



University of Technology Sydney

**Advanced Control Strategies for Vehicle to Grid
Systems with Electric Vehicles as Distributed Sources**

Yanqing Qu


**School of Electrical, Mechanical and Mechatronic Systems
University of Technology Sydney, Australia**

**A thesis submitted to the University of Technology Sydney
for the Degree of Doctor of Philosophy**

CERTIFICATE OF AUTHORSHIP/ORIGINALITY

I certify that the work in this thesis has not previously been submitted for a degree nor has it been submitted as part of requirements for a degree as fully acknowledged with the text.

I also certify that the thesis has been written by me. Any help that I have received in my research work and the preparation of the thesis itself has been acknowledged. In addition, I certify that all information sources and literature used are indicated in the thesis.


Signature of Candidate

Acknowledgements

First of all, I would like to express heartfelt gratitude and appreciation to my supervisor, Professor Jianguo Zhu, for his enthusiastic help, inspiration, patience, unlimited support and consistent encouragement throughout the entire research period providing the opportunity to work in this highly promising research field. I am also grateful to Associate Professor Youguang Guo, my co-supervisor, for his useful suggestions and encouragement of my attitude.

Also, I would like to thank Professor Guoxiu Wang, the external co-supervisor, from the School of Mathematical and Physical Sciences, Faculty of Science for his precious discussion and comments. His research experience on electrochemical energy storage components has made a significant contribution to the hybrid energy storage system development.

I would also like to express thanks to my research group mates, in particular Dr. Jiefeng Hu and Dr. Gang Lei of the Centre for Electrical Machines and Power Electronics, University of Technology Sydney (UTS), for their precious time, professional advice, sharing of knowledge, technical support and friendship. Their opinions and advices have provided me with great assistance in completing my PhD research work.

On a personal aspect, I would like to thank my parents for their love and support given to me during this research period. Their support is so important for me to finish my PhD study and grow up in Australia. I also would like to thank my special friends who helped me and gave me essential support during this period of study.

TABLE OF CONTENTS

CERTIFICATE OF AUTHORSHIP/ORIGINALITY	i
ACKNOWLEDGEMENTS	ii
TABLE OF CONTENTS	iii
LIST OF SYMBOLS	vii
LIST OF ABBREVIATIONS	xi
LIST OF FIGURES	xiv
LIST OF TABLES	xix
ABSTRACT	xx
1. INTRODUCTION	1
1.1 Background and Significance	1
1.2 Development of Electric Vehicles	3
1.3 The Concept of V2G Services	5
1.4 Smart Car Parks in Power Grids	7
1.5 Research Objectives	10
1.6 Outline of the Thesis	12
References	13
2. LITERATURE SURVEY	19
2.1 Introduction	19
2.2 Vehicles and Energy Sources	19
2.3 Battery Charging and Grid Connection	26
2.4 V2G System Requirements and Power Flow	28
2.5 Smart Charging	36

2.6 EV-Grid Models	37
2.7 Control Algorithm for Bidirectional Power Flow	41
2.7.1 Voltage oriented control	41
2.7.2 Direct control	42
2.7.3 Space vector modulation direct control	42
2.7.4 Model predictive control	43
2.8 Grid Support from V2G Services	45
2.8.1 Load balancing and peak power (load management)	46
2.8.2 Support to systems containing renewable energy resources	47
2.8.3 Electric grid interaction for grid support	47
2.9 Economic Issues Related to V2G Services	49
2.10 Summary of the Chapter	55
References	56
3. ENERGY STORAGE SYSTEM FOR ELECTRIC VEHICLES	73
3.1 Introduction	73
3.2 Model Development of Batteries as Energy Storage System in EVs	75
3.2.1 Battery characteristics for model development	75
3.2.2 Battery model development procedure	79
3.3 Model Development of Supercapacitors as Energy Storage System in EVs	81
3.3.1 Supercapacitor characteristics for model development	81
3.3.2 Supercapacitor model parameter calculation	84
3.4 Balancing Circuit Development for Energy Storage System	89
3.4.1 Supercapacitor cell voltage balancing necessity	91
3.4.2 Equalization scheme types	92
3.4.3 Supercapacitor cell voltage balancing methods comparison	93
3.4.4 Novel balancing circuit development for supercapacitor storage bank	99
3.5 Numerical Simulations and Experimental Verifications	108
3.5.1 Supercapacitor experimental test	108
3.5.2 Battery experimental test	122
3.5.3 Test performance of supercapacitor cell balancer	136
3.6 Summary of the Chapter	141

References	142
4 IMPLEMENTATION OF THE V2G SYSTEM AT COMPONENT LEVEL	148
4.1 Introduction	148
4.2 Direct Power Control for Bidirectional Power Flow Control	151
4.3 Model Predictive Control for Bidirectional Power Flow Control	154
4.4 Flexible Power Regulation between Grid and EVs	156
4.5 Numerical Simulation	160
4.5.1 Comparison between MPC and conventional DPC	160
4.5.2 Bidirectional power flow control	165
4.6 Summary of the Chapter	168
References	169
5 GRID SUPPORT FROM V2G SERVICES	175
5.1 Introduction	175
5.2 Modelling of Bidirectional Charger Used for V2G Support to Grid	181
5.3 Aggregator Development of V2G services	183
5.4 V2G Service for Grid Stability from EV Parks	190
5.4.1 Power system and V2G system modelling in the PSCAD/EMTDC	191
5.4.2 Power compensation from EVs to the grid	194
5.5 Simulation Results and Scaled Down Experimental Test Results for V2G Service	202
5.5.1 Experimental results of the generator performance when load changes	205
5.5.2 Simulation results of the V2G support to power system when load changes	207
5.6 Summary of the Chapter	208
References	209
6 ECONOMIC ISSUES RELATED TO V2G SERVICES	212
6.1 Introduction	212

6.2 V2G System Information Collection for SmartPark	213
6.2.1 EVs information collection	214
6.2.2 Grid side information collection	218
6.3 Optimal Charging Based on Different Objectives	226
6.3.1 As fast as possible charging (AFAP)	226
6.3.2 Maximization of the average state of charge (SOC) for all vehicles at the next time step	229
6.3.3 Maximum revenue static charging scheduling problem (R-SCSP) and Minimum cost dynamic charging scheduling problem (C-DCSP)	232
6.4 Summary of the Chapter	237
References	238
7 CONCLUSIONS AND FUTURE WORK	240
7.1 Conclusions	240
7.2 Future work	241
APPENDIX. PUBLICATIONS BASED ON THE THESIS PROJECT	242

List of Symbols

A	Normal distribution of arrival time
$A0, A1, A2$	Control of address signals
a	Regulation prices [\$]
B	Cost upper bound [\$]
$C, C_{1c}, C_{2c}, C_{3c}, C_{4c}$	Capacitor capacitance [F]
$Cap_{r,i}(k)$	Remaining battery capacity needed to be filled [F]
$C_{i,t}$	Cost of charging EV i at timeslot t (\$)
D	Normal distribution of departure time
$d_P d_Q$	Digitized signals by two fixed-band hysteresis comparators
d_t	Energy consumption at time t (Wh)
E	Energy density (Wh/L)
e	Line to line AC Voltage (V)
f	Source voltage frequency (hZ)
g	Electricity prices (\$)
I	Current supplied by the battery (A)
$I_1(t)$	Current value across supercapacitor (A)
I_a	Charger current (A)
I_C	Charge current across R_{1c} (A)
K_f	Infrastructure cost (\$)
K_{T1}	Transformer T1 ratio
K_{T2}	Transformer T2 ratio
K_{T3}	Transformer T3 ratio
l	Base loads (W)
M	Estimated number of miles driven daily (km)
$m_{i,t}$	Aggregator's revenue from EV i at timeslot t (\$)

N	Total number of plug-in electric vehicles (PEVs)
P	Active power exchanged with the grid (W)
P_{EV}	Charging station injects active power (W)
P_{EVavg}	Average constant power requirement for all PEVs (W)
P_i	Active power flows in line i (W)
$p_{i,t}$	Charging rate of EV i at timeslot t (kW)
$\bar{P}_{i,t}$	Maximum charging rate limit of EV i at timeslot t (kW)
P_{Li}	Active load at bus i (W)
P_{ref}	Active power reference (W)
P_t	Price per energy unit at time t (\$)
Q	Reactive power exchanged with the grid (Var)
Q_{EV}	Charging station injects reactive power (Var)
Q_i	Reactive power flows in line i (Var)
Q_{Li}	Reactive load at bus i (Var)
Q_{ref}	Reactive power reference (Var)
R	Transformer delivery capacity (W)
R_0	Series resistor of battery (Ω)
R_l	Parallel resistor of battery (Ω)
$R_{1c}, R_{2c}, R_{3c}, R_{4c}$	Resistor (Ω)
R_L	Leakage resistor of supercapacitor (Ω)
R_S	Series resistor of supercapacitor (Ω)
$r_{i,t}$	Regulation capacity of EV i at timeslot t (kW)
$S_{a1}-S_{a5} S_{b1}-S_{b5}$	Bidirectional switches
S_B	System rated power (W)
S_{EV}	Power supplied by the battery (W)
SOC_{end}	Terminal EV battery SOC
SOC_{init}	Initial EV battery SOC

SOC_{max}	Maximum storage capacity (Ah)
SOC_t	SOC level for at time t
T	Total number of timeslots
$T_{r,i}(k)$	Remaining time for charging the i th vehicle at time step k
T_s	Sample time
U_B	System rated voltage (V)
$U^*(t)$	Voltage value of supercapacitor (V)
V	Voltage of voltage source (V)
$V_1 \sim V_5, V_6 \sim V_{11}$	Terminal voltage (V)
V_a	Grid voltage (V)
V_b	Voltage present voltage (V)
V_b^*	Reference battery voltage (V)
$V_{b,nom}$	Voltage nominal value (V)
V_{dc}	DC bus voltage (V)
V_E	Terminal voltage of capacitor C_{1c} (V)
V_i	Voltage of bus i (V)
V_{oc}	Open-circuit voltage (V)
V_s	Terminal voltage for supercapacitor before charge (V)
ΔV_o	Jump of terminal voltage across capacitor (V)
X	Line reactance between the converter and the utility node (Ω)
$x_{i,t}$	SOC of EV i at time t
Z_t	Location of the EV at time t
Δ	Angle between E and V
λ_t	V2G parameter for at time t
η_c	Charging efficiency
η_d	Discharging efficiency
Ψ_e	Energy-related battery degradation cost (\$/kWh)

Ψ_p	Power-related battery degradation cost (\$/kWh ²)
ϕ	Net charging amount (kWh)
φ_t	Charge parameter for at time t (kWh)
Φ_i	Charging schedule for a given charging task i
$\bar{\varphi}$	Maximum charging amount per time slot (kWh)
$\psi_e \varphi_t$	Line term reflecting the degradation from energy throughput
$\psi_p \varphi_t^2$	Quadratic term reflecting power-related degradation

List of Abbreviations

ACE	Area Control Error
AFAP	As Fast as Possible Charging
AGC	Automatic Generation Control
BESS	Battery Energy Storage System
BEV	Battery Electric Vehicle
BMS	Battery Management System
C-DCSP	Cost Dynamic Charging Scheduling Problem
CNT	Carbon NanoTube
CVT	Continuously Variable Transmission
DER	Distributed Energy Resource
DOD	Depth of Discharge
DPC	Direct Power Control
DSO	Distribution System Operator
DTC	Direct Torque Control
EIS	Electrochemical Impedance Spectroscopy
EMI	Electromagnetic Interference
EMTDC	Electromagnetic Transient and DC
EPA	Environmental Protection Agency
EPRI	Electric Power Research Institute
ESP	Energy Service Provider
EV	Electrical Vehicle
FACTS	Flexible AC Transmission System
FCV	Fuel Cell Vehicle
GV	Grid-able Vehicle
G2V	Grid to Vehicle
HEV	Hybrid Electrical Vehicle
HVDC	High Voltage Direct Current
ICE	Internal Combustions Engine

IGBT	Insulated-gate Bipolar Transistor
IGCT	Integrated-gate Commutated Thyristor
ISO	Independent System Operator
LP	Linear Programming
MPC	Model Predictive Control
NEC	National Electrical Code
NERC	National Electric Reliability Council
OCV	Open Circuit Voltage
PEM	Proton Exchange Membrane
PEV	Plug-in Electric Vehicle
PFCV	Plug-in Fuel Cell Vehicle
PHEV	Plug-in Hybrid Electrical Vehicle
PI	Proportional-integral
PLC	Power Line Communication
PSO	Particle Swarm Optimization
PSCAD	Power System Computer Aided Design
PV	Photovoltaic
PWM	Pulse Width Modulation
R-DCSP	Revenue Dynamic Charging Scheduling Problem
RES	Renewable Energy Resources
R-SCSP	Revenue Static Charging Scheduling Problem
SCs	Supercapacitors
SDPC	Switching Table-based Direct Power Control
SGSS	Smart Grid Stabilization System
SMPS	Switched Mode Power Supply
SOC	State of Charge
STATCOM	Static Compensator
SVM	Space Vector Modulator
V2B	Vehicle to Building
VFC	Voltage to Frequency Converters

V2G	Vehicle to Grid
V2I	Vehicle to Infrastructure
VOC	Voltage Oriented Control
VSI	Voltage Source Inverter
V2X	Vehicle to any Load
WSCC	Western System Coordinating Council

LIST OF FIGURES

- Fig. 1.1 Overview of the proposed PEVs network charging system with renewable resources
- Fig. 1.2 Typical structure of a parking lot for V2G system
- Fig. 2.1 Typical EV configuration
- Fig. 2.2 Toyota Prius configuration (a) HEV, (b) converted PHEV
- Fig. 2.3 Fuel cell vehicle configuration (a) FCV, (b) PFCV
- Fig. 2.4 Typical variable-speed electric motor characteristics
- Fig. 2.5 Typical electric motor efficiency characteristics
- Fig. 2.6 Components and power flow of a V2G system
- Fig. 2.7 EV power electronics configuration with V2G
- Fig. 2.8 AC propulsion V2G model AC-150 (a) electrical schematic, (b) picture of the package
- Fig. 2.9 Single-stage power electronics topologies with (a) Single-phase inverter; (b) Three-phase inverter
- Fig. 2.10 Cascaded power electronic topologies with DC-DC and DC-AC converters
- Fig. 2.11 Bidirectional isolated DC-DC power electronics topology
- Fig. 2.12 Generalized power electronics and control of a battery energy storage system
- Fig. 2.13 Block diagram of VOC
- Fig. 2.14 Block diagram of DPC
- Fig. 2.15 Block diagram of SVM-DPC
- Fig. 2.16 Block diagram of model predictive control
- Fig. 2.17 Envisioned large-scale PHEV/PEV charging/V2G infrastructure in a smart grid environment
- Fig. 2.18 EV charging configuration at AC level 1 and 2 setup (i.e. on-board charger).
- Fig. 2.19 EV charging configuration at DC level 1 and 2 framework (i.e. off-board charger)
- Fig. 2.20 The power output and battery state of charge for an electric vehicle providing frequency regulation ancillary service
- Fig. 3.1 Indicative Ragone plots for different energy storage devices
- Fig. 3.2 Schematic representation of operation of electrochemical cell. (a) Discharge (b) Charge
- Fig. 3.3 Typical battery discharge curve
- Fig. 3.4 Circuit-oriented battery models (a), (b) and (c)
- Fig. 3.5 First-order Thevenin charging model
- Fig. 3.6 Double layer capacitor
- Fig. 3.7 Three layer supercapacitor structure
- Fig. 3.8 Model of supercapacitor used
- Fig. 3.9 EIS Nyquist plot of supercapacitor
- Fig. 3.10 Simplest electric model
- Fig. 3.11 Equivalent charge circuit model
- Fig. 3.12 Cell equalization circuit using switched resistor

- Fig. 3.13 (a) Typical flyback-converter-based equalize, (b) Inductor coupling flyback-converter-based equalizer, (c) Buck-boost-based modular current divider
- Fig. 3.14 Equalization using MOSFET to achieve the balancing
- Fig. 3.15 Equivalent circuit of the proposed cell voltage equalizer: (a) state 1: Sa is ON and Sb is OFF, (b) state 2: Sa is OFF and Sb is ON
- Fig. 3.16 Bidirectional switch
- Fig. 3.17 Circuit diagram of cell balancing circuit using Switched capacitor based on the Cockcroft-Walton scheme
- Fig. 3.18 Simulation results of the voltage waveform using switched capacitor based on the Cockcroft-Walton scheme
- Fig. 3.19 Switchless cell voltage equalizer
- Fig. 3.20 Current flow direction in (a) mode A and (b) mode B
- Fig. 3.21 Circuit diagram of cell balancing circuit using switchless voltage equalizer
- Fig. 3.22 Simulation results of the voltage waveform using switchless voltage equalizer
- Fig. 3.23 Circuit diagram of cell balancing circuit using transformer
- Fig. 3.24 Simulation results of the voltage waveform using transformer
- Fig. 3.25 Energy recovery for a capacitor versus depth of discharge
- Fig. 3.26 Voltage monitoring circuit diagram
- Fig. 3.27 Cell balancer diagram
- Fig. 3.28 Cell Balancer SMPS and VFC
- Fig. 3.29 Local controller with dummy VFC Controller plugged into J32
- Fig. 3.30 Front panel LED display
- Fig. 3.31 Supercapacitor from Jinzhou Kaimei Power Co.
- Fig. 3.32 The charge circuit for supercapacitor
- Fig. 3.33 The self-discharge circuit for supercapacitor
- Fig. 3.34 1.96 Ω load discharge circuit
- Fig. 3.35 Power supply used to charge the supercapacitor
- Fig. 3.36 Power supply used for current sensor board from NI
- Fig. 3.37 Current sensor used to transfer current signal to voltage signal
- Fig. 3.38 DAQ board used to collect the voltage data of supercapacitor and current sensor
- Fig. 3.39 Supercapacitor connected into the circuit
- Fig. 3.40 The waveform view of Labview
- Fig. 3.41 The blocks of Labview to collect data
- Fig. 3.42 The whole work station
- Fig. 3.43 Voltage of No.1 supercapacitor for self-discharge
- Fig. 3.44 Voltage of No.2 supercapacitor for self-discharge
- Fig. 3.45 Voltage of No.3 supercapacitor for self-discharge
- Fig. 3.46 Voltage of No. 1 supercapacitor for 3.15A constant charging
- Fig. 3.47 Voltage of No. 2 supercapacitor for 3.15A constant charging
- Fig. 3.48 Voltage of No. 3 supercapacitor for 3.15A constant charging
- Fig. 3.49 Voltage of No.1 supercapacitor for 1.96 Ω load discharge
- Fig. 3.50 Voltage of No.2 supercapacitor for 1.96 Ω load discharge

- Fig. 3.51 Voltage of No.3 supercapacitor for 1.96 Ω load discharge
- Fig. 3.52 No.1 supercapacitor recovery performance
- Fig. 3.53 No.2 supercapacitor recovery performance
- Fig. 3.54 No.3 supercapacitor recovery performance
- Fig. 3.55 Basic model voltage curve comparison with experiment results
- Fig. 3.56 Voltage error between model and experiment
- Fig. 3.57 Simulink block diagram of supercapacitor model charging
- Fig. 3.58 Constant current charging with 3.15A for 91 seconds
- Fig. 3.59 Voltage of supercapacitor during constant current charging procedure
- Fig. 3.60 Comparison of the experimental and simulation results
- Fig. 3.61 Nanophosphate battery from A123 company
- Fig. 3.62 Schematic illustration of the Nanophosphate structure, with secondary and primary particles
- Fig. 3.63 2A constant current charge for the No. 1 battery
- Fig. 3.64 3A constant current charge for the No. 1 battery
- Fig. 3.65 4A constant current charge for the No. 1 battery
- Fig. 3.66 Comparison of different current charge for the No. 1 battery
- Fig. 3.67 2A constant current charge for the No. 2 battery
- Fig. 3.68 3A constant current charge for the No. 2 battery
- Fig. 3.69 4A constant current charge for the No. 2 battery
- Fig. 3.70 Comparison of different current charge for the No. 2 battery
- Fig. 3.71 3A constant current charge for the No. 3 battery
- Fig. 3.72 4A constant current charge for the No. 3 battery
- Fig. 3.73 Experimental setup for measuring battery charge performance
- Fig. 3.74 First-order Thevenin charging model
- Fig. 3.75 Experiment results of charging behaviour
- Fig. 3.76 Curve fitting of $[U_t(t)-U_{oc}]$ versus time (starting SOC=0%)
- Fig. 3.77 Curve fitting of $[U_t(t)-U_{oc}]$ versus time (starting SOC=10%)
- Fig. 3.78 Curve fitting of $[U_t(t)-U_{oc}]$ versus time (starting SOC=20%)
- Fig. 3.79 Curve fitting of $[U_t(t)-U_{oc}]$ versus time (starting SOC=30%)
- Fig. 3.80 Curve fitting of $[U_t(t)-U_{oc}]$ versus time (starting SOC=40%)
- Fig. 3.81 Curve fitting of $[U_t(t)-U_{oc}]$ versus time (starting SOC=50%)
- Fig. 3.82 Curve fitting of $[U_t(t)-U_{oc}]$ versus time (starting SOC=60%)
- Fig. 3.83 Curve fitting of $[U_t(t)-U_{oc}]$ versus time (starting SOC=70%)
- Fig. 3.84 R_0 variation with different SOC starting
- Fig. 3.85 R_1 variation with different SOC starting
- Fig. 3.86 A single supercapacitor module
- Fig. 3.87 Three supercapacitor modules in test bed
- Fig. 3.88 Input power and efficiency versus cell voltage
- Fig. 3.89 VFC output frequency versus cell voltage using a 250 kHz VFC clock
- Fig. 4.1 V2G charger structure with the AC transmission bus
- Fig. 4.2 Three-phase AC-DC converter topology

- Fig. 4.3 control block of SDPC
- Fig. 4.4 possible voltage vectors
- Fig. 4.5 Control block of model predictive control (MPC)
- Fig. 4.6 Four quadrant operation of power flow through inverter between grid and vehicle
- Fig. 4.7 Branch of a radial distribution system
- Fig. 4.8 Input AC side V_a and I_a (DPC)
- Fig. 4.9 Input AC side V_a and I_a (DPC) (0.15s-0.25s)
- Fig. 4.10 Input I_a , I_b and I_c (DPC)
- Fig. 4.11 Input I_a , I_b and I_c (DPC) (0.15s-0.25s)
- Fig. 4.12 Output DC voltage V_{dc} (DPC)
- Fig. 4.13 Input active power P (DPC)
- Fig. 4.14 Input reactive power Q (DPC)
- Fig. 4.15 Input AC side V_a and I_a (MPC)
- Fig. 4.16 Input AC side V_a and I_a (MPC) (0.15s-0.25s)
- Fig. 4.17 Input I_a , I_b and I_c (MPC)
- Fig. 4.18 Input I_a , I_b and I_c (MPC) (0.15s-0.25s)
- Fig. 4.19 Output DC voltage V_{dc} (MPC)
- Fig. 4.20 Input active power P (MPC)
- Fig. 4.21 Input reactive power Q (MPC)
- Fig. 4.22 Three-phase bidirectional AC-DC converter topology used in V2G system
- Fig. 4.23 Active power P and reactive power Q in one chart
- Fig. 4.24 Grid voltage V_a (1/10 scaled) and charger current I_a , waveforms for each operation mode. (a) Mode#1-discharging operation. (b) Mode#2-discharging and capacitive operation. (c) Mode#3-charging operation. (d) Mode#4-charging and inductive operation.
- Fig. 5.1 Illustrative schematic of power line and wireless control connections between vehicles and the electric power grid
- Fig. 5.2 A single container of A123's Smart Grid Stabilization System (SGSS)
- Fig. 5.3 Power electronics-interfaced EV applications in the power grid
- Fig. 5.4 EVs batteries used as a distributed energy source
- Fig. 5.5 Aggregator in V2G system
- Fig. 5.6 Computer/communication/control network for the framework of V2G system
- Fig. 5.7 Classification of power system stability
- Fig. 5.8 3 generators, 9 buses power system from WSCC
- Fig. 5.9 3 generators, 9 buses power system model block diagram in PSCAD/EMTDC
- Fig. 5.10 V2G system model block diagram in PSCAD/EMTDC
- Fig. 5.11 Frequency recovery performance comparison. (a) Without EVs' active power compensation. (b) With EVs' active power compensation
- Fig. 5.12 Voltage recovery performance at bus 4 (Increase reactive load at bus 4 and use EVs to compensate the reactive power at 4s)

- Fig. 5.13 Different buses voltage variation when there is reactive load change at bus 4 and reactive power from EVs compensated at bus 4. (a) Bus 4. (b) Bus 1. (c) Bus 2. (d) Bus 3. (e) Bus 5. (f) Bus 6.
- Fig. 5.14 Voltage change comparison results among different bus numbers when there is reactive power load change at bus 4 and reactive power from EVs compensated at bus 4
- Fig. 5.15 Connection of transformer and load
- Fig. 5.16 Display and control panels of Easygen-3000 in the laboratory
- Fig. 5.17 PT screen
- Fig. 5.18 Experimental test bed for the generator when load changes
- Fig. 5.19 Output voltage waveform of resistor load without V2G support
- Fig. 5.20 Output voltage waveform of resistor and capacitive load without V2G support
- Fig. 5.21 Output voltage waveform of resistor, capacitive and inductive load without V2G support
- Fig. 5.22 V2G support to power system when load changes
- Fig. 6.1 The probability density function of arrival time A
- Fig. 6.2 The probability density function of arrival time D
- Fig. 6.3 The probability density function of parking time
- Fig. 6.4 Average kilometres travelled, Motor vehicles by state/territory of registration Year ended 30 June 2012
- Fig. 6.5 The probability density function of the daily travel distance
- Fig. 6.6 System load following and regulation
- Fig. 6.7 Electricity load demand data in a typical day in NSW (11/3/2015)
- Fig. 6.8 Load curve and load following line in a typical day in NSW (11/3/2015)
- Fig. 6.9 Power regulation pattern in a typical day in NSW (11/3/2015)
- Fig. 6.10 Electricity load demand data in a typical month in NSW (1/12/2014-31/12/2014)
- Fig. 6.11 Electricity load demand data in a typical month in NSW 24 hours a day 31 days a month (1/12/2014-31/12/2014)
- Fig. 6.12 Electricity price variation in a typical month in NSW (1/12/2014-31/12/2014)
- Fig. 6.13 Electricity price variation in a typical month in NSW 24 hours a day 31 days a month (1/12/2014-31/12/2014)
- Fig. 6.14 The illustration of the remaining battery capacity

LIST OF TABLES

TABLE 2.1	AC/DC Charging Levels Characteristics as per SAE J1772 Standard
TABLE 2.2	Mathematical Model Formulation of V2G Optimization
TABLE 3.1	2005 Comparison of Energy Density of Various Energy Storage Technologies
TABLE 3.2	Extraction Results of Ro and R1
TABLE 4.1	Switching Table of Conventional SDPC
TABLE 4.2	Electrical Parameters of Power Circuit
TABLE 4.3	Electrical Parameter of Power Circuit
TABLE 4.4	Battery Parameters Block Used in the Simulink
TABLE 4.5	Two V2G Mode Worked in the Simulation
TABLE 5.1	Key Features about a Single Container of A123's Smart Grid Stabilization System
TABLE 5.2	Model Parameters of a 3 Generator, 9 Bus Power System Model
TABLE 6.1	Parameters for PEVs in Different Sizes
TABLE 6.2	Average Distance and Electricity Consumption for a Typical PHEV
TABLE 6.3	Total Energy Available For Grid Support
TABLE 6.4	Total Energy Available For Grid Support
TABLE 6.5	Total Energy Required During Charging
TABLE 6.6	Total Energy Required During Charging
TABLE 6.7	Model Parameters
TABLE 6.8	The Symbols and Major Notations

ABSTRACT

This thesis focuses on the control and implementation of the vehicle to grid (V2G) system in a smart grid. Important issues like structure, principle, performance, and control of energy storage systems for electrical vehicles and power systems are discussed.

In recent decades, due to rapid consumption of the earth's oil resources, air pollution and global warming (a result of the "greenhouse effect"), the development of electrical vehicles (EVs), hybrid electrical vehicles (HEVs) and plug-in electric vehicles (PEVs) are attracting more and more attentions. In order to provide regulation services and spinning reserves (to meet sudden demands for power), V2G services have a promising prospective future for grid support. It has been proposed that in the future development, such use of V2G could buffer and support effectively the penetration of renewable sources in power systems. This PhD thesis project aims to develop novel and competitive control strategies for V2G services implementation for EVs in smart electrical car parks or Smartparks.

Through a comprehensive literature review of the current EV development and energy storage systems used for EVs, several energy storage technologies are compared and a hybrid energy storage system consisting of batteries and supercapacitors is proposed. This system combines effectively the advantages of high energy density of battery banks and high power density of supercapacitor banks. Supercapacitor and battery cells are tested in the laboratory using different charging and discharging procedures. Different supercapacitor and battery models are compared, discussed, and verified using the experimental data. For the energy storage system package, a cell voltage balance circuit is developed for the supercapacitor module. The principle of this circuit is also applicable to the battery module. The proposed balancing method is simple and reliable, and presents good performance for voltage balancing to prolong the lifetime of the energy storage system.

The essential technology of V2G is based on the bidirectional power flow control of the charger. Besides charging the EV batteries, it can utilize the stored energy to feed electricity back to the power grid when there is a need. Three-phase AC/DC converters have been extensively used in industrial applications and also the V2G chargers. The power converters used for the V2G services are required to operate more efficiently and effectively to maintain high power quality and dynamic stability. Then the AC/DC

converter used for the bidirectional V2G charger is developed and modelled. For the control aspect of AC/DC converter, a new control approach using a model predictive control (MPC) scheme is developed for V2G applications. With the advanced control strategy, the EVs in Smartparks can exchange both active and reactive power with the grid flexibly. The MPC algorithm presents excellent steady-state and dynamic performance.

When a very large number of EVs are aggregated in Smartparks, the charging and discharging power should be a significant viable contributor to the power grid. New challenges will be introduced into the power system planning and operation. While discharging, the V2G power brings more potential benefits to enhance the power quality and system reliability. Using V2G services, EVs can provide many grid services, such as regulation and spinning reserve, load levelling, serving as external storage for renewable sources. An effective approach to deal with the negligibly small impact of a single EV is to group a large number of EVs. An aggregator is a new player whose role is to collect the EVs by attracting and retaining them so as to result in a MW capacity that can beneficially impact the grid. From the aggregator' decision, the EVs are determined by the optimal deployment. The aggregator can act as a very effective resource by helping the operator to supply both capacity and energy services to the grid. By supplying active power and reactive power from EVs, the aggregation may be used for frequency and voltage regulation to control frequency and voltage fluctuations that are caused by supply–demand imbalances. Different case studies of EVs' support to grid are carried out; the results show that V2G services can stabilize the frequency and voltage variations and have control flexibilities to fulfil system reliability and power quality requirements.

The main attractiveness of V2G to consumers is that it can produce income to the vehicle owner to maximize car use. On the other hand, the utility companies can use EVs to stabilize the frequency in the power system and improve the utility operation. It also makes the utility companies more efficient with less loss because the energy is generated locally. From this point of view, V2G is a source of revenue in both electricity and transportation system, and it can help the environment reduce pollution and global warming. Various data of V2G systems have been collected for economic analysis, such as EV battery capacities, charging time, and grid electricity price and load demands. Then for the economic issues related to V2G services, optimal charging based on different objectives is presented. Dumbing charging, maximization of the average state of charge (SOC), maximum revenue and minimum cost are compared. Economic

issues are a very special aspect of the V2G technology and how a large profit from V2G services can be produced is the main point of attraction to vehicle owners.

Significant conclusions based on the research findings are drawn, and possible future works for further development including commercialisation of the V2G technology are proposed.

CHAPTER 1

INTRODUCTION

1.1 Background and Significance

The worldwide development of automobiles is one of the greatest achievements of modern technology, and has made great contributions to the growth of modern society by satisfying many of the needs for mobility in everyday life. The rapid development of the automotive industry, unlike that of any other industry, has prompted the progress of human beings from a primitive security to a highly developed industrial one [1.1]. The number of automobiles on the planet doubled to about a billion or so in the last 10 years, and thus automobiles constitute an integral part of our everyday life. The automobile industry and the other industries that serve it constitute the backbone of the world's economy and employ the greatest share of the working population.

However, the large number of automobiles in use around the world has caused and continues to cause serious problems for the environment and human life. Air pollution, global warming (a result of the "greenhouse effect"), and rapid depletion of the earth's petroleum resources are now problems of paramount concern. The problems associated with oil consumption have to take into account those induced costs. Although difficult to estimate, the costs associated with these problems are huge and indirect, and may be financial, human, or both. What makes it worse is that it is becoming more and more difficult to discover new reserves of petroleum in the earth. It remains clear that any solutions to these problems will indeed result in cost savings, which will benefit the payers.

Yet the exhaust emissions of the conventional internal combustions engine (ICE) vehicles are to blame as a major source of urban pollution that contributes to the greenhouse effect leading to global warming, and the crisis will inevitably become acute as the oil reserves of the world

diminish. The increasing number of automobiles adding to the pollution problems is also an economic factor inherent in the poor energy conversion efficiency of combustion engines. Environmental as well as economic issues provide a compelling impetus to develop clean, efficient, and sustainable vehicles for urban transportation [1.2]. The subject of electrical and hybrid vehicles is becoming increasingly important. Furthermore, the next generation of conventional automobiles will experience a gradual replacement of the hydraulically driven actuators by electrically driven actuators.

Recently, the research and development activities related to electrical vehicles (EVs), hybrid electrical vehicles (HEVs), and fuel cell vehicles have been emphasized [1.3]. Although the number for alternative electric vehicles is not significantly higher when the efficiency is evaluated on the basis of conversion from crude oil to traction effort at the wheels, it makes a difference [1.4]. EVs paved their way into public use as early as the middle of the 19th century, and the interest and research in EVs soared in the 1990s, with the major automobile manufacturers embarking on plans to introduce their own electric or hybrid electric vehicles. EVs enabled by high-efficiency electric motors and controllers and powered by alternative energy sources can provide a means for establishing a clean, efficient, and environmentally friendly urban transportation system [1.5]. Surprisingly, the concept of HEV is almost as old as the automobile itself. The primary purpose, however, was not so much to lower the fuel consumption but rather to assist the ICE to provide an acceptable level of performance. A hybrid electric vehicle is a vehicle in which at least one of the energy sources, storage units, and converters can deliver electric energy. The HEV serves as a compromise for the environmental pollution problem and the limited range capability of today's purely EV, and vehicle design complexity increases significantly with hybrid vehicles, because control and support systems are needed for a thermal engine and an electrical machine in addition to the components needed for controlled blending of power coming from the two sources [1.6]. The trend is increasing rapidly today, with EVs serving as zero-emission vehicles, and HEVs already filling in for ultralow-emission vehicles.

The Plug-in HEV (PHEV) is to be the focus research area and the trends of HEV with the advantages of improving vehicle fuel efficiency and reduce the emissions. It also drops down the dependence of the vehicle on oil by EV model [1.7]. PHEV takes the electrification of the automobile one step further than the HEV by increasing the battery energy capacity [1.8]. The additional capacity of the battery is used to propel the vehicle without using on-board fuel energy [1.9].

1.2 Development of Electric Vehicles

Electric motive power started in 1827, when Slovak-Hungarian priest Ányos Jedlik built the first crude but viable electric motor, provided with stator, rotor and commutator, and the year after he used it to power a tiny car [1.10]. American blacksmith and inventor Thomas Davenport built a toy electric locomotive, powered by a primitive electric motor, in 1835. In 1838, a Scotsman named Robert Davidson built an electric locomotive that attained a speed of four miles per hour (6 km/h). In England a patent was granted in 1840 for the use of rails as conductors of electric current, and similar American patents were issued to Lilley and Colten in 1847 [1.11]. By the 20th century, electric cars and rail transport were commonplace, with commercial electric automobiles having the majority of the market. Over time their general-purpose commercial use reduced to specialist roles, as platform trucks, forklift trucks, ambulances [1.12], tow tractors and urban delivery vehicles, such as the iconic British milk float; for most of the 20th century, the UK was the world's largest user of electric road vehicles [1.13]. EVs were among the earliest automobiles, and before the pre-eminence of light, powerful internal combustion engines, electric automobiles held many vehicle land speed and distance records in the early 1900s. They were produced by Baker Electric, Columbia Electric, Detroit Electric, and others, and at one point in history out-sold gasoline-powered vehicles. In fact, in 1900, 28 percent of the cars on the road in the USA were electric. EVs were so popular that even President Woodrow Wilson and his secret service agents toured Washington DC in their Milburn Electrics, which covered 60–70 miles per charge [1.14]. A number of developments contributed to the decline of electric cars [1.15]. Improved road infrastructure required a greater

range than that offered by electric cars, and the discovery of large reserves of petroleum in Texas, Oklahoma, and California led to the wide availability of affordable gasoline, making gas-powered cars cheaper to operate over long distances [1.16]. Also gasoline-powered cars became ever easier to operate thanks to the invention of the electric starter by Charles Kettering in 1912 [1.17]. As roads were improved outside urban areas electric vehicle range could not compete with the ICE. Finally, the initiation of mass production of gasoline-powered vehicles by Henry Ford in 1913 reduced significantly the cost of gasoline cars as compared to electric cars [1.18].

During the last few decades, the environmental impact of the petroleum-based transportation infrastructure, along with the peak oil, has led to renewed interest in an electric transportation infrastructure [1.19]. EVs differ from fossil fuel-powered vehicles in that the electricity they consume can be generated from a wide range of sources, including fossil fuels, nuclear power, and renewable sources such as tidal power, solar power, and wind power or any combination of those. The carbon footprint and other emissions of electric vehicles vary depending on the fuel and technology used for electricity generation. The electricity may then be stored on board the vehicle using a battery, flywheel, or supercapacitors. Vehicles making use of engines working on the principle of combustion can usually only derive their energy from a single or a few sources, usually non-renewable fossil fuels. A key advantage of hybrid or plug-in electric vehicles is regenerative braking due to their capability to recover energy normally lost during braking as electricity is stored in the on-board battery.

As of September 2014, series production highway-capable all-electric cars are available in some countries for retail customers include the Mitsubishi i MiEV, Chery QQ3 EV, JAC J3 EV, Nissan Leaf, Smart ED, BYD e6, Bolloré Bluecar, Renault Fluence Z.E., Ford Focus Electric, Tesla Model S, Honda Fit EV, RAV4 EV second generation, Renault Zoe, Roewe E50, Mahindra e2o, Chevrolet Spark EV, Mercedes-Benz SLS AMG Electric Drive, Fiat 500, Volkswagen e-Up!, BMW i3, Kia Soul EV, Volkswagen e-Golf, Mercedes-Benz B-Class Electric Drive and Venucia e30. The Leaf, with over 180,000 units sold worldwide by early

June 2015, is the world's top-selling highway-capable all-electric car in history [1.20]-[1.21]. The Tesla Model S is the world's second best-selling all-electric car of all time, with global deliveries of about 75,000 units by June 2015 [1.22].

As of May 2015, more than 500,000 highway-capable all-electric passenger cars and light utility vehicles have been sold worldwide since 2008, out of total global sales of about 850,000 light-duty plug-in electric vehicles [1.23]-[1.24]. As of May 2015, the United States continued to have the largest fleet of highway-capable plug-in electric vehicles in the world, with about 335,000 highway legal plug-in electric cars sold in the country since 2008, and representing about 40% of the global stock [1.25]-[1.26]. California is the largest plug-in car regional market in the country, with almost 143,000 units sold between December 2010 and March 2015, representing over 46% of all plug-in cars sold in the U.S [1.27]-[1.30].

Norway is the country with the highest market penetration per capita in the world, with four plug-in electric vehicles per 1000 inhabitants in 2013 [1.31]. In March 2014, Norway became the first country where over 1 in every 100 passenger cars on the roads is a plug-in electric [1.32]. Norway also has the world's largest plug-in electric segment market share of total new car sales, 13.8% in 2014, up from 5.6% in 2013 [1.33]. As of May 2015, there were 58,989 plug-in electric vehicles registered in Norway, consisting of 54,160 all-electric vehicles and 4,829 plug-in hybrids [1.34].

1.3 The Concept of V2G Services

With environmental and climate change issues and legislation, rising energy costs, concerns about energy security and fossil energy reserves, and growing consumer expectations, plug-in electric vehicles (PEVs) and plug-in hybrid electric vehicles (PHEVs) are appearing worldwide [1.35]-[1.36]. Even though PEVs have not been widely adopted, in part because of technical limitations, social obstacles, and cost compared to the conventional internal combustion engine (ICE) vehicles [1.37], based on moderate expectations, by 2020 up to 35% of the total vehicles in the USA will be PEVs according to the Electric Power Research Institute (EPRI) [1.38].

PEVs have an advantage compared to self-contained hybrid electric vehicles (HEV) and ICE vehicles: a connection to the electric power grid. A plug-in vehicle can charge its batteries using AC power typically provided by the utility grid. PEVs and PHEVs can also be designed so that power can be sent back to the grid. A vehicle with this type of technology is defined as being vehicle-to-grid (V2G) capable. PEVs can serve in discharge mode as V2G devices and in charge mode as grid-to-vehicle (G2V) devices [1.39].

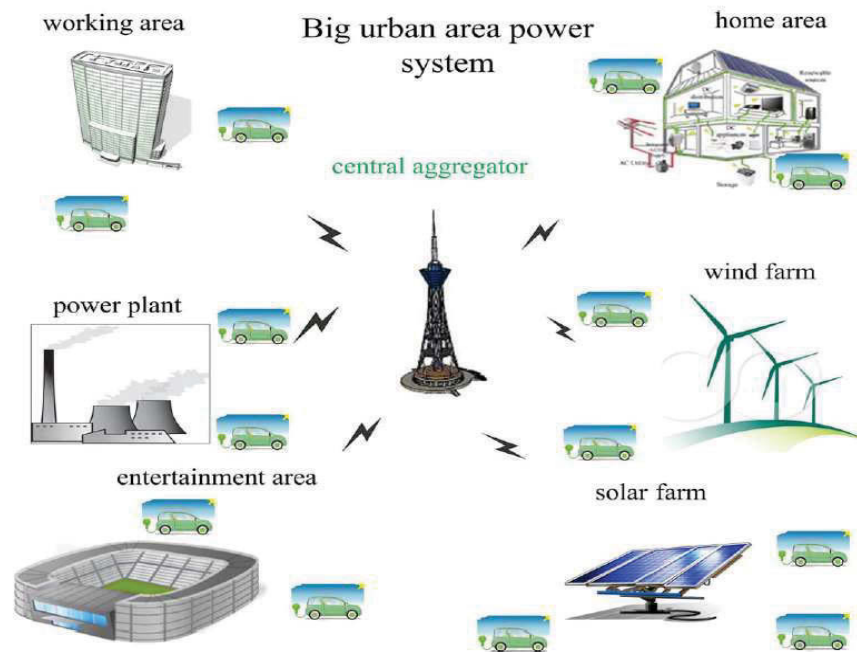


Fig. 1.1 Overview of the proposed PEVs network charging system with renewable resources [1.40]

Fig. 1.1 shows the overview of the proposed PEVs network charging system with renewable resources. The parking lots are located in different areas, such as working area, home area and entertainment area. The concept allows V2G vehicles to provide power to help balance loads by “valley filling” (charging at night when demand is low) and “peak shaving” (sending power back to the grid when demand is high). It can enable utilities with new ways to provide regulation services (keeping voltage and frequency stable) and provide spinning reserves (meet sudden demands for power). For future development, it has been proposed that such use of electric vehicles could buffer renewable power sources such as wind power, for example, by storing excess energy produced during windy periods and providing it back to the grid during

high load periods, thus effectively stabilizing the intermittency of wind power. Some see this application of vehicle-to-grid technology as a renewable energy approach that can penetrate the baseline electric market.

PEVs as a distributed energy resources (DERs) come in many shapes and sizes and may be owned by utilities, system operator, or even utility customers. The integration and control of DER present many unique opportunities and challenges in grid operations. The infrastructure between DER and power grid is the addition of a two-way communications system that would reach from the control centre down into every part of the power grid including homes. The concurrent development of two-way communications and large-scale integration of intelligent devices facilitates the use of distributed control architecture to provide localized autonomous self-healing control. A power network with these infrastructure enhancements along with the resulting (and necessary) changes in grid monitoring and control capabilities is called a smart grid. Transitioning DER to a smart grid provides increased opportunities for advanced communications, automation, and intelligent appliance control. These will enable increased efficiency throughout the system and better integration of distributed energy resources with the goals of a more secure, intelligent, and sustainable system.

1.4 Smart Car Parks in Power Grids

The number of PEVs entering the market has been increasing very rapidly in recent years. In the near future, these vehicles could participate in V2G power transactions in the proposed smart grid framework. Since most personal vehicles are parked more than 95% of the day and generally follow a daily schedule [1.41], their predictable nature can be utilised successfully in V2G transactions. During V2G operations, the PEV fleet can provide many grid services, such as regulation and spinning reserve, load levelling, serving as external storage for renewable sources, and generating revenue by buying and selling power at different times according to variable price curves. Another important service that these PEVs are capable of is reactive power support, which has not been studied extensively. The reactive power compensation

capability of an individual vehicle battery has been reported in [1.42], where the common dc bus of the dc-dc converter and the inverter are responsible for reactive power compensation. Shunt Flexible AC Transmission System (FACTS) devices such as static compensators (STATCOMs) are capable of very fast and accurate reactive power compensation [1.43]. However, the main drawback of FACTS devices is their high cost. On the other hand, the PEVs, while parked in smart car parks or the Smart Park, contain a significant amount of active and reactive power potential and can be utilized for meeting the grid's requirements with little significant infrastructure cost. With the advanced control of power flow between car parks and the grid side, it is possible for these Smart Parks to behave like virtual STATCOMs which can supply not only active power but also reactive power to the grid.

The conventional thinking is based on the idea that EVs would be connected to the grid for charging during the evening until next day morning hours. This point of view lacks a significant proposition that is made possible by the fact that vehicles are parked over 90 percent of the time. If these distributed energy resources are connected to the grid, it could be used to provide possible grid services such as the V2G system [1.44]. In the first step, making the V2G concept practical depends on commercializing EVs because providing the grid services with V2G system requires a large number of vehicles due to their small energy storage. When a large number of EVs are aggregated, there has been little research into the optimal placement of EVs for the services of the V2G approach. Optimal placement and dispatch of EVs is of considerable concern in the distribution sector due to issues such as outage management, system security and emergency conditions. This application raises the importance of parking lots in the system for identifying the optimal placement and locations of parking in order to supply EVs power. The Smart Park can be located in a working area, studying area, home area and entertainment area. Interest in public charging is very important for the success of this approach. Educating and informing consumers regarding available parking lots will be necessary to help promote public charging options for those who may not have charging accessibility at home.

The need for an aggregator is considered in this project for market contribution due to limited and small capacity of EV batteries. This aggregator could be a distribution system operator (DSO), retailer or a private owner like a parking lot owner. The aggregator earns his/her profit from selling energy to EV owners and providing grid services. Additionally, the aggregator is responsible for meeting the participant's requirements based on their contracts and criteria. Besides, one of the important roles of the aggregator is to coordinate the V2G system and renewable energy resources. The aggregator could manage the charging and discharging of EVs when renewable generation exceeds and drops below the demand, respectively. Since EVs are a large number of distributed energy resources in the V2G application, an intelligent and wide communication infrastructure is needed for signalling between distributed EV fleet and DSO.

The Smart Park is appropriate due to the faster development of EVs in comparison with the smart grid technologies such as communication and intelligent sensors and devices. Parking lots reduce the need to establish communication platforms for EVs management and equip the infrastructures like higher levels of power for fast charging and discharging due to fast response to grid services. A parking lot is easier and faster to equip than individual houses. Also parking of EVs within the parking lots helps to make the V2G concept more feasible since the owner behaviour is very stochastic and unpredictable. Constructing the parking lots in the low-load areas of the grid or the areas with high capacity lines and transformers could help the power system to bear the power requirements of EVs. Therefore, parking lots could be effective even if the V2G concept is not considered. A typical structure of smart parking lots is showing in Fig. 1.2 [1.45]. The various issues associated with parking lots are listed below:

1. Parking scheduling for competition in power market to achieve maximum profit or handle system problems such as peak shifting and load curtailment.
2. Defining criteria and incentives for EV owners' satisfaction such as equipping parking lots with protection systems against network transient and failure that damage EVs battery.

- Economic incentives such as battery swapping which allows a driver to exchange a flat battery for a freshly charged battery. This could reduce the battery cost and remove the concern about charging time.

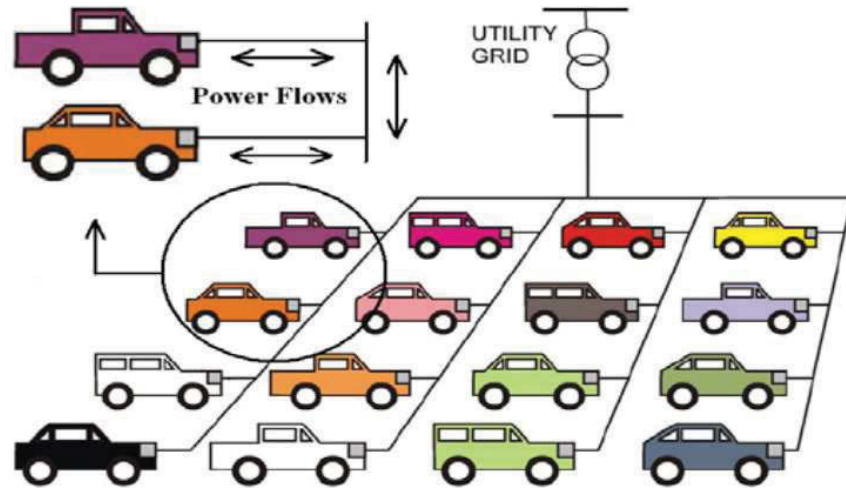


Fig. 1.2 Typical structure of a parking lot for V2G system [1.46]

Nevertheless, from the V2G perspective, the smart parking lot approach could be very useful in existing power grids. EVs make transportation and electricity systems interdependent. This relationship provides a new opportunity for smart grids. With the development of smart grids, employing EVs as energy storage devices would be more strengthened and desirable as V2G. Smart parking lots can be considered as the first and fast approach for making V2G practical.

1.5 Research Objectives

The major research objective of this thesis project is to develop novel advanced grid friendly control strategies for V2G systems (an important component or subsystem in the future smart grids) to help improve the grid power quality, including the control of active and reactive power flows, regulation of voltage and frequency, compensation of power factor and harmonics, and fault ride through, while meeting the energy demand of PEVs.

In this project, the energy storage system in PEVs, the models of PEV power systems, and the interface between them will be firstly developed. Based on the study of these models, novel

autonomous distributed V2G control schemes will then be proposed and implemented for the V2G system. Numerical simulations will be conducted to optimize the control strategies and experimental tests will be conducted for verification of the theory.

PEVs as a distributed energy storage system might require some changes due to the new load levels, patterns, and load characteristics since many distribution systems were designed decades ago considering the load levels at that time. It is essential to do the analysis of the effects of a specific load for the stability and control of power system to identify the effects of a specific load for the stability and control of power system. The key questions relating to how PEVs could feasibly and effectively supply distributed frequency control, shift the peak power of the regional load, and stabilize the power of the distributed generations should be addressed. The research work will be carried out on the following aspects:

- How could distribution system planning and design be impacted as PEVs market penetration increases?
- What impact would the V2G technology have on the lifetime of the battery packs due to frequently charging/discharging?
- Determination of a general approach to find the appropriate amount and duration of power which can contribute to the bulk system frequency control. In other words, to be grid friendly – to help improve the grid power quality besides meeting the needs of both the grid and PEVs for power charging and discharging.
- Characterization of aggregate PEV regulation supply based on supply duration and limits on changes to individual charge rates.
- Evaluation of the economic and technical advantages of PEVs as distributed energy storage units in smart grids.
- The impacts on battery charging and consequently vehicle drivability that can be used to inform vehicle owners as they decide if and how much they would like to participate in supplying frequency regulation through V2G.

It is necessary to study the effects of PEVs as a source of regulation, the real power response of central generation to the changes in system loading and the automatic generation control commands.

The integration of EVs in the power system will impose deep modifications to both sectors. It is necessary to identify grid operational management and control strategies that should be available with the presence of vehicles with plug-in capabilities.

This thesis aims to address key questions when considering the use of PEVs as distributed energy storage system to provide local frequency control to improve power quality of the grid system.

1.6 Outline of Thesis

The thesis is organized as follows:

In Chapter 1 (this chapter), the background, motivation, and significance of this thesis is introduced, defining the main focus in the development of V2G technology. The development of EVs, concept of V2G services and SmartPark are also introduced. After that, the objectives of the thesis are presented.

Chapter 2 presents a comprehensive review of the energy storage systems used for the V2G system, power systems, bi-directional chargers and control algorithms to implement smart charging strategies. The economic issues related to V2G services are also reviewed.

Chapter 3 gives out the detailed structure of energy storage systems. The models of batteries and supercapacitors for EV energy storage systems are discussed. The charging and discharging characteristics of batteries and supercapacitors are presented. Numerical simulation of batteries and supercapacitors are carried out; furthermore, the experimental verifications for the energy storage system are conducted.

Chapter 4 presents the grid support from the V2G services; the modelling of the bidirectional charger used for the V2G system is carried out firstly. Based on the voltage and power rating level of the charger, different control algorithms are applied to the control of converter and the results are compared. Then, the active and reactive power compensation from the V2G system are discussed for grid stability when there is a need from the grid side. Finally, numerical simulations results are presented to verify the theoretical analysis of power compensation.

Chapter 5 carries out the implementation of the V2G system at the component level. Firstly, the model predictive control is applied in the bidirectional power flow control of the charger. Flexible power regulation between grid and EVs including the four quadrants operation of the charger are introduced and then discussed. Then the numerical simulation and scaled down experimental verification of the bidirectional charger are conducted in the laboratory.

Chapter 6 discusses the economic issues related to V2G services. The optimal charging based on different objectives is firstly carried out, such as maximizing the revenue of V2G services, and meeting the requirements of the state of charge (SOC) when EVs leave the Smart Park. Smart Park and cost reduction of the charging infrastructure are also analysed and results are compared.

Chapter 7 concludes this thesis with a general summary of the contributions and offers some remarks and suggestions for the way forward. Key areas that require further investigations are also presented in this chapter.

References

- [1.1] M. Ehsani, Y. Gao and, Ali Emadi, “Modern electric, hybrid electric, and fuel cell vehicles fundamentals, theory, and design,” @2010 by Taylor and Francis Group, LLC.
- [1.2] M. Ehsani, Y. Gao, S. E. Gay, and A. Emadi, Modern Electric, Hybrid Electric, and Fuel Cell Vehicles. Boca Raton, FL: CRC Press, 2005.
- [1.3] J. Larminie and J. Lowry, Electric Vehicle Technology Explained. New York: Wiley,

2003.

- [1.4] S. G. Wirasingha and A. Emadi, "Pihef: Plug-in hybrid electric factor," *IEEE Trans. Veh. Technol.*, vol. 60, no. 3, pp. 1279–1284, Mar. 2011.
- [1.5] B. K. Sovacool and R. F. Hirsh, "Beyond batteries: An examination of the benefits and barriers to plug-in hybrid electric vehicles and a vehicle to-grid transition," *Energy Policy*, vol. 37, no. 3, pp. 1095–1103, 2009.
- [1.6] M. Duvall and E. Knipping, "Environmental assessment of plug-in hybrid electric vehicles. Volume 1: Nationwide Greenhouse Gas Emissions," EPRI/NRDC, Palo Alto, CA, Final Rep. 1015325, 2007, pp. 1–56.
- [1.7] W. Kempton and J. Tomić, "Vehicle-to-grid power implementation: From stabilizing the grid to supporting large-scale renewable energy," *Journal of Power Sources*, vol. 144, no. 1, pp. 268–279, 2005.
- [1.8] IEA (2010), *Energy Technology Perspectives*, IEA/OECD, Paris, France. Available at: http://www.iea.org/publications/free_new_Desc.asp?PUBS_ID=2100. Mark, L., K. Kavi, H. Anders and B. Moss
- [1.9] I. Hadjipaschalis, A. Poullikkas, V. Efthimiou, "Overview of current and future energy storage technologies for electric power applications", *Renewable and Sustainable Energy Reviews*, Volume 13, Issues 6-7, August-September 2009, Pages 1513-1522
- [1.10] M. Guarnieri (2012). "Looking back to electric cars". *Proc. HISTELCON 2012 - 3rd Region-8 IEEE HISTory of Electro - Technology Conference: The Origins of Electrotechnologies*: #6487583.doi:10.1109/HISTELCON.2012.6487583.
- [1.11] "History of Railway Electric Traction". Mikes.railhistory.railfan.net. Retrieved on 2010-12-26. pp.8-9 Batten, Chris Ambulances Osprey Publishing, 04/03/2008
- [1.12] "Escaping Lock-in: the Case of the Electric Vehicle". Cgl.uwaterloo.ca. Retrieved 2010-12-26. *AAA World Magazine*. Jan-Feb 2011, p. 53
- [1.13] S. Bashash and H. K. Fathy, "Transport-based load modelling and sliding mode control of plug-in electric vehicles for robust renewable power tracking," *IEEE Trans. Smart Grid*, vol.3, no. 1, pp. 526-534, Mar. 2012.

- [1.14] D. S. Callaway, "Tapping the energy storage potential in electric loads," *Proc. IEEE*, vol. 99, no.1, pp. 184-199, Jan. 2011.
- [1.15] Loeb, A.P., "Steam versus Electric versus Internal Combustion: Choosing the Vehicle Technology at the Start of the Automotive Age," *Transportation Research Record, Journal of the Tran. Research Board of the National Academies*, No. 1885, at 1. Automobile, retrieved on 18 July 2009.
- [1.16] A. A. Frank, "Plug-in hybrid vehicles for a sustainable future," *Amer. Sci.*, vol. 95, no. 2, pp. 158-165, Mar./Apr. 2007.
- [1.17] Matthe, Roland; Eberle, Ulrich (2014-01-01). "The Voltec System - Energy Storage and Electric Propulsion". Retrieved on 2014-05-04.
- [1.18] M. Bellis, "The Early Years", *The History of Electric Vehicles*, About.com, retrieved on 6 July 2006
- [1.19] Eberle, Ulrich; von Helmholt, Rittmar, "Sustainable transportation based on EV concepts: a brief overview," *Royal Society of Chemistry*. Retrieved on 2010-06-08.
- [1.20] "Renault-Nissan Alliance Sells Its 250,000th Electric Vehicle" (Press release). Paris/Yokohama:Renault-Nissan Alliance. 2015-06-24. Retrieved on 2015-06-26.
- [1.21] J. Cobb, "Tesla Due To Sell 75,000th Model S This Month". *HybridCars.com*. Retrieved on 2015-06-27.
- [1.22] Guinness World Records, "Best-selling electric car". *Guinness World Records*. Retrieved on 2013-01-22.
- [1.23] J. Cobb, "Renault-Nissan And Leaf Lead All In Global EV Proliferation,". *HybridCars.com*. Retrieved on 2015-06-14. About 510,000 battery electric cars and light-duty vans have been sold worldwide by May 2015.
- [1.24] J. Cobb, "European Plug-in Sales Leap Ahead of US For The First Time," *HybridCars.com*. Retrieved on 2015-06-14. Cumulative global sales totaled about 850,000 highway legal plug-in electric passenger cars and light-duty vehicles by May 2015.
- [1.25] J. Cobb, "Top 6 Plug-In Vehicle Adopting Countries – 2014". *HybridCars.com*.

Retrieved 2015-06-26. Cumulative plug-in electric car sales in the U.S. totaled 291,332 units between 2008 and December 2014.

[1.26] J. Cobb, "May 2015 Dashboard". HybridCars.com and Baum & Associates. Retrieved on 2015-06-26. See sections: "May 2015 Plug-in Hybrid Car Sales Numbers and May 2015 Battery Electric Car Sales Numbers." A total of 43,560 plug-in electric cars were sold during the first five months of 2015, consisting of 15,100 plug-in hybrids and 28,460 battery electric cars.

[1.27] J. Cobb, "Californians Bought More Plug-in Cars Than China Last Year". HybridCars.com. Retrieved on 2015-03-18.

[1.28] A. Ohnsman, "Californians Propel Plug-In Car Sales With 40% of Market". Bloomberg News. Retrieved on 2014-09-09.

[1.29] California New Car Dealers Association (CNCDA), "California Auto Outlook Covering Fourth Quarter 2014: New Light Vehicle Registrations Likely to Exceed 1.9 million units in 2015" (PDF). CNCDA. Retrieved on 2015-03-15. Registrations through December 2014 since 2010.

[1.30] California New Car Dealers Association (CNCDA) (May 2015). "New Light Vehicle Registrations in California Should Approach Two million units in 2015" (PDF) 11(2). CNCDA. Retrieved on 2015-06-22. Registrations through March 2015 since 2011. Revised figures for 2014.

[1.31] J. Cobb, "Top 6 Plug-In Vehicle Adopting Countries". HybridCars.com. Retrieved 2014-01-18. Over 172,000 highway-capable passenger vehicles have been sold in the U.S. between 2008 and December 2013.

[1.32] Staff, "Elbilsalget i mars slo alle rekorder" [Electric vehicle sales in March broke all records] (in Norwegian). Grønn bil. Retrieved on 2014-04-03.

[1.33] M. Klippenstein, "One Percent Of Norway's Cars Are Already Plug-In Electrics". Green Car Reports. Retrieved on 2014-04-09.

[1.34] Staff, "Over 20.000 ladbare biler pa norske veier" [Over 20,000 rechargeable electric cars on Norwegian road] (in Norwegian). Grønn bil. Retrieved on 2014-01-13.

- [1.35] M. Ehsani, Y. Gao, S. E. Gay, and A. Emadi, *Modern Electric, Hybrid Electric, and Fuel Cell Vehicles*. Boca Raton, FL: CRC Press, 2005.
- [1.36] J. Larminie and J. Lowry, *Electric Vehicle Technology Explained*. New York: Wiley, 2003.
- [1.37] S. G. Wirasingha and A. Emadi, "Pihef: Plug-in hybrid electric factor," *IEEE Trans. Veh. Technol.*, vol. 60, no. 3, pp. 1279–1284, Mar. 2011.
- [1.38] B. K. Sovacool and R. F. Hirsh, "Beyond batteries: An examination of the benefits and barriers to plug-in hybrid electric vehicles and a vehicle to-grid transition," *Energy Policy*, vol. 37, no. 3, pp. 1095–1103, 2009.
- [1.39] M. Duvall and E. Knipping, "Environmental assessment of plug-in hybrid electric vehicles. Volume 1: Nationwide Greenhouse Gas Emissions," EPRI/NRDC, Palo Alto, CA, Final Rep. 1015325, 2007, pp. 1–56.
- [1.40] Tan Ma, "Economic analysis of real time large scale PEVs network power flow control algorithm with the consideration of V2G services", *IEEE transactions on industry applications*, VOL. 50 No.6 November. 2014
- [1.41] J. Tomic' and W. Kempton, "Using fleets of electric drive vehicles for grid support," *J. Power Sources*, vol. 168, no. 2, pp. 459–468, Jun. 2007.
- [1.42] M. C. Kisacikoglu, B. Ozpineci, and L. M. Tolbert, "Examination of a PHEV bidirectional charger system for V2G reactive power compensation," in *Proc. 2010 25th Annu. IEEE Appl. Power Electron. Conf. Expo. (APEC)*, pp. 458–465.
- [1.43] N. G. Hingorani and L. Gyugyi, *Understanding FACTS: Concepts and Technology of Flexible AC Transmission Systems*. New York: IEEE Press, 2000.
- [1.44] S. Letendre, P. Denholm, and P. Lilienthal, "Electric & Hybrid Cars: New Load or New Resource?" *Public Utilities Fortnightly*, 2006, Dec. [Online]. Available: <http://www.fortnightly.com/pursearch r.cfm>.
- [1.45] C. Hutson, G. K. Venayagamoorthy, and K. A. Corzine, "Intelligent Scheduling of Hybrid and Electric Vehicle Storage Capacity in a Parking Lot for Profit Maximization in Grid Power Transactions," *IEEE Conference Maximization in Grid Power Transactions*,

p.p. 1-8, 2008.

- [1.46] C. Hutson, G. K. Venayagamoorthy, and K. A. Corzine, “Intelligent Scheduling of Hybrid and Electric Vehicle Storage Capacity in a Parking Lot for Profit Maximization in Grid Power Transactions”, *IEEE Conference Maximization in Grid Power Transactions*, p.p. 1-8, 2008.

CHAPTER 2

LITERATURE REVIEW

2.1 Introduction

The society's concerns with oil depletion, global warming, fuel economy and emissions standards have led many automotive manufacturers to produce alternative vehicles such as electrical vehicles (EVs), hybrid EVs (HEVs), and plug-in HEVs (PHEVs), which are more fuel efficient and environmentally friendly without sacrificing the comfort and drive performance of the current internal combustion engine (ICE) powered vehicles. EVs can act as distributed sources which can also support the power grid side when needed to improve the grid power quality. Through the bidirectional chargers used for the smart carpark, the EVs can not only exchange the active power to grid, but also the reactive power. This chapter presents an overview of existing vehicle powertrain architectures: (1) EVs, (2) HEVs, (3) PHEVs, (4) fuel cell vehicles (FCVs), and (5) plug-in FCVs (PFCVs). This chapter also describes a V2G system and power flow between the grid and the EVs, EV-grid models, bidirectional charger and smart charging strategies.

2.2 Vehicles and Energy Sources

An electric vehicle can be defined as a vehicle in which some or all of the driving energy is supplied through electricity from a battery. In a conventional ICE powered vehicle, gasoline or diesel fuel is combusted to create mechanical energy that provides the power to move the vehicle forward. A number of EV technologies are currently in use or under development, as discussed in Jorgenson [2.1]. An HEV has a small electric battery that supplies electricity to the combustion engine. The battery in an HEV can be charged by a generator driven by the engine or through the captured kinetic braking energy from a process called regenerative braking. HEVs are more fuel efficient than ICE vehicles (ICEVs), but ultimately the vehicle is fully

powered by liquid fuels. A PHEV) is similar in concept to an HEV, but with a much larger battery and grid connection. The grid connection allows the battery to be charged by the grid electricity and the larger battery size enables the car to drive a significant distance in all electric-mode. An all-electric range of twenty miles can be denoted through the notation PHEV-20, and a forty mile all-electric range would be PHEV-40. A battery electric vehicle (BEV) is fully powered by grid electricity stored in a large on-board battery. EVs use energy much more efficiently than ICEVs; a traditional ICEV fuel efficiency is 15-18%, while a BEV can be as high as 60-70% efficient [2.1].

The FCV is another type of electric vehicle, in that the fuel cell generates electricity through an electrochemical process in the fuel cell stack. FCVs have an on-board fuel source, such as natural gas or hydrogen, and can either be fully reliant on the fuel cell or designed with a battery in a hybrid arrangement like an HEV or PHEV. Future visions of a hydrogen economy involve the use of FCVs for transportation; if the hydrogen is created through the electrolysis of water using renewable electricity or from biomass sources then the FCVs would be utilizing renewable sources as well. Currently, the vast majority of the world's hydrogen is produced from fossil fuel sources and the creation of a sustainable hydrogen economy still faces a number of hurdles [2.2]. While hydrogen from electrolysis is an important potential use for renewable electricity, the transition to a hydrogen economy is also a broad topic to be considered.

When the plug-in EVs (PEVs) are connected to the grid, the main working part is the energy storage system. Energy storages are defined as devices that store energy, deliver energy outside (discharge), and accept energy from outside (charge). There are several types of energy storage devices/systems that have been proposed for EV and HEV applications, including mainly the chemical batteries, supercapacitors, ultra-high-speed flywheels, and fuel cells. The oldest, classical and most matured battery technology is the Lead-acid battery. New technologies developed recently or still under development include Sodium Sulphurs and Lithium-ion batteries [2.1].

Most advanced battery research and development programs are focusing on the following barriers for the lithium based battery technology in its entrance to the market: calendar life, operating temperature, cost per kW, and sufficient durability for vehicle use. In testing alternative materials for the lithium based battery negative electrode, new materials have been identified showing high power capability, good reactivity, and long life. The long term research and development is focused mainly on stable, low cost lithium based battery materials. Despite their current high cost and fragile nature, the lithium based battery technology is still improving and the selection of such a battery for a PEV based on low mass and high energy density when compared to other technologies is being considered.

Because of the frequent stop-and-go operation of EVs and HEVs, the discharging and charging profile of the energy storage is highly variable. The average power required from the energy storage is much lower than the peak power for acceleration and hill climbing in a relatively short duration. The difficulty in simultaneously obtaining high values of specific power, specific torque, and cycle life has led to some suggestions that the energy storage system of EVs and HEVs should be a hybridization of an energy source and a power source. Power source can be recharged from the energy source during less demanding driving or regenerative braking. The power source that has received wide attention is the supercapacitor. Although the supercapacitor as a part of energy storage sources has been discussed and developed, the main storage source is still battery.

Most of the electric vehicles are of the plug-in type, utilising on-board battery chargers to recharge the batteries from the utility power. The simplest form of a plug-in electric vehicle is shown in Fig. 2.1. This configuration consists of a battery system and a motor controller that provides power to the motor, which in-turn supplies power to the wheels for traction. Many of today's EVs use a permanent magnet electric motor that can also act as a generator to recharge the batteries when the brakes are applied. During regenerative braking, the machine acts as a generator that provides the power back to the batteries and in the process slows down the

vehicle. Friction brakes are used when the vehicle must be stopped quickly or if the batteries are at full charge.

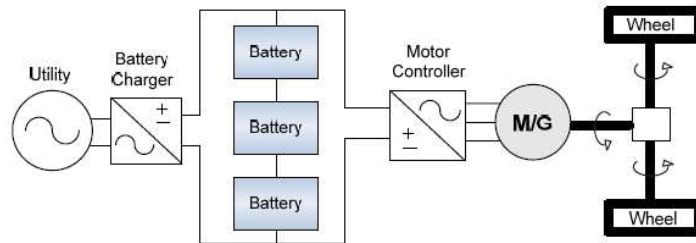
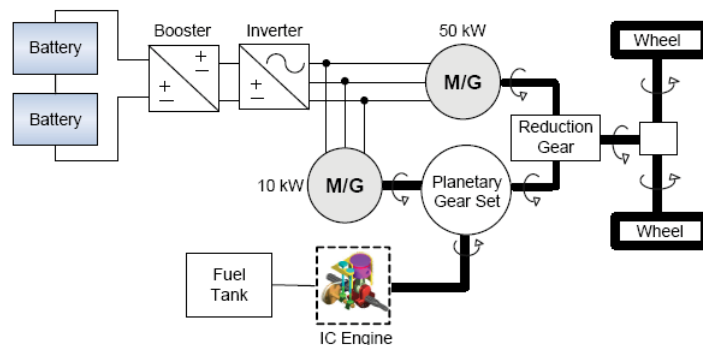


Fig. 2.1 Typical EV configuration [2.3]

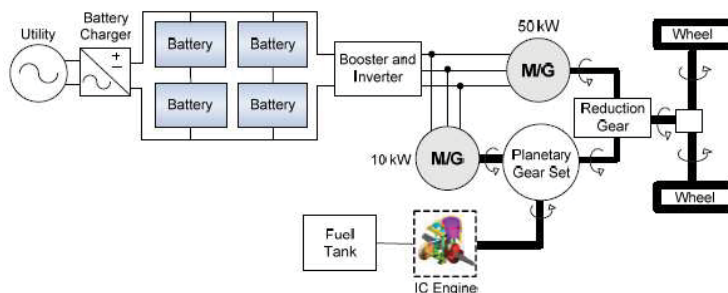
The components that make up a typical HEV include a battery pack, motor controller, motor/generator, internal combustion engine, transmission and driveline components. The primary power electronics include a DC-AC motor controller which provides three-phase power to a permanent magnet motor. The Toyota Prius HEV configuration is given in Fig. 2.2(a). The Prius design uses two permanent magnet motors/generators, one rated as 10kW and the other rated as 50kW. The battery is connected to a booster and inverter before feeding to the motor/generators. The power electronics are bidirectional and used for both charging the battery and powering the motors. The motor/generators and gasoline engine feed into a planetary gear set. The system operates in a continuously variable transmission (CVT) mode where the gear ratio is determined by the power transfer between the battery, motor/generators and gasoline engine [2.3]-[2.4]. The batteries can also be charged using regenerative braking of the large motor/generators. There is no provision to charge the batteries externally.

For plug-in hybrid electric vehicles, batteries are charged when they are not supplying. This is normally accomplished through a utility connected AC-DC converter to obtain DC power from the grid. The batteries can also be charged directly from a solar power source using a DC-DC converter or from a wind power source using an AC-DC converter. The energy flow is unidirectional as power is taken from the utility to charge the battery pack. A Toyota Prius configuration with PHEV conversion is shown in Fig. 2.2(b).

The battery voltage for most converted PHEVs are maintained at the same level as the original design (typically 200-500V DC) and the battery modules are added in parallel to increase the energy capacity of the battery pack, thus allowing the electric motor to run more often than the original HEV design. Some of the PHEV conversion companies include: CalCars, Energy CS, Hymotion, Electrovaya, and Hybrids Plus, and most of them use lithium batteries.



(a)



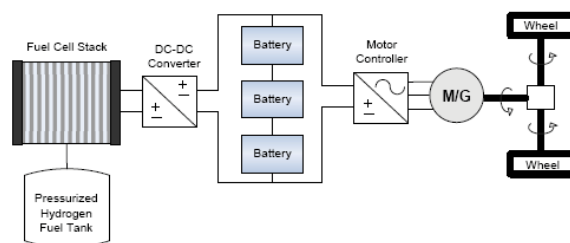
(b)

Fig. 2.2 Toyota Prius configuration (a) HEV, (b) converted PHEV [2.3]

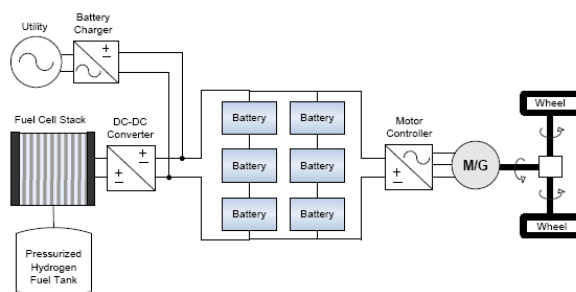
A typical FCV configuration is shown in Fig. 2.3(a). Prototype fuel cell vehicles that are currently under development mostly utilize an on-board tank to store hydrogen pressurized at 5,000 to 10,000 psi. Hydrogen and conditioned air are fed to a Proton Exchange Membrane (PEM) fuel cell stack. As the fuel flow increases, the DC output current increases. The DC output from the stack is fed into a DC-DC converter to a DC power bus. Connected to the DC bus is a battery pack and motor controller. The configuration is very similar to the electric vehicle configuration in which a motor/generator provides the mechanical power for traction.

The on-board batteries allow the energy to be stored during regenerative braking and provide peak power to the motor controller during vehicle acceleration. In field tests, more than 800,000 miles have been placed on a fleet of various fuel cell vehicles. The demonstration showed that the vehicles were performing between 52%-58% efficiency with distances ranged between 100 to 190 miles [2.4].

In the PFCV configuration, the batteries are primarily charged using an on-board utility-connected battery charger. This configuration typically uses a larger battery pack than an FCV to give the vehicle a longer driving range under electric power. The configuration shown in Fig. 2.3(b) uses a PEM fuel cell stack that produces DC power which is then boosted to a higher voltage using a DC-DC converter. Batteries are connected to a DC bus and are used to allow the fuel cell stack to operate at more constant operating conditions. The motor controller draws its power from the DC bus and provides three phase power to the motor/generators. Regenerative braking is also used to store power in the battery pack. An on-board battery charger is connected to the utility to allow the batteries to be recharged when the vehicle is parked.



(a)



(b)

Fig. 2.3 Fuel cell vehicle configuration (a) FCV, (b) PFCV [2.4]

Variable-speed electric motor drives usually have the characteristics shown in Fig. 2.4 [2.5]-[2.7]. At the low-speed region (less than the base speed as marked in Fig. 2.4), the motor has a constant torque. In the high-speed region (higher than the base speed), the motor has a constant power. This characteristic is usually represented by a speed ratio x , defined as the ratio of its maximum speed to its base speed. In low-speed operation, voltage supply to the motor increase with the increase of speed through the electronic converter while the flux is kept constant. At the point of base speed, the voltage of the motor reaches the source voltage. After the base speed, the motor voltage is kept constant and the flux is weakened, dropping hyperbolically with increasing speed. Hence, its torque also drops hyperbolically with increasing speed.

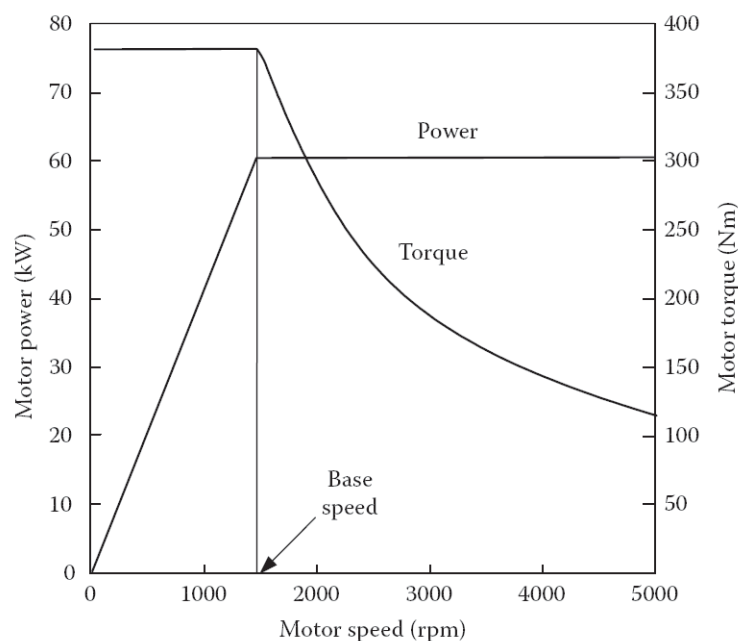


Fig. 2.4 Typical variable-speed electric motor characteristics [2.7]

In transportation, the unit of energy is usually kilowatt-hour (kWh). The energy consumption per unit distance in kWh/km is generally used to evaluate the vehicle energy consumption. However, for traditional vehicles the commonly used unit is a physical unit of fuel volume per unit distance, such as liters per 100 km (L/100 km). On the other hand, for battery-powered EVs, the original energy consumption unit in kWh, measured at the battery terminals, is more suitable. The battery energy capacity is usually measured in kWh and the driving range per battery

charge can be easily calculated.

Energy consumption is an integration of the power output at the battery terminals. For propelling, the battery power output is equal to the resistance power and power losses in the transmission and motor drive, including power losses in the electronics.

When regenerative braking is effective on an EV, a part of the braking energy-wasted in conventional vehicles-can be recovered by operating the motor drive as a generator and restoring it into the batteries.

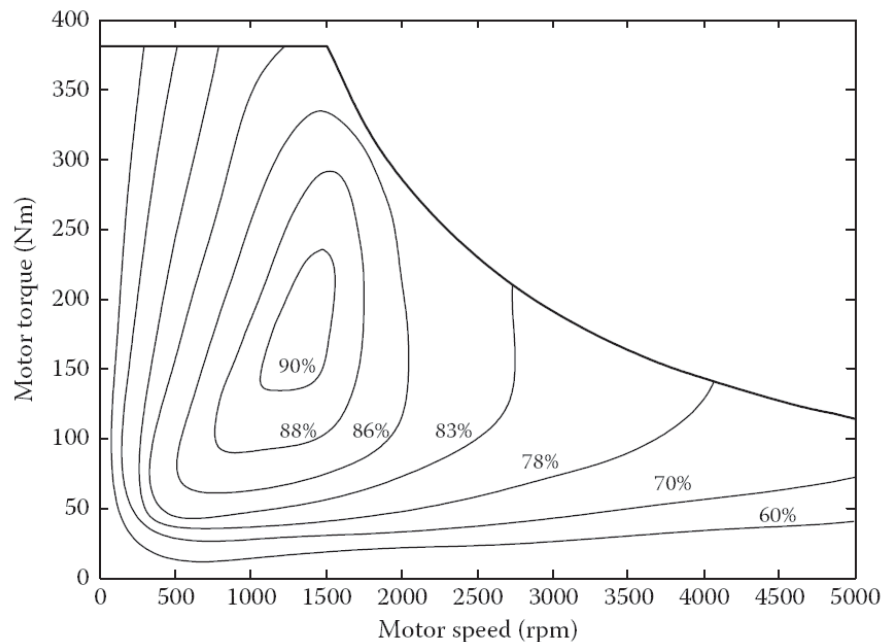


Fig. 2.5 Typical electric motor efficiency characteristics [2.7]

The efficiency of a traction motor varies with its operating points on the speed–torque (speed–power) plane as shown in Fig. 2.5, where the most efficient operating area exists. In power train design, this area should overlap or at least be as close as possible to the area of the greatest operation as mentioned in the previous section.

2.3 Charging and Grid Connection

The battery of an electric vehicle can be recharged from the grid with various measures of external control, labelled here as charge plans. A simple, or unconstrained, charge plan is a

system in which the vehicle immediately begins recharging as soon as it is connected to the grid. A delayed charge plan offsets the battery charging by a set amount of time, for example three hours. Night-time charge plans delay charging to occur over the course of the night when electricity prices are the lowest, with the battery being fully charged for use in the morning. Smart charging implies some measure of intelligent control over the charging of the vehicle by the utility or system operator. This can either be direct charging, through direct control of the vehicle, or indirect charging by designing the vehicle to respond to price signals. Dallinger and Wietschel [2.5] suggested that indirect charging would be a more promising concept as it is more likely to lead to consumer acceptance than direct external control.

The idea behind smart charging is to charge the vehicle when it is the most beneficial, which could be when electricity is at its lowest price, demand is the lowest, when there is excess capacity, or based on some other metrics. The rate of charge can be varied with certain limits set by the driver; the most basic limit being that the vehicle must be fully charged by the morning. Lunzet al. [2.6] suggest that one focus of smart charging should be to manage the battery performance and lifetime, which can improve the lifetime economics of the battery.

A V2G capable EV is able to store electricity and then returns it to the electric grid. V2G power is an interesting concept that was first proposed by Kempton and Letendre [2.7]. The authors suggested that V2G could be used to generate a profit for vehicle owners if the power was used under certain conditions to provide valuable services to the electric grid. These services include regulation (second by second balancing of demand and supply), spinning reserve, and peak power provision. The energy could in theory be supplied from the battery of a BEV or PHEV, from the engine of a PHEV in generator mode, or from the fuel cell of an FCV [2.8]. Pang et al. [2.9] suggest that vehicle-to-building (V2B) technology is closer to being a viable option than V2G; under a V2B scenario the EV would offer demand management and outage management services to the building. A V2G/V2B capable EV could store renewably generated electricity during periods of low demand or excess supply and provide it back to the grid, or building, when required.

2.4 V2G System Requirements and Power Flow

The components and power flow of a V2G system are represented in Fig. 2.6. The system consists of six major subsystems:

- (1) Energy resources and an electric utility;
- (2) An independent system operator and aggregator;
- (3) Charging infrastructure and locations;
- (4) Two-way electrical energy flow and communication between each PEV and independent system operator (ISO) or aggregator;
- (5) On-board and off-board intelligent metering and control; and
- (6) The PEV itself with its battery charger and management.

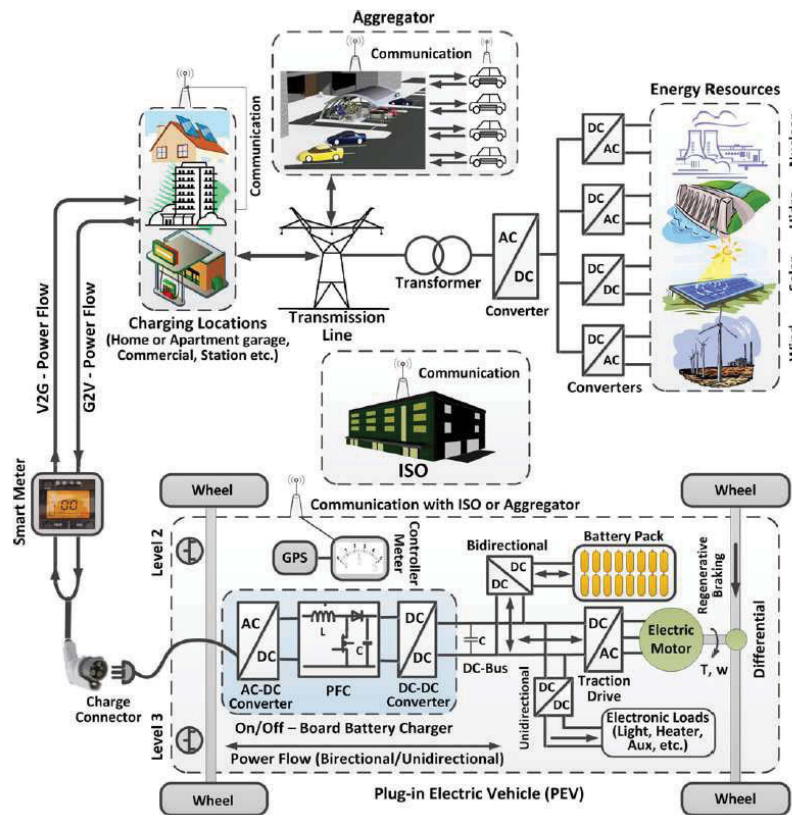


Fig. 2.6 Components and power flow of a V2G system [2.10]

In general, PEVs with V2G interfaces can charge or inject energy into the grid when parked and connected [2.10]. The concept requires three elements: a power connection to the grid, a communication connection with the grid operator, and suitable metering; an efficient power transaction requires substantial information interchange [2.11]. In general, communications must be bidirectional to report battery status and receive commands [2.12]-[2.13]. Intelligent metering and information control that is aware of the battery capacity and state of charge (SOC) are challenging [2.14]-[2.16]. Both on-board and off-board smart meters have been proposed to support V2G methods [2.17]-[2.19]. Smart metering can make PEVs control loads and help combine PEVs and renewable energy [2.20]. GPS locators and on-board meters are useful [2.21]-[2.22]. Sensors and smart meters on charging stations can monitor and exchange information with the control centre through a field area network [2.12].

Control and communication are essential for services such as dynamic adjustments that track intermittent resources and alter charge rates to track power prices, frequency or power regulation, and spinning reserves [2.23]-[2.26]. A variety of communication protocols have been discussed for this purpose, including ZigBee, Bluetooth, Z-Wave, and HomePlug [2.27]-[2.31]. In the U.S., IEEE and SAE provide requirements and specifications on the necessary communications [2.32]-[2.34]. The National Electric Infrastructure Working Council is also working to define a communications standard, enabling PEVs to communicate with chargers [2.35]-[2.36].

PEV chargers without state-of-the-art power electronics can produce deleterious harmonic effects on the distribution system [2.37]. IEEE-519 [2.38], IEEE-1547 [2.39], SAE-2894 [2.40], and International Electrotechnical Commission-IEC-1000-3-6 [2.41] standards limit allowable harmonic and DC current injection into the grid, and PEV chargers are usually designed to comply. Sophisticated active power converter technology has been developed to reduce harmonic currents and provide high power factor [2.42]-[2.45].

Shock hazard risk reduction for PEV charging is addressed in the standard for personnel protection systems for PEV supply circuits [2.46]-[2.47]. Isolation is beneficial for PEV

functions, including the high-voltage battery, DC–DC converter, traction inverter, and charger. Galvanic isolation in electric vehicle supply equipment can be provided either with a line transformer or in the DC–DC converter stage with a high-frequency transformer. High frequency transformer isolation supports voltage adjustment for better control, safety for load equipment, compactness, and suitability for varying applications. Although galvanic isolation is a favourable option in the charger circuits for safety reasons, isolated on-board chargers are usually avoided owing to extra cost. There is a possibility of avoiding these problems by using the traction motor and inverter for the charger circuit, thus providing an integrated drive system and charger. To overcome the isolation problem, various possibilities have been investigated with emphasis on special electric machine configurations that have an extra set of windings.

A V2G vehicle can be designed to provide frequency regulation services by absorbing or providing power back to the utility to match generation with the load. A grid operator could provide commands to the V2G capable vehicle to allow the vehicle to absorb or produce power in order to keep the utilities Area Control Error (ACE) low. ACE is a measure that indicates the deviation of the generation in a power system area from the load. The ACE is generally controlled by controlling individual generators to be within that control area so that it complies with the National Electric Reliability Council (NERC) and the areas electricity governing council prescribed acceptable limits [2.48]-[2.49].

V2G vehicles typically use a high power, high energy battery pack and a bi-directional inverter and controller. An electronic control module controls the power electronics to operate in charge, discharge, or standby modes. Typical V2G vehicles utilize either a Nickel Metal Hydride or Lithium Ion battery pack.

A promising V2G configuration for supplying battery energy to the grid is the integrated motor controller/inverter shown in Fig. 2.7. This configuration shows a utility connection using the same power electronics that are used for the motor controller, thus eliminating the need for a separate battery charger.

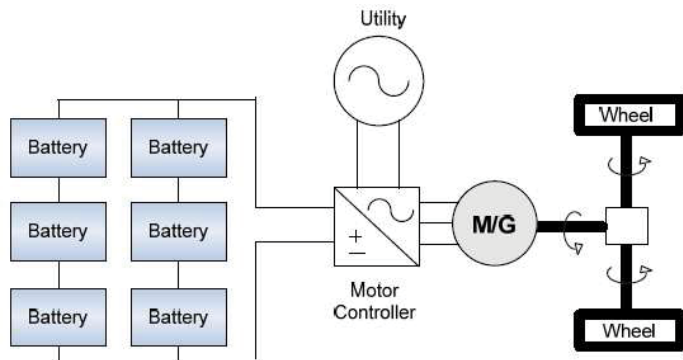
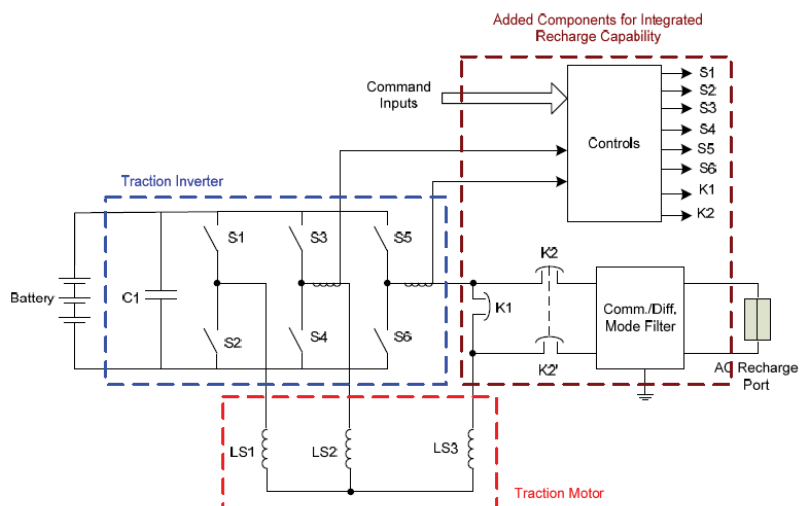


Fig. 2.7 EV power electronics configuration with V2G [2.50]

An example of V2G power electronics topology that is available commercially from AC Propulsion is shown in Fig. 2.8(a). The unique feature of this system is that the same power electronics switching stage can be used for both motor control, battery charging, and for providing power to the utility. A photograph of the system is given in Fig. 2.8(b) [2.50].



(a)



(b)

Fig. 2.8 AC propulsion V2G model AC-150 (a) electrical schematic, (b) picture of the package [2.50]

The AC Propulsion's AC-150 drive system is rated at 150kW (200 HP). The system uses a 20 kW bi-directional grid power interface. The integrated grid interface allows the drive to be used for distributed generation, selling grid ancillary services, and using vehicles to provide uninterruptible backup power to homes or businesses. The system includes a digital interface for instrumentation and recharge control and an integrated DC bus power port for connection of other DC power sources. The system is designed to operate as an induction motor controller with traction control and regeneration. The power electronics allow it to operate as a battery charger or V2G interface to the utility grid [2.50]-[2.51]. The system re-uses the power switches of the propulsion inverter (which drives the traction motor) as the power switches for a grid-tied inverter and uses the motor windings as the inductors needed for the grid-tied inverter. This provides a bi-directional high-power interface to the electric power grid with no extra power components over what are needed for propelling the vehicle. The AC power from the vehicle can be used to power stand-alone loads or it can be fed to the grid. Safety systems, such as anti-islanding protection, prevent the vehicle from feeding power into the grid when grid power is not available [2.51].

The most fundamental topology for utility connection of the Battery Energy Storage System (BESS) is the single-stage, self-commutated voltage-source inverter as shown in Fig. 2.9. While the DC output of the battery system is connected across a filter capacitor, the capacitor itself is used to limit the currents in the battery. The output of the capacitor is connected to a voltage-source inverter (VSI) [2.52]-[2.53]. Depending on the utility connection, the inverter can be single-phase or three-phase. The output of the inverter is then connected to a low-pass filter to prevent high-frequency harmonics injected into the AC system. A synthesized AC-output voltage is produced by appropriately controlling the switches and consists of a controlled series of positive and negative pulses that correspond to the positive and negative half cycles of a sinusoid.

The most common two-stage topology for the BESS consists of a DC-AC grid-connected voltage source pulse width modulation (PWM) inverter with a bidirectional DC-DC converter.

The DC-AC full-bridge inverter controls the grid current by means of PWM, known as a “bang-bang” operation. A simple design for a two-stage power electronics topology, as shown in Fig. 2.10, incorporates a full-bridge DC-DC converter that can operate with any voltage and current polarity. The voltage polarity and amplitude can be set irrespective of the current direction [2.54].

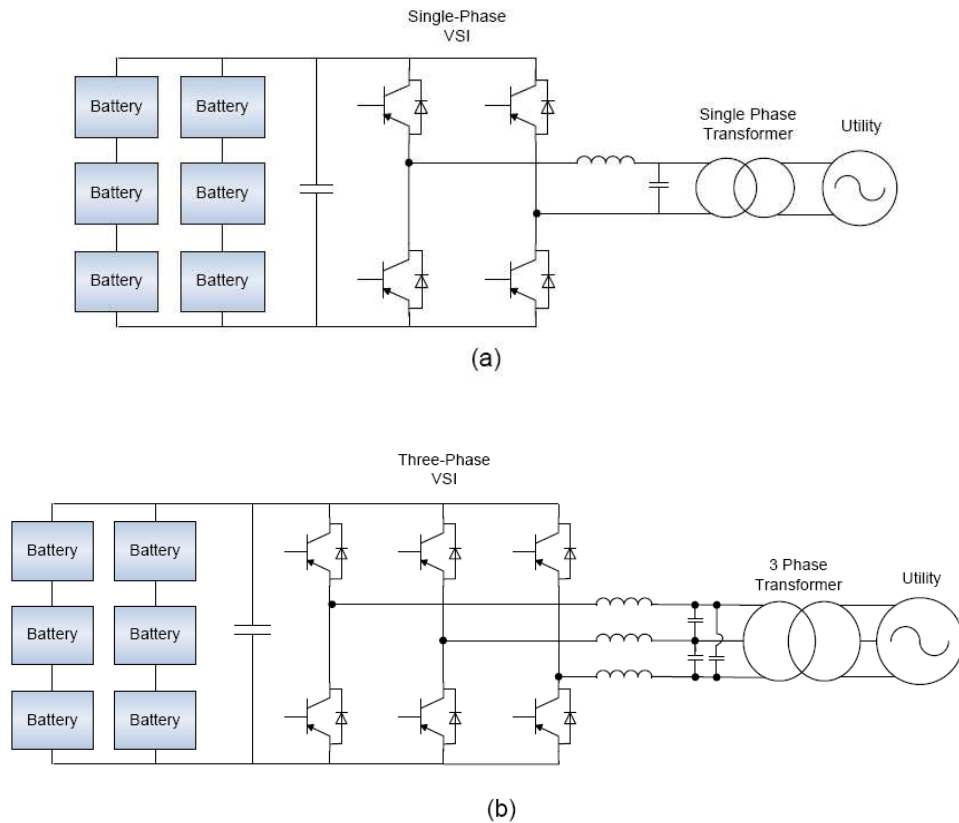


Fig. 2.9 Single-stage power electronics topologies with (a) Single-phase inverter; (b) Three-phase inverter [2.52]

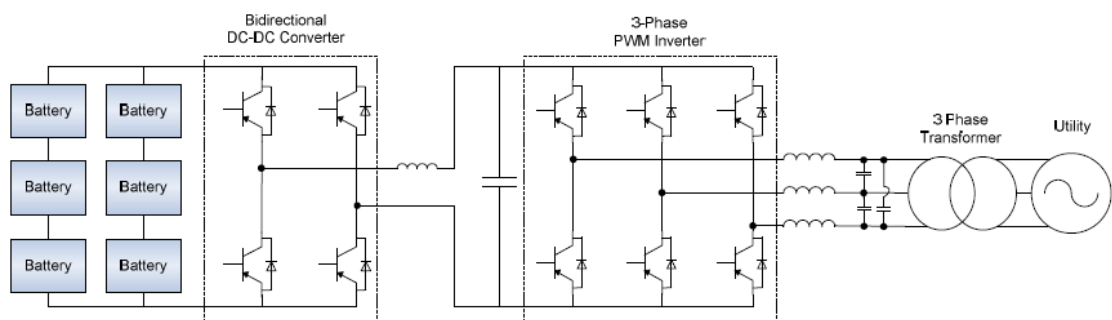


Fig. 2.10 Cascaded power electronic topologies with DC-DC and DC-AC converters [2.54]

All of the power electronics topologies discussed so far have not provided isolation. For utility connection, a line-frequency transformer is used for galvanic isolation. To avoid the bulky, low-frequency transformers (regarded as poor components mainly due to their relatively large size and low efficiency), several bidirectional isolated DC-DC converter topologies have been developed [2.55]-[2.57]. One such topology (see Fig. 2.11) can provide galvanic isolation between the output terminals from the input terminals, and can step up and down its output voltage by using a high-frequency transformer.

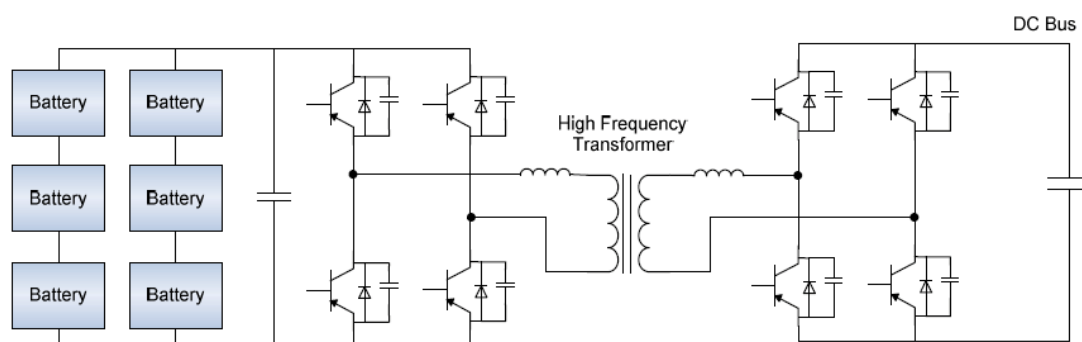


Fig. 2.11 Bidirectional isolated DC-DC power electronics topology [2.55]

From the discussion in the previous survey, it can be observed that the most generalized form of power electronics topologies for the battery energy storage systems is the bidirectional DC-DC converter cascaded with the DC-AC three-phase inverter as shown in Fig. 2.12.

There are different modes of operation for the BESS connected to the utility. The BESS can either send power to the utility by discharging or it can receive power from the utility to charge itself [2.58]. The operation mode control block, as shown in Fig. 2.12, decides the charging/discharging operation for the BESS. The control design for power electronic systems is different for charging and discharging modes. Based on the mode in which the battery is operating, the control signals from charging or discharging blocks are connected to the power electronics system by the selector switches S_{w1} and S_{w2} .

The operation mode control block is designed based on a simple charge-discharge schedule of the BESS. The BESS can send the power to the utility during the peak-load period (i.e., from 6

pm to 10 pm) only if the voltage of BESS is greater than the nominal value ($V_{b,nom}$). During the discharge mode, based on the present voltage (V_b) and SOC of the BESS, the P_{ref} signal determines the amount and rate of discharge to be generated. The BESS can be charged at any other time, provided the SOC of the battery is smaller than the maximum storage capacity (SOC_{max}). The switch control signal is generated based on a lookup table. According to the design, the signal “0” means no charge/discharge, “1” means discharging, and “2” indicates charging. This signal simultaneously controls switches S_{w1} and S_{w2} . Based on the status of this signal, the power electronics converters are either connected to the charging block or the discharging block. Other charge-discharge schedules can also be programmed in the operation mode control depending on the application.

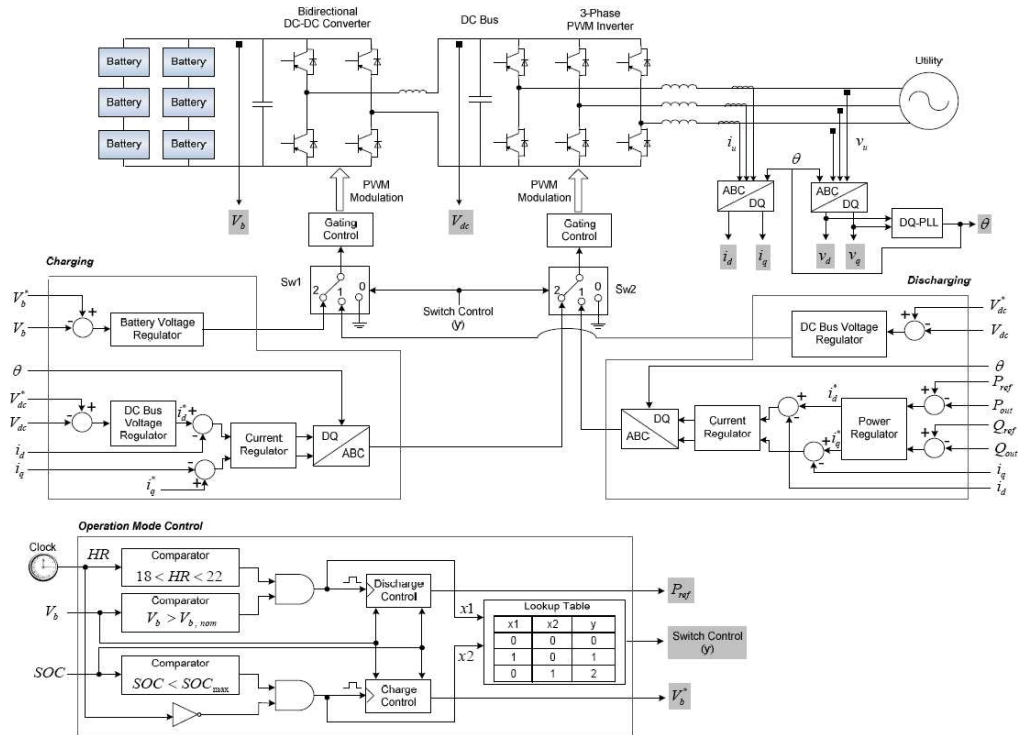


Fig. 2.12 Generalized power electronics and control of a battery energy storage system [2.58]

When the mode of operation for the BESS is charging, the power flows from the utility to the battery system through power electronic converters. The DC-DC converter determines the voltage at the battery terminals (V_b) based on which the battery is charged. The battery voltage

regulator generates the PWM pattern based on the reference battery voltage (V_b^*) (coming from operation mode control) such that V_b follows this reference voltage. For the proper control, the DC-DC converter requires a constant DC input. The DC-AC converter works as the controlled rectifier and the controller maintains the DC bus voltage (V_{dc}) at a preset value. This control design is a variation of the constant power control. Instead of using the active power reference, a DC bus voltage is regulated while the input to the inverter acts as a constant power source to represent the prime mover. In this case, the output of the DC bus regulator is proportional to the active power.

During the discharge mode, the power flows from the BESS to the utility. In this mode, the DC-DC converter maintains the DC bus voltage for the inverter, and the grid connected inverter controls the active and reactive power flow. The control of the utility connected inverter, as shown in Fig. 2.12, provides constant power control [2.59]. Many control functions to deal with practical issues are not shown in the diagram, such as the negative sequence regulation, DQ decoupling. The inner control loop regulates current, and the outer control loop regulates power. In some cases, the reactive power reference, Q_{ref} , could be a power factor reference. By controlling this reference, the injected current to the utility can be maintained at unity power factor. The output of the control system is the high-frequency sinusoidal PWM signals for the voltage-source inverter switches. When the active power reference is increased, the inverter draws more power from the DC bus, thereby decreasing the DC bus voltage. The DC-link voltage regulator, as shown in Fig. 2.12, tries to maintain the constant DC voltage by changing PWM switching pattern for the three-phase controller rectifier switches.

2.5 Smart Charging

Coordinated smart charging and discharging can optimize time and power demand and reduce daily electricity costs, voltage deviations, line current, and transformer load surges [2.60], [2.61]-[2.64]. It can also flatten the voltage profiles of a distribution node [2.65]-[2.66]. Incremental investments and high energy losses can be avoided, and wasting renewable energy

and network congestion prevented. Optimization of charging time and energy flows reduces daily electricity cost with little effect on peak capacity needs. Cao et al. [2.67] proposed an intelligent method to control PEVs' charging loads in response to time-of-use price in a regulated market. A heuristic method was implemented to minimize the charging cost by considering the relation between the acceptable charging power of PEV battery and the SOC. Results showed that the optimized charging pattern is beneficial in reducing cost and flattening the load curve. According to their calculations, optimized patterns can reduce charging cost by about 51% for a single isolated PEV, and almost 40% for multiple coordinated vehicles when penetration is higher.

Smart V2G charging and discharging, in which PEVs are charged from renewable resources and discharged to the grid at peak load, was reported to offer the best potential for maximum utilization of renewable sources to reduce cost and emissions[2.68]-[2.69]. A smart metering and control system must be implemented to combine PEVs and renewable energy. The analysis shows that PEV use could reduce gasoline consumption by about 70% compared to ICE vehicles under both charging scenarios. Schulleret al. [2.70] show that the coordinated charging strategies can increase the relative wind power utilization up to 14.7% for employees and 15.6% for retired EV customers as compared to the average share for 2007 of 8% in the German power system.

An alternative battery charging strategy is to swap depleted batteries with a fresh pack. If this can be automated, exchanges can be compared to duration of conventional vehicle refuelling. This method reduces the impact on distribution systems since more flexible charge timing becomes possible [2.71]-[2.73].

2.6 EV-Grid Models

PEVs can behave either as electric loads or as generators. The charging behaviour of PEVs is affected by different factors, such as the type of connection (unidirectional or bidirectional), geographical location, the number of PEVs being charged in a given vicinity, their charging

voltage and current levels, battery status and capacity, charging duration [2.74]-[2.75]. First generation mass-market PEVs, such as the Chevrolet Volt and Nissan Leaf [2.76]-[2.77], are connected to the grid for battery charging only; the most basic configuration. G2V includes conventional and fast battery charging systems. Fast charging can stress the grid distribution network because of the large power capacity (a typical PEV is more than doubled that of an average household load) [2.78]. Charging practices in different locations also have an effect on the amount of power taken from the electric grid by a fleet of PEVs. Charging at work in congested urban centres, for example, can lead to undesirable peak loads [2.79] and could require investments in expensive peaking generation. Injected harmonics and low power factor can be serious problems if the charger does not employ state-of-the-art conversion [2.80]. Previous studies [2.81]-[2.84] show that night-time charging has minimal impact on the power grid, provided suitable choices are made for intelligent controls.

Several studies about the impact of PEVs on the grid have been reported in the literature. When PEVs have adequate on-board power electronics, intelligent connections to the grid, and interactive charger hardware control, they can serve as stored energy resources and as a reserve against unexpected outages [2.85]-[2.87]. Connection to the grid, control and communication between vehicles and grid operator, and on-board/off-board smart metering are required for beneficial V2G operation [2.88]. While the power flow can be either unidirectional and bidirectional, G2V is a logical first step because it limits hardware requirements, simplifies interconnection issues, and tends to reduce battery degradation. PEVs with unidirectional chargers can be charged but not inject energy into the power grid. A bidirectional V2G system is required to support energy injection back to the grid [2.89]-[2.92].

A few single vehicle proof-of-concept tests have been conducted for V2G vehicles [2.93]-[2.94], but no systems level empirical evaluations have been carried out. The models used in the literature can be broadly divided into two categories: (1) long-term, system scale planning models, and (2) hourly time-series models.

The long-term planning models are run on a regional or national scale over the course of many decades and generally optimize the mix of electric generating units in a system given a set of boundary conditions, which can include the integration of EVs. Time-series models take hourly historical data of electricity supply and demand as well as driving data in order to assess the ability of the system to match supply and demand over the short and medium term. These models are generally run over the course of one week up to one year.

There are other discussions of EVs and the electricity system that do not involve the use of models, including a review of socio-technical barriers to mass adoption [2.95], an outline for a transition path and aggregator framework [2.96] and a discussion of business models and policy options for grid integration [2.97]. These papers provide insight into the practical considerations for integrating the transportation and electricity sectors. However, at this point in time the most effective way to predict the impacts of EVs on the electrical system is through models; therefore some of the key model inputs and constraints in the literature will now be discussed.

One of the more interesting input variables for the models is the selection of PHEVs versus BEVs. Of the 42 studies that included detailed analysis which were reviewed for this study, 18 (43%) analysed PHEVs exclusively, 15 (36%) analysed BEVs, and 9 (21%) of the studies analysed both vehicle types. In the PHEV studies, different all-electric ranges could be modelled [2.98]. In the BEV studies, BEVs were often selected in order to use data and characteristics from actual production vehicles [2.99]-[2.100]. In two of the studies that modelled both BEVs and PHEVs, the models were allowed to endogenously favour vehicle technologies given some optimization constraints; in both cases the models chose PHEVs as preferable to BEVs [2.101]-[2.102]. In a different study, BEVs were assumed to have much lower daily driving ranges than PHEVs [2.103]. From this, it can be seen that PHEVs are slightly more preferred by researchers over BEVs, most likely due to the lower battery costs and an extended driving range.

The penetration, or market share, of EVs in the models was selected in a number of different ways. A few studies chose a set number of EVs and analysed the effects of this level of

penetration in isolation [2.104]. Others evaluated a range of EV penetration scenarios [2.105]. Goransson et al. [2.106] took a novel approach, analysing varying fractions of the total electricity demand that is attributed to EVs. The literature predicting the future market share for EVs offers a wide range of values and scenarios, providing scant insight to modellers on an appropriate penetration level to select [2.107]. Green et al. [2.108] suggested that models should have one scenario run with a 0% market share for EVs, which would be considered as a baseline scenario. This could then be compared with multiple EV penetration levels to produce a sensitivity analysis for the effects of EVs.

The influence of charge plans and different charging scenarios is addressed in a number of ways in the literature. Some studies focus exclusively on simple charging [2.109] or smart charging. Others compare just two charging strategies, such as simple charging versus delayed charging [2.110]. The most prevalent modelling approach is to compare a wide range of charging strategies, with some combination of simple, delayed, night-time, smart, and smart with V2G being considered [2.111].

The availability of accurate and detailed driving patterns is a major issue in the creation of accurate and useful EV/electric grid models [2.108]. In order to know the available EV storage and discharge capacity at any time it is necessary to know the number of available (parked and plugged in) vehicles and the amount of energy stored in each battery. The battery energy level, or SOC, depends on how far the vehicle has been driven since it was fully charged, the vehicle efficiency, and the battery size and characteristics. From a computational perspective it is too difficult to model the driving habits and battery SOC of each individual vehicle, and thus some models choose to aggregate all the vehicle batteries into one large unit and use historical data to predict vehicle availability [2.105]. Kristofferson et al. [2.103] state that this method allows the vehicles to charge faster than would actually be realistic; therefore they construct 30 aggregate driving patterns out of historical data in order to more accurately represent the vehicle fleet. Wang et al. [2.111] aggregate vehicles by size and battery range. Whatever the method, a balance between computational ease and real-world accuracy must be found, and many authors

insist that more work must be done to produce accurate vehicle and energy availability functions.

2.7 Control Algorithm for Bidirectional Power Flow

2.7.1 Voltage oriented control

This classic scheme is illustrated in Fig. 2.13. Since the line current vector, $i = i_d + ji_q$, is aligned with the phase voltage vector, $v = v_d + jv_q$, of the power line supplying the converter, a revolving reference frame aligned with v is used, and the active power of the converter output can be controlled by adjusting the reference value, i_d^* , of the direct component of i , while the reactive power of the converter output can be regulated by adjusting the reference value, i_q^* , of the quadrature component of i [2.112]-[2.113]. Generally, i_q^* is set to zero for unit power factor operation. The current references are compared with the actual values, and the errors are then delivered to the proportional-integral (PI) controllers to produce the voltage references. Finally, the switching signals for individual phases of the rectifier are generated by a classic space vector modulator (SVM).

Voltage oriented control (VOC) has various advantages including fixed switching frequency and insensitivity to the line inductance variation. However, the requirement of coordinate transformation, decoupling between active and reactive components and PI regulators can result in complex algorithms and compromised transient performance.

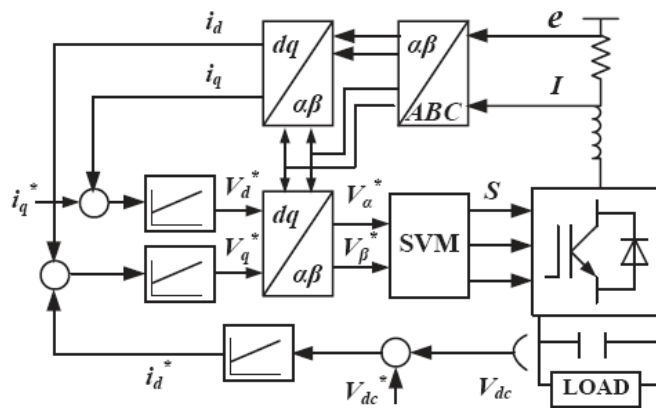


Fig. 2.13 Block diagram of VOC

2.7.2 Direct control

Over the past few years, an interesting emerging control technique has been the direct control strategy. Among the existing direct control methods for power converter control, the direct power control (DPC) is one of the most commonly used approaches. The conventional switching table-based direct power control (SDPC) is derived from the original direct torque control (DTC) for AC machine drives [2.114]-[2.115], and has now become one of the most popular control strategies, because of its excellent transient performance, robustness, and simplicity. Fig. 2.14 shows the control block of DPC. In the SDPC, the converter switching states are determined using a switching table, which is built up from the output signals of hysteresis active and reactive controllers as well as the position of grid voltage vector or virtual-flux vector [2.116]-[2.119]. Since then, several switching tables have been proposed, trying to improve system behaviour [2.120]-[2.122].

Compared to VOC, SDPC does not need any internal current loop and modulator because the converter's switching states are selected via a switching table, and hence the coordinate transformation is also eliminated. However, large power ripples and variable switching frequency are two major significant challenges faced by these SDPC approaches.

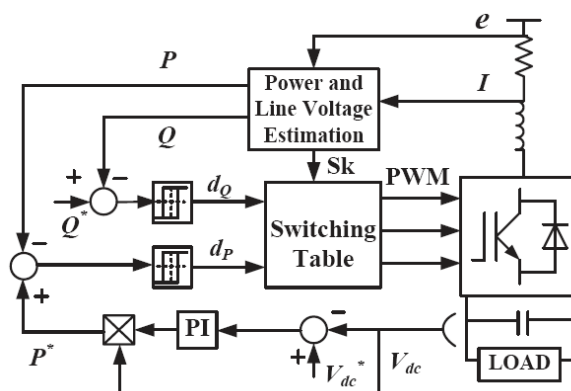


Fig. 2.14 Block diagram of DPC

2.7.3 Space vector modulation direct control

New approaches, for example, the space vector modulation (SVM), have been incorporated into direct control to reduce the power ripples and achieve a constant switching frequency

[2.123]-[2.124]. The error obtained by comparing the commanded and estimated power values is sent to the PI regulators, and the average voltage vector is then delivered to the SVM to produce the switching signals. Whilst these approaches bring some benefits, complicated coordinate transformation and much tuning effort are required to ensure the system stability.

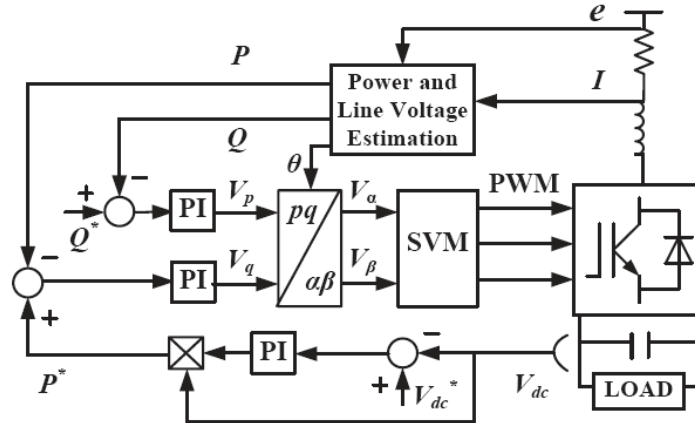


Fig. 2.15 Block diagram of SVM-DPC

By using SVM, the average voltage vector of the converter is produced by integrating linear voltage vectors in a fixed period, and thus constant switching frequency can be achieved. Various researchers have studied integration of SVM into DPC. The key to this approach is to select the referenced voltage vector for the modulator. Instead of using the hysteresis comparators and a switching table, the errors between the referenced and estimated active and reactive power values are fed directly to two PI regulators, as shown in Fig. 2.15. The output signals from the PI regulators are transformed into V_α and V_β in the stationary coordinate system before being sent to the SVM to generate the switching signals. Constant switching frequency and power ripple reduction can be achieved by integrating SVM into DPC. However, such an approach requires two additional PI regulators together with the coordinate transformation, which complicates the system and demands large computing power. The steady-state and transient performance is highly sensitive to the PI control parameters.

2.7.4 Model predictive control

The model predictive control (MPC) uses the system model to predict the behaviour of variables over an N -step time horizon, and a cost function subsequently as the criterion for selecting the

appropriate switching states in the future [2.125]-[2.131]. Generally, the design of MPC controller can be divided into three steps: system predictive model, cost function and parameters selection. Firstly, the system model can be expressed as a discrete-time state-space model, the output of which is determined by the input, the current state of the model, and the discrete interval. In this way, the future behaviour of the system can be predicted until a certain horizon of time. Secondly, the control problem can be defined as the determination of an appropriate control action that will force a generic system variable, $x(t)$, as close as possible to a desired reference value, x^* . A cost function over a finite horizon of length N is then utilized to evaluate each switching state, and the one minimizing the error between $x(t)$ and x^* will be selected for the next sampling period. Finally, as the MPC allows the easy inclusion of system constraints and nonlinearities by revising the cost function, a trade-off between different control objectives should be taken into account in order to obtain a satisfactory performance.

Fig. 2.16 depicts the block diagram of the MPC system, where one step prediction is employed. The essential concept of this predictive DPC is to predict the power of the $(k+1)^{th}$ instant for different voltage vectors. By evaluating the effects of each voltage vector on the active and reactive powers according to a specific cost function, the voltage vector that produces the least power ripple can be determined. In the rectifier control, the control objectives are chosen as the DC-link voltage and the power factor of the AC input, which can be regulated by controlling the active power, P , and reactive power, Q , respectively.

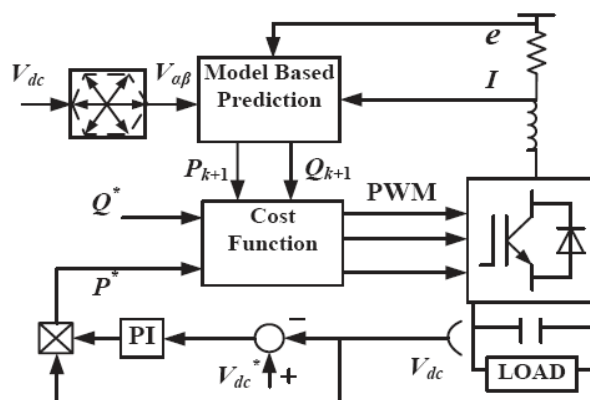


Fig. 2.16 Block diagram of model predictive control

2.8 Grid Support from V2G Services

The increasing number of electric vehicles is demanding a new approach to solving grid issues and has a lot of potential as a source of power system services [2.132]. The most relevant of these is the use of electric vehicles to balance out the power and frequency fluctuations. This approach is known as vehicle to grid (V2G). V2G is the concept of treating electric vehicles as controllable loads which can be used as a source or sink of power as required by the power system. Electric vehicles parked at charging stations such as in a car park, in offices or at home are connected to an aggregator which communicates with the grid and the aggregators. The aggregators can then issue control signals to each vehicle connected to it either as a whole or to each vehicle individually [2.133].

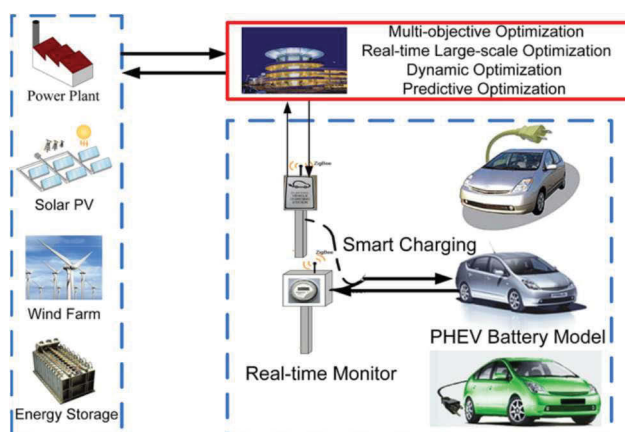


Fig. 2.17 Envisioned large-scale PHEV/PEV charging/V2G infrastructure in a smart grid [2.134]

With large-scale PHEV/PEV aggregated in smart car park, the smart car park can provide power support to the grid. Fig. 2.17 illustrates an envisioned architecture of a large-scale PHEV/PEV enabled municipal parking deck in a smart grid environment. As shown in Fig. 2.17, the system consists of three major subsystems: (1) the traditional power utility and local-scale renewable energy resource (PHEV/PEV on-board energy storage systems are recharged using either renewable energy or traditional energy source); (2) an intelligent grid aggregator/operator (online charging algorithms for large population of PHEV/PEV); and (3) PHEV/PEV with on-board battery management system, battery chargers, and customers. A reliable two-way communication network is needed to enable the successful integration of a large number of

PHEVs/PEVs. Having effective communication technologies is critical to achieve the optimal results.

The first step in implementing V2G technology is the regulation services due to more value in the market and lesser stress on the power system of EV [2.135]-[2.136]. Balanced supply and demand of active power is achieved by frequency regulation [2.137]. Cycling large generators are used for frequency regulation but with a high cost [2.138]. Batteries of EVs provide a fast charging and discharging rate in a V2G system which makes this system an efficient alternative for frequency regulation [2.139]. Balanced supply and demand for reactive power is achieved by voltage regulation. EVs take action in a very short time to regulate signals that could be managed by each EV separately. The battery charger is used to embed the voltage control. Proper selection of current phase angle by the EV charger can help to compensate capacitive and inductive reactive power [2.140]. Charging of EVs can stop when voltage of the supply grid is less, and it can start when voltage is high [2.141]. To maintain stable frequency, union for the coordination of transmission of electricity is defined for three types of control i.e. primary, secondary and tertiary control [2.142]-[2.143]. Down regulation could be achieved by charging the battery of EVs, and if the battery is discharged in the grid then this can achieve up regulation.

2.8.1 Load balancing and peak power (load management)

The V2G system can manage the power load by discharging the battery into the grid at peak time and charge when there is low demand, i.e. overnight and off-peak hours. Intelligent scheduling of charging helps to manage peak load and shifts the load curve [2.144]. The impact of EVs fleet on the grid effectively is reduced by shifting of load and this task can be achieved by charging coordination. The purpose of controlled battery charger is to shift demand for energy and to level the peak load [2.145]. The author in [2.146] suggests that controlling the peak power is the most economical solution for load management.

2.8.2 Support to renewable energy resources

The EVS having a V2G system offers a source of backup for renewable energy resources (RES), e.g. wind and solar, by providing alternating power production [2.147]-[2.149]. If the power produced from RES is very high, in order to restore balance, the centralized power plants should decrease the production or curtail distributed generator units. The solution in terms of matching the generation and consumption, provided by EVs is achieved by charging and discharging of batteries. EVs can store excess energy by RES to meet the needs of driving or providing power to the grid when the demand is higher. The author in Ref. [2.150] showed that DNs with smart grid facility having RES reduce emissions and save \$3.58 per vehicle per day for industries.

2.8.3 Electric grid interaction for grid support

EV charging is one of the fundamental schemes in the electric vehicles' applications. There are several charging levels for EVs that reflect the power capability and charging duration. These levels have been standardized to reveal the EV slow or fast charging scenarios. The slow charging can be experienced at home or office areas whereas the fast charging (typically 15 min to 1 h) can be achieved at dedicated charging stations in commercial or public places. As shown in Table 2.1 [2.151]-[2.153], the AC Level 1 is practically realized at the home environment while the AC Level 2 is suitable for public and commercial areas like workplace, movie theatres, shopping mall and so on. However, the DC fast charging (DC Level 1–3) is envisioned to cover the public, private or commercial charging stations [2.152].

The revised version of the SAE standard J1772 released in October 2012 [2.151] introduced more flexibility to accommodate the EVs particularly for the V2G and charging solutions in the smart grid environment. This includes the DC fast charging levels, electric vehicle supply equipment requirements and reverse energy flow communication portfolios for the PHEVs. In addition, the National Electrical Code (NEC) in article 625 (NEC 625) and IEC 62196 covers other details on the EV charging systems. The advances in bidirectional power converters for electric chargers with low electromagnetic interference (EMI) to support the V2G may well become standard for the EVs. Fig. 2.18 and Fig. 2.19 illustrate the EV charging configurations

for the AC Level 1 & 2 requirements (EV includes an on-board charger) and for the DC Level 1 & 2 (electric vehicle supply equipment includes an off-board charger), respectively. The two figures illustrate the setup of the facilities at the charging point and embedded EV kits for charging scenarios by considering the AC and DC charging levels as depicted in Table 2.1. With the AC Level 1 and 2 configurations in Fig. 2.18, the electric vehicle supply equipment is provided at the charging point by supplying the AC power to an on-board charger. However, with the DC Level 1 and 2 configurations in Fig. 2.19, the charging point supplies the DC current to the EV battery pack.

TABLE 2.1 AC/DC Charging Levels Characteristics as per SAE J1772 Standard [2.153]

Power level type	Voltage level (V)	Current capacity (A)	Power capacity (kW)	Remark (s)
AC level 1	120VAC	12 16	1.4 1.9	1-phase supply (EV contains an on-board charger) Charging time PHEV: 7h BEV: 17h
AC level 2	240VAC	Up to 80	19.2	1 or 3-phase supply (EV contains an on-board charger) 3.3 kW charger PHEV: 3h BEV: 7h 7 kW charger PHEV: 1.5h BEV: 3.5h
AC level 3	-	-	>20	Under development
DC level 1	200-500VDC	<80	Up to 40	3-phase supply (EVSE contains an off-board charger) 20 kW charger PHEV: 22 min BEV: 1.2h
DC level 2	200-500VDC	<200	Up to 100	3-phase supply (EVSE contains an off-board charger) 45 kW charger PHEV: 10 min BEV: 20 min
DC level 3	200-600VDC	<400	Up to 240	Under development

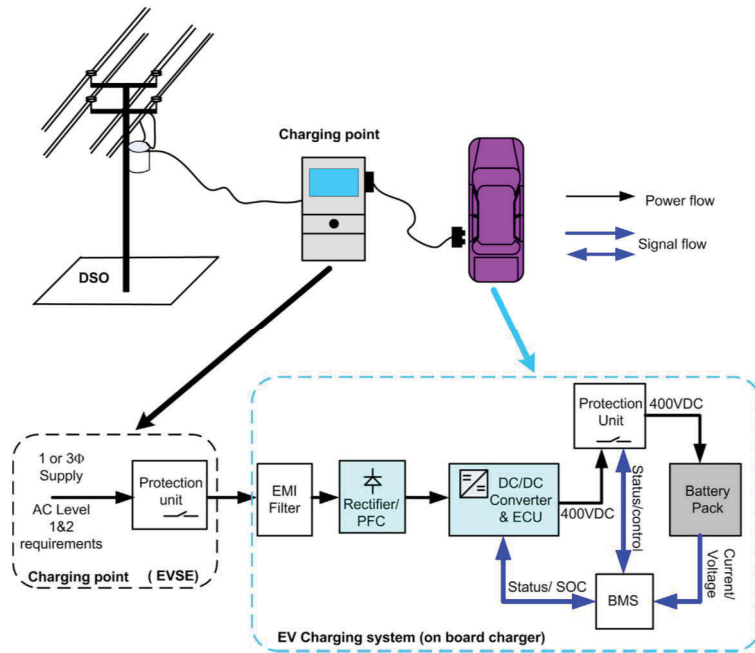


Fig. 2.18 EV charging configuration at AC level 1 and 2 setup (i.e. on-board charger).

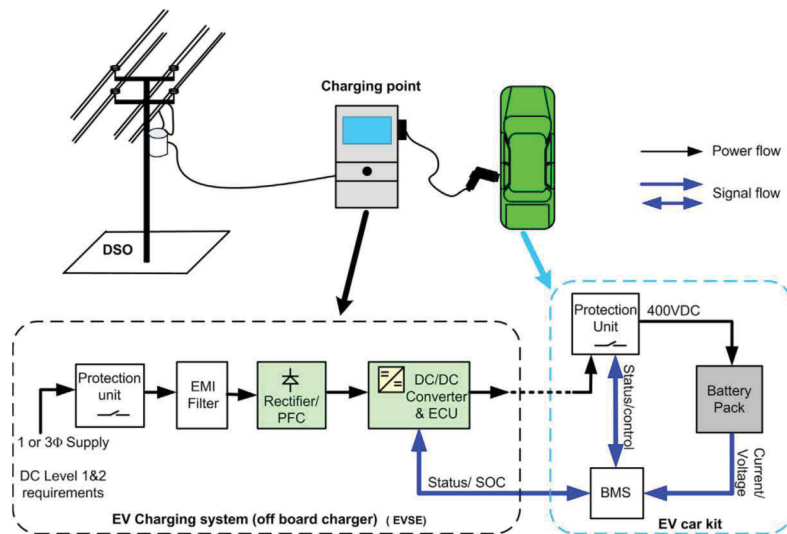


Fig. 2.19 EV charging configuration at DC level 1 and 2 framework (i.e. off-board charger) [2.153]

2.9 Economic Issues Related to V2G Services

In 2000, Kempton and Kubo presented an analysis of using V2G to provide peaking power in Japan [2.154]. In this work, they included the effect of the driving pattern in Japan and concluded that without a reduction in the cost of EV batteries or a change in the current rate

structure, it is uneconomical for EV owners to sell energy from their batteries for peaking use. Later, in 2002, Letendre and Kempton extended on their previous work to include an economic assessment of other V2G applications, namely providing power for baseload, spinning reserve, and frequency regulation [2.155]. Fig. 2.20 provides an illustration of the power flow and the SOC for an EV battery that is used for frequency regulation ancillary service. The EV is assumed to be plugged in at both home and work except when it is used for commuting at 8 am and 6 pm; this can be seen from the large positive power output at these times while the negative spikes are due to regenerative braking during the commute. The net transfer of energy in the battery is small because this V2G application is assumed to be providing both up and down regulation, except after each commute, i.e. the regulation is controlled to provide a net charge. They concluded that due to the high per kilowatt-hour (kWh) cost, V2G cannot be used for baseload application. However, there is economic value for V2G to provide ancillary services in California such as spinning reserve and regulation according to their study. The benefit is enough to offset the high initial cost of EVs. However, this requires design modifications to the current EVs as well as a review of current policies.

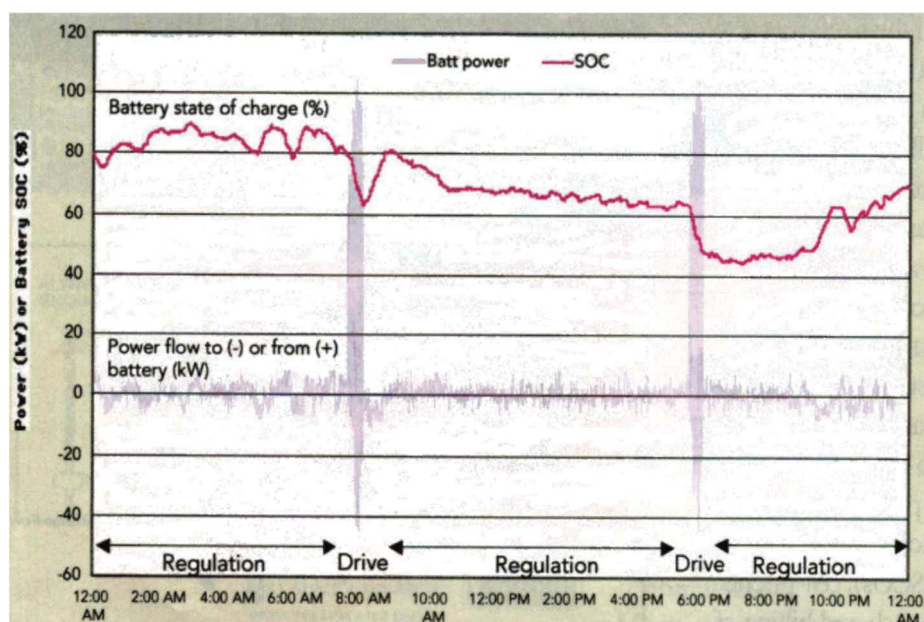


Fig. 2.20 The power output and battery state of charge for an electric vehicle providing frequency regulation ancillary service [2.155].

In 2005, Kempton and Tomić presented similar research on three different types of electric vehicles, battery EV, fuel cell EV, and hybrid EV for V2G applications [2.156]. Their conclusion was that V2G is economically beneficial when there is a capacity payment, i.e. a payment for having the EV batteries online and available for dispatch, with an additional energy payment for when power is actually dispatched. This is often the case for participating in the ancillary service market in the US. In such an environment, V2G can make a profit from the capacity payment even if it is losing money for energy dispatched at low prices.

More recently in 2014, Parsons et al. presented their research on consumer willingness to pay for vehicle-to-grid electric vehicles and their contract terms [2.157]. They conducted a national survey in the US with more than three thousand respondents and found that drivers do not like fixed requirements such as minimum monthly plug-in time even if the target can be easily achieved. The results indicate that drivers prefer a more flexible arrangement such as a variable payment scheme where the payment depends on the amount of time the EVs stay connected to the grid.

In 2009, Peterson et al. presented a paper on the economics of using plug-in hybrid EV batteries for electricity arbitrage in the cities of Boston, Rochester, and Philadelphia [2.158]. These three cities were chosen because their annual mean temperatures were not likely to have an impact on the modelled battery state of charge. They assumed that the batteries were charged when power cost was low and discharged back into the grid when the power cost was high. They also assumed that the batteries were fully charged every morning ready for the daily commute. The results show that with the cost of battery degradation due to the extra charging cycles, the annual profit is between 6 to 72 US dollars which in their opinion was not sufficient incentive for EV owners to want to participate in such a programme. However, in the same year, Peterson et al. also published their findings on the degradation of lithium-ion batteries due to realistic driving patterns and V2G utilisation. They quantified the loss of battery capacity as a function of driving usage as well as a function of the energy processed due to V2G application. From

their results, they claim that a PHEV battery pack can be cycled through a very broad state of charge range without significantly decreasing its capacity.

For public buses, there are some researches who have focused on public fleet vehicles and V2G capabilities. Of all public fleet vehicles, school buses are of particular interest because they cause disproportionate health effects, especially on school children's health. School buses, for example, have a significant impact on local aerosol levels that could directly influence the health of children [2.159]. Such concern has been the impetus for several policies requiring the reduction of school bus exhaust pollution. For this reason, the cost-effectiveness of an electric school bus is analysed because it avoids such health impacts.

While other studies have investigated the costs and benefits of electrifying privately owned vehicles [2.160], this analysis is novel for its focus on public fleet vehicles and V2G capabilities. For example, Al-Alawi and Bradley compared the costs and benefits of privately-owned conventional vehicles and plug-in hybrids, and found a payback period of 7 to 10 years [2.161], but did not include the possibility of V2G revenues, which the analysis found to be essential for cost-effectiveness. Feng and Figliozzi found that the electric commercial fleet vehicles were not competitive with conventional diesel commercial vehicles unless either battery costs decreased by 10 to 30% or both the diesel fuel economy was particularly low and vehicles were highly utilized [2.162]. However, this differs from this analysis in that it does not include V2G revenues and focuses on commercial rather than public fleet vehicles. Furthermore, articles that focus on buses tend not to focus on the costs and benefits, but rather the performance and fuel efficiency of differing types of buses. Hu et al. found that plug-in hybrid buses were more efficient than diesel buses from tank to wheel, and that increases in battery capacity further increased tank to wheel efficiency [2.163]. While the article determines the efficiencies of the buses, it does not account for any costs, and also does not include V2G capacity. In addition, Dawood and Emadi compared the different fuel efficiencies of differing types of buses, and found that parallel electric hybrid buses had the highest fuel economy and fastest acceleration [2.164]. Likewise, the article does not explore purely electric buses, V2G capacity, or account

for any costs. Peterson et al. investigate the economics of using plug-in hybrid electric vehicles for V2G services, and found benefits of \$10 to \$120 per year [2.165] per vehicle. However Peterson et al does not include frequency regulation participation, driving behavior, or purely electric vehicles with higher capacity as this analysis does.

For V2G charging optimization for economic benefits, the complexity of the mathematical model is further increased as the economic factors are integrated by adding the electricity market data.

At the early stage, the general revenue of V2G operation by providing ancillary services is discussed and the conclusion is drawn that EVs could generate substantial profits even though the cost for grid reinforcement and V2G infrastructure are taken into account [2.166]-[2.167]. Among various ancillary services, such as spinning reserve, load shifting, black start, the regulating power market is lucrative for V2G service. The total market value can reach 770 million euros and 11000 MW in the context of German regulating power market [2.168]. However, the mathematical formulation for the V2G power control is not presented in detail.

For multiple control objectives in V2G mathematical formulation, the control scheme of V2G is usually formulated as an optimal problem in which V2G power at different time steps is the decision variable and the electricity market data is included in equations as constants or coefficients. Research on the cost and emission optimization with V2G discusses the benefits of utilizing V2G power to reduce the dependencies on small expensive units and therefore reduce the cost. The control objective contains both cost and emission minimization with the V2G power regulation. Particle swarm optimization (PSO) is used to solve the constrained optimization problem [2.169]. The solutions of this modified intelligent unit commitment problem show that V2G integration reduces effectively operational cost and emissions, and increases profit, reserve and reliability. Other research focuses on the profit offered for EV owners participating in the V2G operation. The revenue to provide grid services as spinning reserves and peak power supply is examined by using the profit earned from existing grid supports [2.167-2.169]. Furthermore, the V2G power can be utilized for multiple uses

simultaneously. The load regulation and frequency regulation are combined in a “dual-use” program to obtain a much higher profit than either of the single-use programs [2.170]. Table 2.2 summarizes the objective function, constraints and solutions for the V2G optimization consisting of EV and power grid models.

While most of the studies focus on the control of EV aggregation as a generating unit, there are still challenges for the design of aggregator. In most of the V2G applications, the EVs are not engaged in the optimal control individually. Instead, the EVs in a certain region are clustered under an aggregator which will collect the available V2G capacity from each vehicle and bid in the power market. The V2G operation is mostly considered from the power system point of view and mathematically formulated by extending an existing power system optimization problem to have V2G power included. Other than studying the V2G applications in the transmission or distribution grid level, the control of the clustered vehicles under supervision of the aggregator is investigated in [2.171]-[2.172]. The detailed model of EV model is formed as the different features of vehicle batteries are included as the parameters of the optimal charging method and the criteria for regulating the power of vehicle battery in a proper sequence is derived.

TABLE 2.2 Mathematical Model Formulation of V2G Optimization [2.173]

EV	Power grid	V2G characteristics
Objectives		
Minimize the cost of electricity and gasoline for driving hybrid EV	Maximize the renewable energy efficiency through EV power coordination	Revised within the current power system optimization and EV energy management structure
Maximize the profit from V2G participation	Minimize the unit commitment cost	Three types of objectives in integrated V2G optimization model: 1. EV-centric objective with the power grid state as input data 2. Grid-centric objective with fixed EV
Maximize the tailpipe emission	Minimize the power losses of the distribution grid involving the economic dispatch in electricity market	
Minimize battery degradation by EV energy management system	Minimize the operating cost of the power system	
	Improve power system	

	reliability, i.g. minimize the loss of load expectation (LOL)	parameters 3. Multi-objective optimization with both components and decision variables from the two sides
Constrains		
EV availability considering parking location and parking period Charing/discharging power limits of EV converter	Voltage regulatory range throughout the power grid Primary and secondary transformer loading limits Transmission line loading	EV model characterized by three components: EV mobility behaviors, battery charging method, and the EV converter
Battery energy storage for mobility needs Battery power and energy capacity Battery charging and discharging patterns	Frequency deviation limits Power balance Output limits of generation units including renewable energies	V2G power aligned with intermittent renewable generation model V2G power flow restricted by the local power network structure such as building, DC microgrid in islanded mode
Solutions		
EV charging power on the timescale of seconds to hours EV charging time sequences EV parking places for the optimum size of charging station Optimum size of EV fleet in cooperation with renewable energy EV reactive power injection via power-electronic charging facility	Selected settings of regulatory electric equipment such as voltage regulator and multi-tap transformer Allowed penetration degree of renewable energies associated with the size of EV aggregation Combination of grid ancillary services provided by EVs Partition and grid restoration scheme with V2G engaged	Coordinated control of EV charging (smart charging) as fundamental V2G stage Various timescales of V2G optimal power fit for the corresponding ancillary services Battery charging/discharging is control along with electric motor driving to minimize the total energy cost

2.10 Summary of the Chapter

Based on the literature review conducted on the EVs and power system and works of other researchers and successful automakers, several aspects of V2G system have been reviewed and different methods have been compared. For the hybrid energy storage system, the

supercapacitor and battery are considered as the most promising components for the energy storage system. The V2G system requirements and power flow of V2G services are also illustrated and discussed. For bidirectional power flow control of V2G system, the working principle of different control algorithm are compared and discussed. Grid support from V2G services includes active power and reactive power support; the grid can maintain stability when power compensation is supplied by vehicles. The V2G system can manage the power load by discharging the battery into the grid at peak time and charge when there is low demand, i.e. overnight and off-peak hours. For economy issues of V2G service, the revenue to provide grid services as spinning reserves and peak power supply is examined by using the profit earned from existing grid supports. The car's battery ultimately acts as an energy storage system for the electrical company so that they can buy back energy from EV owner whenever they want to. Ideally, the electric utility company will implement the idea of valley shaving, charging at night when demand is low, and peak shaving, sending power back to the grid when demand is high. The profit making is the most attractive and important aspect of the V2G service.

The effects of V2G on power quality improvement should be included in the summary as well as this is also one of the major reasons for developing the V2G technology.

References

- [2.1] I. Hadjipaschalis, A. Poullikkas, V. Efthimiou, "Overview of current and future energy storage technologies for electric power applications", *Renewable and Sustainable Energy Reviews*, Volume 13, Issues 6-7, August-September 2009, Pages 1513-1522
- [2.2] Harvey LDD. Energy and the new reality 2: carbon-free energy supply. London: Earthscan; 2010.
- [2.3] T. Jahns and V. Blasko, "Recent advances in power electronics technology for industrial and traction machine drives," *Proc. of the IEEE*, vol. 89, no. 6, pp. 963 – 975, June 2001.
- [2.4] K. Wipke, S. Sprik, J. Kurtz, and H. Thomas, "Learning demonstration progress report – September 2007," National Renewable Energy Laboratory Report, NREL TP-560-42264,

- pp. 41, September 2007.
- [2.5] D. Dallinger, M. Wietschel, “Grid integration of intermittent renewable energy sources using price-responsive plug-in electric vehicles,” *Renewable Sustainable Energy Reviews* 2012; 16:3370–82.
- [2.6] B. Lunz, Z. Yan, J. Gerschler, D. Sauer, “Influence of plug-in hybrid electric vehicle charging strategies on charging and battery degradation costs,” *Energy Policy* 2012;46:511–9.
- [2.7] W. Kempton, S. Letendre, “Electric vehicles as a new power source for electric utilities,” *Transportation Research Part D* 1997, vol. 2, pp. 157–175.
- [2.8] W. Kempton, J. Tomic, “Vehicle-to-grid power fundamentals: calculating capacity and net revenue,” *Journal of Power Sources* 2005; 144:268–79.
- [2.9] C. Pang, P. Dutta, M. Kezunovic, “BEVs/PHEVs as dispersed energy storage for V2B uses in the smart grid,” *IEEE Transactions on Smart Grid* 2012; 3(1): 473–82.
- [2.10] C. Pang, P. Dutta, S. Kim, M. Kezunovic, and I. Damnjanovic, “PHEVs as dynamically configurable dispersed energy storage for V2B uses in the smart grid,” in *Proc. 7th Mediterranean Power Gener., Transm., Distrib. Energy Convers. Conf. Exhib.*, 2010, pp. 1–6.
- [2.11] W. Su, H. Eichi, W. Zeng, and M. Y. Chow, “A Survey on the electrification of transportation in a smart grid environment,” *IEEE Trans. Ind. Inform.*, vol. 8, no. 1, pp. 1–10, Feb. 2012.
- [2.12] J. DiPeso, “Cars to grid: An electrifying idea,” *Environ. Qual. Manage.*, vol. 18, no. 2, pp. 89–94, 2008.
- [2.13] D. P. Tuttle and R. Baldick, “The evolution of plug-in electric vehicle grid interactions,” *IEEE Trans. Smart Grid*, vol. 3, no. 1, pp. 500–505, Mar. 2012.
- [2.14] A. Y. Saber and G. K. Venayagamoorthy, “Plug-in vehicles and renewable energy sources for cost and emission reductions,” *IEEE Trans. Ind. Elect.*, vol. 58, no. 4, pp. 1229–1238, Apr. 2011.
- [2.15] “Plug-in electric vehicles: A practical plan for progress: The report of an expert panel,”

- School of Public and Environ. Affairs at Indiana Univ., Bloomington, Feb. 2011.
- [2.16] Electrification of the transportation system, MIT Energy Initiative Symp., Cambridge, Apr. 8, 2010.
- [2.17] W. Shireen and S. Patel, "Plug-in hybrid electric vehicles in the smart grid environment," in *Proc. Rec. IEEE Power Energy Syst. Transm. Distrib. Conf. Expo.*, 2010, pp. 1–4.
- [2.18] S. D. Breucker, P. Jacqmaer, D. Brabandere, J. Driesen, and R. Belmans, "Grid power quality improvements using grid-coupled hybrid electric vehicles," in *Proc. Power Electron., Mach. Drives Conf.*, 2006, pp. 505–509.
- [2.19] J. Tomi'c and W. Kempton, "Using fleets of electric-drive vehicles for grid support," *J. Power Sources*, vol. 168, no. 2, pp. 459–468, Jun. 2007.
- [2.20] D. Rua, D. Issicaba, F. J. Soares, P. M. R. Almeida, R. J. Rei, and J. A. P. Lopes, "Advanced metering infrastructure functionalities for electric mobility," in *Proc. Rec. IEEE Power Energy Syst. Innovative Smart Grid Tech. Conf., Innovative Smart Grid Tech. Conf. Eur.*, Oct. 2010, pp. 1–6.
- [2.21] A. K. Srivastava, B. Annabathina, and S. Kamalasan, "The challenges and policy options for integrating plug-in hybrid electric vehicle into the electric grid," *The Electr. J.*, vol. 23, no. 3, pp. 83–91, 2010.
- [2.22] W. Kempton and J. Tomi'c, "Vehicle-to-grid power implementation: From stabilizing the grid to supporting large-scale renewable energy," *J. Power Sources*, vol. 144, no. 1, pp. 268–279, 2005.
- [2.23] C. Quinn, D. Zimmerle, and T. H. Bradley, "The effect of communication architecture on the availability, reliability, and economics of plug in hybrid electric vehicle-to-grid ancillary services," *J. Power Sources*, vol. 195, no. 5, pp. 1500–1509, 2010.
- [2.24] W. Kempton and S. Letendre, "Electric vehicles as a new power source for electric utilities," *Transport. Res.-D*, vol. 2, no. 3, pp. 157–175, 1997.
- [2.25] K. Clement-Nyns, E. Haesen, and J. Driesen, "The impact of vehicle to-grid on the distribution grid," *Electr. Power Syst. Res.*, vol. 81, no. 1, pp. 185–192, 2011.
- [2.26] T. Markel, M. Kuss, and P. Denholm, "Communication and control of electric drive

- vehicles supporting renewables,” in *Proc. IEEE Veh. Power Propulsion Conf.*, 2009, pp. 27–34.
- [2.27] W. Su, W. Zeng, and M. Y. Chow, “A digital test bed for a PHEV/PEV enabled parking lot in a smart grid environment,” in *Proc. Rec. IEEE Power Energy Syst. Innovative Smart Grid Tech. Conf.*, Jan. 2012.
- [2.28] H. Chaudhry and T. Bohn, “Security concerns of a plug-in vehicle,” in *Proc. Rec. IEEE Power Energy Syst. Innovative Smart Grid Tech. Conf.*, Jan. 2012.
- [2.29] ZigBee Smart Energy Overview. (2011). [Online].
Available:<http://www.zigbee.org/Standards/ZigBeeSmartEnergy/Overview.aspx>
- [2.30] P. Kulshrestha, K. Swaminathan, M.-Y. Chow, and S. M. Lukic, “Evaluation of ZigBee communication platform for controlling the charging of PHEVs at a municipal parking deck,” in *Proc. IEEE Veh. Power Propulsion Conf.*, 2009, pp. 1211–1214.
- [2.31] M. K. Lee, R. E. Newman, H. A. Latchman, S. Katar, and L. Yonge, “HomePlug 1.0 power line communication LANs—Protocol description and performance results,” *Int. J. Commun. Syst.*, vol. 16, pp. 447–473, 2003.
- [2.32] Communication Between Plug-In Vehicles and the Utility Grid, SAE Int. Standard J2847/1, May 2011.
- [2.33] Communication between Plug-In Vehicles and Off-Board DC Chargers, SAE Int. Standard J2847/2, 2011.
- [2.34] “Communication between Plug-In Vehicles and the Utility Grid for Reverse Power Flow, SAE Int. Standard J2847/3, 2011.
- [2.35] V. Gungor, D. Sahin, T. Kocak, S. Ergut, C. Buccella, C. Cecati, and G. Hancke, “Smart grid technologies: Communications technologies and standards,” *IEEE Trans. Ind. Informat.*, vol. 7, no. 4, pp. 529–539, Sep. 2011.
- [2.36] J. C. Ferreira, V. Monteiro, and J. L. Afonso, “Smart electric vehicle charging system,” in *Proc. IEEE Intell. Veh. Symp. (IV)*, 2009, pp. 758–763.
- [2.37] S. Bai and S. Lukic, “Design considerations for DC charging station for plug-in vehicles,” in *Proc. IEEE Veh. Power Propulsion Conf.*, 2011, pp. 1–6.

- [2.38] W. Xu, “Comparisons and comments on harmonic standards IEC1000-3-6 and IEEE Std. 519,” in *Proc. Harmonics, Quality Power Conf.*, 2000, vol. 1, pp. 260–263.
- [2.39] M. Geske, T. Winkler, P. Komarnicki, and G. Heideck, “Controlled battery charger for electric vehicles,” *PIERS Online*, vol. 6, no. 6, pp. 532–536, 2010.
- [2.40] Power Quality Requirements for Plug-in Vehicle Chargers—Part 1: Requirements,” SAE Int. Standard J2894, 2011.
- [2.41] Electromagnetic Compatibility—Part 3: Limits—Section 2: Limits for Harmonic Current Emissions, IEC Standard IEC1000-3-2, 1995.
- [2.42] C. C. Chan and K. T. Chau, “An overview of power electronics in electric vehicles,” *IEEE Trans. Ind. Electron.*, vol. 44, no. 1, pp. 3–13, Feb. 1997.
- [2.43] C. Aguilar, F. Canales, J. Arau, J. Sebastian, and J. Uceda, “An integrated battery charger/discharger with power-factor correction,” *IEEE Trans. Ind. Electron.*, vol. 44, no. 5, pp. 597–603, Oct. 1997.
- [2.44] Y. Lee, A. Khaligh, and A. Emadi, “Advanced integrated bi-directional AC/DC and DC/DC converter for plug-in hybrid electric vehicles,” *IEEE Trans. Veh. Technol.*, vol. 58, no. 3, pp. 3970–3980, Oct. 2009.
- [2.45] J. C. Gómez and M. M. Morcos, “Impact of EV battery chargers on the power quality of distribution systems,” *IEEE Trans. Power Del.*, vol. 18, no. 3, pp. 975–981, Jul. 2003.
- [2.46] D. Aggeler, F. Canales, H. Zelaya-De La Parra, A. Coccia, N. Butcher, and O. Apeldoorn, “Ultra-fast DC-charge infrastructures for EV-mobility and future smart grids,” in *Proc. IEEE Innovative Smart Grid Technol. Conf. Eur.*, 2010, pp. 1–8
- [2.47] D. Flynn, “Power System Reserve from Electric Vehicles,” *Proceeding of ITRN 2011*, August 2011, University College Cork.
- [2.48] E. Hirst and B. Kirby, “What is system control,” *Proc. of American Power Conference*, Chicago, IL, April 1999.
- [2.49] B. Kirby, “Frequency regulation basics and trends,” Oak Ridge National Laboratory Report, ORNL TM-2004-29, pp. 32, December 2004.
- [2.50] ACPropulsion, “AC-150 EV power system”,

<http://www.acpropulsion.com/technology/gen2.htm>

- [2.51] A. Brooks, "Vehicle-to-grid demonstration project: grid regulation ancillary service with a battery electric vehicle," AC Propulsion, Inc. Report, pp. 61, December 2002.
- [2.52] Ponnaluri, S.; Linhofer, G.O.; Steinke, J.K.; Steimer, P.K., "Comparison of Single and Two Stage Topologies for Interface of BESS or Fuel Cell System Using the ABB Standard Power Electronics Building Blocks." European Conference on Power Electronics and Applications, September 2005.
- [2.53] K. Leng, Sutanto, D. (April 2000). "Using Battery Energy Storage System in a Deregulated Environment to Improve Power System Performance." *International Conference on Electric Utility Deregulation and Restructuring and Power Technologies (DRPT)*, April 2000.
- [2.54] N. Mohan, T.M. Undeland, Power Electronics: John Wiley & Sons, Inc, 2003
- [2.55] S. Inoue; H. Akagi, "A Bidirectional Isolated DC–DC Converter as a Core Circuit of the Next-Generation Medium-Voltage Power Conversion System." *IEEE Transactions on Power Electronics*; Vol. 22, March 2007.
- [2.56] H. Li, F.Z. Peng, J.S. Lawler, "A Natural ZVS Medium-Power Bidirectional DC–DC Converter with Minimum Number of Devices." *IEEE Transactions on Industry Applications*; Vol. 39, March 2003
- [2.57] M. Jain, Daniele, "A Bidirectional DC–DC Converter Topology for Low Power Application." *IEEE Transactions on Power Electronics*; Vol. 15, July 2000.
- [2.58] S.J. Chiang, K.T. Chang, "Residential Photovoltaic Energy Storage System." *IEEE Transactions on Industrial Electronics*, Vol. 45, June 1998.
- [2.59] Z. Ye, M. Dame, "Reliable, Low-Cost Distributed Generator/Utility System Interconnect", NREL Report No. SR-560-38017, 2006.
- [2.60] M. A. S. Masoum, P. S. Moses, and S. Hajforoosh, "Distribution transformers stress in smart grid with coordinated charging of plug-in electric vehicles," in *Proc. Rec. IEEE Power Energy Syst. Innovative Smart GridTech. Conf.*, Jan. 2012.
- [2.61] J. A. P. Lopes, F. J. Soares, P. M. Almeida, and M. M. Silva, "Smart charging strategies

- for electric vehicles: Enhancing grid performance and maximizing the use of variable renewable energy resources,” in *Proc.EVS24 Int. Battery, Hybrid Fuel Cell EV Symp.*, May 2009, pp. 1–11.
- [2.62] P. Fairley, “Speed bumps ahead for electric-vehicle charging,” *IEEE Spectrum* [Online]. Available:
<http://spectrum.ieee.org/greentech/advanced-cars/speed-bumps-ahead-for-electricvehicle-charging>
- [2.63] “European electricity industry views on charging electric vehicles,” AEURELECTRIC Position Paper, Apr. 2011.
- [2.64] S. Vandael, N. Boucke, T. Holvoet, and G. Deconinck, “Decentralized demand side management of plug-in hybrid vehicles in a smart grid,” in *Proc. 1st Int. Workshop Agent Technol. Energy Syst.*, 2010, pp. 67–74.
- [2.65] M. Singh, P. Kumar, and I. Kar, “Implementation of vehicle to grid infrastructure using fuzzy logic controller,” *IEEE Trans. Smart Grid*, vol. 3, no. 1, pp. 565–577, Mar. 2012.
- [2.66] D. Crabtree, T. Faney, K. Koudigkelis, A. Papavasiliou, I. Sidhu, P. Kaminsky, and B. Tenderich, “Optimal charging of electric vehicles,” Center for Entrepreneurship & Technology Technical Brief No.2009.6.v.1.1.1, Sep. 2009.
- [2.67] Y. Cao, S. Tang, C. Li, P. Zhang, Y. Tan, Z. Zhang, and J. Li, “An optimized EV charging model considering TOU price and SOC curve,” *IEEE Trans. Smart Grid*, vol. 3, no. 1, pp. 388–393, Mar. 2012.
- [2.68] A. Schuller, J. Ilg, and C. Van Dinther, “Benchmarking electric vehicle charging control strategies,” in *Proc. Rec. IEEE Power Energy Syst. Innovative Smart Grid Tech. Conf.*, Jan. 2012.
- [2.69] A. T. Al-Awami and E. Sortomme, “Coordinating vehicle-to-grid services with energy trading,” *IEEE Trans. Smart Grid*, vol. 3, no. 1, pp. 453–462, Mar. 2012.
- [2.70] R. Sioshansi, R. Fagiani, and V. Marano, “Cost and emissions impacts of plug-in hybrid vehicles on the Ohio power system,” *Energy Policy*, vol. 38, pp. 6703–6712, 2010.
- [2.71] R. Doctors, “A systems approach to battery powered vehicles,” in *Proc. Battery Conf.*

Appl. Adv., 1995, pp. 117–122.

- [2.72] O. Worley and D. Klobjan, “Optimization of battery charging and purchasing at electric vehicle battery swap station,” in *Proc. IEEE Veh. Power Propulsion Conf.*, 2010, pp. 1–4.
- [2.73] C. D. Waldron and P. Kobylarek, “The reality of electric vehicles and the grid,” *Electric Light & Power*, vol. 89, no. 1, pp. 54–56, Jan./Feb. 2011.
- [2.74] J. Lassila, J. Haakana, V. Tikka, and J. Partanen, “Methodology to analyze the economic effects of electric cars as energy storages,” *IEEE Trans. Smart Grid*, vol. 3, no. 1, pp. 506–516, Mar. 2012.
- [2.75] G. Li and X. P. Zhang, “Modeling of plug-in hybrid electric vehicle charging demand in probabilistic power flow calculations,” *IEEE Trans. Smart Grid*, vol. 3, no. 1, pp. 492–499, Mar. 2012.
- [2.76] GM-Volt: Latest Chevy Volt battery pack and generator details and clarifications. (2011). [Online]. Available: <http://gmvolt.com/2007/08/29/latest-chevy-volt-battery-pack-and-generator-details-and-clarifications>.
- [2.77] Nissan Zero Emission Website, Leaf specs. (2010). [Online]. Available: <http://www.nissan-zeroemission.com/EN/LEAF/specs.html>
- [2.78] W. Shireen and S. Patel, “Plug-in hybrid electric vehicles in the smart grid environment,” in *Proc. Rec. IEEE Power Energy Syst. Transm. Distrib. Conf. Expo.*, 2010, pp. 1–4.
- [2.79] G. T. Heydt, “The impact of electric vehicle deployment on load management strategies,” *IEEE Trans. Power App. Syst.*, vol. PAS-1, no. 144, pp. 1253–1259, May 1983.
- [2.80] S. Meliopoulos, J. Meisel, G. Cokkinides, and T. Overbye, “Power system level impacts of plug-in hybrid vehicles,” PSERC Document 09-12, Oct. 2009.
- [2.81] H. Lund and W. Kempton, “Integration of renewable energy into the transport and electricity sectors through V2G,” *Energy Policy*, vol. 36, no. 9, pp. 3578–3587, 2008.
- [2.82] C. H. Stephan and J. Sullivan, “Environmental and energy implications of plug-in hybrid electric vehicles,” *Environ. Sci. Technol.*, vol. 42, pp. 1185–1190, 2008.
- [2.83] S. Ramtean and P. Denholm, “Emissions impacts and benefits of plug in hybrid electric

- vehicles and vehicle-to-grid services,” *Environ. Sci. Technol.*, vol. 43, pp. 1199–1204, 2009.
- [2.84] C. Samaras and K. Meisterling, “Life cycle assessment of greenhouse gas emissions from PHEVs: Implications for policy,” *Environ. Sci. Technol.*, vol. 42, no. 9, pp. 3170–3176, 2008.
- [2.85] E. Larsen, D. K. Chandrashekhara, and J. Ostergaard, “Electric vehicles for improved operation of power systems with high wind power penetration,” in *Proc. IEEE Energy 2030 Conf.*, Nov. 2008, pp. 1–6.
- [2.86] F. Locment, M. Sechilariu, and C. Forgez, “Electric vehicle charging system with PV grid-connected configuration,” in *Proc. IEEE Veh. Power Propulsion Conf.*, 2010, pp. 1–6.
- [2.87] Y. Gurkaynak and A. Khaligh, “Control and power management of a grid connected residential photovoltaic system with plug-in hybrid electric vehicle (PHEV) Load,” in *Proc. IEEE Appl. Power Energy Conf.*, 2009, pp. 2086–2091.
- [2.88] W. Kempton and J. Tomić, “Vehicle-to-grid power fundamentals: Calculating capacity and net revenue,” *J. Power Sources*, vol. 144, no. 1, pp. 268–279, 2005.
- [2.89] B. Singh, B. N. Singh, A. Chandra, K. Al-Haddad, A. Pandey, and D. P. Kothari, “A review of single-phase improved power quality AC–DC converters,” *IEEE Trans. Ind. Electron.*, vol. 50, no. 5, pp. 962–981, Oct. 2003.
- [2.90] B. Singh, B. N. Singh, A. Chandra, K. Al-Haddad, A. Pandey, and D. P. Kothari, “A Review of three-phase improved power quality AC–DC converters,” *IEEE Trans. Ind. Electron.*, vol. 51, no. 3, pp. 641–660, Jun. 2004.
- [2.91] X. Zhou, S. Lukic, S. Bhattacharya, and A. Huang, “Design and control of grid-connected converter in bi-directional battery charger for plug-in hybrid electric vehicle application,” in *Proc. IEEE Veh. Power Propulsion Conf.*, 2009, pp. 1716–1721.
- [2.92] X. Zhou, G. Wang, S. Lukic, S. Bhattacharya, and A. Huang, “Multi function bi-directional battery charger for plug-in hybrid electric vehicle application,” in *Proc. IEEE Energy Convers. Congr. Expo.*, 2009, pp. 3930–3936.

- [2.93] A. Brooks, "Vehicle-to-grid demonstration project: grid regulation ancillary service with a battery electric vehicle. Sand Dimas," CA, California: Air Resources Board and the California Environmental Protection Agency; 2002.
- [2.94] W. Kempton, S. Baker, "A test of vehicle-to-grid (V2G) for energy storage and frequency regulation in the PJM system," University of Delaware; 2008.
- [2.95] B. Sovacool, "Beyond batteries: an examination of the benefits and barriers to plug-in hybrid electric vehicles (PHEVs) and a vehicle-to-grid (V2G) transition," *Energy Policy* 2009; 37:1095–103.
- [2.96] C. Guille, G. Cross, "A conceptual framework for the vehicle-to-grid (V2G) implementation," *Energy Policy* 2009; 37: 4379–90.
- [2.97] P. Andersen, "Integrating private transport into renewable energy policy: the strategy of creating intelligent recharging grids for electric vehicles," *Energy Policy* 2009; 37: 2481–6.
- [2.98] W. Short, "Preliminary assessment of plug-in hybrid electric vehicles on wind energy markets," Golden, CO: National Renewable Energy Laboratory; 2006.
- [2.99] W. Kempton, "Electric-drive vehicles for peak power in Japan," *Energy Policy* 2000; 28: 9–18.
- [2.100] J. Tomic, W. Kempton, "Using fleets of electric-drive vehicles for grid support," *Journal of Power Sources* 2007; 168:459–68.
- [2.101] H. Turton, "Vehicle-to-grid systems for sustainable development: an integrated energy analysis," *Technological Forecasting & Social Change* 2008; 75:1091–108.
- [2.102] N. Juul, P. Meibom, "Optimal configuration of an integrated power and transport system," *Energy* 2011; 36:3523–30.
- [2.103] T. Kristofferson, K. Capion, "Optimal charging of electric drive vehicles in a market environment," *Applied Energy* 2011; 88: 1940–8.
- [2.104] J. Kiviluoma, "Methodology for modeling plug-in electric vehicles in the power system and cost estimates for a system with either smart or dumb electric vehicles," *Energy* 2011; 36:1758–67.

- [2.105] C. Ekman, "On the synergy between large electric vehicle fleet and high wind penetration — an analysis of the Danish case," *Renewable Energy* 2011; 36: 546–53.
- [2.106] L. Goransson, "Integration of plug-in hybrid electric vehicles in a regional wind-thermal power system," *Energy Policy* 2010; 38: 5482–92.
- [2.107] Oak Ridge National Laboratory. A comparative study of emerging vehicle technology assessments. Oak Ridge, TN: Oak Ridge National Laboratory; 2011.
- [2.108] R. Green, "The impact of plug-in hybrid electric vehicles on distribution networks: a review and outlook," *Renewable Sustainable Energy Review* 2011; 15:544–53.
- [2.109] B. Hodge, S. Huang, "The effects of vehicle-to-grid systems on wind power integration in California," *Computer Aided Chemical Engineering* 2010; 28:1039–44.
- [2.110] S. Hadley, "Impact of plug-in hybrid vehicles on the electric grid," Oak Ridge, TN: Oak Ridge National Laboratory; 2006.
- [2.111] J. Wang, C. Liu, "A. Impact of plug-in hybrid electric vehicles on power systems with demand response and wind power," *Energy Policy* 2011; 39: 4016–21.
- [2.112] J. Holz, "Pulsewidth modulation – a survey," *IEEE Trans. Ind. Electron.*, vol. 39, pp 410-420, Oct. 1992.
- [2.113] M. P. Kazmierkowski, R. Krishnan, and F. Blaabjerg, *Control in Power Electronics*. London, U.K.: Academic, 2002.
- [2.114] I. Takahashi and T. Noguchi, "A new quick-response and high efficiency control strategy of an induction machine," *IEEE Trans. Ind. Appl.*, vol. IA-22, pp 820- 827, 1986.
- [2.115] G. S. Buja and M. P. Kazmierkowski, "Direct torque control of PWM inverter-fed AC motor – a survey," *IEEE Trans. Ind. Electron.*, vol. 51, no. 4, pp. 744-757, August 2004.
- [2.116] T. Ohnishi, "Three phase PWM converter/inverter by means of instantaneous active and reactive power control," in *Proc. IEEE IECON*, 1991, vol. 1, pp. 819- 824.
- [2.117] Noguchi, H. Tomiki, S. Kondo and I. Takahashi, "Direct power control of PWM converter without power-source voltage sensors," *IEEE Trans. Ind. Appl.*, vol. 34, pp 473-479, 1998.
- [2.118] M. Malinowski, M. P. Kazmierkowski S. Hansen, F. Blaabjerg and G. D. Marques,

- “Virtual-flux-based direct power control of three-phase PWM rectifiers,” *IEEE Trans. Ind. Appl.*, vol. 37, no. 4, pp. 1019-1027, 2001.
- [2.119] M. Malinowski, M. P. Kazmierkowski and A. M. Trzynadlowski, “A comparative study of control techniques for PWM rectifiers in AC adjustable speed drives,” *IEEE Trans. Power Electron.*, vol. 18, no. 6, pp. 1390-1396, November 2003.
- [2.120] A. Bouafia, J. P. Gaubert and F. Krim, “Analysis and design of new switching table for direct power control of three-phase PWM rectifier,” in *Proc. IEEE Int. Power Electronics and Motion Control Conf. EPE-PEMC’ 08*, pp. 1-6, 2008.
- [2.121] J. Alonso-Martinez, J. Eloy-Garcia, and S. Arnaltes, “Table-based direct power control: A critical review for microgrid applications,” *IEEE Trans. Power Electron.*, vol. 25, no. 12, pp. 2949-2916, December 2010.
- [2.122] A. Sato and Toshihiko Noguchi, “Voltage-source PWM rectifier – inverter based on direct power control and its operation characteristics,” *IEEE Trans. Power Electron.*, vol. 26, no. 5, pp. 1559-1567, May 2011.
- [2.123] M. Malinowski, M. Jasinski and M. P. Kazmierkowski, “Simple direct power control of three-phase PWM rectifier using space-vector modulation (DPCSVM),” *IEEE Trans. Ind. Electron.*, vol. 51, no. 2, pp. 447-454, April 2004.
- [2.124] D. Zhi, L. Xu, B. W. Williams, L. Yao, and M. Bazargan, “A new direct control strategy for grid connected voltage source converters,” *Int. Conf. Electrical Machines and Systems, 2008 (ICEMS 2008)*, pp. 1157-1162.
- [2.125] A. Bouafia, F. Krim and J. P. Gaubert, “Fuzzy-logic-based switching state selection for direct power control of three-phase PWM rectifier,” *IEEE Trans. Ind. Electron.*, vol. 56, no. 6, pp. 1984-1992, June 2009.
- [2.126] V. S. C. Raviraj and P. C. Sen, “Comparative study of proportional-integral, sliding mode, and fuzzy logic controllers for power converters,” *IEEE Trans. Ind. Appl.*, vol. 33, no. 2, pp 518-524, 1997.
- [2.127] J. Hu, L. Shang, Y. He, and Z. Zhu, “Direct active and reactive power regulation of grid-connected DC/AC converters using sliding mode control approach,” *IEEE Trans.*

- Power Electron.*, vol. 26, no. 1, pp 210-222, 2011.
- [2.128] P. Cortes, M. P. Kazmierkowski, R. M. Kennel, D. E. Quevedo and J. Rodriguez, "Predictive control in power electronics and dirves," *IEEE Trans. Ind. Electron*, vol. 55, no. 12, pp. 4312-4324, December 2008.
- [2.129] D. Zhi, L. Xu, and B. W. Williams, "Model-based predictive direct power control of doubly fed induction generators," *IEEE Trans. Power Electron.*, vol. 25, no. 2, pp. 341-351, Feb. 2010.
- [2.130] J. M. Espí, J. Castelló, R. García-Gil, G. Garcerá, and E. Figueres, "An adaptive robust predictive current control for three-phase grid-connected inverters," *IEEE Trans. Ind. Electron*, vol. 58, no. 8, pp. 3537-3546, August 2011.
- [2.131] Q. Zeng and L. Chang, "An advanced SVPWM-based predictive current controller for three-phase inverters in distributed generation systems," *IEEE Trans. Ind. Electron*, vol. 55, no. 3, pp. 1235-1246, Mar. 2008.
- [2.132] E. Keane and D. Flynn, "Potential for electric vehicles to provide power system reserve," In *Innovative Smart Grid Technologies (ISGT), 2012 IEEE PES*, pp 1-7, jan. 2012.
- [2.133] Willett Kempton and Jasna Tomic, "Vehicle to grid power fundamentals: Calcula-- -ting Capacity and net revenue," *Journal of Power Sources*, 144(1), pp.268-279, 2005.
- [2.134] W. Su, M, Chow, "Computational intelligence-based energy management for a large scale PHEV/PEV enabled municipal parking deck," *Journal of Applied Energy*, 96, pp. 171-182, 2012.
- [2.135] J. Tomic, W. Kempton, Using fleets of electric-drive vehicles for grid support, *J. Power Sources* 168 (2) (2007) 459e468.
- [2.136] A. De Los Rios, J. Goentzel, K.E. Nordstrom, C.W. Siegert, Economic analysis of vehicle-to-grid (V2G)-enabled fleets participating in the regulation service market, in: *Rec. IEEE PES Innovative Smart Grid Tech. Conf. (ISGT)*, January 2012.
- [2.137] D. Wu, K.T. Chau, C. Liu, S. Gao, F. Li, Transient stability analysis of SMES for smart grid with vehicle-to-grid operation, *IEEE Trans. Smart Grid* 3 (1) (2012) 1e4.

- [2.138] C. Wu, H. Mohsenian-Rad, J. Huang, Vehicle-to-aggregator interaction game, *IEEE Trans. Smart Grid* 3 (1) (2012) 434e442.
- [2.139] W. Kempton, J. Tomi_c, "Vehicle-to-grid power fundamentals: calculating capacity and net revenue," *J. Power source*, 144 (1) (2005) 268e279.
- [2.140] C. Wu, H.M. Rad, J. Huang, J. Jatskevich, "PEV-based combined frequency and voltage regulation for smart grid," in: *Rec. IEEE PES Innovative Smart Grid Tech. Conf. (ISGT)*, January 2012.
- [2.141] K. Clement-Nyns, E. Haesen, J. Driesen, The impact of vehicle-to-grid on the distribution grid, *Electr. Power Syst. Res.* 81 (1) (2011) 185e192.
- [2.142] M.D. Galus, M. Zima, G. Andersson, "On integrations of PHEVs into existing power system structures," *Energy Policy* 38 (11) (2010) 6736e6745.
- [2.143] Union for the Coordination of Transmission of Electricity (UCTE), *Operation Handbook*, 2008.
- [2.144] K. Mets, T. Verschueren, W. Haerick, C. Develder, F. De Turck, Optimizing smart energy control strategies for plug-in hybrid electric vehicle charging, in: *Proc. IEEE/IFIP Network Oper. Manage. Symp. Workshops (NOMS)*, 2010, pp. 293e299.
- [2.145] IEEE Std. 1547, IEEE Standard for Interconnecting Distributed Resources with Electric Power Systems, 2003.
- [2.146] W. Kempton, T. Kubo, "Electric-drive vehicles for peak power in Japan," *Energy Policy* 28 (2000) 9e18.
- [2.147] V. Marano, G. Rizzoni, Energy and economic evaluation of PHEVs and their interaction with renewable energy sources and the power grid, in: *Proc. IEEE Veh. Electronics and Safety Conf.*, 2008, pp. 84e89.
- [2.148] W. Short, P. Denholm, Preliminary Assessment of Plug-in Hybrid Electric Vehicles on Wind Energy Markets, Tech. Report National Renewable Energy Lab NREL/TP-620-39729, April 2006.
- [2.149] A. Ramos, L. Olmos, J.M. Latorre, I.J. Perez-Arriaga, "Modeling medium term hydroelectric system operation with large-scale penetration of intermittent generation," in:

Proc. XIV Latin and Iberian Conf. Operations Research, 2008.

- [2.150] A.Y. Saber, G.K. Venayagamoorthy, "Plug-in vehicles and renewable energy sources for cost and emission reductions," *IEEE Trans. Ind. Elect.* 58 (4) (2011) 1229e1238.
- [2.151] SAE Electric vehicle and plug-in hybrid electric vehicle conductive charge coupler. SAE standard J1772; 2012.
- [2.152] Yilmaz M, Krein PT. "Review of battery charger topologies, charging power levels, and infrastructure for plug-in electric and hybrid vehicles," *IEEE Trans Power Electron* 2013; 28(5):2151–69.
- [2.153] F. Mwasilu, J. John Justo, "Electric vehicles and smart grid interaction: a review on vehicle to grid and renewable energy sources integration," *Journal of renewable and sustainable energy reviews* 24 (2014) p.p 501-516.
- [2.154] Kempton, Willett and Toru Kubo. 2000. "Electric-drive Vehicles for Peak Power in Japan," *Energy Policy* 28(1): 9-18.
- [2.155] Letendre, Steven and W. Kempton, 2002. "The V2G Concept: A New Model for Power?" *Public Utilities Fortnightly* 140(4): 16-26, February 2002.
- [2.156] Kempton, Willett and Jasna Tomić, "Vehicle to Grid Fundamentals: Calculating Capacity and Net Revenue," *Journal of Power Sources*, Volume 144, Issue 1, 1 June 2005, Pages 268-279.
- [2.157] Parsons, R. George, K. Michael, "Willingness to pay for vehicle-to-grid (V2G) electric vehicles and their contract terms," *Energy Economics* , 42 (2014), p313-324.
- [2.158] Peterson, "Lithium-ion battery cell degradation resulting from realistic vehicle and vehicle-to-grid utilization," *Journal of Power Sources*, Volume 195, Issue 8, 15 April 2010, Pages 2385–2392.
- [2.159] C. Li, Q. Nguyen, "School bus pollutions and changes in the air quality at schools: a case study," *J Environ Monit* 2009; 11: 1037-42.
- [2.160] DM. Lemoine, DM. Kammen, "An innovation and policy agenda for commercially competitive plug-in hybrid electric vehicles," *Environ Res Lett* 2008; 3
- [2.161] BM. Alawi, TH. Bradley, "Total cost of ownership, payback and consumer preference

- modelling of plug-in hybrid electric vehicles,” *Appl Energy* 2013; 103: 488-506.
- [2.162] W. Feng, M. Figliozzi, “Conventional vs electric commercial vehicle fleets: A case study of economic and technological factors affecting the competitiveness of electric commercial vehicles in the USA,” *ProcedSoc Behav Sci* 2012; 39: 702-11.
- [2.163] X. Hu, N. Murgovski, “Energy Efficiency analysis of a series plug-in hybrid electric bus with different energy management strategies and battery sizes,” *Appl Energy* 2013; 111: 1001-9
- [2.164] V. Dawood, A. Emadi, “Performance and fuel economy comparative analysis of conventional, hybrid, and fuel cell heavy-duty transit buses,” *Veh Technol Conf* 2003; 5: 3310-5
- [2.165] SB. Peterson, JF. Whitacre, “The economics of using plug-in hybrid electric vehicle battery packs for grid storage,” *J Power Sources* 2010; 195: 2377-84.
- [2.166] N. Roterling and M. Ilic, “Optimal charge control of plug-in hybrid electric vehicles in deregulated electricity markets,” *IEEE Transactions on Power Systems*, vol. PP, pp. 1-1, 2010.
- [2.167] J. Kiviluoma and P. Meibom, “Methodology for modeling plug-in electric vehicles in the power system and cost estimates for a system with either smart or dumb electric vehicles,” *Energy*, vol. 36, pp. 1758-1767, 2011.
- [2.168] S. L. Andersson, A. K. Elofsson, M. D. Galus, L. Göransson, S. Karlsson and F. Johnsson, “Plug-in hybrid electric vehicles as regulating power providers: Case studies of Sweden and Germany,” *Energy Policy*, vol. 38, pp. 2751-2762, 2010.
- [2.169] A. Y. Saber and G. K. Venayagamoorthy, “Intelligent unit commitment with vehicle-to-grid --A cost-emission optimization,” *Journal of Power Sources*, vol. 195, pp. 898-911, 2010.
- [2.170] C. D. White and K. M. Zhang, “Using vehicle-to-grid technology for frequency regulation and peak-load reduction,” *Journal of Power Sources*, vol. 196, pp. 3972-3980, 2011.
- [2.171] H. Sekyung, H. Soohee, and K. Sezaki, “Development of an optimal 191 References

Vehicle-to-Grid aggregator for frequency regulation,” *IEEE Transactions on Smart Grid*, vol. 1, pp. 65-72, 2010.

[2.172] M. D. Galus, M. Zima, and G. Andersson, “On integration of plug-in hybrid electric vehicles into existing power system structures,” *Energy Policy*, vol. 38, pp. 6736-6745, 2010.

[2.173] G. Shuang, “Design, analysis and control of vehicle to grid services,” Ph. D thesis of Department of Electrical and Electronic Engineering, The University of Hong Kong, January 2014.

CHAPTER 3

ENERGY STORAGE SYSTEM FOR ELECTRIC VEHICLES

3.1 Introduction

Energy storage systems are tailored to the type of fuel used and the form of energy stored, for example: mechanical, electrochemical, chemical, thermal, or electrical. Whilst mechanical storage systems, including flywheels, pneumatic (hydraulic) and elastic mediums store energy in its kinetic form, electrical storage system, such as batteries and supercapacitor store energy in its potential form. One measure to characterise a storage system is to determine the energy to weight ratio (Wh/kg, namely E) and energy to volume ratio (Wh/L, that is, energy density). These two parameters are compared for different forms of energy storage system in Table 3.1 [3.1].

TABLE 3.1 2005 Comparison of Energy Density of Various Energy Storage Technologies [3.1]

Type of Storage	Wh/kg	Wh/L
Compressed air carbon tanks Isothermal 4500 psi	137	48
Hydrogen carbon tanks 5,000 psi	2,000	700
Hydrogen carbon tanks 10,000 psi	1,666	1,165
Lead acid battery	30	70
NiMH battery	70	180
Lithium Ion battery	120	250
Supercapacitor	5	6.5
Conventional Flywheel	3	2
Hydraulics	2	2
Gas oil	11,660	8,750

However, in hybrid traction applications a more important factor must be considered, that is the power density of the storage system (W/kg namely P). Whilst energy density translates into the

ability to supply power for protracted lengths of time, power density is an indication of the ability to deliver pulse power at higher levels for a short time. The classical relationship between energy density, E , and power density, P , is known as a Ragon plot [3.2], in which a collection of data points is plotted with specific energy density E on the Y-axis and specific power density P on the X-axis are shown in Fig. 3.1.

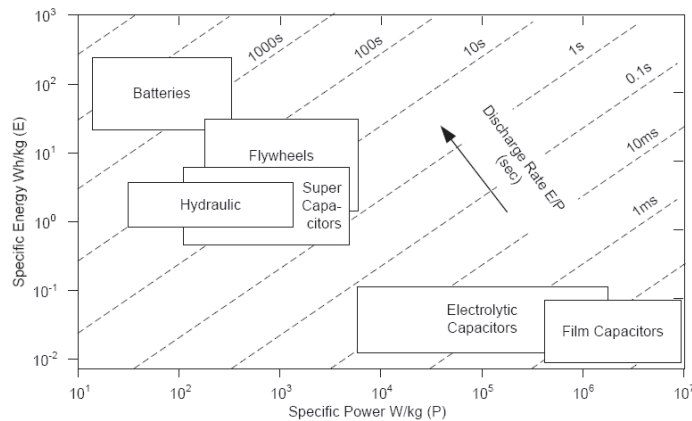


Fig. 3.1 Indicative Ragon plots for different energy storage devices [3.2]

Fig. 3.1 shows indicative characteristics of different types of storage systems. It is important to consider the trends rather than the absolute levels as there could be discrepancies between different published data. One parameter to consider is the P/E ratio. This is important for traction applications as it indicates the ability of the storage device to deliver peak power compared to its energy storage capacity. The inverse ratio E/P gives the discharging time of the storage system as shown in Fig. 3.1.

Fig. 3.1 also shows that some mechanical systems, such as the flywheel, are as good as, or could be better than, electrical storage systems.

To allow EV to become the effective sustainable transportation solution, a great effort has to be made to overcome the major technical issue in EVs energy storage system. At present and in the foreseeable future, the viable EVs energy sources seem to be batteries, fuel cells, supercapacitors and ultra-high speed flywheels.

For EV in high power demand operation, such as acceleration and hill climbing, both basic energy storages deliver their power to the load. On the other hand, in low-power demand operation, such as constant-speed cruising operation, the high specific energy storage will deliver its power to the load and charge the high specific power storage to recover its charge lost during high-power demand operation. In regenerative braking operation, the peak power will be absorbed by the high specific power storage, and only a limited part is absorbed by the high specific energy storage. In this way, the whole system would be much smaller in weight and size than if any one of them alone was the energy storage.

Based on the discussion carried out, batteries have been widely used in EVs in the past ten years. Lithium ion batteries are considered as the only viable solution for EV and PHEV at the present time. Supercapacitors have also been investigated for use in PHEV due to their very high power density and long cycle life. Integrated hybrid energy storage systems that contain high energy lithium ion batteries and high power supercapacitors could potentially provide the best solutions for EV and PHEV.

3.2 Model Development of Batteries as Energy Storage System in EVs

3.2.1 Battery characteristics for model development

A. Electrochemical cell

A rechargeable battery is one or more electrochemical cells that convert stored chemical energy into electrical energy during a discharge process or convert electrical energy into chemical energy during a charge process [3.3].

An electrochemical cell is a chemical device for generating or storing electric energy. It consists of a positive electrode and a negative electrode, separated by electrolyte as shown in Fig. 3.2. The electrolyte is capable of conducting ions between the two electrodes, but is itself an electronic insulator. The positive and negative electrodes are immersed in the electrolyte and the reacting substances usually are stored within the electrodes, sometimes also in the electrolyte.

The chemical reactions associated with the energy conversion take place at the two electrodes. During discharge shown in Fig. 3.2a, the negative electrode contains the substance that is oxidized (i.e. releases electrons), while the positive electrode contains the oxidizing substance that is reduced (i.e. accepts electrons). Those electrons pass through the external load, thereby doing useful work. When the battery is charged, this reaction is reversed and a corresponding amount of energy from an external source is supplied to the cell shown in Fig. 3.2b [3.4].

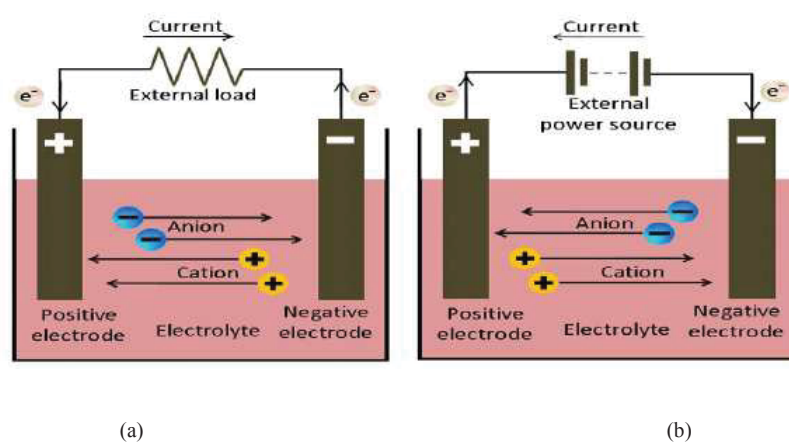


Fig. 3.2 Schematic representation of operation of electrochemical cell. (a) Discharge (b) Charge

B. Current flow and polarization

The current in the battery arises from the transfer of electrons from one electrode to the other. When there is no current flow through a cell, the difference between the potentials of the positive and negative electrodes gives an open-circuit voltage (OCV) of the cell. When current flows, however, mass transport is required to bring the reacting substances to the electrode surface or carry them away. As a result, the voltage under current flow is different from the OCV and the difference comprises (i) an overvoltage at the electrodes caused by electrochemical reactions and concentration deviations on account of transport phenomena and (ii) ohmic voltage drops caused by the electronic as well as the ionic current flows in the conducting parts including the electrolyte, current-collectors and active masses [3.5].

C. Other factors affecting battery models

Other important factors affecting battery performance and models include: battery capacity, state-of-charge (SOC), rate of charge and discharge, temperature, and age [3.5].

The battery capacity represents the maximum amount of energy that can be extracted from the battery under certain conditions, and is determined by the mass of active material contained in the battery.

The SOC is defined as the fraction of the full capacity that is available for further discharge. The OCV of a battery is normally a function of the SOC due to the polarization impact, which is a factor that must be considered in battery modelling.

The charging/discharging rates affect the rated battery capacity. According to the Peukert's equation, if the battery is being discharged very quickly, then the amount of energy that can be extracted from the battery is reduced [3.4]-[3.5]. Consequently, effective modelling of Peukert's relation is particularly important for design and analysis of power converter controlled battery charge and discharge.

The age and history of a battery have impacts on the capacity of a battery. Even when following manufacturers' depth of discharge (DOD) specifications, the battery capacity only stays at the rated capacity for a limited number of charge/discharge cycles. If the battery has been taken below its maximum DOD during its usage, battery capacity may be prematurely reduced.

The temperature of a battery also affects the energy that can be extracted from the battery. At higher temperatures, the battery capacity is usually higher than that at lower temperatures. However, intentionally elevating battery temperature is not an effective method to increase battery capacity as this also decreases battery lifetime.

The viable EV and HEV batteries consist of the lead-acid battery, nickel-based batteries, such as nickel/iron, nickel/cadmium, and nickel-metal hydride (Ni-MH) batteries, and lithium-based

batteries such as lithium-polymer (Li-P) and lithium-ion (Li-I) batteries. It seems that cadmium-based and lithium-based batteries would be the major candidates for EVs and HEVs.

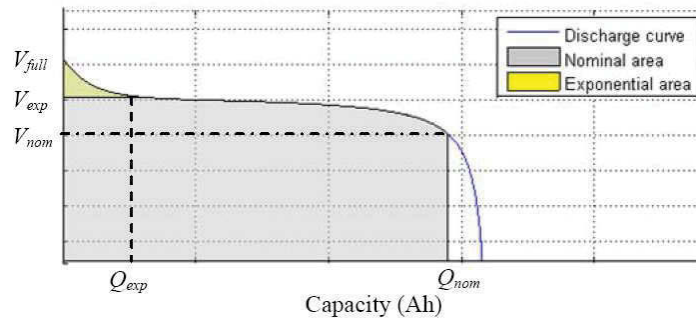


Fig. 3.3 Typical battery discharge curve [3.5]

Fig. 3.3 is the typical battery discharge curve, an exponential area represents dynamic voltage to reflect a non-linear hysteresis phenomenon between discharge and charge. Battery manufacturers usually specify the battery with coulometric capacity (ampere-hours), which is defined as the number of ampere-hours gained when discharging the battery from a fully charged state until the terminal voltage drops to its cut-off voltage. It should be noted that the same battery usually has a different number of ampere-hours at different discharging current rates. Another important parameter of a battery is the SOC. SOC is defined as the ratio of remaining capacity to fully charged capacity. With this definition, a fully charged battery has an SOC of 100% and a fully discharged battery has an SOC of 0%. However, the term “fully discharged” sometimes causes confusion, because of the different capacities at different discharge rates, and different cut-off voltages. In this project, the 20Ah nanophosphate battery cell from A123 Company was used to construct the battery storage bank.

Circuit-oriented battery models use a combination of voltage and current sources, resistors, and capacitors to model battery performance. Most of these electrical models fall under three basic categories: Thevenin-based [3.6]-[3.10], impedance-based [3.11]-[3.12], and runtime-based models [3.13]-[3.14]. Normally, it is more complicated to change battery parameters for different conditions and states of the battery. In addition, to account for variations between

charge and discharge states, two opposing diodes have to be used for each circuit element, making circuit-oriented battery models more complex.

3.2.2 Battery model development procedure

In its most basic form, a Thevenin-based model [3.6]-[3.10], shown in Fig. 3.4(a), consists of a voltage source (at $V_{oc}(SOC)$) in series with a resistor (internal resistance R_0) and a parallel combination of a capacitor and resistor to predict battery response to transient load events at a particular SOC, by assuming the open-circuit voltage [$V_{oc}(SOC)$] is constant.

Impedance-based models, shown in Fig. 3.4(b), employ the method of electrochemical impedance spectroscopy to obtain an AC-equivalent impedance model in the frequency domain, and then use a complicated equivalent network (Z_{ac}) to fit the impedance spectra [3.13]-[3.15]. The fitting process is difficult and complex. In addition, impedance-based models only work for a fixed SOC and temperature setting [3.16], and therefore they cannot predict dc response or battery runtime.

Runtime-based models [3.13]-[3.14] use a complex circuit network to simulate battery runtime and dc voltage response. Fig. 3.4c shows a recent runtime-based battery model [3.14]. On the left side of the model, a capacitor having the value of battery capacity plus a current-controlled current source describes how the battery SOC, represented by V_{SOC} , varies with the battery current. On the right side, the RC networks, similar to that used in the Thevenin-based model, simulate the relation between the battery current and terminal voltage.

The proposed simplified nonlinear dynamic model shown in Fig. 3.5 is based on the first-order Thevenin model. The nonlinear characteristic is reflected by model parameters, which depend on different values of OCV. Since this research only focuses on charging behaviour, the discharging behaviour, self-discharging behaviour, and voltage recovery behaviour are neglected in the Thevenin model. For the further development of energy storage system including battery bank, all the behaviour should be considered for the whole system performance. Following are the equations of this model.

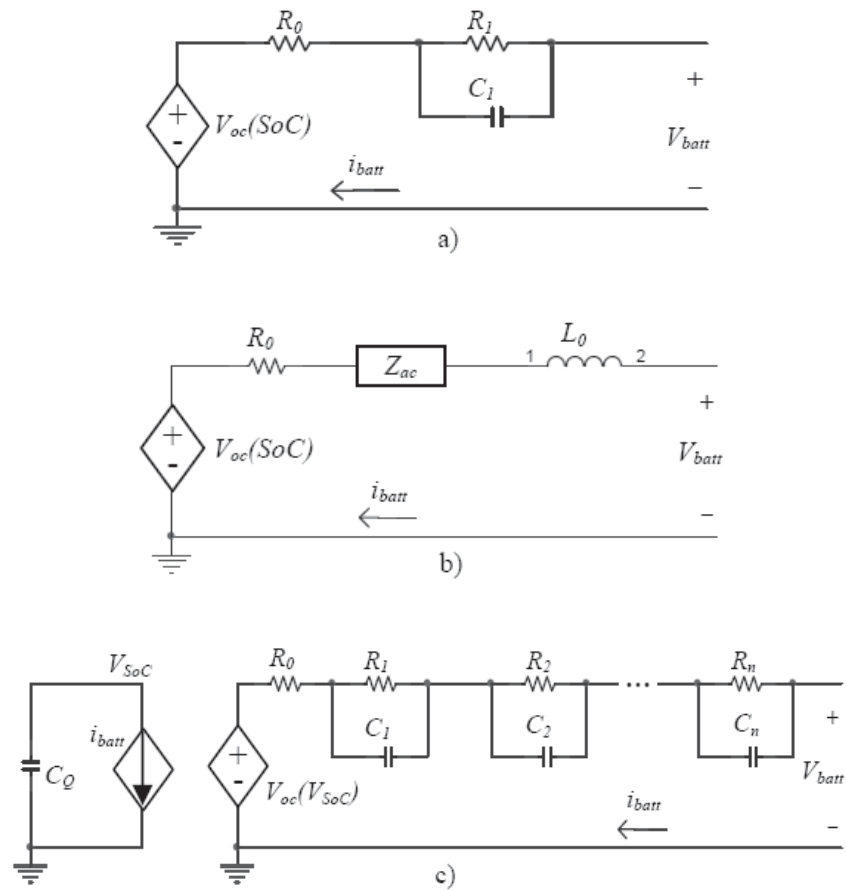


Fig. 3.4 Circuit-oriented battery models (a), (b) and (c)

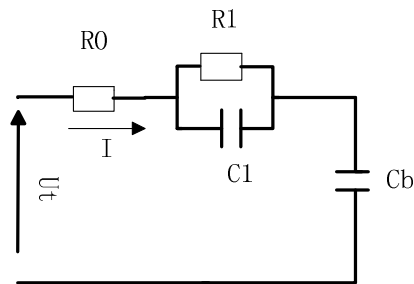


Fig. 3.5 First-order Thevenin charging model

For the model presented in Part A, in the complex field, using the Laplace equations (3.1),

$$U_{c1}(s) = I(s) \cdot \frac{R_1}{R_1 \cdot SC_1 + 1} \quad (3.1)$$

Using the inverse Laplace transfer the (3.1) to (3.2),

$$U_{c1}(t) = I \cdot \int_0^t \frac{1}{C_1} \cdot \exp\left(\frac{1}{-R_1 \cdot C_1}\right) \quad (3.2)$$

Convert the equation (3.2) to (3.3),

$$U_{c1}(t) = I \cdot R_1 \cdot [1 - \exp(\frac{-t}{\tau_1})] \quad (3.3)$$

where $\tau_1 = R_1 \cdot C_1$ $K = \frac{1}{C_b}$

By applying the Kirchhoff's voltage law for the charging model,

$$U_t(t) - U_{oc} = I \cdot R_0 + I \cdot R_1 \cdot [1 - \exp(\frac{-t}{\tau_1})] + k \cdot I \cdot t \quad (3.4)$$

The equation used for curve fitting is given by

$$U_t(t) - U_{oc} = a - b \cdot \exp(-c \cdot t) + d \cdot t \quad (3.5)$$

Based on the simplified nonlinear dynamic model and experimental results, it is essential to give out the model parameters for the model in the section 3.5.

3.3 Model Development of Supercapacitors as Energy Storage

System in EVs

3.3.1 Supercapacitor characteristics for model development

What makes supercapacitors different from the other capacitors types are the electrodes used in these capacitors. Supercapacitors are based on a Carbon NanoTube (CNT) technology; this technology creates a very large surface area with an extremely small separation distance [3.17]. Capacitors consist of two metal electrodes separated by a dielectric material. The dielectric not only separates the electrodes but also has electrical properties that affect the performance of a capacitor. Supercapacitors do not have a traditional dielectric material like ceramic, polymer films or aluminum oxide to separate the electrodes. Instead they have a physical barrier made

from activated carbon that when an electrical charge is applied to the material a double electric field is generated which acts like a dielectric. The thickness of the electric double layer is as thin as a molecule. The surface area of the activated carbon layer is extremely large yielding several thousands of square meters per gram. This large surface area allows for the absorption of a large amount of ions. The charging/discharging occurs in an ion absorption layer formed on the electrodes of activated carbon [3.18].

The activated carbon fiber electrodes are impregnated with an electrolyte where positive and negative charges are formed between the electrodes and the impregnate. The electric double layer formed becomes an insulator until a large enough voltage is applied and current begins to flow. The magnitude of voltage where charges begin to flow is where the electrolyte begins to break down. This is called the decomposition voltage.

The double layers formed on the activated carbon surfaces can be illustrated as a series of parallel RC circuits. In Fig. 3.6 is shown how a supercapacitor is fabricated.

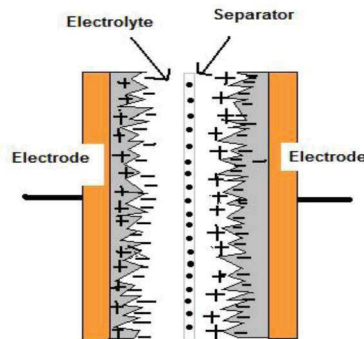


Fig. 3.6 Double layer capacitor

Fig. 3.7 shows the supercapacitor is constituted of three layers: a carbon powder layer (conducting carbon layer) compressed on the current collector layer and an activated carbon layer added to the conducting carbon.

In an SC modelling field, most of the proposed models are equivalent electrical models [3.19]-[3.27]. The problem with this kind of modelling is the lack of physical meaning in the circuit components. Such a meaning should be useful for aging analysis or failure diagnosis.

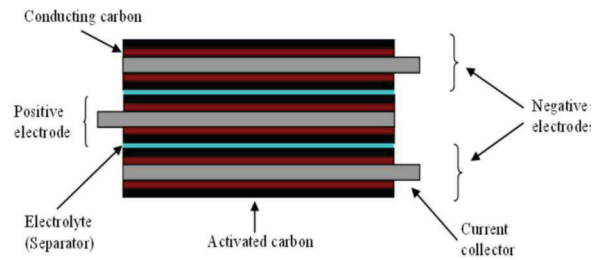


Fig. 3.7 Three layer supercapacitor structure

To take into account species diffusion phenomena that take place inside a double layer capacitor (long range phenomena), several solutions have been proposed. In the simpler one, it is suggested to use a two-branch RC model [3.25]-[3.26], one for the fast dynamics and one for the slow ones. In other models, infinite RC ladder circuits required to take into account these phenomena are replaced by finite RC ladder circuits [3.21]. The inconvenience of most of these models is the complex determination of the different elements: a large number of parameters must be identified. This determination involves nonlinear optimization algorithms or model discretization (using Euler approximation) and a least square method [3.19]. Long range phenomena observed during SC relaxation are also taken into account through the introduction of fractional differentiation in modelling [3.28]-[3.29].

As discussed in the literature review, from the documents [3.30]-[3.31], the simplified model is easy to use to calculate the parameters of the supercapacitor and is good enough to represent the supercapacitor performance. In the following part it can be observed that this model can give a good result.

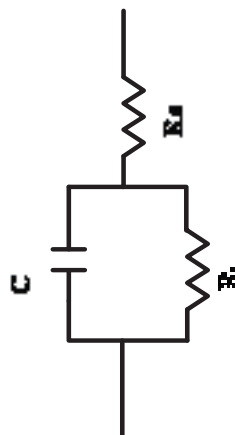


Fig. 3.8 Model of supercapacitor used

Fig. 3.8 is the simplest model of a supercapacitor, R_L is the leakage resistor, R_S is the series resistor, C is the capacitor. According to the self-discharge and load discharge experiments, the results of the 3 main parameters of the supercapacitor in our lab can be given out.

3.3.2 Supercapacitor model parameter calculation

A. Different parameter calculation methods

There are several parameter calculation methods used in the supercapacitor model parameter calculation. In short, the most important parameters of a supercapacitor include capacitance (abbreviated as C), ESR (series resistance) and EPR (which is also called leakage resistance). C decides the energy capability that can be stored in a supercapacitor. Generally speaking, ESR consists of electrode resistance, electrolyte resistance and contact resistance and wastes power as internal heating when charging and discharging. For the supercapacitor, ESR is almost less than one milliohm but influences the energy efficiency and power density. EPR is an inner equivalent parallel resistance usually hundreds of kilo ohms and decides the leakage current when the supercapacitor is in a stand-by mode.

When a supercapacitor is charged to the rated voltage, it can be discharged and the instantaneous voltage drop and current can be recorded by the two probes of an oscillograph. The voltage drop and discharging current can be measured through resistor sampling, thus the ESR is the quotient of them.

EPR measurement is a self-discharging method described as follows. When the supercapacitor is charged to a specified voltage, the power supply is disconnected and left in a self-discharging state. The voltage of the supercapacitor declines approximately according to equation:

$$U = U_0 e^{\frac{-t}{RC}} \quad (3.6)$$

The EPR can be calculated by the equation as follows,

$$EPR = \frac{-(t_2 - t_1)}{\ln \frac{U_2}{U_1} C} \quad (3.7)$$

This method focuses on the experiments result curves to get the parameters of the supercapacitor model; it can be implemented in the laboratory, but they have poor veracity. Besides this method, EIS (Electrochemical Impedance Spectroscopy) testing is an effective method to measure and analyse the parameters of supercapacitors. A sinusoidal voltage perturbation power source is applied to the supercapacitor at a well-defined frequency range. The amplitude and phase of the voltage is recorded when the signal sweeps through the range repeatedly and the Nyquist curve is plotted to get the equivalent impedance of the supercapacitor. A typical Nyquist plot is shown in Fig. 3.9. At high frequencies, the supercapacitor can be equivalent to ESR, which is represented by a vertical straight line shifted on the real axis by its ESR. At low frequencies a supercapacitor is presented as an impedance including EPR in series with ESR and approaches a near vertical straight line shifted on the real axis by the sum of ESR and EPR.

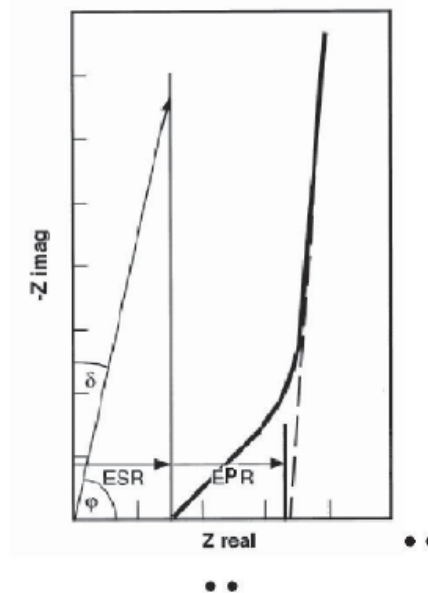


Fig. 3.9 EIS Nyquist plot of supercapacitor

B. Model development of single supercapacitor

(1) Simplified model

In the experiment and the model parameters extraction process, the least squares method is used to minimize the error between the proposed model and the experiment results. When the error is minimized, the parameters to get the minimization are the model parameters.

The detailed process is shown in Fig. 3.10,

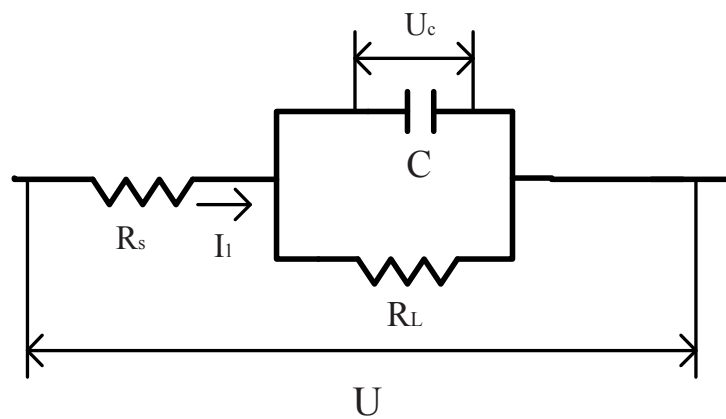


Fig. 3.10 Simplest electric model

Based on the model shown in Fig. 3.10, the equations of the model can be carried out according to the Kirchhoff theory,

$$U(t) = I_1(t)R_s + U_c(t) \quad (3.8)$$

$$I_1(t) = \frac{U_c(t)}{R_L} + C \frac{dU_c(t)}{dt} \quad (3.9)$$

From the equations, we could get the relationship between $U(t)$ and $I_1(t)$, that is $U(t) = f(I_1(t))$, $U(t)$ is the function of $I_1(t)$.

(2) Four-order T-style model

A more complicated model for the supercapacitor is four-order T-style RC network shown in Fig. 3.11. As far as the charging model, the four capacitors are C_{1c} , C_{2c} , C_{3c} , C_{4c} , whose

charge/discharge time constant are $R_{1c} C_{1c}$, $(R_{1c} + R_{2c}) C_{2c}$, $(R_{1c} + R_{2c} + R_{3c}) C_{3c}$, $(R_{1c} + R_{2c} + R_{3c} + R_{4c}) C_{4c}$, the left one is smaller than right one, $R_{1c} C_{1c} \ll (R_{1c} + R_{2c}) C_{2c} \ll (R_{1c} + R_{2c} + R_{3c}) C_{3c} \ll (R_{1c} + R_{2c} + R_{3c} + R_{4c}) C_{4c}$. Therefore, the terminal voltage of the supercapacitor is changed by the different capacitor in different time. During charge process, terminal voltage varies nonlinearly and is decided by $R_{1c}C_{1c}$ and $R_{2c}C_{2c}$ branches. $R_{3c}C_{3c}$ mainly affects the change of terminal voltage during less than 100 seconds after power source is off. $R_{4c}C_{4c}$ mainly affects the equivalent model after 100 seconds since power off. R_L mainly affects the change of terminal voltage during half an hour to two hours after power is off.

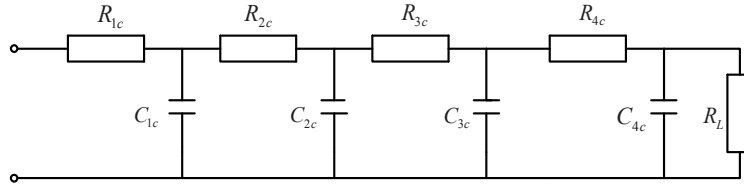


Fig. 3.11 Equivalent charge circuit model

The equations of the model and model parameters identification are presented as follows. At the moment of charge power is on, it appears a jump in the terminal voltage for capacitor. There is a jump in the terminal voltage for capacitor because a voltage drop for the charge current I_C across R_{1c} . Let the jump of terminal voltage across capacitor in the moment of charge power is on is ΔV_0 , then

$$R_{1c} = \frac{\Delta V_0}{I_C} \quad (3.9)$$

Assuming the terminal voltage is $V_1 \sim V_5$ respectively in $t_1 \sim t_5$, in the 15 seconds charging period.

Voltage on C_{1c} in the five different time is

$$V_{C_{1c},i} = V_i - I_C R_{1c} \quad (i = 1, 2, 3, 4, 5) \quad (3.10)$$

Assuming the terminal voltage for supercapacitor before charge is V_s ,

$$(C_{1c} + C_{2c})(V_{C_{1,i}} - V_S) - I_C t_i = (I_C - C_{1c} \left. \frac{dV_{C1}}{dt} \right|_{t=t_i}) R_{2c} C_{1c} \quad (i = 2, 3, 4) \quad (3.11)$$

Assuming the terminal voltage is $V_6 \sim V_{11}$ respectively in $t_6 \sim t_{11}$ when the power is off more than 50 seconds. It is considered that the six value of $V_6 \sim V_{11}$ decrease little by little in the six moments.

$$i_{C_{1,i}} = C_{1c} \left. \frac{dV_{C1}}{dt} \right|_{t=t_i} \approx C_{1c} \frac{V_{i-1} - V_{i+1}}{t_{i+1} - t_{i-1}} \quad (i = 7, 8, 9, 10) \quad (3.12)$$

$$V_{C_{2,i}} \approx V_{C_{1,i}} - i_{C_{1,i}} R_{2c} \quad (i = 7, 8, 9, 10) \quad (3.13)$$

At $t=t_8, t_9$, the current of C_{2c} and R_{3c} are

$$i_{C_{2,i}} = C_{2c} \left. \frac{dV_{C2}}{dt} \right|_{t=t_i} \approx C_{2c} \frac{V_{C_{2,i-1}} - V_{C_{2,i+1}}}{t_{i+1} - t_{i-1}} \quad (i = 8, 9) \quad (3.14)$$

$$i_{R_{3,i}} = i_{C_{1,i}} + i_{C_{2,i}} \quad (i = 8, 9) \quad (3.15)$$

$$R_{3c} i_{R_{3,8}} + V_{C_{3,8}} = V_{C_{2,8}} \quad (3.16)$$

$$R_{3c} i_{R_{3,9}} + V_{C_{3,9}} = V_{C_{2,9}} \quad (3.17)$$

Assuming pulse charge time is t_c , according to charge conservation law

$$\Delta Q_{C_{3,i}} \approx I_C t_C - C_{1c} (V_{C_{1,i}} - V_S) + C_{2c} (V_{C_{2,i}} - V_S) \quad (3.18)$$

$$R_{3c} = \frac{(V_{C_{2,8}} - V_S) \Delta Q_{C_{3,9}} - (V_{C_{2,9}} - V_S) \Delta Q_{C_{3,8}}}{i_{R_{3,8}} \Delta Q_{C_{3,9}} - i_{R_{3,9}} \Delta Q_{C_{3,8}}} \quad (3.19)$$

$$C_{3c} = \frac{i_{R_{3,9}} \Delta Q_{C_{3,8}} - i_{R_{3,8}} \Delta Q_{C_{3,9}}}{(V_{C_{2,8}} - V_S) i_{R_{3,9}} - (V_{C_{2,9}} - V_S) i_{R_{3,8}}} \quad (3.20)$$

After charge power off half an hour, terminal voltage of capacitor C_{1c} is V_E ,

$$(C_{1c} + C_{2c} + C_{3c} + C_{4c})(V_E - V_S) = I_C t_C \quad (3.21)$$

$$C_{4c} = \frac{I_C t_C}{V_E - V_S} - C_{1c} - C_{2c} - C_{3c} \quad (3.22)$$

R_L mainly affects the change of terminal voltage during half an hour to two hours after charge power off. During this period, four capacitor discharge through R_L slowly. The terminal voltage of capacitor is V_E after half an hour since power off.

$$V_F = V_E e^{-5400 / (R_L (C_{1c} + C_{2c} + C_{3c} + C_{4c}))} \quad (3.23)$$

$$R_L = \frac{5400}{(C_{1c} + C_{2c} + C_{3c} + C_{4c}) \ln(V_E / V_F)} \quad (3.24)$$

3.4 Balancing Circuit Development for Energy Storage System

In multi-cell batteries or supercapacitors, because of the large number of cells used, we can expect that they will be subject to a higher failure rate than single cell batteries. The more cells used, the greater the opportunities to fail and the worse the reliability.

Because of the discrepancy in operating characteristics due to internal and external sources among individual cells in the bank, the residual capacities before recharging or the restored capacities during charging may not be the same.

The major internal sources are manufacturing variance in charge storage volume, variation in internal impedance, and differences in self-discharge rate. The external sources can be some multi-rank pack protection ICs, which drain charge unequally, differential loading of ranks with the pack, the thermal difference across the pack results in different self-discharge rates. The self-discharge rate approximately doubles with every 10°C rise in cell temperature, and thus good thermal design of the host equipment thoughtful location of the module (battery pack) can obviously minimize this effect.

Energy storage cells such as those used for EV and HEV applications are made up from long strings of cells in series in order to achieve higher operating voltages of 200 to 300 volts or more and are particularly vulnerable. The problems can be compounded if parallel packs of cells are required to achieve the desired capacity or power levels. With a battery made up from n cells, the failure rate for the battery will be n times the failure rate of the individual cells.

All cells are not created equal. The potential failure rate is even worse than this however due to the possibility of interactions between the cells. Because of production tolerances, uneven

temperature distribution and differences in the ageing characteristics of particular cells, it is possible that individual cells in a series chain could become overstressed leading to premature failure of the cell. During the charging cycle, if there is a degraded cell in the chain with a diminished capacity, there is a danger that once it has reached its full charge it will be subject to overcharging until the rest of the cells in the chain reach their full charge. The result is temperature and pressure build up and possible damage to the cell. With every charge-discharge cycle the weaker cells will get weaker until the battery fails. During discharging, the weakest cell will have the greatest depth of discharge and will tend to fail before the others. It is even possible for the voltage on the weaker cells to be reversed as they become fully discharged before the rest of the cells also resulting in early failure of the cell. Various methods of cell balancing have been developed to address this problem by equalising the stress on the cells.

The first approach to solving this problem should be to avoid it if possible through cell selection. Batteries should be constructed from matched cells, preferably from the same manufacturing batch. Testing can be employed to classify and select cells into groups with tighter tolerance spreads to minimise variability within groups.

Another important avoidance action is to ensure at all times an even temperature distribution across all cells in the battery. Note that in an EV or HEV passenger car application, the ambient temperature in the engine compartment, the passenger compartment and the boot or trunk can be significantly different and dispersing the cells throughout the vehicle to spread the mechanical load can give rise to unbalanced thermal operating conditions. On the other hand, if the cells are concentrated in one large block, the outer cells in contact with ambient air may run cooler than the inner cells which are surrounded by warmer cells unless steps are taken to provide an air (or other coolant) flow to remove heat from the hotter cells. After cell selection, equalising the temperature across the battery pack should be the first design consideration in order to minimise the need for cell balancing.

To provide a dynamic solution to this problem which takes into account the ageing and operating conditions of the cells, the Battery Management System (BMS) may incorporate a cell

balancing scheme to prevent individual cells from becoming overstressed. These systems monitor the State of Charge (SOC) of each cell, or for less critical, low cost applications, simply the voltage across each cell in the chain. Switching circuits then control the charge applied to each individual cell in the chain during the charging process to equalise the charge on all the cells in the pack. In automotive applications the system must be designed to cope with the repetitive high energy charging pulses such as those from regenerative braking as well as the normal trickle charging process.

Several Cell Balancing schemes have been proposed and there are trade-offs between the charging times, efficiency losses and the cost of components.

In this part of the research, the current version of cell balancer is designed for use with supercapacitors. When the battery storage bank is developed in the future, the same principle can be applied to the battery bank and the circuit can also be used for the battery cell balancer. Supercapacitors and batteries can be made for the hybrid energy storage system for EVs or HEVs.

3.4.1 Supercapacitor cell voltage balancing necessity

Supercapacitors, not like batteries, are a novel energy storage device based on the principle of the double layer-electrolyte capacity, which has many merits such as long lifetime, high efficiency and fast dynamic response. So it is a power storage technology that has a bright future in power storage development. Supercapacitors are used for storing energy which the electromotor generates and brakes energy when the load is falling; the supercapacitors release the energy which has been stored when the load is rising. Thus the original energy which is consumed by the braking resistance is recycled totally, then the purpose of energy saving and environment protection is realized [3.32].

Due to the lower voltage of a single supercapacitor, generally speaking, the series and parallel connection of supercapacitors from the energy storage module meet the energy storage capacity and higher voltage requirement. Series connection of supercapacitor cells leads to cell-voltage

imbalance because of differing individual cell properties that occur due to limitations in the manufacturing process, such as capacitance, internal resistance, self-discharge rate, and environmental conditions. Equalization techniques are usually employed to eliminate such an imbalance.

There are two main ways to achieve the balancing; passive and active balancing. The passive balancing methods remove the excess charge from the fully charged cells through passive, resistor, element until the charge matches those of the lower cells in the pack or charge reference. The resistor element will be either in fixed mode or switched according to the systems as described in [3.33-3.37]. The active cell balancing methods remove charge from higher energy cells and deliver it to lower energy cells. This study compares the several proposed balancing methods from different viewpoints and, as well, simulates some balancing methods and provides a conclusion.

3.4.2 Equalization scheme types

There are generally four existing equalization schemes: dissipative, capacitive shuttling balancing, inductor/transformer balancing and energy converter balancing methods. Dissipative methods of equalization such as the switched resistor or zener clamp methods described in [3.38] and shown in Fig 3.12, are perceived to be too inefficient except for low budget systems and will not be analysed here. Capacitive cell balancing, also known as “Charge Shuttling” equalization [3.39]-[3.45], utilises basically external energy storage devices, capacitor(s) for shuttling the energy between the pack cells so as to achieve the balancing. There are a number of coupled coil equalization schemes presented in literature (in [3.46]-[3.48]) and these usually offer advantages in sensor reduction and sometimes switching device number. The drawback of these converters is that they use on-standard multi-winding transformers which have to be made bespoke to the system – they are not widely available components. The principle of dc/dc converters is to transfer energy from the higher voltage cell to the lower voltage cell or to the whole stack with less power loss. Most of them employ a large-scale voltage detection network to help find the higher voltage cell and the lower voltage cell. Fig. 3.13(a) shows an equalization

circuit of this type [3.49]. A type of equalizer based on the flyback converter and the inductor coupling structure, as shown in Fig. 3.13(b), has been studied because it needs no voltage detection [3.50]-[3.51]. There is also a modular structure equalization scheme [3.52]-[3.53] that can simplify the control algorithm, as shown in Fig. 3.13(c), where only the nearest two cells are voltage compared and energy transferred. This circuit should have a long equalizations time because the energy-transfer route is not global; therefore, it is not suited for high-power application.

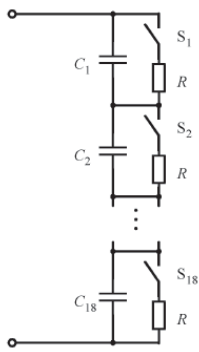


Fig. 3.12 Cell equalization circuit using switched resistor.

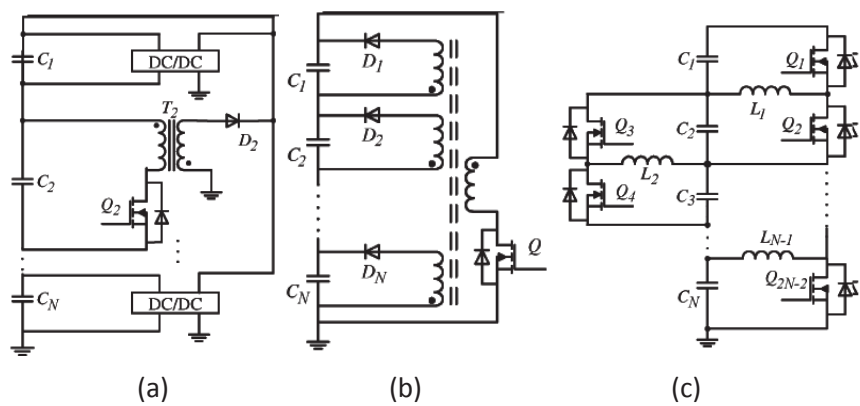


Fig. 3.13 (a) Typical flyback-converter-based equalize, (b) Inductor coupling flyback-converter-based equalizer, and (c) Buck-boost-based modular current divider.

3.4.3 Supercapacitor cell voltage balancing methods comparison

A. Switched capacitor based on the Cockcroft-Walton scheme

Equalization circuit composed of supercapacitors C_1 - C_6 , a voltage source V , a resistance R and bidirectional switches S_{a1} - S_{a5} and S_{b1} - S_{b5} as described in [3.54] is shown in Fig. 3.14. When S_V is ON and S_R is OFF, the system is charged by the voltage source V . When S_V is OFF and S_R is ON, the system supplies the power to the resistance R . While the system is charged it takes two states, which are shown in Fig. 3.15. In state 1, S_a is on and S_b is off as shown in Fig. 3.15(a). In state 2, S_a is off and S_b is on as shown in Fig. 3.15(b). Fig. 3.16 is the MOSFETs composed of bidirectional switches.

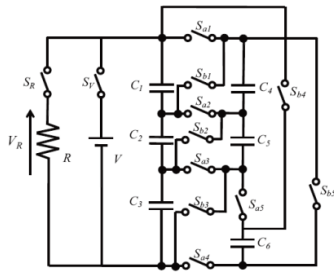
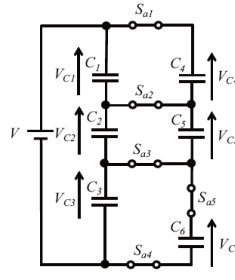
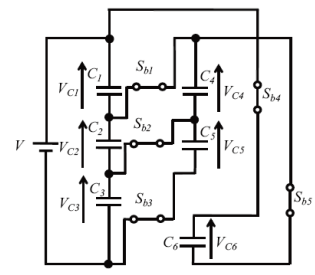


Fig. 3.14 Equalization using MOSFET to achieve the balancing.



(a)



(b)

Fig. 3.15 Equivalent circuit of the proposed cell voltage equalizer: (a) state 1: Sa is ON and Sb is OFF, (b) state 2: Sa is OFF and Sb is ON.

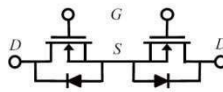


Fig. 3.16 Bidirectional switch

State 1 and state 2 appear one after another by switching S_a and S_b . Switching pulses are with 50% duty cycle. Repeating turning on S_a and S_b , all of the supercapacitor's voltages become equal.

Fig. 3.17 is the equalization circuit diagram established in PSIM simulation software; in this simulation, the switching frequency is 1kHz, and the capacitance of supercapacitor is 120F, the initial voltages of C_1 , C_2 and C_6 are 1.5V, 2V and 3V. When the supercapacitors meet the same voltage level in about 50 seconds, the S_R is turned on, the resistor is 6 Ω ; we could see equalization acts very well at the same time when the supercapacitors are discharging. After discharging for 50 seconds, the S_V is connected again, we could see the system can achieve equalization very quickly, in about 10 seconds. Fig. 3.18 is the simulation results of this method; this simulation results show that the equalization time for 6 cells is about 50 seconds, so the topology is not good for a great number of supercapacitors connected in series, because the equalization is achieved through transferring energy between every adjacent supercapacitor, it will take a considerable time to get the whole system balancing. The simplicity in control method and lack of magnetic components are the main advantages of this balancing method, and it is effective in making cell voltages equal and does not include resistive components generating heat.

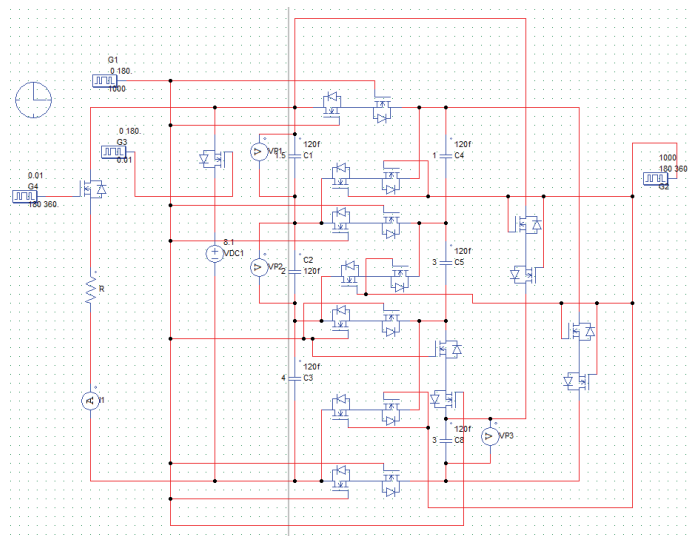


Fig. 3.17 Circuit diagram of cell balancing circuit using Switched capacitor based on the Cockcroft-Walton scheme

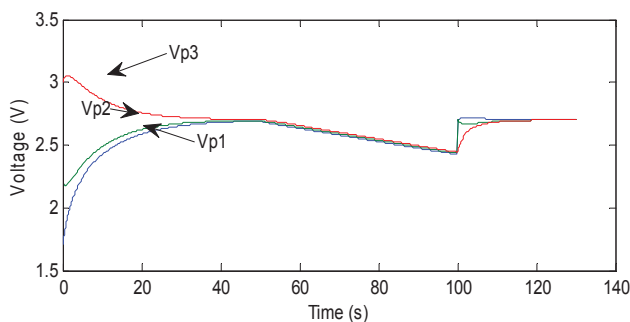


Fig. 3.18 Simulation results of the voltage waveform using switched capacitor based on the Cockcroft-Walton scheme

B. Switchless voltage equalizer

A switchless voltage equalizer for three series-connected SCs as described in [3.55] and as shown in Fig. 3.19 operates as a charger with an equalization function; the charge is provided by an AC power source. Two series-stacked diodes are connected to each SC and the junctions of stacked diodes are connected to the ac power source via energy transfer capacitors C1--C3. The advantages of this equalizer are it consists of passive components only, resulting in reduced circuit complexity, improved reliability and good modularity. The drawback of this circuit is the equalization speed is still slow.

Fig. 3.20 shows the equalizer operates in two modes; each SC can be charged to a uniform voltage level by the ac power source. In mode A, odd-numbered diodes are turned on and C1--C3 are charged by the ac power source and SC1-SC2. In mode B, C1-C3 are discharged to the SCs via even-numbered diodes.

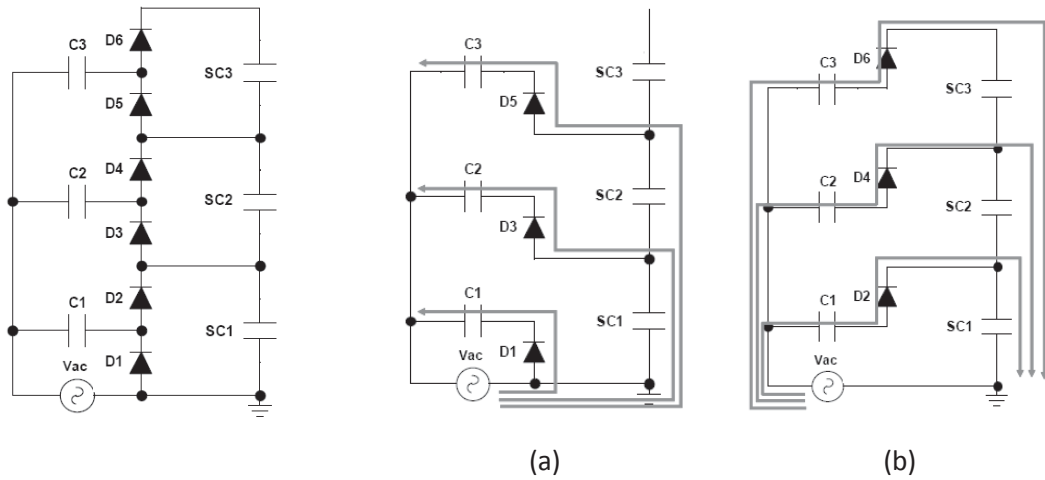


Fig. 3.19 Switchless cell voltage equalizer

Fig. 3.20 Current flow direction in (a) mode A and (b) mode B

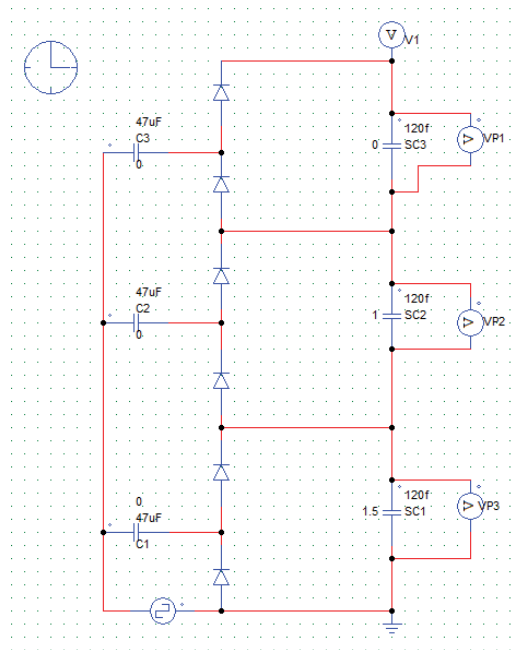


Fig. 3.21 Circuit diagram of cell balancing circuit using switchless voltage equalizer

Fig. 3.21 is the equalization circuit diagram established in PSIM simulation software, in the simulation, the ac voltage for the equalizer is peak amplitude 2V and is provided by a 60Hz

utility power via a transformer, three supercapacitor modules with 120F are connected in series and from an initially voltage-imbalanced condition with 0V, 1V and 1.5V, respectively, all electrolytic capacitors having capacitance of $470\mu\text{F}$ each were used for C1--C3.

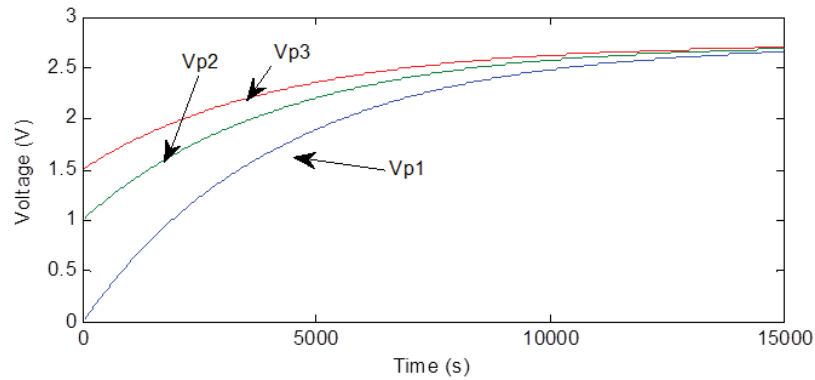


Fig. 3.22 Simulation results of the voltage waveform using switchless voltage equalizer

Fig. 3.22 is the simulation results of the voltage waveform, it can be seen the equalization speed is very slow, three supercapacitors take about 3 hours to achieve the equalization. The main advantage of this circuit is that the structure is quite simple and the components for each supercapacitor are fewer than the other kinds of topology. From the analysis, the simplicity in control and lack of magnetic components cannot outweigh this scheme's lack of suitability to a high power charging/discharging energy storage system.

C. Cell balancing circuit using transformer

This cell balancing circuit method using transformer as described in [3.56] applies the fact that the voltages are the same if each transformer tap has the same turns ratio to the cell balancing circuit. The charger is provided from the EV, and the charger is ac power supply 2.7V, the switched transformers sharing the same primary side, and the same turns of secondary side in order for the supercapacitor cells to have same charging voltage. Every supercapacitor connects a rectifier to charge it since the current from transformers is ac current. The disadvantages of this kind of circuit using transformers are this circuit is heavy and voluminous for the iron core of the transformer, and another disadvantage is the current should be controlled under the specification for preventing from burning of transformer coils or rectifier circuit.

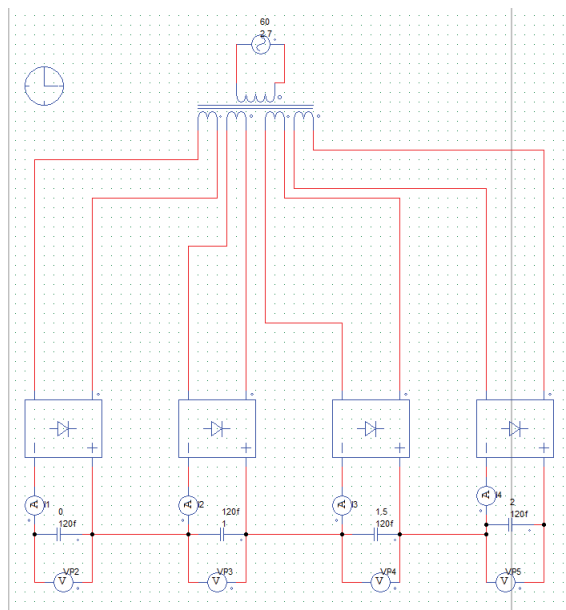


Fig. 3.23 Circuit diagram of cell balancing circuit using transformer

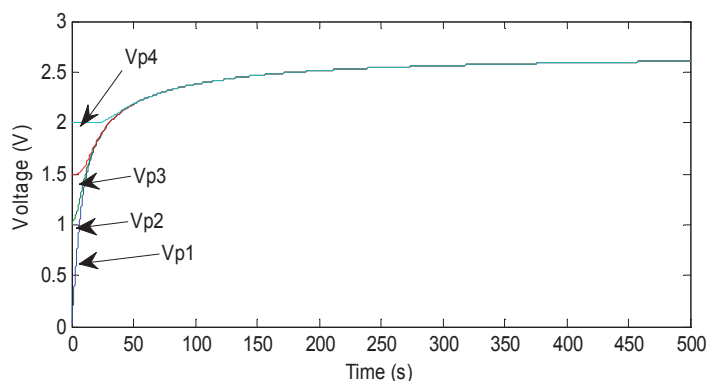


Fig. 3.24 Simulation results of the voltage waveform using transformer

Fig. 3.23 is the equalization circuit diagram established using PSIM simulation software; in this simulation, four 120F supercapacitors are connected in series, and the initial voltages of supercapacitor are 0V, 1V, 1.5V and 2V, respectively, the ac power supply is 2.7V, all supercapacitors connect with a voltage measurement and a current measurement so we could see the diversification of the current and the voltages of each supercapacitor.

Fig. 3.24 is the simulation results of the voltage waveform; it can be seen that the balancing speed is quicker than the former two methods, the four supercapacitors take about 50 seconds to achieve the same voltage, but it is still slow, it takes more than 500 seconds to get the final

voltage (2.7V). This balancing circuit is also designed for charging balancing; if we could solve the former problems, this balancing method is a very effective method for cell balancing.

3.4.4 Novel balancing circuit development for supercapacitor storage bank

Based on the comparison and discussion in the last section, a novel balancing circuit is developed for the supercapacitor bank. This section contains the detailed balancer circuit description, balancer operation and cell voltage measurement.

In the novel balancing circuit development, each cell has a flyback switched mode power supply (SMPS) connected across it with the output feeding energy to the whole supercapacitor bank. Only overvoltage cells are discharged and many such cell can be discharged simultaneously. The discharge power can be as high as required and is proportional to cell voltage so equalisation is fast. The excess cell energy goes directly to the whole supercapacitor bank from each SMPS so multiple SMPS efficiencies are not cascaded.

The disadvantages are increased cost, complexity and size with one SMPS transformer per cell. Performance may be judged by the time taken to discharge an overvoltage of 100mV. In this cell bank there are forty five 120F supercapacitors in parallel per cell (5400F), the SMPS draws 20W at 2.7V and the time required to achieve balance is 73 seconds.

The rate of discharge (1.37mV/second) is independent of the actual cell voltage: the discharge is in a straight line, not exponential decay.

The current version of cell balancer is designed for use with supercapacitors rather than battery cells but the same principle applies. When the battery storage bank is developed in the future, the circuit can also be used for the battery cell balancer. There are two major differences between supercapacitor bank and battery bank:

- (1) A supercapacitor bank is meant for short term energy storage and so has less capacity than a battery.

(2) The supercapacitor is essentially a capacitor, it must operate over at least a two to one voltage range if 75% of the stored energy is to be accessible and three to one if 90% is to be achieved as shown in Fig. 3.25. Compare this to the Leaf battery voltage range of 4.2V to 2.5V (1.66 range) for 100% of its accessible energy.

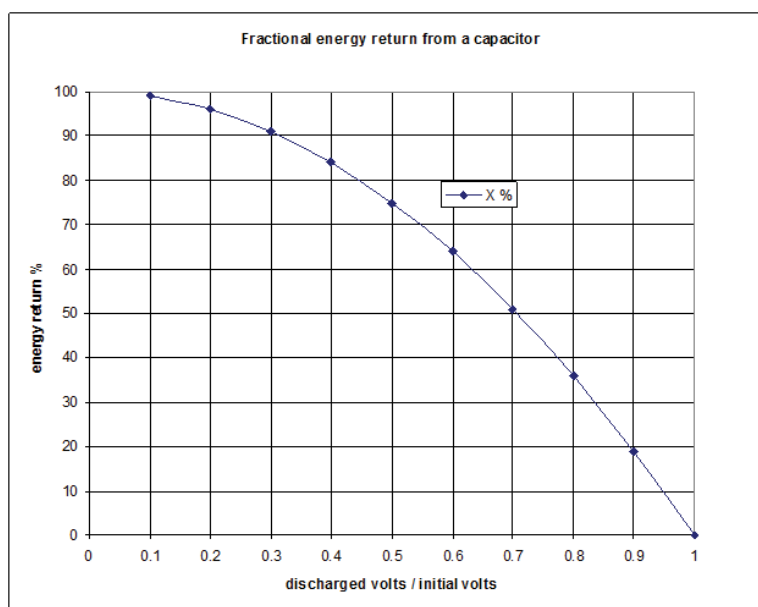


Fig. 3.25 Energy recovery for a capacitor versus depth of discharge

A. Cell balancer operation

Because the cell balancer is to be used in a research environment, individual cell voltage monitoring is included as an electrically separate but physically integrated part of the equipment. The block diagram is thus presented in two parts, the first being for the voltage monitoring circuit is shown in Fig. 3.26 and the second of the cell balancer is shown in Fig. 3.27.

The cell balancing is performed by independent transformer coupled SMPS, one per cell consisting of a number of paralleled supercapacitors. These flyback SMPS continuously and independently discharge overvoltage cells down to the average cell voltage in the bank. The energy so obtained is transformed up to the cell bank voltage and used to recharge all cells in series. Thus this system strongly discharges overvoltage cells, rather than strongly recharging under voltage ones.

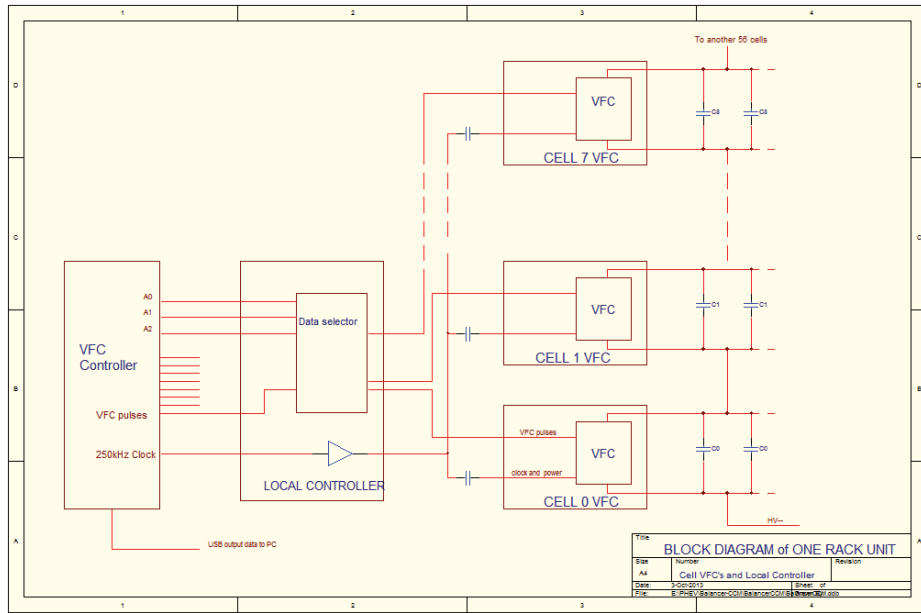


Fig. 3.26 Voltage monitoring circuit diagram

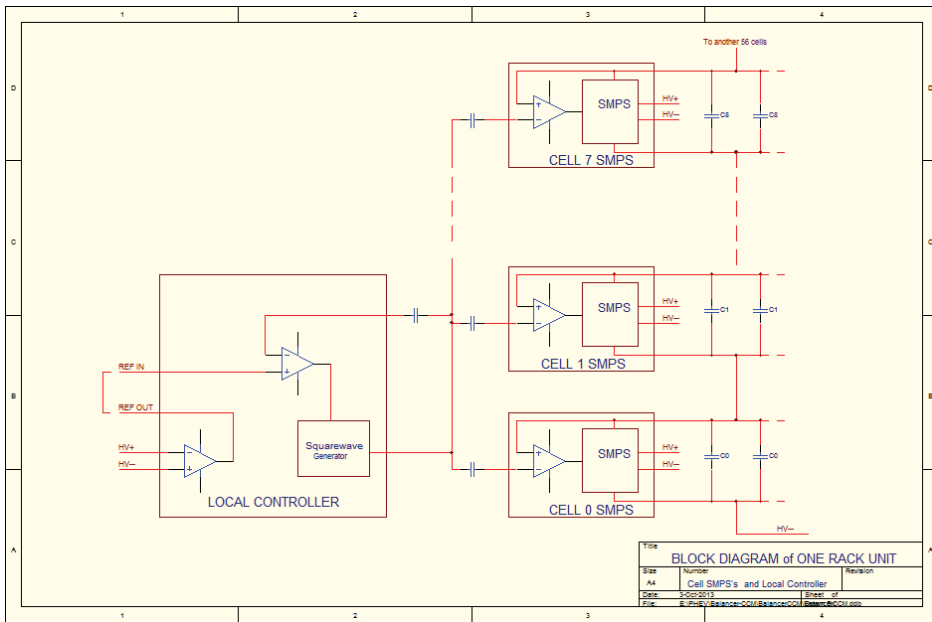


Fig. 3.27 Cell balancer diagram

The SMPS are controlled locally by comparing the local cell voltage to the average cell voltage, which is fed to them via a capacitively coupled square wave from a remotely located bank voltage monitoring circuit. This same square wave also powers the SMPS control circuitry. Each cell balancer includes an optocoupler which drives a remote monitoring LED so that the

operator can see which cells are more frequently going into discharge and hence may be in need of attention.

Currently, one local controller is required for each group of eight cells. Thus for 64 cells in series there is a requirement for eight controllers. The PCBAs have been built so that a controller and its eight associated cells fit in one rack unit tray and the eight trays fit one above the other into a standard 2m high rack frame.

Theoretically, one controller could control all 64 cells if it were designed for rather higher DRIVE-signal output power but the present system allows each set of eight to be tested independently.

The controllers are locally powered from the cells in the same rack unit and hence, as long there is enough charge, the cell balancer system continues to operate even when the cell bank is isolated from the rest of the PHEV Test Bed.

B. Cell voltage monitoring

Cell voltage monitoring is performed by a voltage to frequency converter IC on the same PCBA as the SMPS and the cells to be monitored. It is fed a capacitively coupled square wave which provides both voltage to frequency converters (VFC) clock and power for all the VFC's in the rack unit. The pulse outputs from the eight VFCs are coupled capacitively back to the controller where external address signals control which VFC pulse stream is delivered to an external VFC counter/controller (yet to be built) to be converted back to a voltage for use by some external Test Bed control system.

C. Detailed circuit description

(1) Cell discharger SMPS

The cell discharger may be divided into the SMPS itself, the comparator which turns the SMPS on when the cell voltage is above the reference voltage, the optocoupler which drives a LED telltale on the front panel and the isolated power supply which provides start-up power to the

cell SMPS. The cell PCBAs are built with two sets of connectors and cell fuse holders so that they may be mounted either way up. This allows the cells to be easily connected in series via high current (500A) M6 threaded 12mm diameter aluminium posts which are installed in the middle of the PCBA top edge. Fig. 3.28 shows the cell balancer SMPS and VFC.

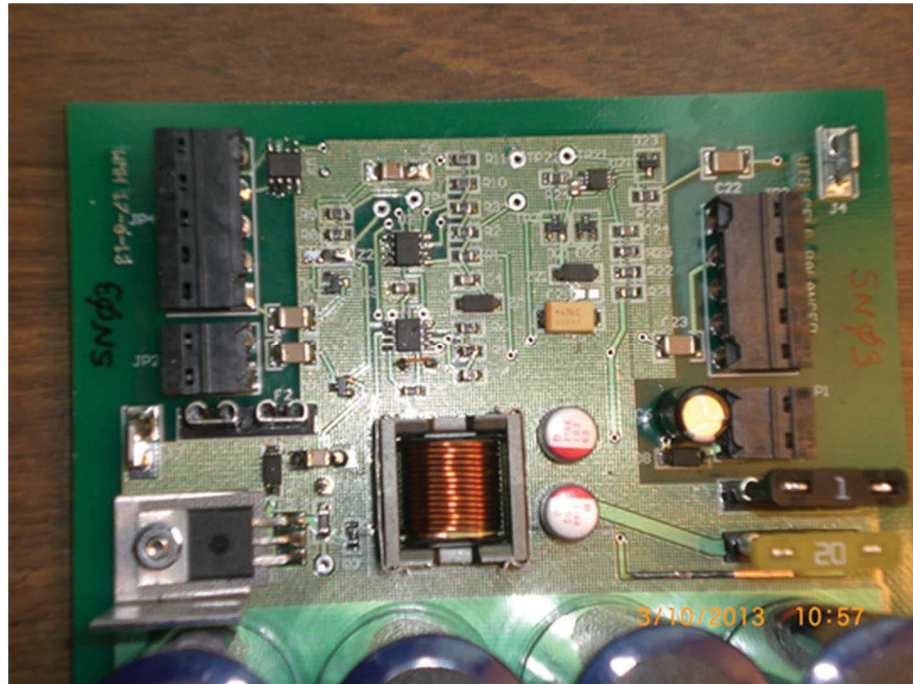


Fig. 3.28 Cell Balancer SMPS and VFC

(2) Isolated power, comparator and optocoupler

A 35kHz square wave generated by the controller at up to 24V_{pp} is capacitively coupled to each cell PCBA. This provides the minimum 8V supply voltage required by the SMPS IC (U1: HV9910) as well as, by dividing down at R8/R9, the reference cell voltage which is compared to the local voltage at R1 by the comparator U2b. If the local voltage is higher, the comparator output voltage goes high, turning on U1, the optocoupler diode and the discharge process.

(3) SMPS and overvoltage protection

U1 is a hysteretic SMPS controller which senses T1 inductor current at R12 and turns Q1 MOSFET off when the R12 voltage reaches a value set by the voltage at U1/pin7. T1 steps the resulting inductor voltage up to feed power into the high voltage output which connects across

the entire bank of cells. The energy in T1 leakage inductance is harvested by D7 and used to boost the raw supply voltage at U1/pin1 and C3. Should the high voltage output become disconnected from its load, the voltage at C3 rises to the point where Z2 turns on and causes the reference voltage to exceed the local cell voltage, at which point U2b turns the SMPS off, protecting the SMPS components Q1, C6 and D8.

(4) Cell discharger local controller

The controller shown in Fig. 3.29 is comprised of a differential amplifier, which samples the total cell bank voltage to provide an average cell voltage at REF OUT, and a REF IN-controlled square wave generator which provides the DRIVE signal to the capacitors feeding the reference voltage to the SMPS stages. Separately there is a demultiplexer which selects which VFC output to feed to the remote VFC Controller/counter, the VFC clock/power signal generator and interfaces between the local controller and the cells, remote VFC Controller and a front panel LED display. There are also two power supplies, one to provide 24V using the variable output from seven series cells and another to provide a negative supply locally.

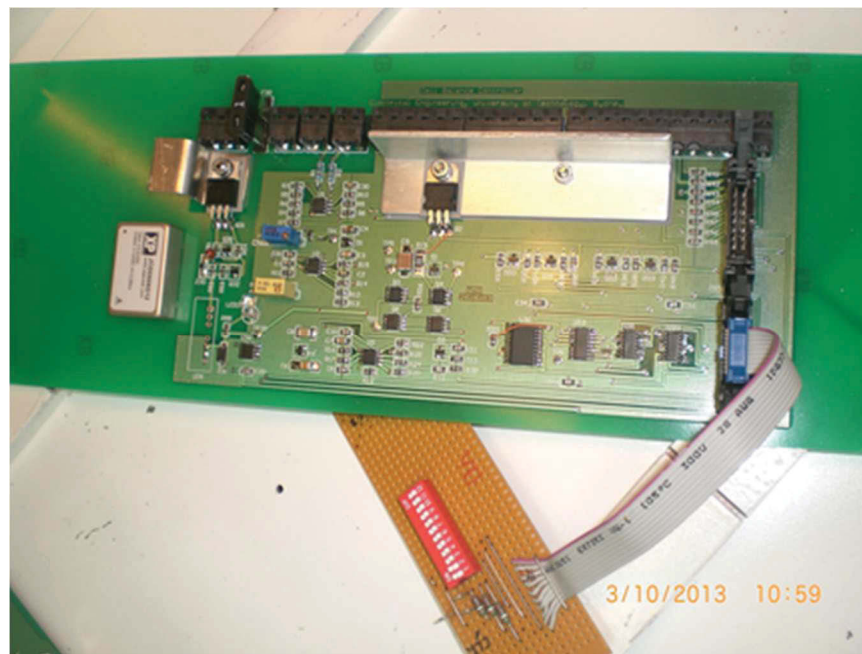


Fig. 3.29 Local controller with dummy VFC Controller plugged into J32

(5) Differential amplifier

U1b reads the DC voltage across the cell bank and U1a subtracts the high voltage common mode signal from what U1b sees. U1b output is filtered at C1 and scaled by POT2 to produce REF OUT at U2a output which may be used to feed directly to REF IN. There is a connection to POT2, available on J33, to allow a front panel potentiometer to be fitted which would allow more convenient adjustment of the reference voltage. The REF OUT front panel output may be fed directly to REF IN. Alternatively, any REF OUT signal may be used to feed the same signal to all controller REF IN inputs in parallel.

(6) Drive generator

U3b generates a 35 kHz square wave to drive Q3 to Q6 output stage which produces the DRIVE power and reference signal capacitively coupled to all eight SMPS. U3a controls Q2 and hence the supply volts fed to Q3 to Q6 and the amplitude of DRIVE. U3a inputs compare REF IN with the output from a rectifier/filter network which is identical to those feeding the SMPS comparators and so the SMPS comparator reference signals should all match REF IN closely. A green front panel LED is powered by the DRIVE signal and gives an indication of the DRIVE amplitude.

(7) LED display

Each cell SMPS has an optocoupler output which controls its own orange LED on the front panel, indicating when the SMPS is functioning. Thus it is possible to see if any cell units are going overvoltage too often or too long. Fig. 3.30 shows the LED display box. There is also a green LED to monitor the DRIVE level (and hence the average cell voltage). Two BNC connectors allow the local average cell voltage to either be fed in or fed out as required.

(8) Power supplies

A DC to DC converter with internal high voltage isolation provides 24V to run the controller. There is a voltage limiting circuit feeding this converter because its input is only rated at 9V yet

it needs to be fed from seven cell stages in series which results in an input voltage between 6V and 21V (or more).

U2b oscillates at about 3kHz to produce a negative voltage to supply the differential amplifier.



Fig. 3.30 Front panel LED display

D. VFC cell voltage measurement

(1) VFC demultiplexer, VFC clock and power

A 250kHz clock signal, supplied externally from the VFC Controller, is buffered in U30 and capacitively coupled to all cell VFCs to provide both clock and local power supply. The VFC outputs are fed to U32 to be demultiplexed under the control of address signals A0, A1, A2 provided from the VFC Controller via J32. The chosen signal is fed to the VFC Controller, to be counted and fed, probably via a USB port, to some external computer for use by researchers.

(2) Calibration

The VFC IC (U21 AD7740) is operated with an externally provided clock which eliminates one source of error; however the voltage divider chain R21, R22, R25 tolerance error and the VFC offset voltage (+-7mV typical, +- 35mV max) need to be addressed. One solution is to measure

the output of each of the 64 VFCs individually at two known voltages and store span and zero errors in software. This could be done conveniently under software control while constructing the PCBAs, by connecting all the stages in parallel with appropriate known voltages. Alternatively, accept the errors implied by the data sheet zero error together with the likely 1% error in the divider chain. (Alternatively, hand select the divider resistors).

(3) Cabling

Six cables connect to the local controller. A two wire cable connects to quick-connect connectors present on the lowest and highest cell PCBAs to feed seven cell's worth of voltage at J34 to provide power for the local controller. The three other two-wire cables connect the controller and its eight cells' high voltage inputs in parallel and to the cell bank high voltage.

Because each alternate PCBA has to be fitted inverted, the connectors alternate from one side of the rack unit to the other and there are two high voltage cables each connecting four cells. For the same reason there are two cables connecting the DRIVE/VFC/optocoupler outputs to the controller. Cells are numbered 0 though to 7 starting from the front (nearest the LED panel) and one cable connects to cells 0,2,4,6 and the other to cells 1,3,5,7.

(4) VFC controller

A tentative circuit has been drawn up for this controller for further research. It has been assumed that it should simply present any of the 64 cell voltages on demand via a USB connection to some external computer and that it should devote itself at other times to continuously refreshing its stored cell voltages.

E. Time to rebalance a single stage by 100mV at any voltage

The speed of discharge in volts/sec is theoretically constant irrespective of cell voltage.

$$E = \frac{CV^2}{2} \tag{3.25}$$

$$P = kV \tag{3.26}$$

$$\frac{\partial E}{\partial V} = CV \quad (3.27)$$

$$\frac{\partial V}{\partial E} = \frac{1}{CV} \quad (3.28)$$

$$\frac{\partial V}{\partial t} = \frac{\partial E}{\partial t} \times \frac{\partial V}{\partial E} = kV \times \frac{1}{CV} = \frac{k}{C} \quad (3.29)$$

Here $k = 20\text{W}/2.7\text{V} = 7.4 \text{ W/V}$ and $C = 5400\text{F}$, hence $dV/dt = 1.37 \text{ mV/s}$

In section 3.5, the performance of testing cell balancer will be carried out and further work needing to be done will be illustrated.

3.5 Numerical Simulations and Experimental Test

To develop the energy storage system used for the EVs, numerical simulations and experimental verifications were carried out. In order to get the model of the battery and supercapacitors, different batteries and supercapacitors were chosen. A test bench was also implemented. This part presents the characteristics and testing performance of battery and supercapacitor. By focusing on studying and verifying the characteristics, the experiments were performed in very narrow confines.

3.5.1 Supercapacitor experimental test

The experimental testing performance is first carried out for the model development in this part. The supercapacitor cell used in the EV project in our Laboratory is the 120F supercapacitor from Jinzhou Kaimei Power Co. as shown in Fig.3.31.

A. Experimental test circuit diagram

Fig. 3.32-3.34 show the test circuit diagram of the supercapacitor. Fig. 3.32 is the charge circuit for the supercapacitor, the voltage of the supercapacitor is measured by the voltmeter and through Labview software to collect voltage data to PC. Fig. 3.33 is the self discharge circuit for the supercapacitor, same voltage measurement applies. Fig. 3.34 is the discharge circuit of supercapacitor which uses 1.96Ω load. When supercapacitors are charged to full capacity, the

load is connected to the cell and the voltage data collected in the PC to get the experimental results.



Fig. 3.31 Supercapacitor from Jinzhou Kaimei Power Co.

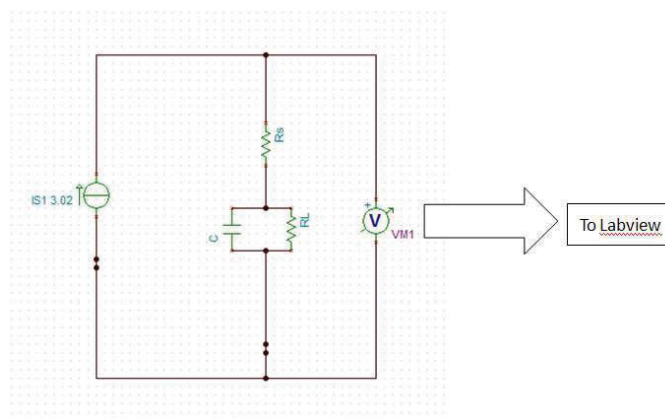


Fig. 3.32 The charge circuit for supercapacitor

B. Experimental test bench set up

Fig. 3.35-3.42 show the experimental test bench setup for the supercapacitor; there are two power supplies, current sensor, DAQ board and Labview software to collect supercapacitor cell information. The whole test bench is shown in Fig. 3.42.

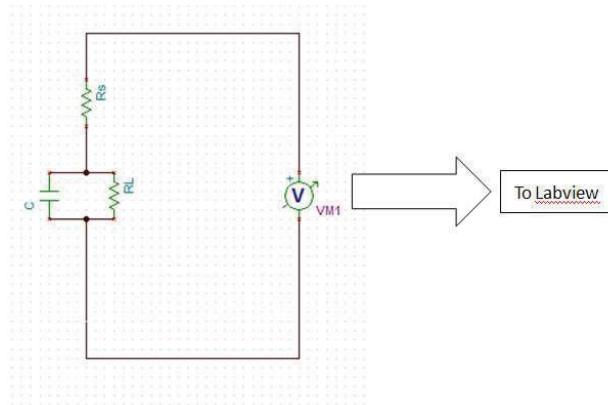


Fig. 3.33 The self-discharge circuit for supercapacitor

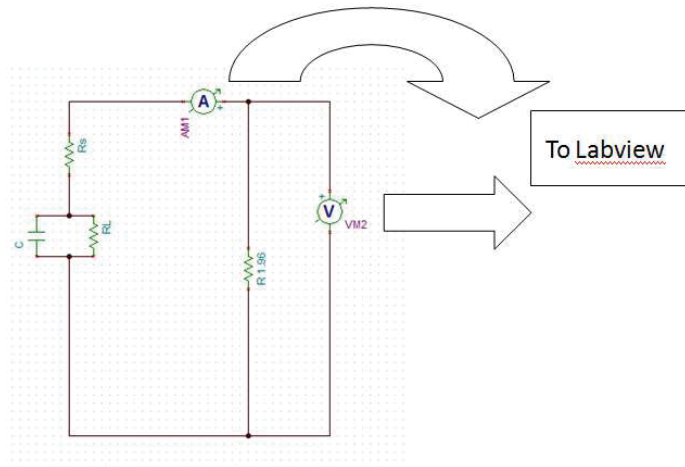


Fig. 3.34 1.96Ω load discharge circuit

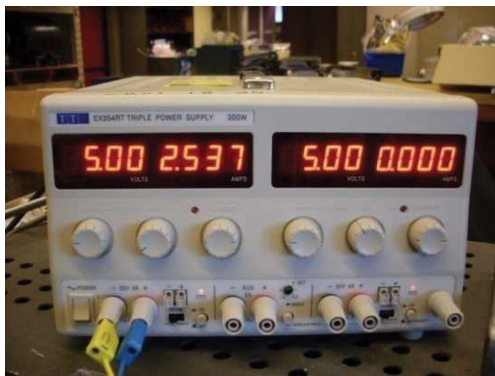


Fig. 3.35 Power supply used to charge the supercapacitor



Fig. 3.36 Power supply used for current sensor board from NI

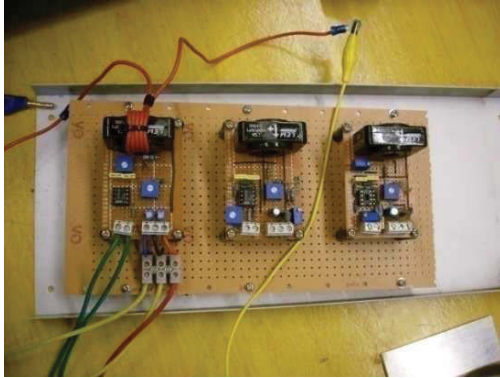


Fig. 3.37 Current sensor used to transfer current signal to voltage signal

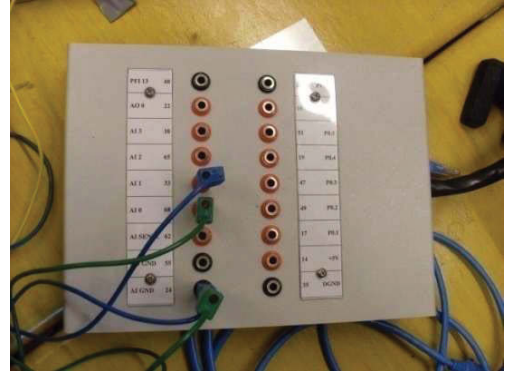


Fig. 3.38 DAQ board used to collect the voltage data of supercapacitor and current sensor

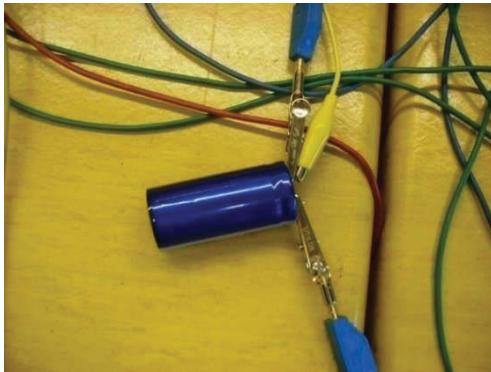


Fig. 3.39 Supercapacitor connected into the circuit

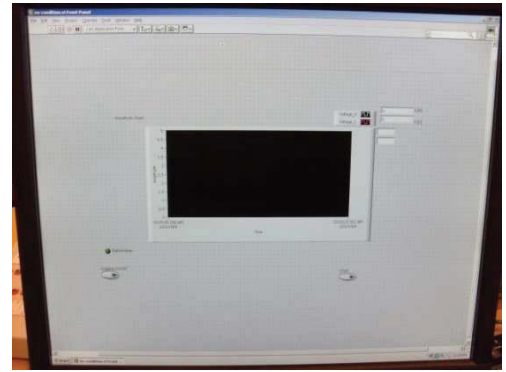


Fig. 3.40 The waveform view of Labview

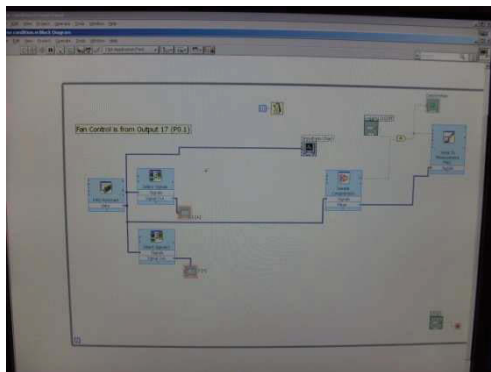


Fig. 3.41 The blocks of Labview to collect data

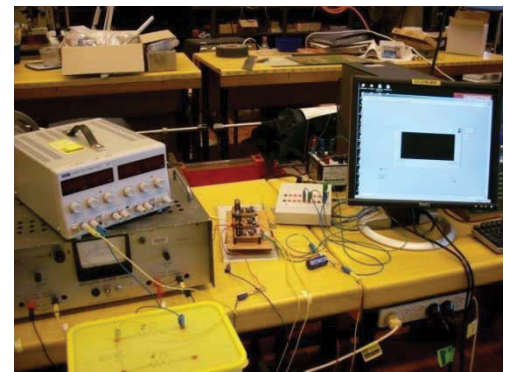


Fig. 3.42 The whole work station

C. Experiment test results

This part provides the experiment test results of the supercapacitor. It includes self-discharge, constant current charge, load discharge and repeat self-discharge performance. For every test procedure, three supercapacitor cells are tested separately. Every cell's test performance result is presented in this part.

(1) Self-discharge

Fig. 3.43-3.45 shows the self-discharge performance of three different supercapacitors. From these figures we could observe supercapacitors' voltage drops slowly in the self-discharge test, the voltage of supercapacitor will drop below 2V. However, from these Figures it can be observed that each cell's self-discharge performance is different. If a number of supercapacitors are connected together, it is essential to develop the cell balancer to avoid accelerating the deterioration of the supercapacitor lifetime.

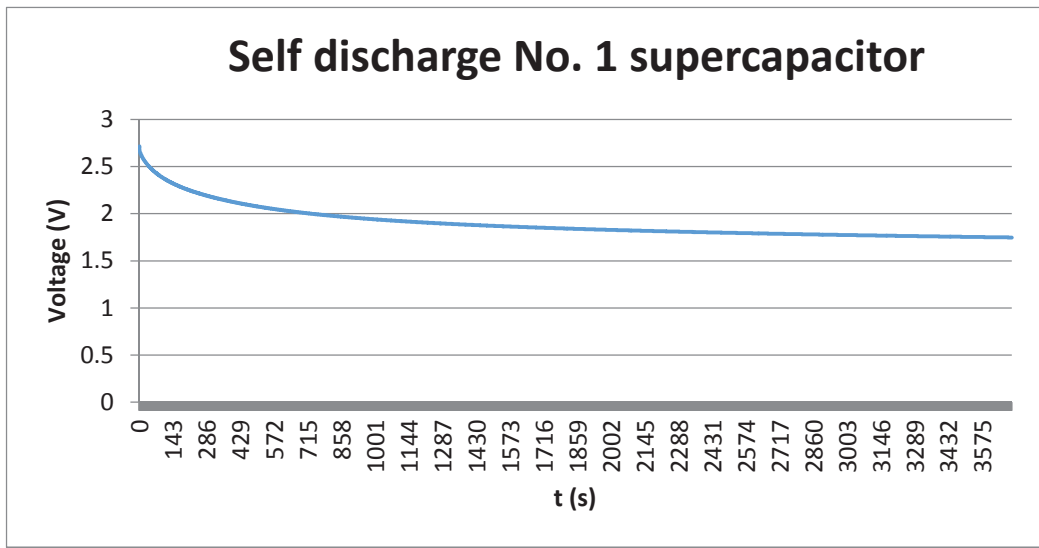


Fig. 3.43 Voltage of No.1 supercapacitor for self-discharge

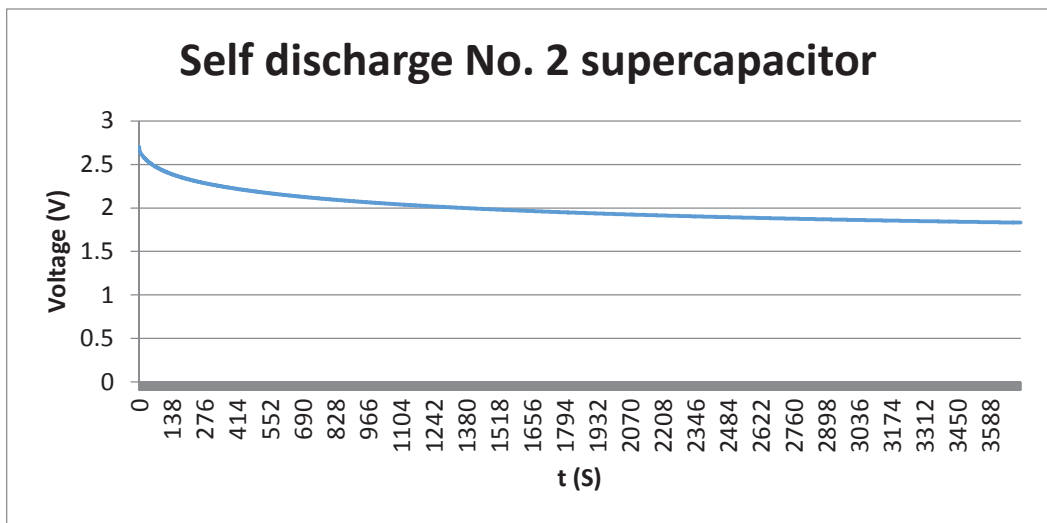


Fig. 3.44 Voltage of No.2 supercapacitor for self-discharge

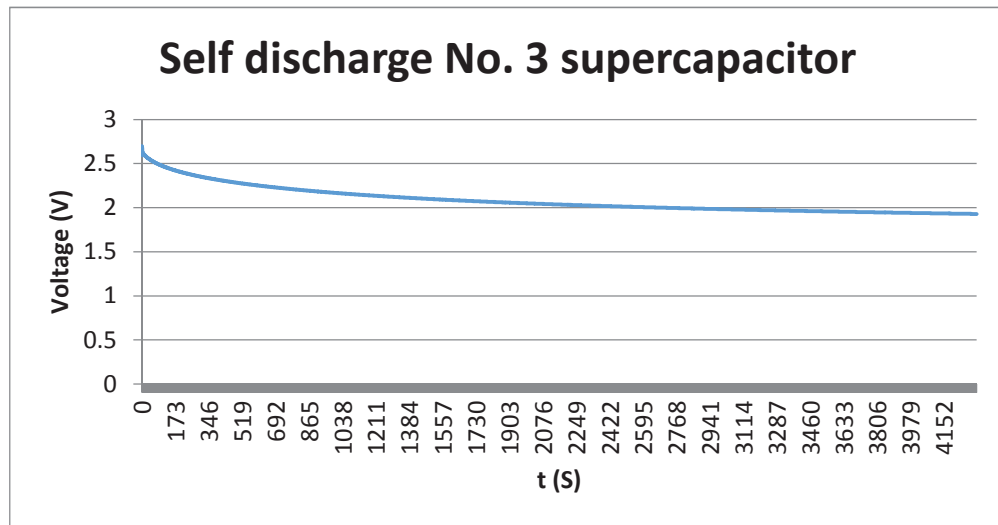


Fig. 3.45 Voltage of No.3 supercapacitor for self-discharge

(2) 3.15A constant current charging

Fig. 3.46-3.48 shows the 3.15A constant current charge performance of three different supercapacitors. From these figures it can be observed that supercapacitors' voltage rises quickly to rated voltage, less than two minutes in constant charge test, which is the main advantage of the supercapacitor (quick charging).

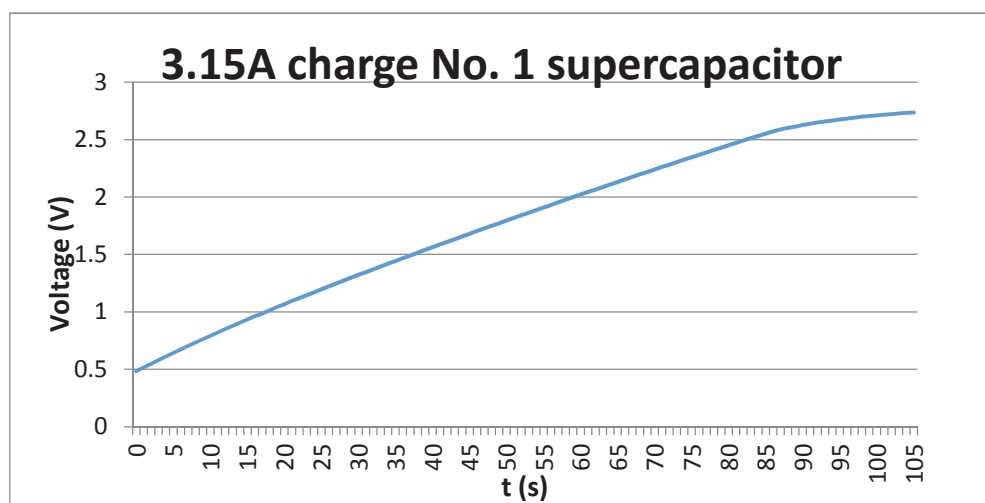


Fig. 3.46 Voltage of No. 1 supercapacitor for 3.15A constant charging

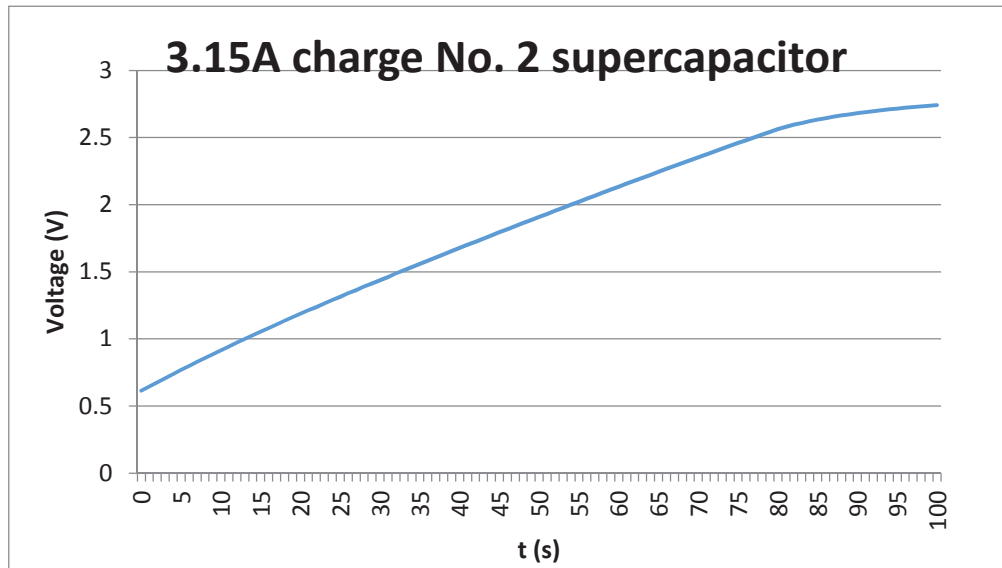


Fig. 3.47 Voltage of No. 2 supercapacitor for 3.15A constant charging

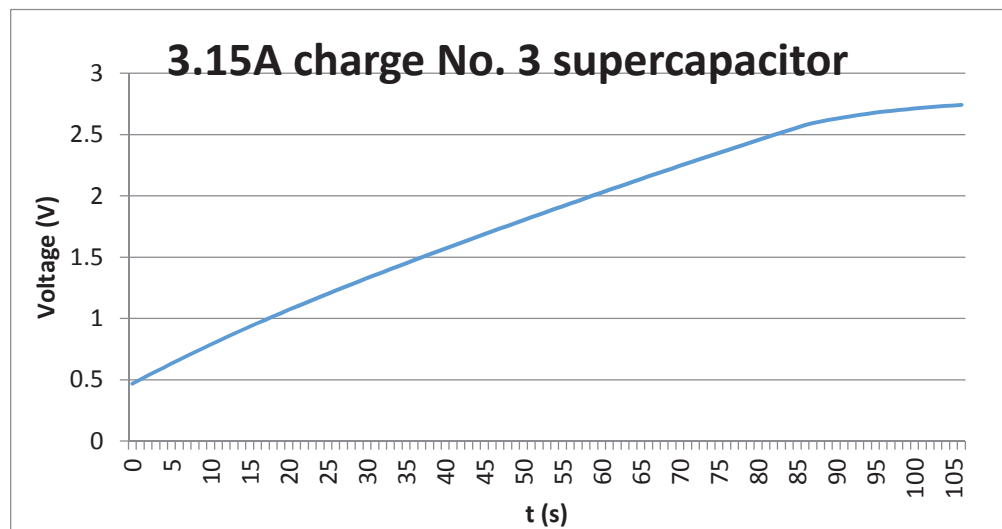


Fig. 3.48 Voltage of No. 3 supercapacitor for 3.15A constant charging

(3) 1.96Ω load discharge

Fig. 3.49-3.51 shows the 1.96Ω load discharge performance of three different supercapacitors. From these figures it can be observed supercapacitors' voltage drops quickly especially in the first two minutes. Finally the voltage of supercapacitor drops below 0.5V. This characteristic also is the main advantage of a supercapacitor (quick discharging).

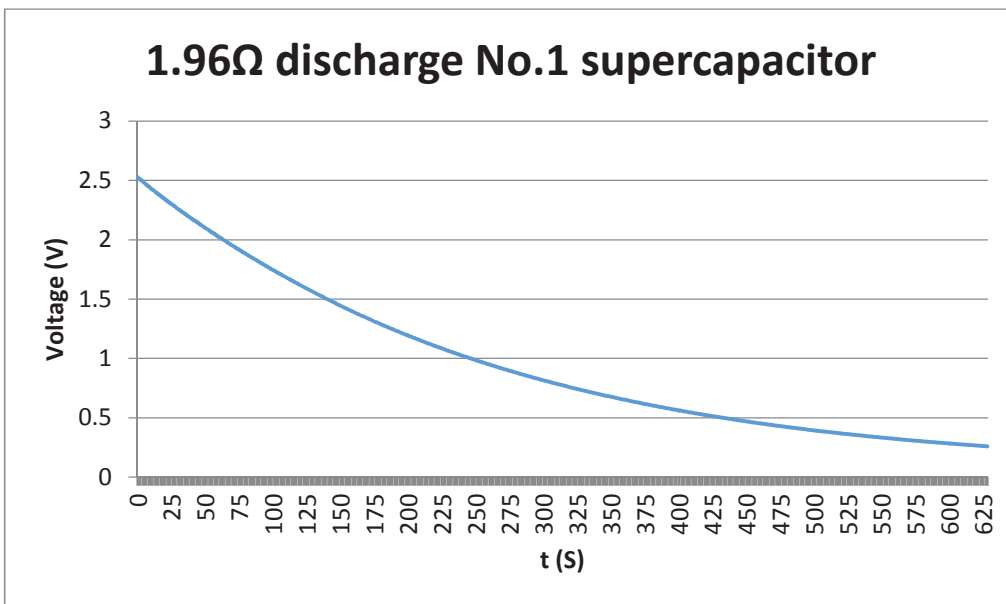


Fig. 3.49 Voltage of No.1 supercapacitor for 1.96Ω load discharge

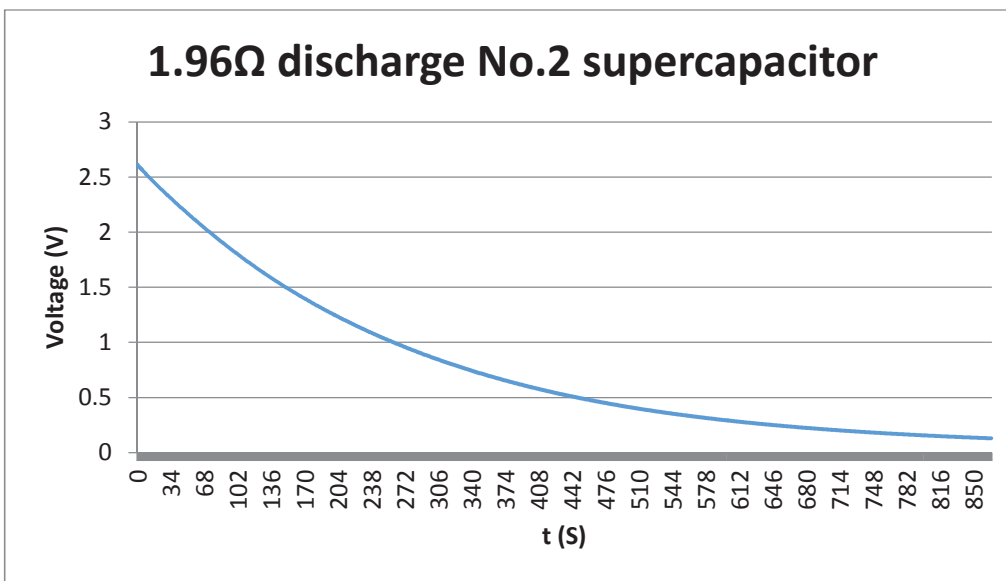


Fig. 3.50 Voltage of No.2 supercapacitor for 1.96Ω load discharge

(4) Self-discharge for 3 times to see different supercapacitors self-recovery performances

Repeat self-discharge procedures:

- Charge the supercapacitor to 2.7V, and then let it sit on the desk for more than half hour to

see its self-discharge performance.

- Charge the supercapacitor again to 2.7V, and then let it sit on the desk for more than half hour to see its self-discharge performance.
- Repeat this cycle for 3 times.

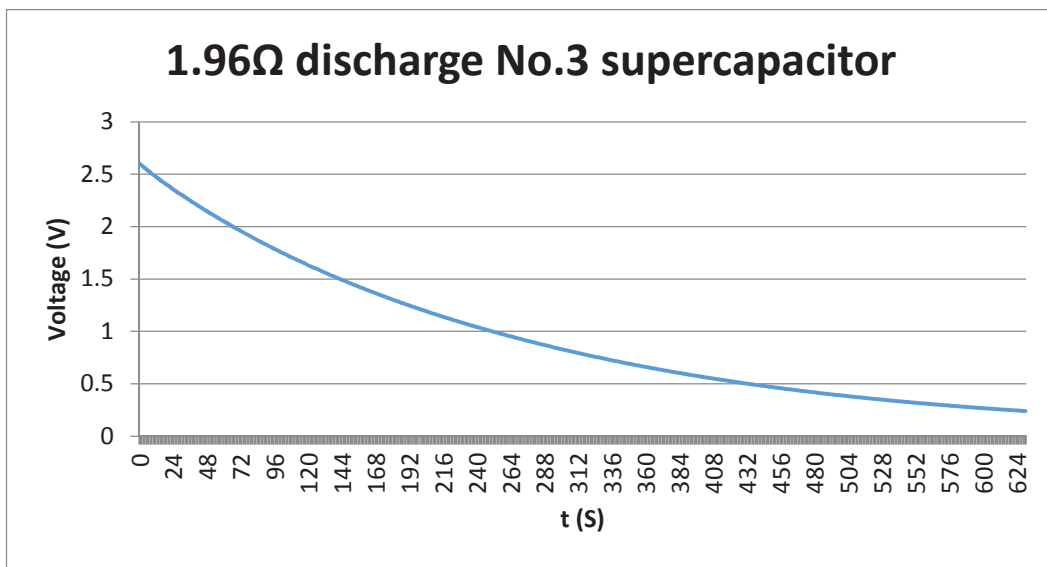


Fig. 3.51 Voltage of No.3 supercapacitor for 1.96Ω load discharge

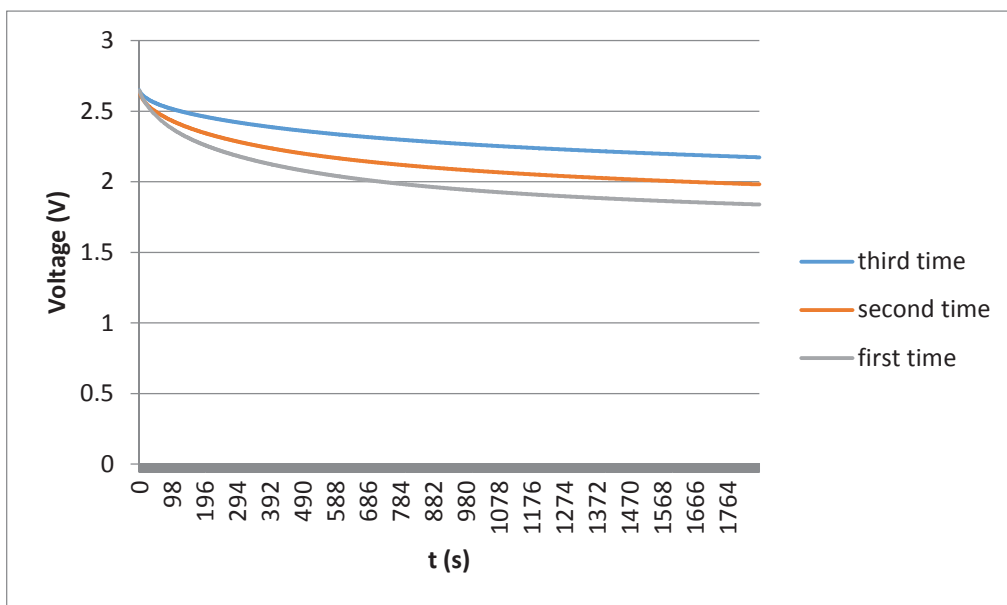


Fig. 3.52 No.1 supercapacitor recovery performance

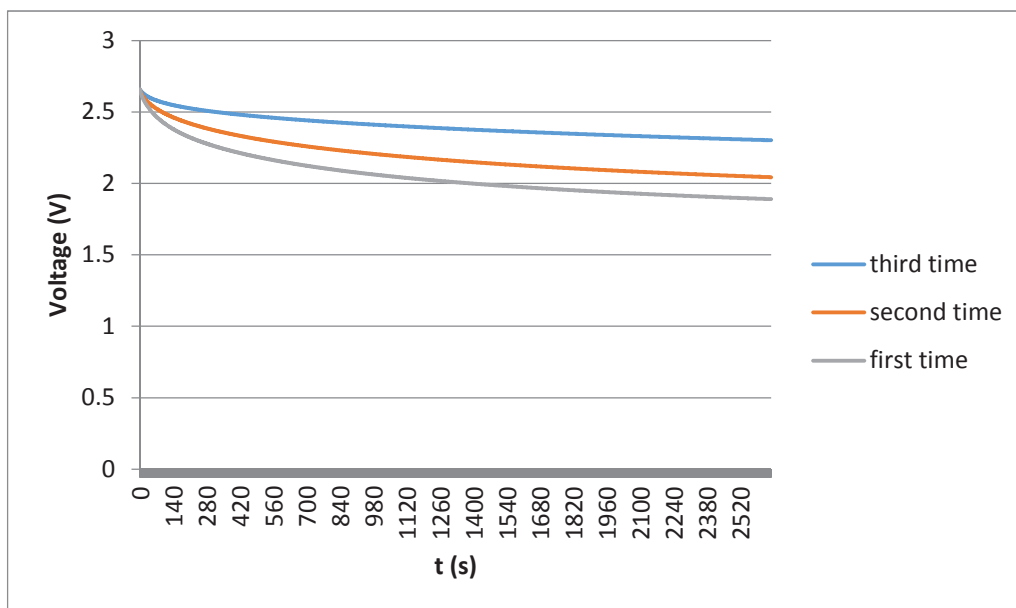


Fig. 3.53 No.2 supercapacitor recovery performance

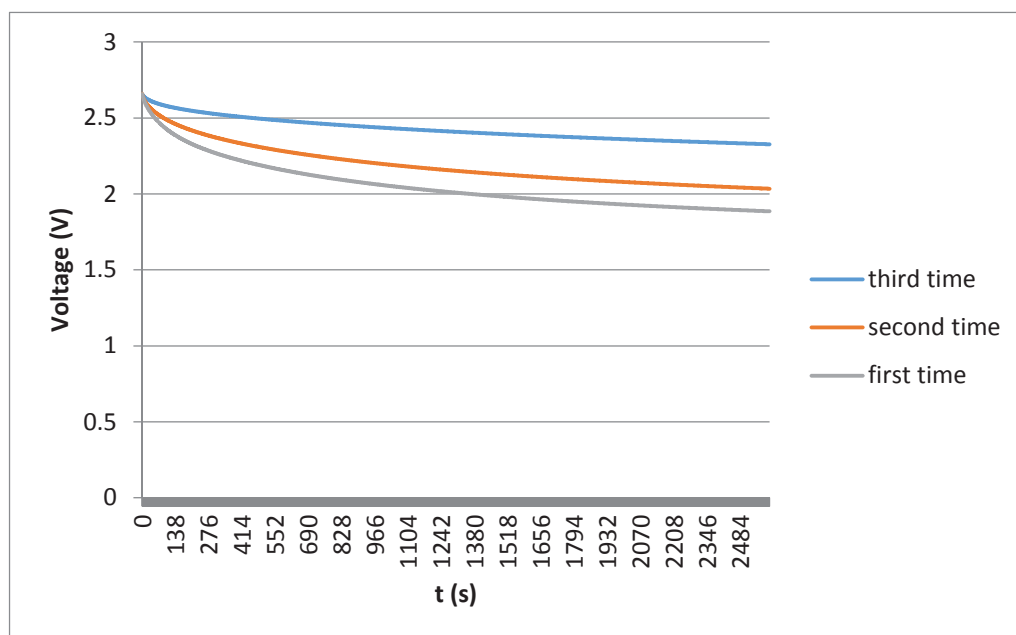


Fig. 3.54 No.3 supercapacitor recovery performance

Fig. 3.52-3.54 show the self-discharge performance for three times of three different supercapacitors. The test can also be treated as a supercapacitor recovery performance. From these figures it can be observed that supercapacitors' voltage drops slower as self-discharge time increases. A new supercapacitor has a "babyhood" for the first period discharging. With

the test time increasing, the self-discharge performance can be improved with testing cycle repeating.

D. Model verification

(1) Simplified model verification

From the test of charge experiment, the voltage and current value $U^*(t)$ and $I_1(t)$ can be obtained. From the simplified model of the supercapacitor, the function can be obtained as: $U(t) = f(I_1(t))$. Based on the results of $U^*(t)$ and $U(t)$, the error between the $U^*(t)$ and $U(t)$ can be obtained as $\text{Error} = U(t) - U^*(t)$. Then by using squares method in MATLAB to minimize the error between the experiment data and the basic model, the results of basic parameters R_1 , C_1 and R_2 are given out.

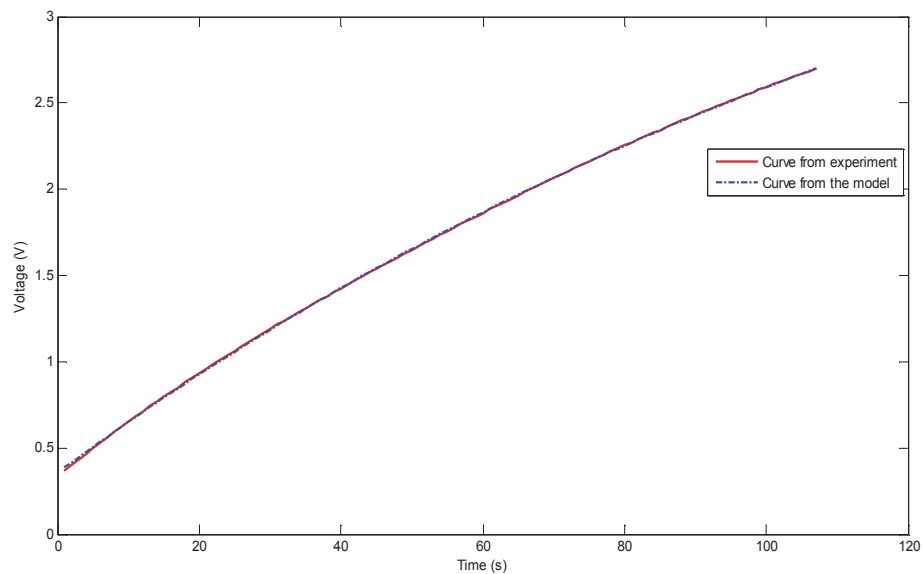


Fig. 3.55 Basic model voltage curve comparison with experiment results

Fig. 3.55 is the result of basic model voltage curve comparison with experiment results according to squares method to minimize the error. It can be observed that the fitting is nearly perfect, this method is very suitable for parameters extraction. Fig. 3.56 is the extracted voltage error based on the results of Fig. 3.55; the error is tiny so the model could track the experiment results very closely. From the experiment results and simplest model it can be concluded that

the simplest model can represent the supercapacitor behaviour very well, and it could be very useful for future research work on energy storage model with battery pack.

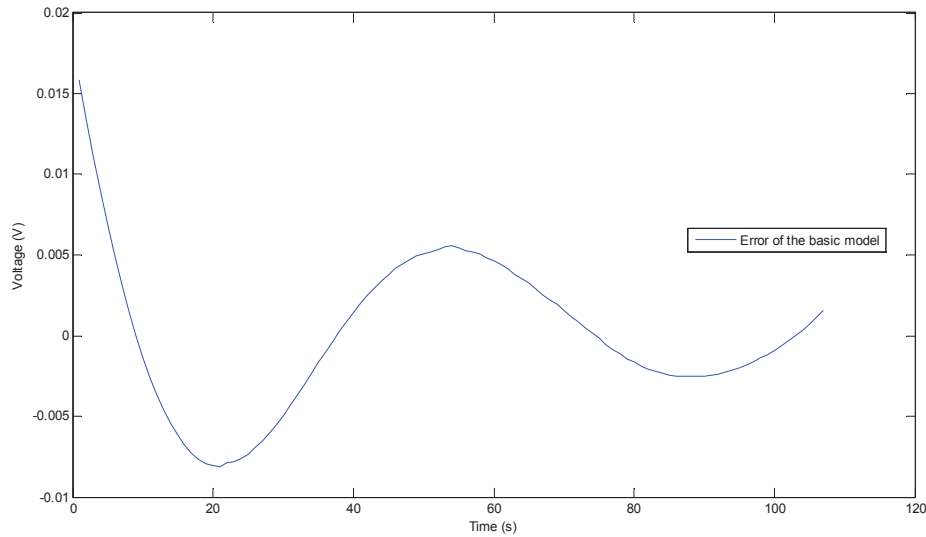


Fig. 3.56 Voltage error between model and experiment

(2) *Complicated model verification*

For the more complicated model for the supercapacitor, it is a four-order T-style RC network. According to the experiment data collected and the four-order model and after calculation using the equations given out in section 3.3.2, the results of each component value were found to be as follows:

$$\begin{array}{llll}
 R_{1c}=0.04 \Omega & C_{1c}=83.06 \text{ F}; & R_{2c}=0.382 \Omega & C_{2c}=59.90 \text{ F} \\
 R_{3c}=2.51 \Omega & C_{3c}=98.095 \text{ F}; & R_{4c}=12.51 \Omega & C_{4c}=75 \text{ F} \\
 R_L=446.93 \Omega & & &
 \end{array}$$

To verify the model parameters, a simulation model is constructed in SIMULINK. The different constant current charging signals are applied to compare the different charging phenomenon.

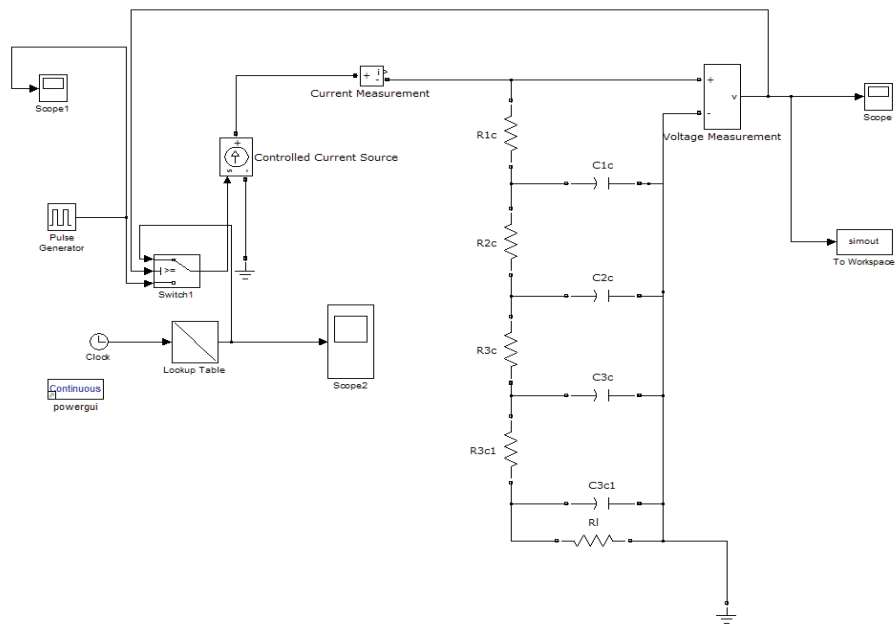


Fig. 3.57 Simulink block diagram of supercapacitor model charging

Fig. 3.57 is the Simulink diagram of supercapacitor model charging; different current charging is applied in the simulation. Figs.3.58 and 3.59 illustrate the charging procedure and simulation charging results with a constant current of 3.15A for 91 seconds.

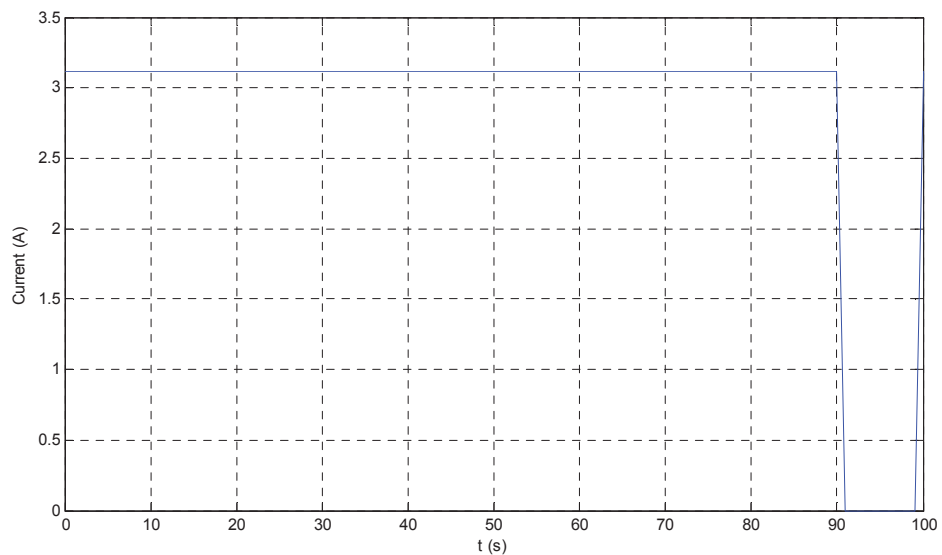


Fig. 3.58 Constant current charging with 3.15A for 91 seconds

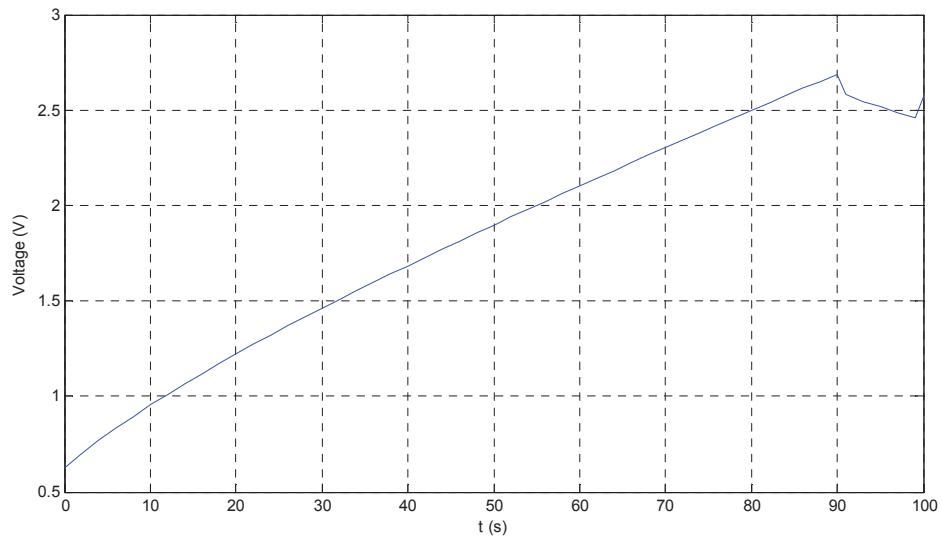


Fig. 3.59 Voltage of supercapacitor during constant current charging procedure

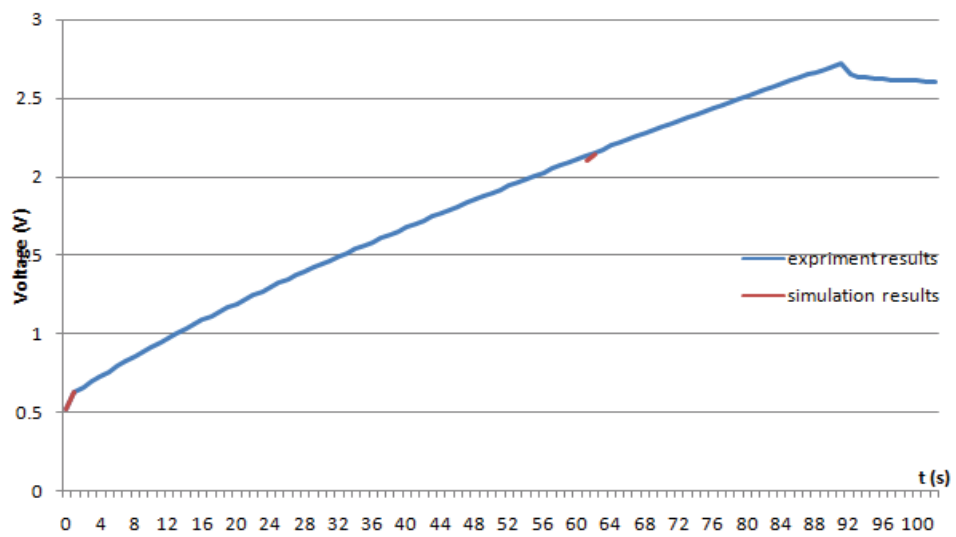


Fig. 3.60 Comparison of the experimental and simulation results

Fig. 3.60 is the result of complicated model voltage curve comparison with experiment results. It can be observed that the fitting is nearly perfect, so this model is also good for supercapacitor bank development.

3.5.2 Battery experimental test

The viable EV and HEV batteries consist of the lead-acid battery, nickel-based batteries, such as nickel/iron, nickel/cadmium, and nickel-metal hydride (Ni-MH) batteries, and lithium-based batteries such as lithium-polymer (Li-P) and lithium-ion (Li-I) batteries. Considering the development history of battery, it seems that cadmium-based and lithium-based batteries would be the major candidates for EVs and HEVs.

Battery manufacturers usually specify the battery with coulometric capacity (ampere-hours), which is defined as the number of ampere-hours gained when discharging the battery from a fully charged state until the terminal voltage drops to its cut-off voltage. It should be noted that the same battery usually has a different number of ampere-hours at different discharging current rates. Another important parameter of a battery is the SOC. SOC is defined as the ratio of remaining capacity to fully charged capacity. With this definition, a fully charged battery has an SOC of 100% and a fully discharged battery has an SOC of 0%. However, the term “fully discharged” sometimes causes confusion, because of the different capacities at different discharge rates, and different cut-off voltages.

The battery cell used in the EV project in our Laboratory is the 20Ah nanophosphate battery from A123 company as shown in Fig.3.61.

Nanophosphate is A123 Systems’ patented lithium ion battery cathode active material, originally developed by professor Yet-Ming Chiang and his group at the Massachusetts Institute of Technology (M.I.T.). They reported their work in the seminal paper entitled, “Electronically conductive phosphor-olivines as lithium storage electrodes,” which was published in the journal Nature Materials in the October 2002 issue [3.57].

Nanophosphate is an engineered nanoscale material with specific structural and chemical properties designed to maximize the performance of lithium-ion batteries [3.58]. Fig. 3.62 schematically illustrates this structure. The image on the left is a cathode electrode, with the

aluminum current collector foil covered with Nanophosphate particles. The middle image is the Nanophosphate secondary particle and the image on the right illustrates the primary particles.



Fig. 3.61 Nanophosphate battery from A123 company

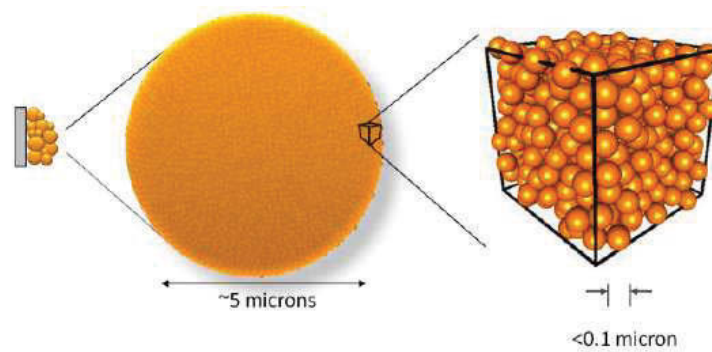


Fig. 3.62 Schematic illustration of the Nanophosphate structure, with secondary and primary particles

[3.58]

The primary Nanophosphate particles are on the order of one-tenth of a micron in diameter and are agglomerated into much larger secondary particles, which have diameters on the order of a

few microns. So, although the primary particle may have a length scale in the order of several tens of nanometers, the secondary particle is on the length scale of microns, making it well above the Environmental Protection Agency (EPA) definition of what is considered a nanomaterial. Micron-sized secondary particles allow the Nanophosphate powder to be handled and processed more easily.

This unique electrochemical structure of Nanophosphate enables a number of performance advantages, including higher power, excellent safety, long life and greater usable energy.

In order to optimally manage the battery bank, experimental tests are essential in order to give out the charge-discharge behaviour, the model of the battery and SOC estimation of the battery.

A. Experimental test circuit diagram

The battery cell experimental test circuit diagram is similar to the supercapacitor cell experimental test circuit. For the model development, the charging behaviour using different charging currents is carried out in the test.

B. Experimental test results

The battery experimental test bench setup is similar to the supercapacitor cell experimental test bench. Different currents are applied to charge the battery.

Fig. 3.63-3.65 show the charging results of different current (2A, 3A, 4A) charge for the No. 1 battery. From the figures it can be observed that the different current charging has different full capacity charging time. Fig. 3.66 shows different current charging profiles in one figure. From Fig. 3.66 it can be observed that the terminal voltage of the battery can be different with different current charging. The higher the charging current, the higher the terminal voltage of battery will be charged. In the experimental test shown in Fig. 3.63, the battery is overcharged in the last stage. When batteries are connected together and packed as an energy storage system, it is essential to use a battery management system to control the battery charging status to avoid over-charged or over-discharged.

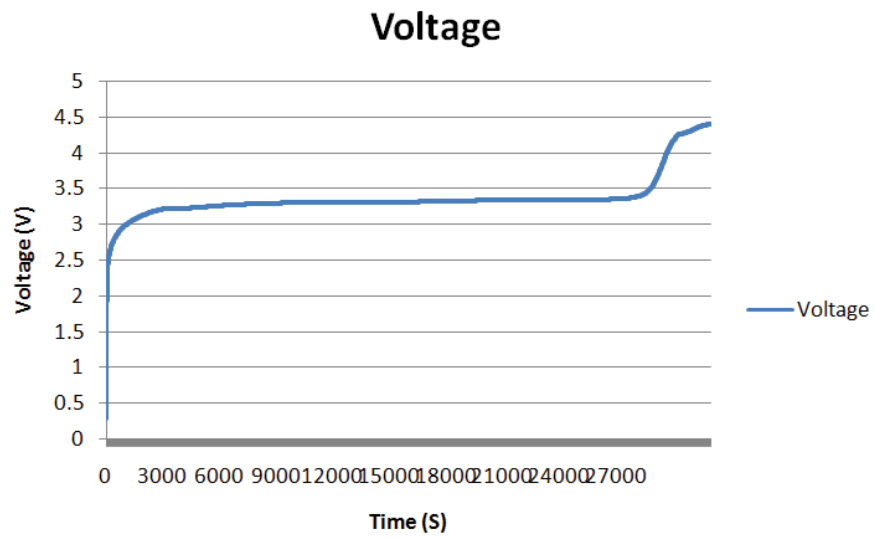


Fig. 3.63 2A constant current charge for the No. 1 battery

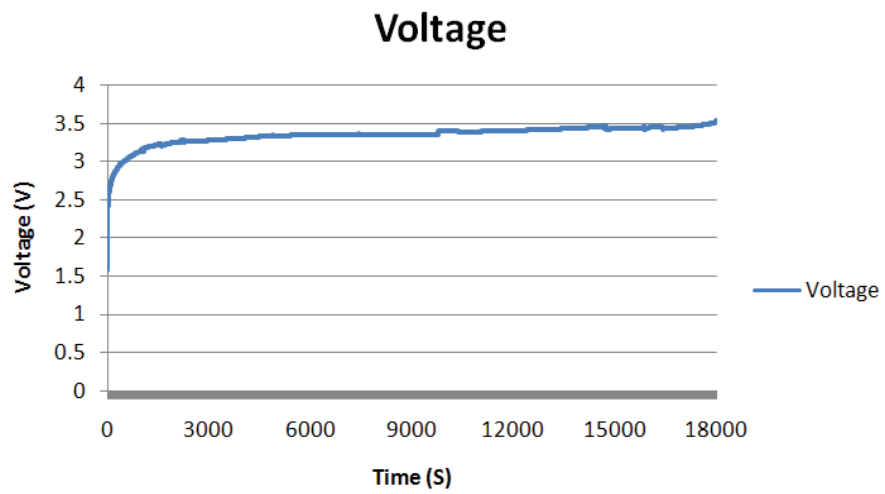


Fig. 3.64 3A constant current charge for the No. 1 battery

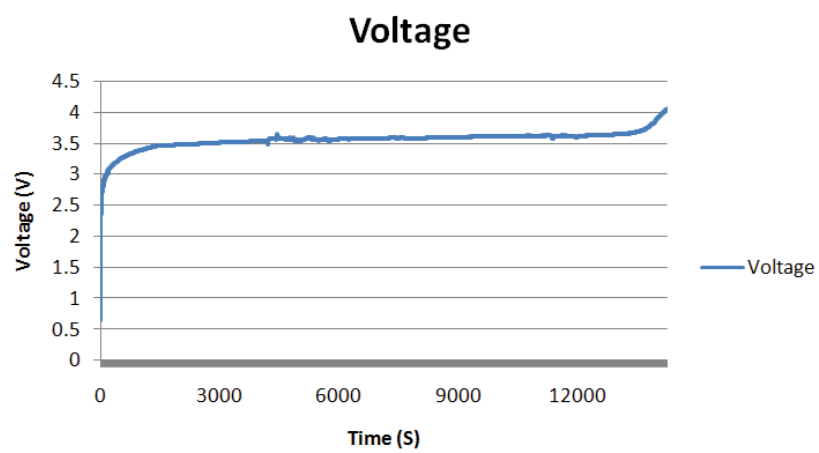


Fig. 3.65 4A constant current charge for the No. 1 battery

Fig. 3.67-3.69 show the charging results of different current (2A, 3A, 4A) charge the No. 2 battery. The charging characteristic has difference with No.1 battery. Fig. 3.70 shows the different current charging profiles in one figure. The voltage of battery using 4A charging rises very quickly compared with other charging profile. The terminal voltage of different current charging is almost the same.

Fig. 3.71 and Fig. 3.72 are the 3A and 4A charge for the No. 3 battery. For No. 3 battery, the 4A charging profile shown in Fig. 3.72 is not very smooth since the charging current is not stable during the experiment test.

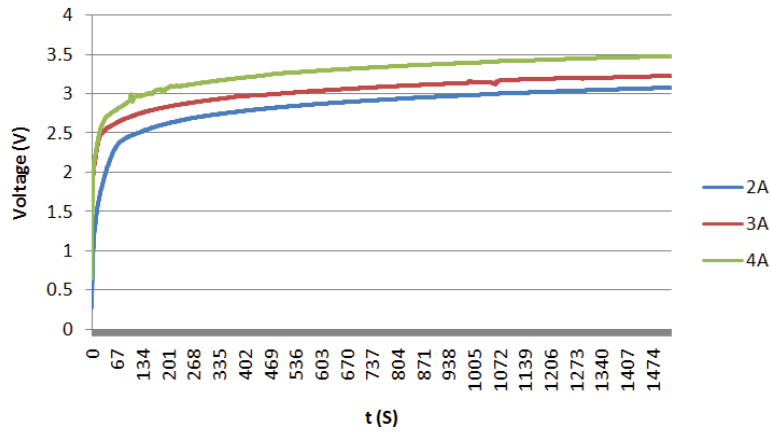


Fig. 3.66 Comparison of different current charge for the No. 1 battery

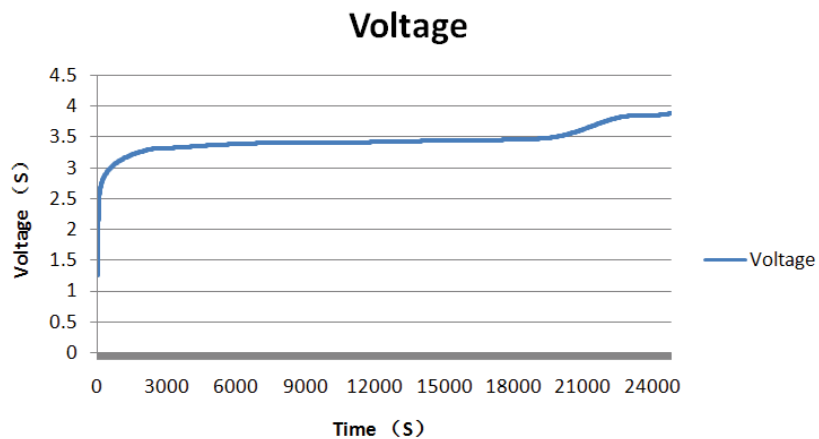


Fig. 3.67 2A constant current charge for the No. 2 battery

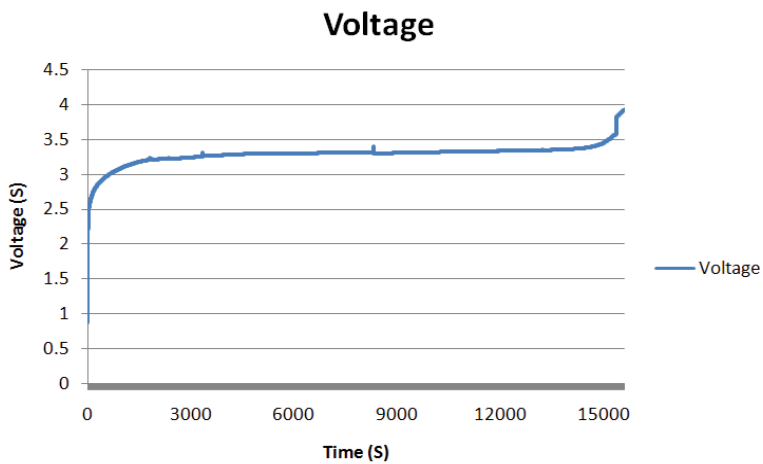


Fig. 3.68 3A constant current charge for the No. 2 battery

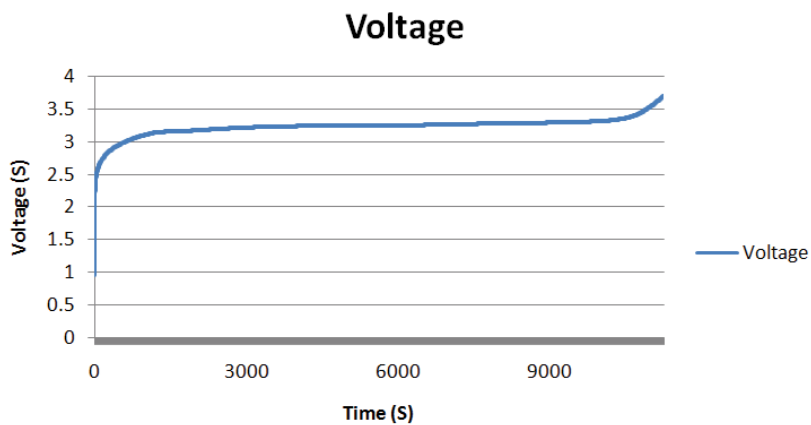


Fig. 3.69 4A constant current charge for the No. 2 battery

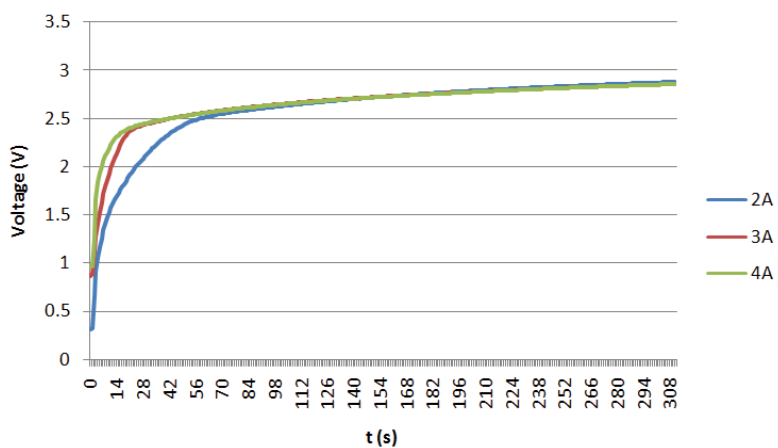


Fig. 3.70 Comparison of different current charge for the No. 2 battery

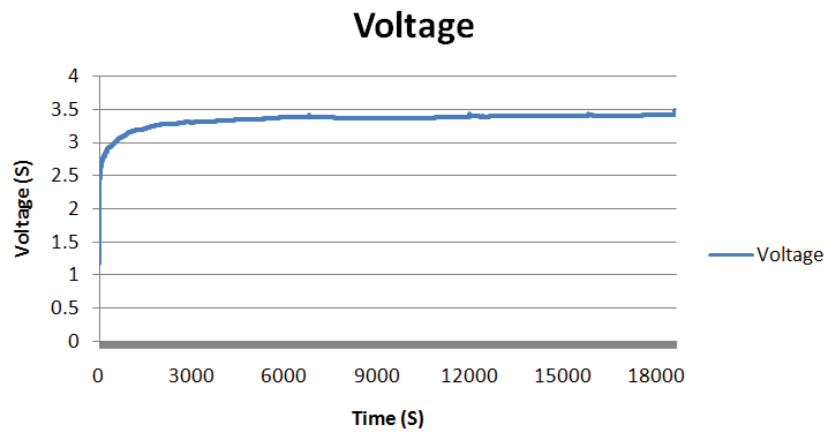


Fig. 3.71 3A constant current charge for the No. 3 battery

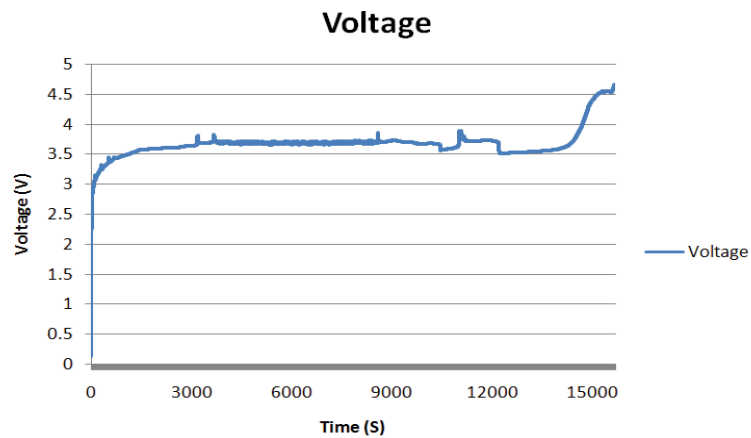


Fig. 3.72 4A constant current charge for the No. 3 battery

C. Battery model parameters extraction

(1) Experiment setup and battery model calculation

Battery is not like the supercapacitor, the electric circuit model is nonlinear, so an experiment was designed to measure the terminal voltage response by charging the battery with a constant current. Fig. 3.73 is the diagram of the experimental setup. The voltage across the battery terminals corresponding to a constant charging current was measured by a data acquisition system and recorded by LABVIEW software.

In the charging experiment, the battery was charged by a constant current from empty to full capacity, and the behaviour at eight different SOC values was measured by repeating the following procedure of two steps: (a) Charge the battery by a 4A constant current source for an increment of 2Ah, and (b) Disconnect it from the charging current source and keep it at rest to wait for the stabilization of OCV before the next charging step, i.e. (a). By this procedure, the correspondence between the SOC and OCV can be determined.

The influence of temperature on model parameters is an interesting and important part for the battery used in HEV applications, and has been studied by various researchers [3.59]-[3.62]. Due to the lack of experimental facility for temperature control, however, all experiments in this study were conducted at 18°C, the ambient temperature.

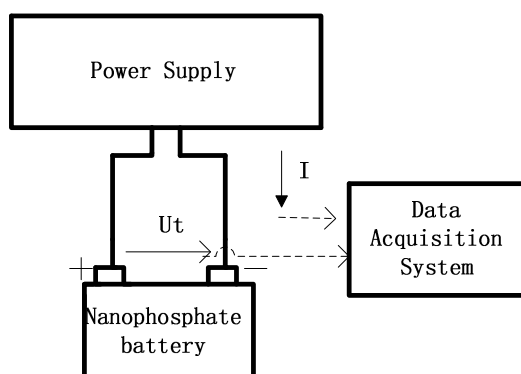


Fig. 3.73 Experimental setup for measuring battery charge performance

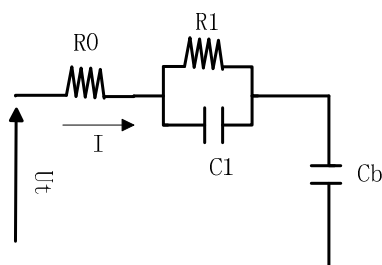


Fig. 3.74 First-order Thevenin charging model

The proposed nonlinear dynamic model for parameters extraction is shown in Fig. 3.74; this model is based on the first-order Thevenin model. The nonlinear characteristic is reflected by model parameters, which depend on different values of OCV. Because this study focuses only on charging behaviour, the discharging behaviour, self-discharging behaviour, and voltage recovery behaviour are neglected in the Thevenin model. Following are the equations of this model.

For the model presented in Part A, in the complex field, using the Laplace equations (3.30),

$$U_{cl}(s) = I(s) \cdot \frac{R_1}{R_1 \cdot sC_1 + 1} \quad (3.30)$$

Using the inverse Laplace transfer the (3.30) to (3.31),

$$U_{cl}(t) = I \cdot \int_0^t \frac{1}{C_1} \cdot \exp\left(\frac{1}{-R_1 \cdot C_1}\right) \quad (3.31)$$

Convert the equation (3.31) to (3.32),

$$U_{cl}(t) = I \cdot R_1 \cdot \left[1 - \exp\left(\frac{-t}{\tau_1}\right)\right] \quad (3.32)$$

where $\tau_1 = R_1 \cdot C_1$ $K = \frac{1}{C_b}$

By applying the Kirchhoff's voltage law for the charging model,

$$U_t(t) - U_{oc} = I \cdot R_0 + I \cdot R_1 \cdot \left[1 - \exp\left(\frac{-t}{\tau_1}\right)\right] + k \cdot I \cdot t \quad (3.33)$$

The equation used for curve fitting is given by

$$U_t(t) - U_{oc} = a - b \cdot \exp(-c \cdot t) + d \cdot t \quad (3.34)$$

(2) *Experiment results and discussions*

In the experiment test, apply the charging procedures in the last section. The experimental results are shown in Fig. 3.75. Fig. 3.75 plots the recorded experiment results of charging behaviour. The charge procedure stops to avoid the overcharge of the Nanophosphate battery.

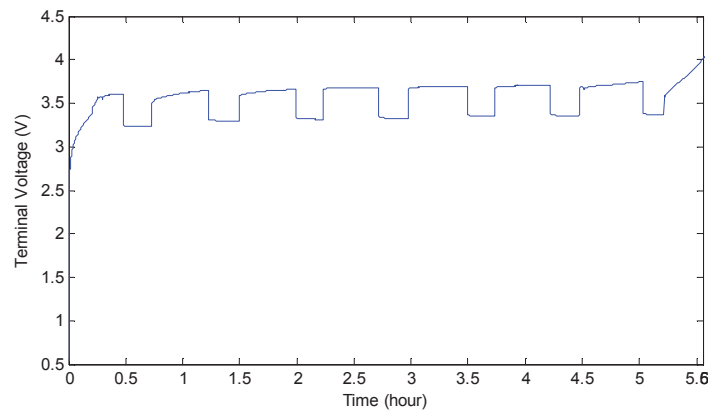


Fig. 3.75 Experiment results of charging behaviour

(3) *Curve fitting of $[U_t(t)-U_{oc}]$ versus time*

In order to get the parameters of the model of battery proposed in the last section, according to (4) and (5), curve fitting box in MATLAB was used to extract different parameters values with different SOC starting. Figs. 3.76 to 3.83 depict a set of curves at different initial OCV values, corresponding to different starting SOC. As shown in Figs. 3.76 to 3.83, with different starting SOC, the curves of the terminal voltage subtracting the OCV of the battery are different, indicating different parameters of battery model with different starting OCVs, or starting SOC. Figs. 3.76 to 3.83 clearly shows that the battery model is strongly nonlinear. The Thevenin electrical model (Fig. 3.74), which consists of R-C blocks, is capable of catching the dynamic behaviour. Due to the linear structure of all electrical models, the nonlinear behaviour can only be reflected by the dependence of model parameters on different OCV. Thus, according to the analysis above, the model parameters are different with corresponding OCV.

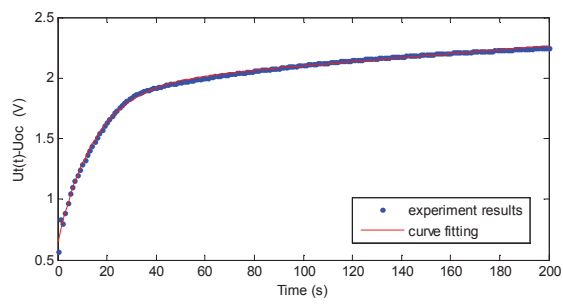


Fig. 3.76 Curve fitting of $[U(t)-U_{oc}]$ versus time (starting SOC=0%)

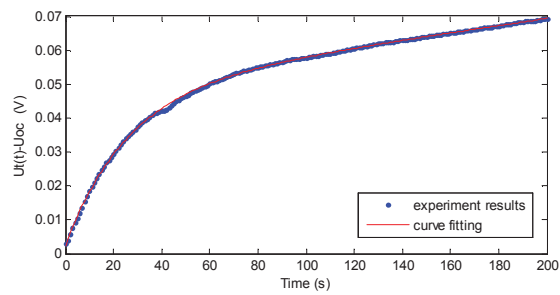


Fig. 3.77 Curve fitting of $[U(t)-U_{oc}]$ versus time (starting SOC=10%)

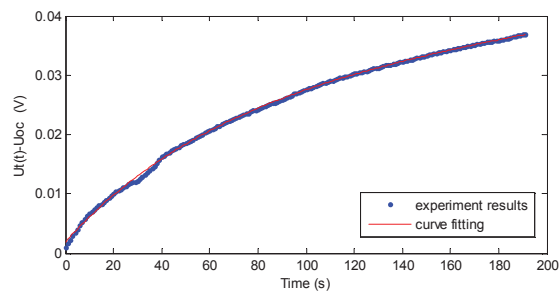


Fig. 3.78 Curve fitting of $[U(t)-U_{oc}]$ versus time (starting SOC=20%)

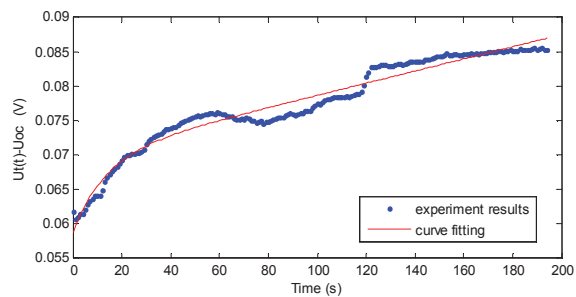


Fig. 3.79 Curve fitting of $[U(t)-U_{oc}]$ versus time (starting SOC=30%)

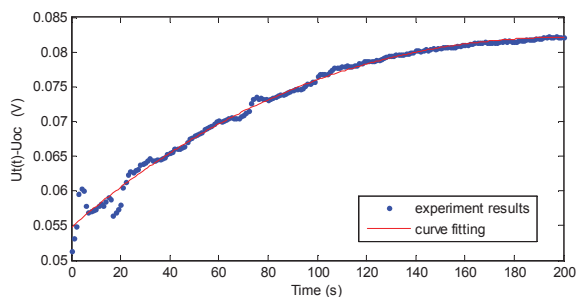


Fig. 3.80 Curve fitting of $[U(t) - U_{oc}]$ versus time (starting SOC=40%)

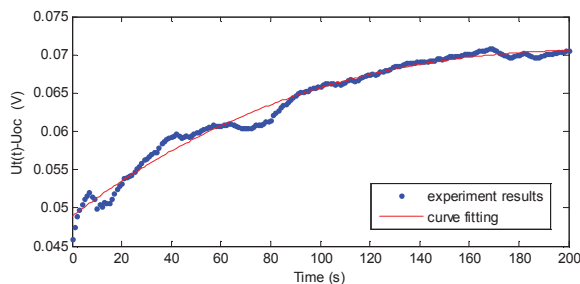


Fig. 3.81 Curve fitting of $[U(t) - U_{oc}]$ versus time (starting SOC=50%)

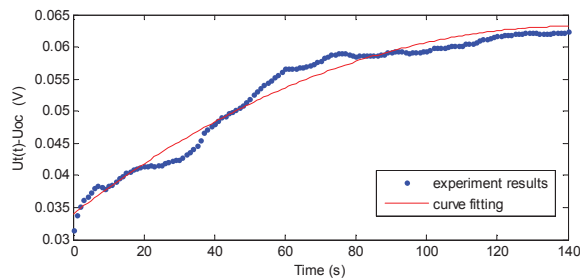


Fig. 3.82 Curve fitting of $[U(t) - U_{oc}]$ versus time (starting SOC=60%)

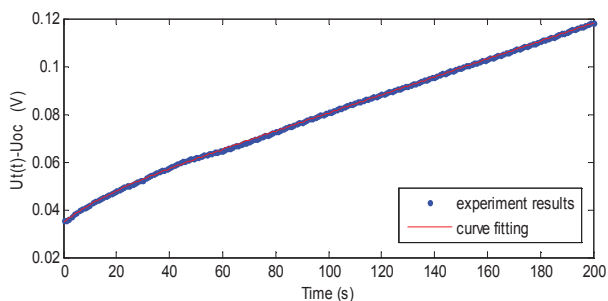


Fig. 3.83 Curve fitting of $[U(t) - U_{oc}]$ versus time (starting SOC=70%)

(4) Parameter calculation

Having obtained the equations of the proposed model and the curve fitting results, the parameters of this model have been extracted. By curve fitting using the MATLAB, the parameters can be easily obtained by (3.35) to (3.38),

$$R_0 = \frac{a-b}{I} \quad (3.35)$$

$$R_1 = \frac{b}{I} \quad (3.36)$$

$$\tau_1 = \frac{1}{c} \quad (3.37)$$

$$k = \frac{d}{I} \quad (3.38)$$

From 0% to 70% SOC starting, the battery has the different OCV starting, and the extraction result of R0 and R1 are given in Table 3.2.

TABLE 3.2 Extraction Results of R₀ and R₁

SOC	R ₀	R ₁
0%	0.16	0.32
10%	0.0058	0.0115
20%	0.00045	0.0063
30%	0.01476	0.0027
40%	0.0137	0.0438
50%	0.012	0.02
60%	0.0085	0.38375
70%	0.0087	0.002

It can be observed that the R₀ and R₁ variation curves with different SOC starting in Fig. 3.84 and Fig. 3.85.

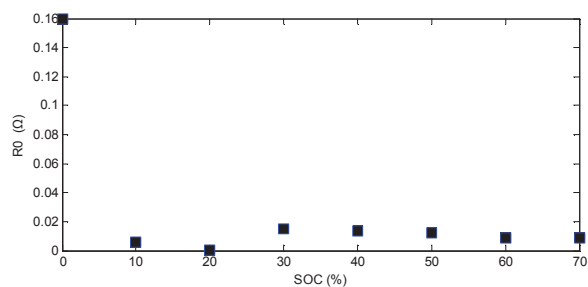


Fig. 3.84 R0 variation with different SOC starting

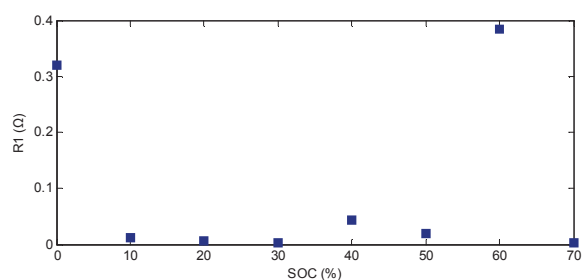


Fig. 3.85 R1 variation with different SOC starting

From Figs. 3.84 and 3.85, it can be observed that the R_0 is a maximum value at 0% SOC, and from 10% to 70% SOC, the R_0 varies slightly from 0.45mΩ to 14.76mΩ. While the parameter R_1 is not like the R_0 , it has a maximum value at 60% SOC, and the second maximum value at 0% SOC. In other different SOC starting percentages, it is under 2.7mΩ.

After obtaining the results of the parameters at different SOC starting, we know more characteristics about the Nanophosphate battery. From the results of the analysis above, the parameters variations are not like the other lithium ion batteries. This work could be very useful for an exact model for a Nanophosphate battery to be carried out in the future.

By focusing on the studying and verifying the nonlinear characteristic, the experiments were performed in rather narrow confines. From this research work, according to the analysis of the charging experiments results, the charging characteristic of the 20Ah Nanophosphate battery was obtained. The author used the results of the battery charging behavior, gave out the relationship between the parameters of the battery model and the different SOC starting for charging. To the best of the authors' knowledge, no in-depth studies of charging behavior and

nonlinear modelling for Nanophosphate battery have been carried out. So the work done in this part could be very helpful and useful for the future research on the Nanophosphate battery. This work only focuses on the charging behavior, so discharging behavior, self-discharging behavior, self-recovery behavior need to be carried out in the future; the parameters value variation of battery in these behaviors should be different from the charging behavior.

3.5.3 Test performance of supercapacitor cell balancer

The operation of a supercapacitor cell balancer is given out in a previous section. This part shows the test performance of the supercapacitor cell balancer.

The supercapacitors are connected in a PCB board, Fig. 3.86 shows a single supercapacitor module board. There are forty five 120F supercapacitors in parallel per cell bank.



Fig. 3.86 A single supercapacitor module

Fig. 3.87 shows three supercapacitor modules in test bed. For energy storage system, it is essential to connect supercapacitor modules together to afford the energy. To test the performance of supercapacitor modules, testing devices are needed to get the results for further research.

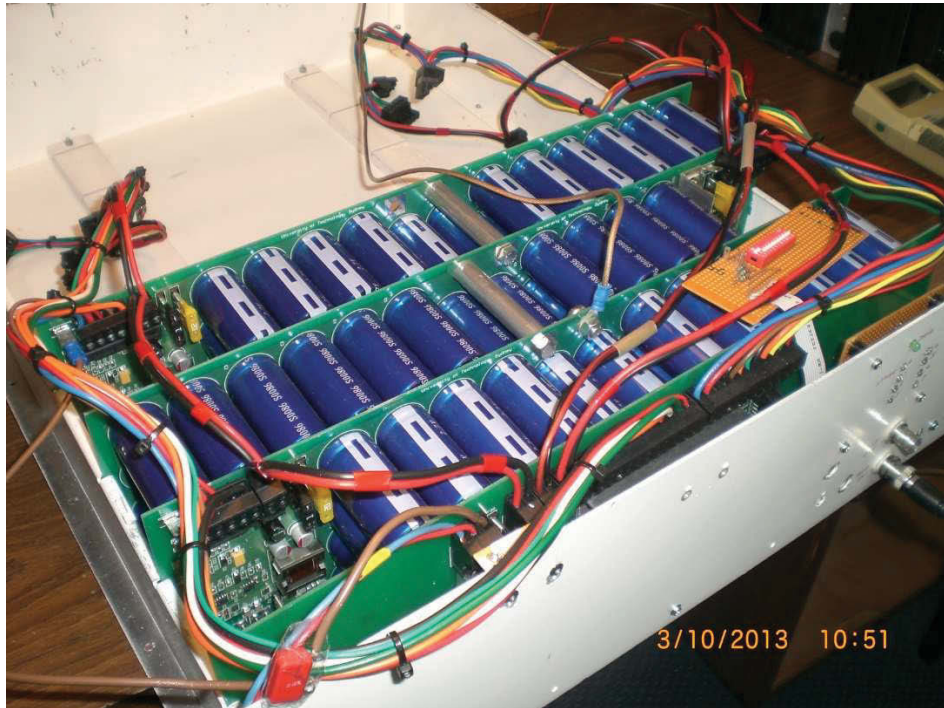


Fig. 3.87 Three supercapacitor modules in test bed

A. Two devices have been built to allow testing with just three cells and a local controller.

(1) Power Zener diode

This unit provides a high voltage load for the cell SMPS's. The “zener” voltage is adjustable via the knob in the range 43.8V to 208.4V. The circuit consists of an opamp comparing a fraction of the “zener” voltage to a fixed reference and driving the gates of two paralleled MOSFETs to achieve equality. The unit should be capable of dissipating 150W with the assistance of a fan.

(2) Dummy VFC controller

This unit allows the output of the particular cell VFC selected by the binary code on the DIP switch to be fed to the OUT terminal on the unit where a counter may be connected to monitor the VFC frequency. Switch section 1 is A0, section 2 is A1 and section 3 is A2.

A second terminal, CLOCK, is provided for the 250 kHz clock signal required by the VFC's to be fed in from a square wave oscillator.

Note that +5V must be provided to the dummy controller on pin 4 of the ribbon cable by pulling the SPARE line high, by linking R30 to +5V.

(3) Controller to cell bank connector

Note the quick-connect wire from the plug at controller socket J34. This is to complete the return circuit for the DRIVE signal and may be connected anywhere on the cell bank. It has a 1.5uF capacitor in series so that the DC levels may be independent for testing purposes. In a completed Cell Balancer this wire would be omitted since the connection is made via at each local controller power supply.

Note that if this connection is not present then there is very little power supply or reference voltage developed at any of the cell dischargers in spite of a normal DRIVE signal voltage.

B. Discharge power, cell voltage and efficiency

As expected the SMPS input power is linearly related to cell voltage, Fig. 3.88 shows the results.

Efficiencies of the three cell SMPS's at 2.6V are approximately 80%. This can be observed from Fig. 3.88.

C. VFC operation

For VFC operation test performance, Fig. 3.89 shows the VFC output frequency versus cell voltage using a 250 kHz VFC clock.

D. What is required to complete the cell balancer

(1) New PCBAs

The three cells and one local controller which have been constructed are sufficient to demonstrate the performance of the cell balancing scheme. The other 61 cells together with 7 local controllers and the VFC Controller are yet to be built. Each group of eight supercapacitor

cells with accompanying local controller fits into a rack unit and the wiring for each rack unit is shown in the circuit diagrams.

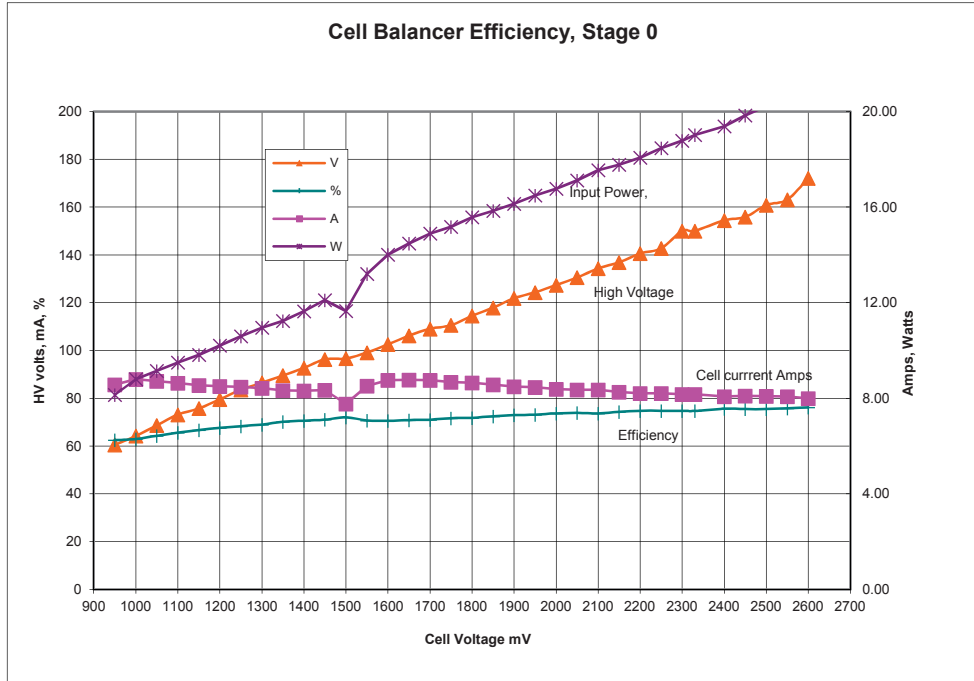


Fig. 3.88 Input power and efficiency versus cell voltage

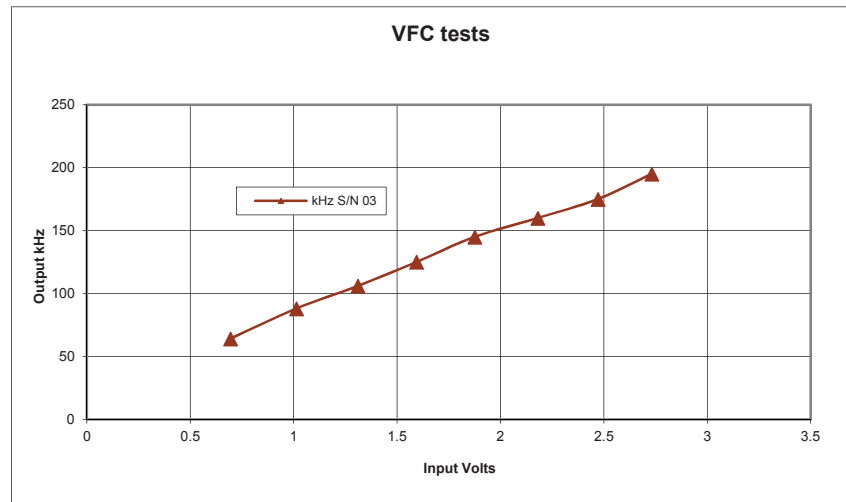


Fig. 3.89 VFC output frequency versus cell voltage using a 250 kHz VFC clock

Both of the PCB designs have had the latest modifications applied. All of the existing PCBAs should be replaced by the new version (10/10/13) so that everything is standard.

A further modification would be to incorporate some way of conveniently turning the system off. At present the system is self-powered and will continue balancing forever so long as there is sufficient supercapacitor charge. Currently, the only way to turn the system completely off is to remove all 64 of the 20A SMPS fuses as well as one 1A fuse in each local controller power supply. Turning the balancing process off while leaving the local controllers operating may be achieved by feeding REF IN with a DC voltage of 3V (or more), possibly from a couple of torch batteries. However the local controllers would still be drawing power (about 2.5W each).

(2) Rack unit fitout

Each group of eight supercapacitor stages with accompanying local controller fits into a rack unit and the existing 2m high rack frame has space for eight such units plus a small DC-DC converter.

(3) Cabling

The internal wiring will include high current (500A peak, welding cable would be ideal), between rack units and also linking them to the DC-DC converter. There will also be a high voltage (173V, 5A) cable linking rack units to distribute the SMPS output energy. Eight ribbon cables carrying the VFC clock signal, the three low order address lines and the local VFC outputs will link the local controllers with the VFC Controller. External connections will comprise two high current cables from the DC-DC converter and a USB cable from the VFC controller to an external computer which is shown in the circuit diagram.

(4) Mechanical

The rack frame will need seven more rack unit trays with tray supports fitted to the vertical rails for each unit. There are two sides to the rack frame which clip on and two doors. The doors will have to have hinges fitted to the rack frame to suit. To allow the rack frame to be moved, heavy duty 125mm castors or wheels should be fitted to the underside.

(5) DC to DC buck/boost converter

Because the supercapacitor bank (and for that matter the battery bank) operate over a range of voltages there is a need for a two quadrant DC-DC converter to convert the energy at the bank voltage to the motor operating voltage. This converter would need to handle 100kW on a peak basis (supercapacitor bank) or continuous basis (battery bank). The output voltage would be the range of designed motor voltages and the input voltage would be the maximum supercapacitor bank voltage (173V) down to perhaps one third of this, if 90% of the energy in the supercapacitors is to be utilised. The range for the battery bank would be smaller, but nevertheless appreciable, and based on the maximum LiPF₆ voltage range of perhaps 2.5V to 4.2V.

3.6 Summary of the Chapter

This chapter presents the basic working principles of battery and supercapacitor, specific battery and supercapacitor are chosen based on the energy system requirements. Different battery models are compared and developed for the hardware implementation of a hybrid energy storage system. The supercapacitor is not like a battery, the charging and discharging speed is quicker than for a battery. When supercapacitor cells are discharged, the instantaneous power supplied by the supercapacitor is very high so EVs can get enough traction power to start up. After doing the experimental testing for the battery and supercapacitor cell, different tests are conducted and results are carried out which are very useful for the hybrid energy storage system implementation. Another contribution of the work in this chapter is to develop a novel balancing circuit for an energy storage system. The current version of cell balancer developed in this chapter is designed for use with supercapacitors rather than battery cells but the same principle applies. The cell balancer development is an essential part of an energy storage system when a large number of cells are connected together to afford the energy.

References

- [3.1] http://gcep.stanford.edu/pdfs/ChEHeXOTnf3dHH5qjYRXMA/14_Burke_10_12_trans.pdf.
- [3.2] T Christian and M W Carlen, "Theory of Ragon Plots," *Journal of Power Sources*, 2000.
- [3.3] R. Dell, D.A.J. Rand, "Understanding batteries," Royal Society of Chemistry, 2001.
- [3.4] D. Linden and T.B. Reddy, "Handbook of Batteries," 3rd ed., McGraw- Hill, August 30, 2001.
- [3.5] O. Tremblay and L.A. Dessaint, "Experimental Validation of a Battery Dynamic Model for EV Applications," *World Electric Vehicle Journal* Vol. 3, ISSN 2032-6653, 2009.
- [3.6] Z. M. Salameh, M. A. Casacca, and W. A. Lynch, "A mathematical model for lead-acid batteries," *IEEE Trans. Energy Conversion*, vol. 7, no. 1, pp. 93–98, Mar. 1992.
- [3.7] M. Valvo, F. E. Wicks, D. Robertson, and S. Rudin, "Development and application of an improved equivalent circuit model of a lead acid battery," in *Proc. Energy Convers. Eng. Conf.*, vol. 2, Aug. 1996, pp. 1159–1163.
- [3.8] M. Ceraolo, "New dynamical models of lead-acid batteries," *IEEE Trans. on Power Systems*, vol. 15, no. 4, pp. 1184–1190, Nov. 2000.
- [3.9] S. Barsali and M. Ceraolo, "Dynamical models of lead-acid batteries: Implementation issues," *IEEE Trans. Energy Conversion*, vol. 17, no. 1, pp. 16–23, Mar. 2002.
- [3.10] L. Benini, G. Castelli, A. Macci, E. Macci, M. Poncino, and R. Scarsi, "Discrete-time battery models for system-level low-power design," *IEEE Trans. on VLSI Systems*, vol. 9, no. 5, pp. 630–640, Oct. 2001.
- [3.11] B. Schweighofer, K. M. Raab, and G. Brasseur, "Modeling of high power automotive batteries by the use of an automated test system," *IEEE Trans. on Instrument Measurement*, vol. 52, no. 4, pp. 1087–1091, Aug. 2003.
- [3.12] L. Gao, S. Liu, and R. A. Dougal, "Dynamic lithium-ion battery model for system simulation," *IEEE Trans. Compon. Packag. Technol.*, vol. 25, no. 3, pp. 495–505, Sep. 2002.

- [3.13] M. Chen and G.A. Rincon-Mora, "Accurate Electrical Battery Model Capable of Predicting Runtime and I-V Performance," *IEEE Trans. Energy Conversion*, vol. 21, no. 2, pp. 504-511, June 2006.
- [3.14] H. Zhang and Mo-Yuen Chow, "Comprehensive Dynamic Battery Modeling for PHEV Applications," in *Proceedings of 2010 IEEE PES General Meeting*, Minneapolis, MN, July 26-29, 2010.
- [3.15] X. Feng and Z. Sun, "A battery model including hysteresis for State-of-Charge estimation in Ni-MH battery," in *Proceedings of Vehicle Power and Propulsion Conference*, 2008. VPPC. IEEE, 2008, pp. 1-5.
- [3.16] S. Buller, M. Thele, R. W. D. Doncker, and E. Karden, "Impedance based simulation models of supercapacitors and Li-ion batteries for power electronic applications," *IEEE Transactions on Industry Applications*, Vol. 41, Issue 3, May-June 2005, pp. 742 – 747.
- [3.17] M. Endo, S. Iijima, M. S. Dresselhaus, "Carbon Nanotubes", Elsevier Science Limited, ISBN 008 0426824, 1996.
- [3.18] R. A. Dougal, L. Gao, and S. Liu, "Ultracapacitor model with automatic order selection and capacity scaling for dynamic system simulation", *Journal of Power Sources*, vol. 126, pp. 250-257, 2004.
- [3.19] W. Yang, J. E. Carletta, T. T. Hartley, and R. J. Veillette, "An ultracapacitor model derived using time-dependent current profiles," in *Proc. 51st MWSCAS*, Aug. 10–13, 2008, pp. 726–729.
- [3.20] A. Grama, L. Grama, D. Petreus, and C. Rusu, "Supercapacitor modelling using experimental measurements," in *Proc. ISSCS*, Jul. 9–10, 2009, pp. 1–4.
- [3.21] R. M. Nelms, D. R. Cahela, and B. J. Tatarchuk, "Modeling double-layer capacitor behavior using ladder circuits," *IEEE Trans. Aerosp. Electron. Syst.*, vol. 39, no. 2, pp. 430–438, Apr. 2003.
- [3.22] L. Zubieta and R. Bonert, "Characterization of double-layer capacitor (DLCs) for power electronics application," *IEEE Trans. Ind. Appl.*, vol. 36, no. 1, pp. 199–205, Jan./Feb. 2000.

- [3.23] S. Buller, E. Karden, D. Kok, and R. W. De Doncker, "Modeling the dynamic behavior of supercapacitors using impedance spectroscopy," *IEEE Trans. Ind. Appl.*, vol. 38, no. 6, pp. 1622–1626, Nov./Dec. 2002.
- [3.24] F. Rafik, H. Gualous, R. Gallay, A. Crausaz, and A. Berthon, "Frequency, thermal and voltage supercapacitor characterization and modeling," *Journal of Power Sources*, vol. 165, no. 2, pp. 928–934, Mar. 2007.
- [3.25] R. Faranda, M. Gallina, and D. T. Son, "A new simplified model of doublelayer capacitors," in *Proc. Int. Conf. Clean Elect. Power*, May 21–23, 2007, pp. 706–710.
- [3.26] F. Belhachemi, S. Rael, and B. Davat, "A physical based model of power electric double-layer supercapacitors," in *Conf. Rec. IEEE IAS Annu. Meeting*, Oct. 8–12, 2000, vol. 5, pp. 3069–3076.
- [3.27] R. L. Spyker and R. M. Nelms, "Classical equivalent circuit parameters for a double-layer capacitor," *IEEE Trans. Aerosp. Electron. Syst.*, vol. 36, no. 3, pp. 829–836, Jul. 2000.
- [3.28] J. J. Quintana, A. Ramos, and I. Nuez, "Identification of the fractional impedance of ultracapacitors," in *Proc. IFAC Workshop FDA*, 2006. [CD-ROM].
- [3.29] D. Riu, N. Reitere, and D. Linzen, "Half order modelling of supercapacitor," in *Conf. Rec. IEEE IAS Annu. Meeting*, 2004, vol. 4, pp. 2550–2554.
- [3.30] B. Lunz, Z. Yan, J. Gerschler, "Influence of plug-in hybrid electric vehicle charging strategies on charging and battery degradation costs," *Energy Policy* 2012;46:511–9.
- [3.31] W. Kempton, S. Letendre, "Electric vehicles as a new power source for electric utilities," *Transportation Research Part D* 1997, vol. 2, pp. 157–175.
- [3.32] Research of supercapacitor voltage equalization strategy on rubber tyred gantry crane energy saving system
- [3.33] J. Cao, N. Schofield and A. Emadi, "Battery balancing methods: A comprehensive review," *IEEE Vehicle Power and Propulsion Conference*, VPPC 08. pp. 1-6, 2008.
- [3.34] K. Zhi-Guo, Z. Chun-Bo, L. Ren-Gui and C. Shu-Kang, "Comparison and Evaluation of Charge Equalization Technique for Series Connected Batteries," *37th IEEE Power Electronics Specialists Conference*, pp. 1-6, 2006.

- [3.35] S. Moore and P. Schneider, "A Review of Cell Equalization Methods for Lithium Ion and Lithium Polymer Battery Systems," in *Proceedings of the SAE 2001 World Congress*, 2001.
- [3.36] M. J. Isaacson, R. P. Hollandsworth, P. J. Giampaoli, F. A. Linkowsky, A. Salim and V. L. Teofilo, "Advanced lithium ion battery charger," *15th Annual Battery Conference on Applications and Advances*, pp. 193-198, Jan. 2000.
- [3.37] N. H. Kutkut, and D. M. Divan, "Dynamic Equalization Techniques for Series Battery Stacks," *IEEE Telecommunications Energy Conference*, INTELEC, pp. 514-521, 1996.
- [3.38] D. Linzen, S. Buller, E. Karden, "Analysis and Evaluation of Charge-Balancing Circuits on Performance, Reliability, and Lifetime of Supercapacitor Systems," *IEEE Transactions on Industry Applications*, vol. 41, no. 5, pp. 1135 - 1141, Sept/Oct 2005.
- [3.39] S. West, and P.T. Krein, "Switched-Capacitor Systems For Battery Equalization," *IEEE Modern Techniques and Technology (MTT 2000). Proceedings of the VI International Scientific and Practical Conference of Students, Post-graduates and Young Scientists*, pp. 57-59, 2000.
- [3.40] C. Pascual, and P.T. Krein, "Switched Capacitor System for Automatic Series Battery Equalization," *IEEE Applied Power Electronics Conference and Exposition, APEC '97 Conference Proceedings*, 12th Vol. 2, pp. 848-854, 1997.
- [3.41] Carmelo Speltino, Anna Stefanopoulou and Giovanni Fiengo, "Cell Equalization in Battery Stacks Through State Of Charge Estimation Polling," *American Control Conference (ACC)*, pp. 5050-5055, 2010
- [3.42] A.C. Baughman, and M. Ferdowsi, "Double-Tiered Switched-Capacitor Battery Charge Equalization Technique," *IEEE Transactions on Industrial Electronics*, Vol. 55. pp. 2277-2285, 2008.
- [3.43] A. Baughman, and M. Ferdowsi, "Double-Tiered Capacitive Shuttling Method for Balancing Series-Connected Batteries," *IEEE Conference on Vehicle Power and Propulsion*, pp. 109-113, 2005.

- [3.44] P. Hong-Sun, K. Chol-Ho, and L. Joong-Hui, "Design of a Charge Equalization Based on Battery Modularization," *IEEE Trans. on Vehicular Technology*, Vol. 58, pp. 3938-3946, 2009.
- [3.45] T. H. Phung, J. C. Crebier, and N. T. Van Nguyen, "Optimized Structure for Next-to-Next Balancing of Series- Connected Lithium-ion Cells," *26th Annual IEEE Applied Power Electronics Conference and Exposition (APEC)*, pp. 1374-1381, 2011.
- [3.46] P. Barrade, "Series Connection of Supercapacitors: Comparative Study of Solutions for the Active equalization of the Voltages," in *7th International Conference on Modeling and Simulation of Electric Machines, Converters and Systems*, Montréal, Canada, 2002.
- [3.47] A. Xu, Liu X., and S. Xie, "Research on dynamic voltage equalization circuit for series connected ultracapacitors," in *IEEE International Conference on Industrial Technology*, 2009.
- [3.48] A. Xu, S. Xie, and X. Liu, "Dynamic Voltage Equalization for Series-Connected Ultracapacitors in EV/HEV Applications," *IEEE Transaction on Vehicular Technology*, vol. 58, pp. 3981-3987, October 2009.
- [3.49] D. C. Hopkins, C. R. Mosling, and S. T. Hung, "Dynamic equalization during charging of serial energy storage elements," *IEEE Trans. Ind. Appl.*, vol. 29, no. 2, pp. 363–368, Feb. 1993.
- [3.50] H. Schmidt and C. Siedle, "The charge equalizer—A new system to extend battery lifetime in photovoltaic systems, UPS and electric vehicles," in *Proc. INTELEC Conf.*, 1993, pp. 146–151.
- [3.51] N. H. Kutkut and D. M. Divan, "Dynamic equalization techniques for series battery stacks," in *Proc. IEEE Telecommun. Energy Conf.*, 1996, pp. 514–521.
- [3.52] N. H. Kutkut, "A modular non-dissipative current diverter for EV battery charge equalization," in *Proc. IEEE Appl. Power Electron. Conf. Expo.*, 1998, vol. 2, pp. 686–690.

- [3.53] Y. S. Lee and G. T. Cheng, "Quasi-resonant zero-current switching bidirectional converter for battery equalization applications," *IEEE Trans. Power Electron.*, vol. 21, no. 5, pp. 1213–1224, Sep. 2006.
- [3.54] T. Inoue, H. Koizumi, "A voltage equalizer applying a charge pump for energy storage systems," *Circuit theory and design*, 2009, ECCTD 2009.
- [3.55] M. Uno, "Supercapacitor-based Electrical Energy Storage System," Japan Aerospace Exploration Agency.
- [3.56] W. Moore, J. Schneider, "A Review of Cell Equalization Methods for Lithium Ion and Lithium Polymer Supercapacitor Systems," Society of Automotive Engineers Inc., 2001-01-0959, 2001.
- [3.57] S. Chung., T. Bloking, "Electronically conductive phospho-olivines as lithium storage electrodes," *Nature Materials*, pp.123-128, 2002.
- [3.58] A123 Systems whitepaper, Inc, "Nanophosphate basics: an overview of the structure, properties and benefits of A123 systems' proprietary lithium ion battery technology."
- [3.59] Z.M. Salameh, M. A. Casacca, and W. A. Lynch, "A mathematical model for lead–acid batteries," *IEEE Trans. Energy Conversion management*, vol. 7, no. 1, pp. 93–98, Mar. 1992.
- [3.60] M. A. Casacca, "Determination of lead–acid battery capacity via mathematical modeling techniques," *IEEE Trans. Energy Conversion and management*, vol. 7, no. 3, pp. 442–446, Sep. 1992.
- [3.61] M. Ceraolo, "New dynamical models of lead–acid batteries," *IEEE Trans. Power Syst.*, vol. 15, no. 4, pp. 1184–1190, Nov. 2000.
- [3.62] S. Barsali and M. Ceraolo, "Dynamical models of lead–acid batteries: Implementation issues," *IEEE Trans. Energy Conversion and management*, vol. 17, no. 1, pp. 16–23, Mar. 2002.

CHAPTER 4

IMPLEMENTATION OF THE V2G SYSTEM AT COMPONENT LEVEL

4.1 Introduction

As mentioned in previous chapters, enormous advantages arise from the interaction of EVs with the power grid. Focusing the interaction of electric vehicles (EVs) with the different systems where they can be connected for vehicle to grid (V2G) system implementation is the essential stage in this study. The concept of G2V is the simplest way of integration of the EV batteries charging system with the power grid. It does not require any communication between both systems and only allows energy flow from the power grid to the EVs. Nowadays, this is the most common (and almost unique) batteries charging process for EVs, and it will be the first approach to the massive integration of these vehicles. The V2G technology utilizes the stored energy in the EV batteries to contribute electricity back to the electrical power grid, when the grid operators request it. This way EVs can receive energy during the excess of production and deliver it back to the power grid during the periods of great demand, balancing the energy production and consumption, and also stabilizing the intermittent production from renewable energy sources, improving their integration into the power grid. Each vehicle should have two fundamental elements: a connection for the bidirectional flow of the electrical energy; and a logical connection for the communication and control on both sides. The control signal from the power grid operator to the vehicles can be implemented through a broadcast radio signal, through a cell phone network, through an internet connection, or through Power Line Communication (PLC) [4.1].

In high power applications, such as flexible alternating current transmission systems (FACTS) [4.2], high voltage direct current (HVDC) transmission systems [4.3], and large capacity renewable energy (wind and PV) systems [4.4]-[4.5], low switching frequencies are employed

to reduce the switching losses. However, it is of very high priority to control the power converters intelligently to maintain high power quality in the current. This is important in a distributed power generation system, and also in the micro and smart grids in the future [4.6]-[4.7].

High power converters for distributed generation need a grid-friendly operation, low harmonic conductive electromagnetic emission for low electromagnetic interference, and at the same time converters must be controlled with low switching frequency in order to reduce the commutation losses. The power-switching devices used in these converters, such as high-voltage insulated-gate bipolar transistor (IGBT) and integrated-ate commutated thyristor (IGCT), are capable of switching at a modest frequency of 3-5 kHz. In high-power applications, it is often desirable to switch at even lower frequencies for lower switching power losses and higher power-handling capability. proper selection of the switching frequency and PWM scheme is critical in minimizing harmonics and imbalance, and therefore, to achieve the desired system performance and to avoid costly and complex filters.

For bidirectional power control of the charger used for the V2G services, a large variety of pulse-width modulation (PWM) converters have been developed, and the control strategies have been an ongoing research subject over the last few decades.

Three-phase AC/DC converters have been extensively used in industrial application such as speed drives [4.8], renewable energies [4.9], active filters [4.10]-[4.11], micro-grid systems [4.12]-[4.13], and so on. Compared with a conventional diode rectifier, they have several advantages: bidirectional power flow, unity power factor, and sinusoidal input AC. Therefore, AC/DC converters are adopted in applications that require less distortion in the current waveforms for the purpose of observing the strict regulations on electrical harmonic pollutions. Since the AC/DC converters have abilities to control the input currents in sinusoidal waveforms, the unity power factor can be easily controlled by regulating the currents in phase with the grid voltages. Additionally, it has an advantage of reducing the size of the capacitor required by the system because the dc-link voltage is regulated by controlling the input power [4.14]-[4.20].

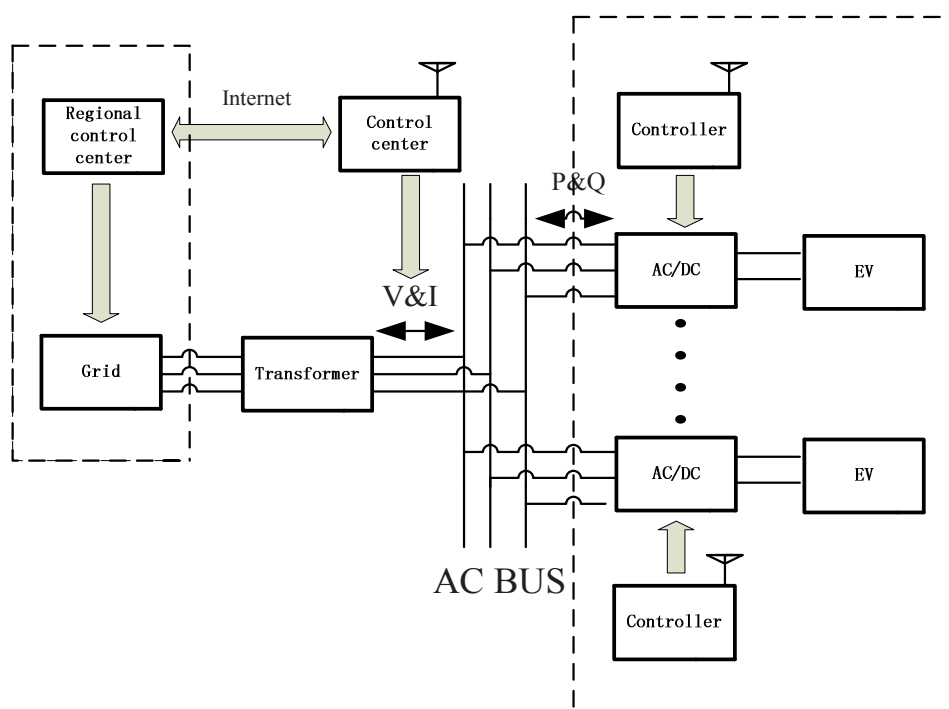


Fig. 4.1 V2G charger structure with the AC transmission bus

Fig. 4.1 shows the main topology used for the V2G charger structure in the smart car park. Fig. 4.1 is the AC bus topology. The AC bus topology has 3 levels of control: EV charger control, V2G control and economic related issues.

The AC transmission bus is composed of two main parts, the grid side and EV side. The regional control centre exchanges information with control centre through internet connection. Then the regional control centre gives signals to the grid side to determine how much electricity should be supplied to the smart car park. The controllers used in the EV side control the AC/DC converter used for charging and discharging based on the energy required by the EV owners and their behaviours. The controllers used for the EV side communicate with the control center through wireless communication. The AC bus topology only uses AC/DC converters, the power loss should be lower than the DC bus topology. However, for AC bus topology, there should be two parts of control for the active and reactive power (P&Q) control.

For V2G system implementation, the interface between grid and vehicle is a bidirectional charger. There are several ways to classify battery chargers. Based on the type of connection there is conductive charging and inductive charging (contactless charging). Based on the power flow direction, there are uni-directional chargers and bi-directional chargers. Based on the utilization of the drive train, there are integrated chargers and stand-alone chargers. Based on the location of the battery charger, there are on-board chargers and off-board (stationary) chargers. Based on the number of power stages, there are two-stage chargers and single-stage chargers.

A bi-directional battery charger can be either a two-stage solution or a single-stage solution. Two-stage indicates a bi-directional AC/DC stage and a bi-directional DC/DC stage. Contrary to a two-stage structure, single stage topology will be a promising solution which will reduce cost and increase system density. The controller design for single-stage topology will be also an interesting topic because the control structure is different compared to the well defined two-stage converter control structure. Municipal charging deck architecture addresses the fast charging technique with the integration of available renewable resources and the utilization of ultra-capacitors to compensate for the power demand during the peak charging [4.21].

The power converters used for the V2G services are required to operate more efficiently and effectively to maintain high power quality and dynamic stability [4.22]-[4.23]. To fulfil these requirements, advanced control techniques are desired.

4.2 Direct Power Control for Bidirectional Power Flow Control

Effective performance control strategies for electrical drives and power converters have been an ongoing research subject for several decades. With the development of more forms of electric transportation, this is becoming more so [4.24]. The direct torque control (DTC) has become a powerful control scheme since its first proposal in the 1980s [4.25]-[4.28]. Because of its fast transient performance, simple control structure and robustness, DTC has been further utilized in renewable energy applications [4.29]-[4.30]. Among the control techniques used in power

converters, the direct power control (DPC), which is adapted from DTC for AC machines, has become one of the most popular control strategies, again, because of its robustness and simplicity [4.31]-[4.35]. In the conventional switching table based DPC (SDPC), the converter states are chosen by using a switching table, which is constructed from the instantaneous errors between the estimated and the referenced values of active and reactive power. Unlike the voltage oriented control (VOC), it does not need internal current loops and modulators, and thus the coordinate transformation is also eliminated. However, the main drawback is the large power ripples, leading to distorted line currents.

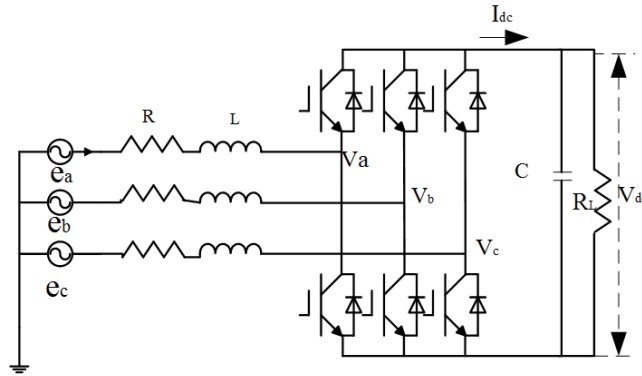


Fig. 4.2 Three-phase AC-DC converter topology

A three-phase two-level AC/DC converter, as shown in Fig. 4.2, is used as an example to illustrate the direct power control and model predictive power control strategy. Three IGBT half-bridge units are connected to the main grid via a choke consisting of three series-connected inductors L and resistors R . On the DC side, a purely resistive load R_L is connected to the IGBT bridge with a capacitor C in parallel. The converter input voltage can be expressed as the complex space vectors where

$$e_{\alpha\beta} = \begin{bmatrix} e_\alpha \\ e_\beta \end{bmatrix} = \frac{2}{3} \begin{bmatrix} 1 & -1/2 & -1/2 \\ 0 & \sqrt{3}/2 & -\sqrt{3}/2 \end{bmatrix} \begin{bmatrix} e_a \\ e_b \\ e_c \end{bmatrix} \quad (4.1)$$

$$I_{\alpha\beta} = \begin{bmatrix} I_\alpha \\ I_\beta \end{bmatrix} = \frac{2}{3} \begin{bmatrix} 1 & -1/2 & -1/2 \\ 0 & \sqrt{3}/2 & -\sqrt{3}/2 \end{bmatrix} \begin{bmatrix} I_a \\ I_b \\ I_c \end{bmatrix} \quad (4.2)$$

$$e_{\alpha\beta} = L \frac{dI_{\alpha\beta}}{dt} + RI_{\alpha\beta} + V_{\alpha\beta} \quad (4.3)$$

$$C \frac{dV_{dc}}{dt} = \frac{3}{2} (I_\alpha S_\alpha + I_\beta S_\beta) - I_L \quad (4.4)$$

The active and reactive power exchanged with the grid can be calculated as

$$\begin{bmatrix} P \\ Q \end{bmatrix} = \frac{3}{2} \begin{bmatrix} e_\alpha & e_\beta \\ e_\beta & -e_\alpha \end{bmatrix} \begin{bmatrix} I_\alpha \\ I_\beta \end{bmatrix} \quad (4.5)$$

Since SDPC is a widely employed and accepted control strategy, it is always used as a benchmark reference for other control strategies in research work. Fig. 4.3 illustrates the SDPC scheme, where the reference active power P^* is delivered from the PI DC voltage regulator while the referenced reactive power Q^* is generally set to zero for unity power factor. The digitized signals d_P and d_Q are then generated by two fixed-band hysteresis comparators using the tracking errors between the estimated and referenced values of the active and reactive powers. The converter switching signals are then selected from a look-up switching table (Table 4.1) according to d_Q , and d_P and the position of system input voltage vector $e_{\alpha\beta}$ in the α - β plane, which has 12 sectors as shown in Fig. 4.4.

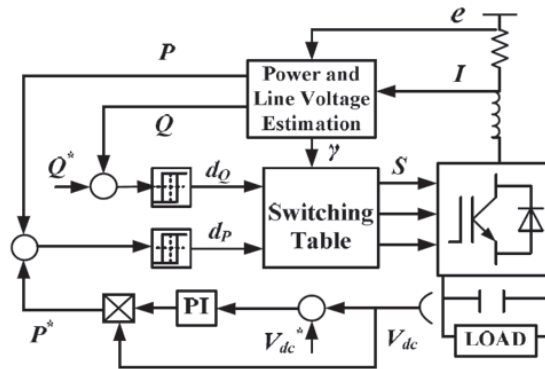


Fig. 4.3 Control block of SDPC

TABLE 4.1 Switching Table of Conventional SDPC

d_p	d_Q	S_1	S_2	S_3	S_4	S_5	S_6	S_7	S_8	S_9	S_{10}	S_{11}	S_{12}
1	0	V_6	V_7	V_1	V_0	V_2	V_7	V_3	V_0	V_4	V_7	V_5	V_0
	1	V_7	V_7	V_0	V_0	V_7	V_7	V_0	V_0	V_7	V_7	V_0	V_0
0	0	V_6	V_1	V_1	V_2	V_2	V_3	V_3	V_4	V_4	V_5	V_5	V_6
	1	V_1	V_2	V_2	V_3	V_3	V_4	V_5	V_5	V_5	V_6	V_6	V_1

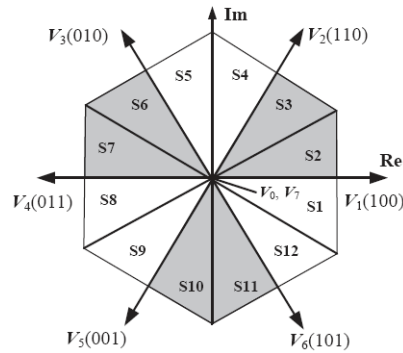


Fig. 4.4 Possible voltage vectors

An in-depth analysis of the SDPC switching table reveals that the voltage vector selected is not necessarily the best one to correct the power errors in some sectors. For example, V_7 is selected using the table if $d_p > 0$ and $d_Q > 0$ in sector S1. However, the reactive power derivative (or “slope”) of V_7 is near zero, which means that activating V_7 just keeps the reactive power constant rather than increasing it, resulting in large power ripples and current distortion. In this case, the more suitable vector to control the power is V_3 rather than V_7 .

4.3 Model Predictive Control for Bidirectional Power Flow Control

Very recently, a new control strategy, known as the predictive control, was introduced in electrical drives [4.36]-[4.38], [4.39]-[4.45]. It has many merits, such as reduced torque, flux

and active/reactive power ripples, constant switching frequency, and excellent steady-state and transient responses.

The main characteristic of predictive DPC strategy of converters is the use of the converter model to predict the behavior of the controlled variables in the following sampling instants. The predictive behavior is then used to obtain the most effective voltage vector to control the active and reactive power with excellent performance. The key to the scheme is the prediction of power at the $(k+1)$ th sampling instant for different voltage vectors. This assumes that an optimal voltage vector is able to minimize the power ripple effectively when applied during the interval between the k th and $(k+1)$ th instants. Fig. 4.5 shows a block diagram of the MPC.

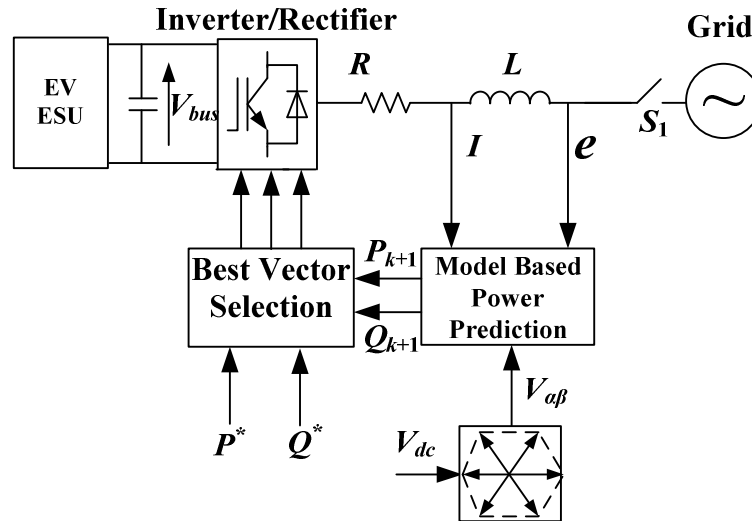


Fig. 4.5 Control block of model predictive control (MPC)

For sinusoidal and balanced line voltage,

$$\bar{e} = e_{\alpha} + je_{\beta} = |\bar{e}| e^{j\omega t} \quad (4.6)$$

The following expression can be deduced as

$$\frac{d}{dt} \begin{bmatrix} e_{\alpha} \\ e_{\beta} \end{bmatrix} = \omega \cdot \begin{bmatrix} -e_{\beta} \\ e_{\alpha} \end{bmatrix} \quad (4.7)$$

The instantaneous active and reactive power derivation can be calculated by

$$\frac{d}{dt} \begin{bmatrix} P_i \\ Q_i \end{bmatrix} = -\frac{R}{L} \begin{bmatrix} P_i \\ Q_i \end{bmatrix} + \omega \begin{bmatrix} -Q_i \\ P_i \end{bmatrix} + \frac{3}{2L} \begin{bmatrix} (|\bar{e}|^2 - \text{Re}(\bar{e}\bar{V}_i^*)) \\ -\text{Im}(\bar{e}\bar{V}_i^*) \end{bmatrix} \quad (4.8)$$

Therefore, the predictive power at the end of the sampling period T_s for each converter switching state can be expressed as

$$\begin{bmatrix} P_i^{k+1} \\ Q_i^{k+1} \end{bmatrix} = T_s \left(-\frac{R}{L} \begin{bmatrix} P_i^k \\ Q_i^k \end{bmatrix} + \omega \begin{bmatrix} -Q_i^k \\ P_i^k \end{bmatrix} + \frac{3}{2L} \begin{bmatrix} (|\bar{e}|^2 - \text{Re}(\bar{e}\bar{V}_i^*)) \\ -\text{Im}(\bar{e}\bar{V}_i^*) \end{bmatrix} \right) + \begin{bmatrix} P_i^k \\ Q_i^k \end{bmatrix} \quad (4.9)$$

Then the system can evaluate the effects of each converter switching state on active and reactive power, and select the one producing the least power ripple according to a specific cost function, which is defined as

$$J_i = \sqrt{(P^* - P_i^{k+1})^2 + (Q^* - Q_i^{k+1})^2} \quad (4.10)$$

4.4 Flexible Power Regulation between Grid and EVs

EV chargers are of critical importance to strengthen the interaction between the grid and the vehicle in a responsible way so that neither vehicle nor grid is harmed in the short and long term. It can afford flexible power regulation between grid and vehicles. A simple unidirectional charger is enough to charge a vehicle battery with required voltage and current waveforms. In contrast, an advanced bidirectional charger is capable of making the grid integration beneficial to the utility and the owner of the vehicle. Usually, a vehicle stays parked during 90-95% of their total lifetime. Therefore, the utility can benefit from this valuable asset and utilize alternative vehicle technologies, a valuable investment.

EV chargers can provide the grid with the following services that can be included in V2G: 1) voltage support, 2) reactive power compensation, 3) harmonic filtering, 4) power factor regulation, 5) load balancing, and 6) peak shaving. Also, if the grid electricity is lost, the charger should be suitable for islanded operation for emergency power which is often called vehicle to home (V2H) or vehicle to any load (V2X).

Other than management of V2G energy, power regulation services of V2G can provide dynamic regulation power to compensate for the continuous power imbalance between the demand and the supply. It is more suitable for EVs to perform in the advanced distribution grid with a large share of renewable generation [4.46]-[4.48]. On the one hand, the dynamic regulation is performed on the time scale of seconds, which requires alternating charging and discharging of EV batteries to provide positive and negative regulations. Consequently, EVs characterized by fast power response and bi-directional four-quadrant power flow via the power electric charger are perfect candidates for dynamic power regulations aiming to stabilize the grid frequency and voltage. Moreover, the reactive power can be independently injected at the AC terminal even without the EV connected to the charging facility, by virtue of the capacitor positioned at the DC link of the converter. On the other hand, the positive regulations over a long time must be equivalent to the negative regulations, which makes the net energy to be roughly zero. This is a significant advantage of dynamic regulation performed by EVs as no energy change occurs on the battery storage. Also, small energy decline only involves shallow discharging that has a minimal impact on the battery cycle, and therefore prevents the battery from wearing out which is one key challenge of V2G application.

From the previous discussion, with the bidirectional converter, the battery can behave both as a source or sink, i.e., the vehicles at the charging station can collectively discharge or charge respectively. Hence, EVs with the help of converters can support not only the active power, but also the reactive power. When EVs can afford the reactive power to the grid, the V2G services will attract more and more EVs owner's willingness to support the grid.

When EVs are parking at the car park, according to the grid and EV owners' behaviour, the batteries can absorb or inject power from the grid during charging and discharging. Fig. 4.6 shows the four quadrant operation of power flow through inverter between grid and the vehicles.

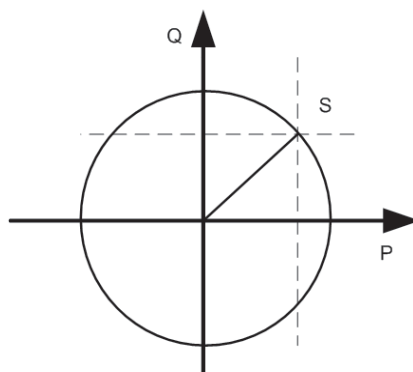


Fig. 4.6 Four quadrant operation of power flow through inverter between grid and vehicle

A charger used for the V2G services can be configured in two different ways in terms of its active power P and reactive power Q transfer capability with the utility grid. Fig. 4.6 describes the available operation regions for the bidirectional charger (positive P or Q means that the power is sent to the charger by the grid). P_{max} and Q_{max} are equal to the apparent power rating of the charger. The unidirectional chargers that are in use in today’s PHEVs and EVs operate at the positive x-axis of the P-Q plane. They operate close to unity power factor (pf) and allow control of the active power used to charge the battery. The four-quadrant bidirectional charger that operates in all four regions is shown in Fig. 4.6.

From the last section, we could see that through the four quadrant operation, the vehicles can afford V2G services (both active and reactive power) to the grid side. For a typical radial distribution system shown in Fig. 4.7, the batteries of the EVs, behaving as a distributed energy resource (DER), are connected at bus i via a charging station. This charging station injects active power P_{EV} and reactive power Q_{EV} when grid side needs it.

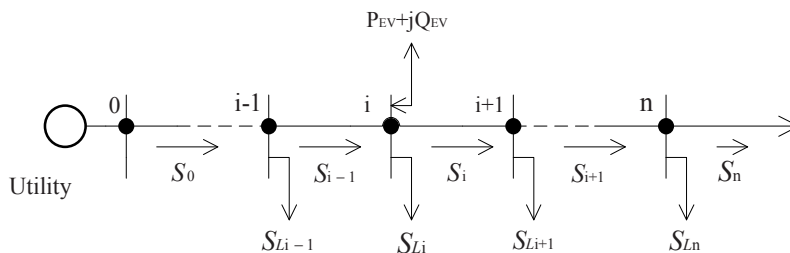


Fig. 4.7 Branch of a radial distribution system

In Fig. 4.7, $S_0=P_0+jQ_0$, $S_{i-1}=P_{i-1}+jQ_{i-1}$, $S_i=P_i+jQ_i$, $S_{i+1}=P_{i+1}+jQ_{i+1}$, and $S_n=P_n+jQ_n$ are the total apparent power flowing in the respective branch.

$S_{Li-1}=P_{Li-1}+jQ_{Li-1}$, $S_{Li}=P_{Li}+jQ_{Li}$ and $S_{Li+1}=P_{Li+1}+jQ_{Li+1}$ are the load at respective node. V_i is the voltage of bus i , P_i and Q_i are the real and reactive power flows in line i . P_{Li} and Q_{Li} are the load at bus i . The batteries of the EVs connected at bus i injects active and reactive power. The equations for voltages at $(i+1)$ th bus can be described as

$$V_{i+1}^2 = V_i^2 - 2(P_i r_i + Q_i x_i) + \left(\frac{P_i^2 + Q_i^2}{V_i^2} \right) (r_i^2 + x_i^2) \quad (4.11)$$

$$P_{i+1} = P_i - P_{Li+1} - P_{lossi} \quad (4.12)$$

$$Q_{i+1} = Q_i - Q_{Li+1} - Q_{lossi} \quad (4.13)$$

$$P_{Lossi} = \left(\frac{P_i^2 + Q_i^2}{V_i^2} \right) r_i \quad (4.14)$$

$$Q_{Lossi} = \left(\frac{P_i^2 + Q_i^2}{V_i^2} \right) x_i \quad (4.15)$$

$$\Delta V_{EV} = \frac{P_{EV} r_i + Q_{EV} x_i}{V_i} \quad (4.16)$$

From Fig. 4.7 and equations, it is found that the power injection by EVs' batteries reduce power losses and improve the bus voltage of the network. This is due to the fact that power flow in the transmission and distribution systems is reduced, as EV battery generates power locally to fulfil demand. This reduction in power losses is one of the main features of V2G. Other benefits of V2G are peak demand management, frequency and voltage stability, and reactive power support.

From the research and discussion above, EVs parking in the Smartpark can afford both active power and reactive power to grid according to grid and EV owners' requirements. The bidirectional power flow can be controllable and benefit both grid and EVs.

4.5 Numerical Simulation

4.5.1 Comparison results for the DPC and MPC

To check feasibility of the DPC applied for the V2G bidirectional charger, numerical simulations were carried out by using Matlab/Simulink. The system parameters are listed in Table 4.2. The nominal DC-link voltage is 300V. The frequency of the AC power grid is 50Hz.

TABLE 4.2 Electrical Parameters of Power Circuit

Resistance of reactor	R	450 m Ω
Inductance of reactor	L	4.5 mH
DC-bus capacitor	C	3000 μ F
Load resistance	R_L	90 Ω
Line to line ac Voltage	e	120 V(rms)
Source voltage frequency	f	50 Hz
Power	P	1 kW
DC-bus voltage	V_{dc}	300 V
Sample time	T_s	40 μ s

The reference DC-link voltage V_{dc} is set to be 300V, and the reference reactive power Q^* is set to 0 VAR for unity power factor operation. Fig. 4.8-4.14 shows the steady and dynamic state performance of the DPC,

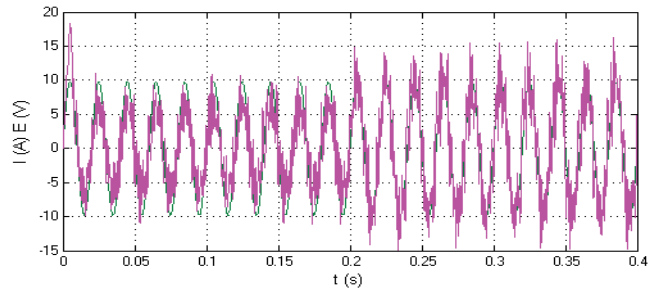


Fig. 4.8 Input AC side V_a and I_a (DPC)

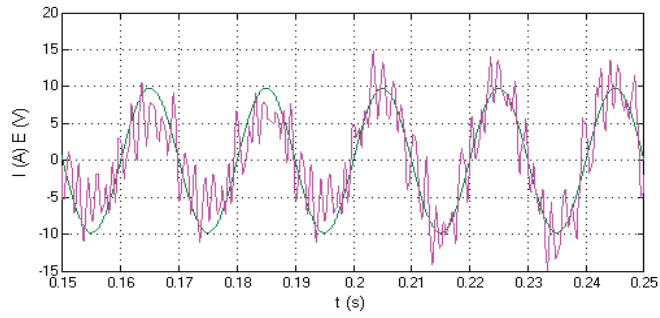


Fig. 4.9 Input AC side V_a and I_a (DPC) (0.15s-0.25s)

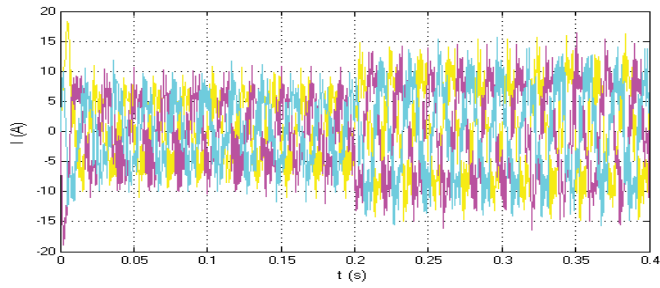


Fig. 4.10 Input I_a , I_b and I_c (DPC)

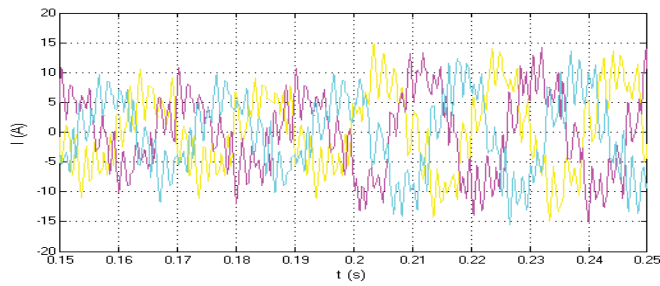


Fig. 4.11 Input I_a , I_b and I_c (DPC) (0.15s-0.25s)

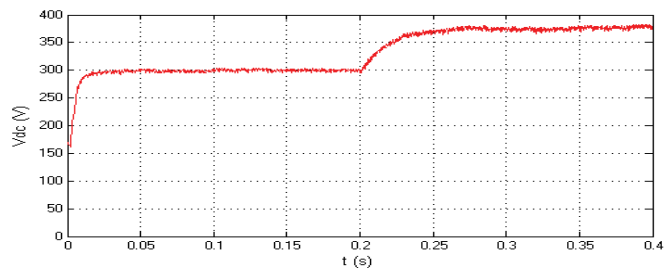


Fig. 4.12 Output DC voltage Vdc (DPC)

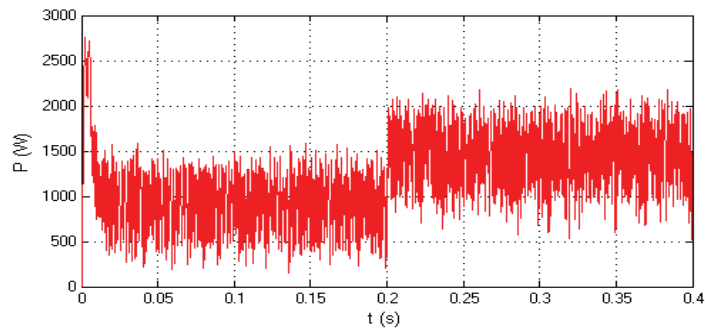


Fig. 4.13 Input active power P (DPC)

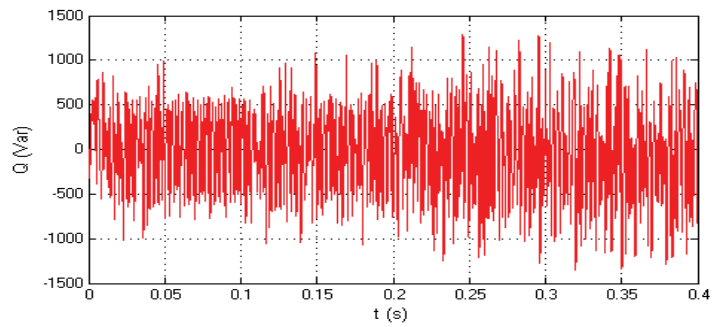


Fig. 4.14 Input reactive power Q (DPC)

Fig. 4.8 shows the input AC side current and voltage waveform for phase A when input active power increased under DPC algorithm. Fig. 4.9 is the enlargement of the current and voltage waveform for phase A between 0.15s to 0.25s. From Fig. 4.9 it can be observed that the current and voltage are same phase. Fig. 4.10 is the input three phase current waveform when input active power increased.

Following are simulation results of the MPC results. The reference DC-link voltage V_{dc} is set to be 300V, and the reference reactive power Q^* is set to 0 VAR for unity power factor operation. Fig. 4.15-4.21 shows the steady and dynamic state performance of the MPC. Fig. 4.16 to Fig. 4.18 show the input AC side current and voltage waveform when input active power increased under MPC algorithm. From them it can be observed that the power factor is same when active power changed.

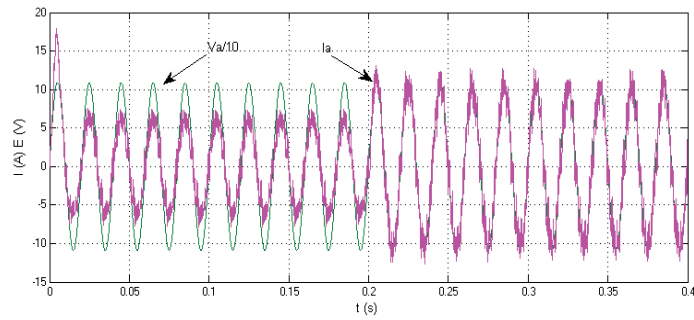


Fig. 4.15 Input AC side V_a and I_a (MPC)

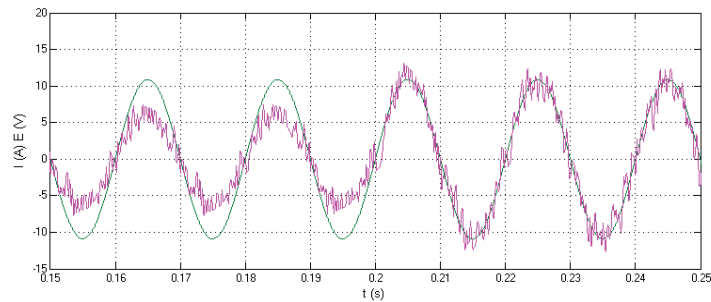


Fig. 4.16 Input AC side V_a and I_a (MPC) (0.15s-0.25s)

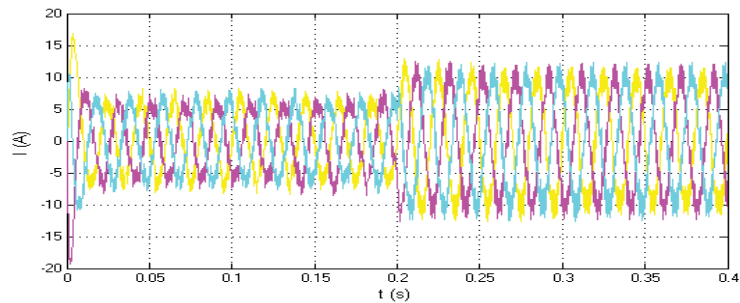


Fig. 4.17 Input I_a , I_b and I_c (MPC)

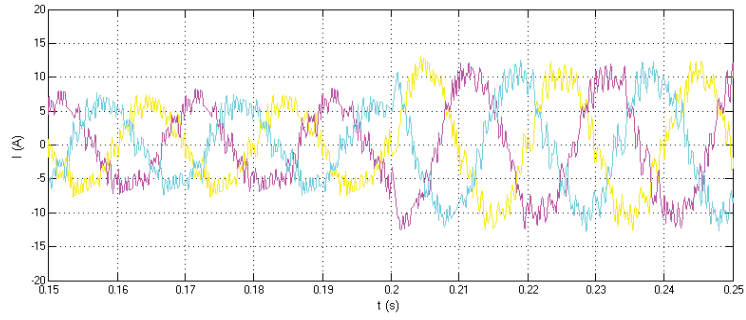


Fig. 4.18 Input Ia, Ib and Ic (MPC) (0.15s-0.25s)

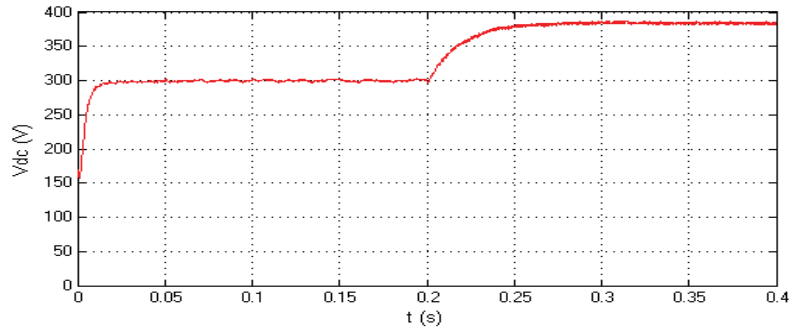


Fig. 4.19 Output DC voltage Vdc (MPC)

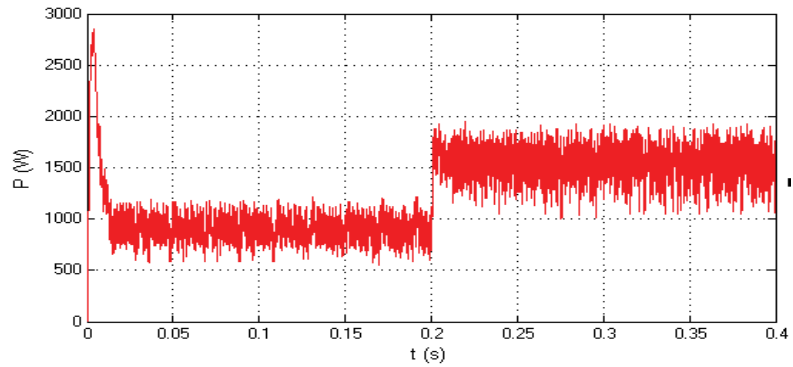


Fig. 4.20 Input active power P (MPC)

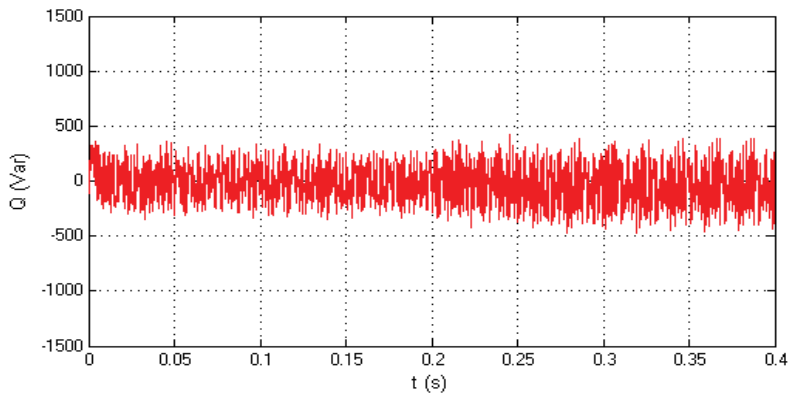


Fig. 4.21 Input reactive power Q (MPC)

From the comparison of DPC and MPC control strategy, MPC yields much smaller power ripple and more sinusoidal line current. The active power and reactive power ripples are reduced, DC-link voltage is more stable under MPC control strategy.

4.5.2 Bidirectional power flow control

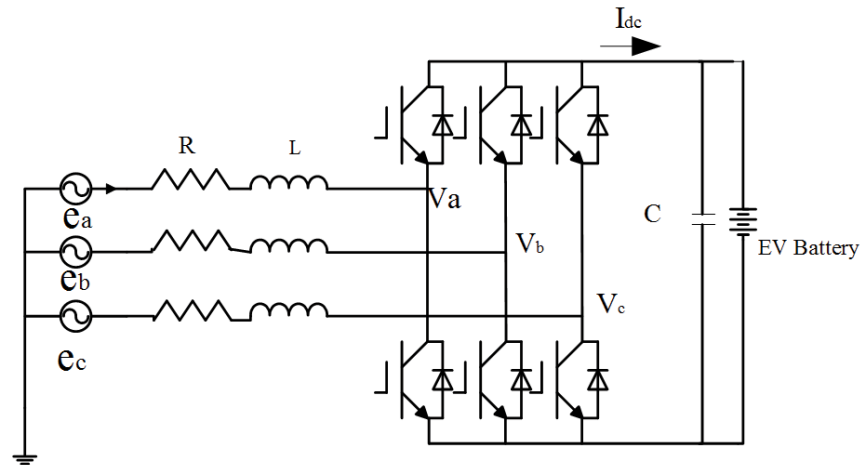


Fig. 4.22 Three-phase bidirectional AC-DC converter topology used in V2G system

Fig. 4.22 shows the bidirectional AC-DC converter topology for V2G and G2V applications of the EV. The first mode is the rectifier mode, the second mode is the inverter mode.

A. Description of working principle

The bidirectional AC-DC converter operates in two modes

- Rectifier mode (V2G) in which the bidirectional AC-DC converter operates as a front end rectifier and allows power transfer from the three-phase grid to the EV battery.
- Inverter mode (G2V) whereby power flows from the EV battery to the three-phase grid and the AC-DC converter acts as a voltage source inverter.

To check the feasibility of the dynamic performance of the V2G bidirectional charger, numerical simulations were carried out by using Matlab/Simulink. The system parameters are listed in Table 4.3.

TABLE 4.3 Electrical Parameter of Power Circuit

Resistance of reactor	R	450 m Ω
Inductance of reactor	L	4.5 mH
DC-bus capacitor	C	4000 μ F
Load resistance	R_L	90 Ω
Line to line ac Voltage	e	415 V(rms)
Source voltage frequency	f	50 Hz
DC-bus voltage	V_{dc}	300 V
Sample time	T_s	40 μ s

TABLE 4.4 Battery Parameters Block Used in the Simulink

Battery parameters	
Nominal voltage	250V
Rated capacity	6.5Ah
Fully charged voltage	294.5V
Internal resistance	0.384Ohms
Initial state of charge (SOC)	20%

TABLE 4.5 Two V2G Mode Worked in the Simulation

V2G bidirectional mode	P (W)	Q (Var)
Inverter mode (0.04s-0.8s)	14000	0
Inverter mode (1s-1.8s)	14000	6000
Rectifier mode (2s-2.8s)	21000	0
Rectifier mode (3s-4s)	21000	6000

Table 4.4 shows the battery parameters used in the simulation, the battery is modelled for lithium-ion battery. The initial SOC is set as 20%. Table 4.5 shows the two V2G working modes. The first one is inverter mode and the other one is rectifier mode. These two modes are the two different working stages of V2G services.

B. Simulation results for bidirectional power flow

Fig. 4.23 is the active power P and reactive power Q output from the V2G charger ($P > 0$ means charging and $P < 0$ means discharging). According to the different direction of the P and Q , the charger has inverter mode and rectifier mode. Fig. 4.24 shows the zoomed versions of grid voltage V_a and charger current I_a during each operation mode. The operation modes include the inverter (discharging) and rectifier (charging) mode. From (a)-(d) of Fig. 4.24 it can be observed that the bidirectional power flow can be achieved with different power output based on the MPC control algorithm.

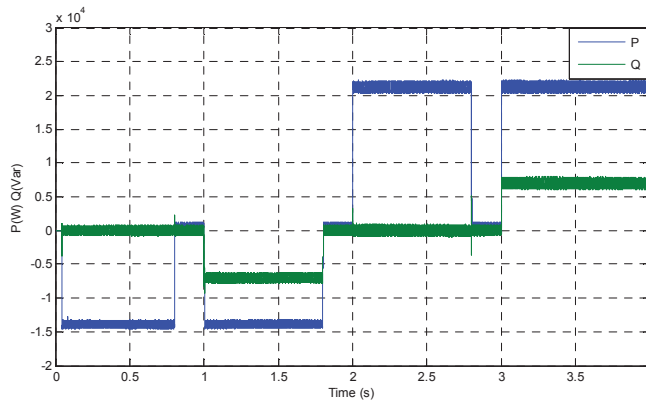


Fig. 4.23 Active power P and reactive power Q in one chart

From the simulation results, it can be concluded that the proposed MPC is much better than DPC switching table both in steady state and transient state performance. In rectifier mode, with MPC control, instantaneous active power and instantaneous reactive power track their references with good accuracy and stability during all sectors of the main period. Unity power factor operation of the converter is successfully achieved by maintaining reactive power close to zero. In inverter state, after a very short transient with step change of load power, active power tracks its reference with good approximation and stability, the reactive power is successfully

maintained close to zero. The MPC strategy shows excellent dynamic response. The conclusions can provide the guidelines for experimental setup of V2G system.

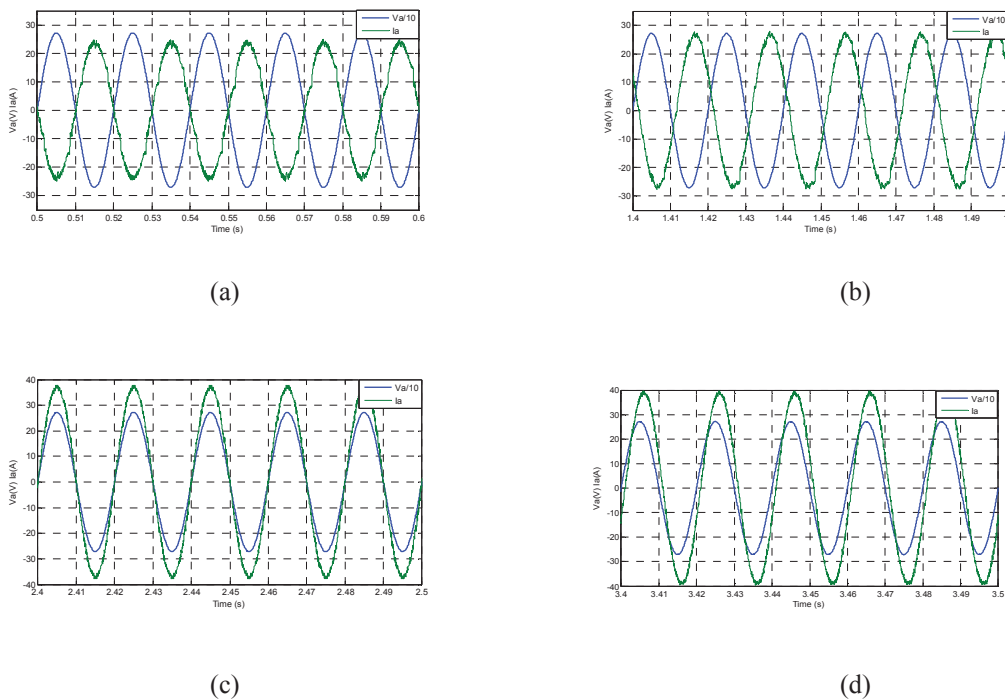


Fig. 4.24 Grid voltage V_a (1/10 scaled) and charger current I_a , waveforms for each operation mode. (a) Mode#1-discharging operation. (b) Mode#2-discharging and capacitive operation. (c) Mode#3-charging operation. (d) Mode#4-charging and inductive operation.

4.6 Summary of the Chapter

In this chapter, different control strategies have been compared. The results of using DPC strategy to control the bidirectional AC/DC converter used as a V2G charger are provided firstly. A new MPC strategy has been proposed later, by using the system model to predict the behaviour of system variables, a cost function is employed as a criterion to select the optimal switching states. Compared with the DPC control strategy, the MPC yields much smaller power ripple and more sinusoidal line current. The active power and reactive power ripples are reduced, DC-link voltage is more stable under the MPC control strategy. By using the MPC strategy, EV charger can afford flexible power regulation to the grid by acting as a rectifier or inverter. Finally, the simulation results of bidirectional charger used for the V2G system are carried out.

The proposed MPC method presents excellent steady-state and dynamic performances. This takes into account different control objectives by using the cost function flexibly and correctly, which makes this method very attractive in terms of controlling power converters and in the development of EV Smartparks in smart grids.

References

- [4.1] W. Kempton, J. Tomic, "Vehicle-to-Grid Power Fundamentals: Calculating Capacity and net Revenue," *Journal of Power Sources*, vol.144, issue:1, pp.268-279, 2005.
- [4.2] X. Jiang, X. Fang, J. H. Chow, and L. Hopkins, "A novel approach for modeling voltage-sourced converter-based FACTS controllers," *IEEE Trans. Power. Del.*, vol. 23, no. 4, pp. 2591–2598, October 2008.
- [4.3] Z. Miao, L. Fan, D. Osborn, and S. Yuvarajan, "Wind farms with HVDC delivery in inertial response and primary frequency control," *IEEE Trans. Energy. Convers.*, vol. 25, no. 4, pp. 1171–1178, December 2010.
- [4.4] F. Blaabjerg, "Power electronics in renewable energy systems," Tutorial in SAAEI'06 Conf. 2006.
- [4.5] Z. Chen, J. M. Guerrero, and F. Blaabjerg, "A review of the state of the art of power electronics for wind turbines," *IEEE Trans. Power Electron.*, vol. 24, no. 8, pp. 1859-1875, August 2009.
- [4.6] J. Wang, Q. Huang, W. Sung, Y. Liu, and B. J. Baliga, "Smart grid technologies," *IEEE Magazine. Ind. Electron.*, pp. 16–23, June 2009.
- [4.7] H. Farhangi, "The path of the smart grid," *IEEE Magazine. Power & Energy.*, vol. 4, no. 1, pp. 18–28, January/February 2010.
- [4.8] M. Malinowski, M. P. Kazmierkowski, and A. M. Trzynadlowski, "A comparative study of control techniques for PWM rectifiers in ac adjustable speed drives," *IEEE Trans. Power Electron.*, vol. 18, no. 6, pp. 1390– 1396, Nov. 2003.

- [4.9] F. Blaabjerg, R. Teodorescu, M. Liserre, and A. Timbus, "Overview of control and grid synchronization for distributed power generation systems," *IEEE Trans. Ind. Electron.*, vol. 53, no. 5, pp. 1398–1409, Oct. 2006.
- [4.10] B. Chen and G. Joos, "Direct power control of active filters with averaged switching frequency regulation," *IEEE Trans. Power Electron.*, vol. 23, no. 6, pp. 2729–2737, Nov. 2008.
- [4.11] Q. N. Trinh and H. H. Lee, "An advanced current control strategy for three-phase shunt active power filters," *IEEE Trans. Ind. Electron.*, vol. 60, no. 12, pp. 5400–5410, Dec. 2013.
- [4.12] X. Liu, C. Loh, P. Wang, and F. Blaabjerg, "A direct power conversion topology for grid integration of hybrid AC/DC energy resources," *IEEE Trans. Ind. Electron.*, vol. 60, no. 12, pp. 5696–5707, Dec. 2013.
- [4.13] J. Alonso-Martinez, J. E. Carrasco, and S. Arnaltes, "Table-based direct power control: A critical review for microgrid applications," *IEEE Trans. Power Electron.*, vol. 25, no. 12, pp. 2949–2961, Dec. 2010.
- [4.14] J. Rodriguez, J. Dixon, J. Espinoza, J. Pontt, and P. Lezana, "PWM regenerative rectifiers: State of the art," *IEEE Trans. Ind. Electron.*, vol. 52, no. 1, pp. 5–22, Feb. 2005.
- [4.15] D. S. Wijeratne and G. Moschopoulos, "A three-phase single-stage AC–DC PWM buck-type full-bridge converter: Analysis, design, and characteristics," *IEEE Trans. Ind. Electron.*, vol. 60, no. 10, pp. 4201–4214, Oct. 2013.
- [4.16] J. H. Kim, S. T. Jou, D. K. Choi, and K. B. Lee, "Direct power control of three-phase boost rectifiers using a sliding-mode scheme," *J. Power Electron.*, vol. 13, no. 6, pp. 1000–1007, Nov. 2013.
- [4.17] J. Dai, D. Xu, B. Wu, and N. R. Zargari, "Unified DC-link current control for low-voltage ride-through in current-source-converter-based wind energy conversion systems," *IEEE Trans. Power Electron.*, vol. 26, no. 1, pp. 288–297, Jan. 2011.

- [4.18] J. Dai, D. D. Xu, and B. Wu, "A novel control scheme for current-source converter-based PMSG wind energy conversion systems," *IEEE Trans. Power Electron.*, vol. 24, no. 4, pp. 963–972, Apr. 2009.
- [4.19] Y.W. Li, M. Pande, N. Zargari, and B. Wu, "An input power factor control strategy for high-power current-source induction motor drive with active front-end," *IEEE Trans. Power Electron.*, vol. 25, no. 2, pp. 352–359, Feb. 2010.
- [4.20] S. Kwak and H. A. Toliyat, "Design and rating comparisons of PWM voltage source rectifiers and active power filters for AC drives with unity power factor," *IEEE Trans. Power Electron.*, vol. 20, no. 5, pp. 1133–1142, Sep. 2005.
- [4.21] Y. Du, X. Zhou, and A. Huang, "Review of non-isolated bi-directional DC-DC converters for plug-in hybrid electric vehicle charge station application at municipal parking decks," *Proc IEEE APEC'10*, pp. 1145-1151, 2010
- [4.22] F. Blaabjerg, M. Liserre, and K. Ma, "Power electronics converters for wind turbine systems," *IEEE Trans. Ind. Appl.*, vol. 48, no. 2, pp. 708-719, March/April.2012.
- [4.23] J. Hu, J. Zhu, and D. G. Dorrell, "A Comparative Study of Direct Power Control of AC/DC Converters for Renewable Energy Generation," in *Proc. IEEE IECON Conf.*, pp. 3453–3458, 2011.
- [4.24] B. Fahimi and J. Wang, "Electric transportation – a transformation around the globe," *IEEE Magazine. Power & Energy*, vol. 9, no. 4, pp 14-16, June 2011.
- [4.25] I. Takahashi and T. Noguchi, "A new quick-response and high efficiency control strategy of an induction machine," *IEEE Trans. Ind. Appl.*, vol. IA-22, pp 820-827, 1986.
- [4.26] "Direct torque control – The world's most advanced AC drive technology," ABB Finland, Helsinki, Tech. Guide 1, 1996.
- [4.27] K-B. Lee, S-H. Huh, and F. Blaabjerg, "Performance improvement of DTC for induction motor-fed by three-level inverter with an uncertainty observer using RBFN," *IEEE Trans. Energy. Convers.*, vol. 20, no. 2, pp. 276–283, June 2005.

- [4.28] S. M. A. Cruz, H. A. Toliyat, and A. J. Marques, “DSP implementation of the multiple reference frames theory for the diagnosis of stator faults in a DTC induction motor drive,” *IEEE Trans. Energy. Convers.*, vol. 20, no. 2, pp. 329–335, June 2005.
- [4.29] J. Arbi, M. J.-B. Ghorbal, and L. Charaabi, “Direct virtual torque control for doubly fed induction generator grid connection,” *IEEE Trans. Ind. Electron.*, vol. 56, no. 10, pp. 4163–4173, October 2009.
- [4.30] G. Abad, M. A. Rodriguez, and J. M. Canales, “Direct torque control for doubly fed induction machine-based wind turbines under voltage dips and without crowbar protection,” *IEEE Trans. Energy. Convers.*, vol. 25, no. 2, pp. 586–588, June 2010.
- [4.31] N. H. Tomiki, S. Kondo and I. Takahashi, “Direct power control of PWM converter without power-source voltage sensors,” *IEEE Trans. Ind. Appl.*, vol. 34, pp. 473–479, 1998.
- [4.32] M. Malinowski, M. P. Kazmierkowski, S. Hansen, F. Blaabjerg, and G. D. Marques, “Virtual-flux-based direct power control of three-phase PAWM rectifier,” *IEEE Trans. Ind. Appl.*, vol. 37, no. 4, pp. 1019–1027, 2001.
- [4.33] M. Malinowski, M. P. Kazmierkowski and A. M. Trzynadlowski, “A comparative study of control techniques for PWM rectifiers in AC adjustable speed drives,” *IEEE Trans. Power Electron.*, vol. 18, no. 6, pp. 1390–1396, 2003.
- [4.34] L. Xu and P. Cartwright, “Direct active and reactive power control of DFIG for wind energy generation,” *IEEE Trans. Energy. Convers.*, vol. 21, no. 3, pp. 750–758, September 2006.
- [4.35] D. Zhi and L. Xu, “Direct power control of DFIG with constant switching frequency and improved transient performance,” *IEEE Trans. Energy. Convers.*, vol. 22, no. 1, pp. 110–118, March 2007.
- [4.36] G. Abad, M. A. Rodriguez, and J. Poza, “Two-level VSC based predictive direct torque control of the doubly fed induction machine with reduced torque and flux ripples at low constant switching frequency,” *IEEE Trans. Power. Electron.*, vol. 23, no. 3, pp. 1050–1061, May 2008.

- [4.37] D. Zhi, L. Xu, and B. W. Williams, "Model-based predictive direct power control of doubly fed induction generators," *IEEE Trans. Power. Electron.*, vol. 25, no. 2, pp. 341–351, February 2010.
- [4.38] J. Hu, J. Zhu, Y. Zhang, Q. Ma, and Y. Guo, "Simple and Robust Predictive Direct Control of DFIG with Low Constant Switching Frequency and Reduced Torque and Flux Ripples," in *Proc. IEEE Int. Electric Machines and Drives Conf.* 2011, pp. 781–786.
- [4.39] P. Cortes, M. P. Kazmierkowski, R. M. Kennel, D. E. Quevedo and J. Rodriguez, "Predictive control in power electronics and drives," *IEEE Trans. Ind. Electron.*, vol. 55, no. 12, pp. 4312–4324, December 2008.
- [4.40] T. Geyer, G. Papafotiou and M. Morari, "Model predictive direct torque control—Part I: concept, algorithm, and analysis," *IEEE Trans. Ind. Electron.*, vol. 56, no. 6, pp. 1894–1905, June 2009.
- [4.41] S. Kouro, P. Cortes, R. Vargas, U. Ammann and J. Rodriguez, "Model predictive control—A simple and powerful method to control power converters," *IEEE Trans. Ind. Electron.*, vol. 56, no. 6, pp. 1826–1838, June 2009.
- [4.42] J. Hu, J. Zhu, Y. Zhang, and Y. Guo, "Predictive Direct Power Control of Doubly Fed Induction Generator with Power Ripples Reduction and One Step Delay Compensation for Wind Power Generation," in *Proc. IEEE ICEMS Conf.*, pp. 1–6, 2011.
- [4.43] J. Hu, J. Zhu, Q. Ma, and Y. Zhang, "Predictive Direct Virtual Torque Control of Doubly Fed Induction Generator for Grid Synchronization," in *Proc. IEEE ICEMS Conf.*, pp. 1–6, 2011.
- [4.44] Y. Zhang and J. Zhu, "A novel duty cycle control strategy to reduce both torque and flux ripples for DTC of permanent magnet synchronous motor drives with switching frequency reduction," *IEEE Trans. Power. Electron.*, vol. 26, no. 10, pp. 3055–3067, October 2011.
- [4.45] Y. Zhang, J. Zhu and J. Hu, "Model Predictive Direct Torque Control for Grid Synchronization of Doubly Fed Induction Generator," in *Proc. IEEE IEMDC Conf.*, pp. 765–770, 2011.

- [4.46] S. Han, S. Jang, K. Sezaki, and S. Han, "Quantitative modeling of an energy constraint regarding V2G aggregator for frequency regulation," in *2010 9th International Conference on Environment and Electrical Engineering (EEEIC)*, 2010, pp. 114-116.
- [4.47] H. Liu, Z. Hu, Y. Song, and J. Lin, "Decentralized Vehicle-to-Grid control for primary frequency regulation considering charging demands," *IEEE Transactions on Power Systems*, vol. 28, pp. 1-10, 2013.
- [4.48] H. Sekyung, H. Soohye, and K. Sezaki, "Estimation of achievable power capacity from plug-in electric vehicles for V2G frequency regulation: case studies for market participation," *IEEE Transactions on Smart Grid*, vol. 2, pp. 632-641, 2011.

CHAPTER 5

GRID SUPPORT FROM V2G SERVICES

5.1 Introduction

The fundamental concept of V2G power is using V2G capable electric vehicles to provide electric power to the grid while they are parked and properly connected. The electric vehicles can be fuel cell vehicles, plug-in hybrids, or battery-electric vehicles. Most vehicles are parked on average for 95 percent of the time each day; the electrochemical energy stored in their batteries is able to provide electricity to the power grid when connected, with economic benefits both for the utilities and the vehicles owners [5.1].

To be able to provide V2G power, the vehicle must have three required elements [5.2]: (a) a connection to the grid for electric energy flow, (b) control or logical connection necessary for communication with the grid operator, and (c) controls and metering on-board the vehicle.

In contrast to the traditional one-way trip from grid to the vehicles, the electricity now flows two-way between the grid and the connected vehicles as needed. Illustrated in Fig. 5.1, the electric power system operator (labelled ISO, Independent System Operator) sends out a control signal wirelessly, requesting for electricity. The signal can go directly to each individual vehicle (upper right of Fig. 5.1), or to a fleet manager controlling a fleet of parked vehicles (lower right of Fig. 5.1), or through a third-party aggregator managing dispersed individual vehicles' power.

As discussed earlier, energy storage-based technologies are considered technically superior to traditional generation-based technologies for regulation. Generally, there are two reasons. Firstly, an energy storage system with a finite capacity can accomplish regulation because regulation is a “zero-energy” service – it neither generates nor consumes energy over a measurable amount of time. Second, energy storage can respond virtually instantaneously and

provide the power asked for precisely without significant efficiency losses associated with performing regulation.

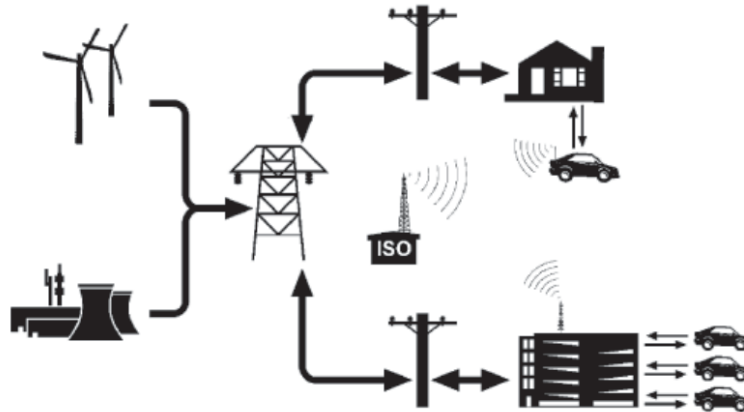


Fig. 5.1 Illustrative schematic of power line and wireless control connections between vehicles and the electric power grid [5.3]

V2G emerged as a side product with the introduction of electric vehicles to transportation. It is considered highly competitive for regulation by some researchers. Three reasons are presented in supporting V2G to be suitable for regulation by Tomic and Kempton in their study: (a) regulation service has the highest market value for V2G, (b) stresses on battery are minimized, and (c) battery-electric vehicles are well suited to provide regulation services [5.4]. Their study suggests that “large profits come from providing V2G for regulation up and down” while admitting the estimated \$290 annual net income may be too small to justify transaction costs [5.5].

Some other analysts have questioned the economic merits behind V2G based on the fact that the profit depends on the efficiency of battery systems and the difference in peak and off-peak electricity prices. First, if the efficiency works for V2G, then the grid-dedicated battery storage systems like battery banks would be more suitable for grid support. Secondly, with the mass adoption of EVs to provide V2G power, the price of grid balancing would eventually fall and thus make V2G no longer profitable.

The price issue is not within the scope of the analysis in this chapter. However, a brief understanding of how the regulation prices are determined in a market-based power system is necessary. In practice, the opportunity costs associated with maneuvering generation assets performing regulation are driving the high market prices. First of all, to be able to perform regulation, the generator has to operate at a reduced power output instead of the rated output. Then, when a generator is required to regulate down, it further incurs an opportunity cost for being unable to sell more electricity. There is also an opportunity cost for regulation-performing generators to keep running at minimal capacity even if the electricity prices are lower than their marginal costs. Finally, regulation requires frequent ramping up and down, and the increased cost of wear and tear and reduced efficiency must also be compensated for.

It is not yet clear about the long-term effects of using V2G for regulation on a battery cycle life (typically defined as the number of times a battery can be charged and discharged before its capacity falls below 70 to 80 percent of its original capacity or nameplate energy). However, unlike the thermal generators, battery-electric vehicles already have energy storage that is designed for large and frequent power fluctuations over short time periods, making V2G a strong candidate for supplying grid-balancing power. Interestingly, it was noted in a demonstration project of V2G for regulation in California that the battery capacity increased by about 10% during the testing [5.6].

The battery packs of plug-in electrical vehicles (PEVs) have to be charged for driving. When parked, PEVs can also act as an energy resource to feed power to the grid. When a large number of PEVs are plugged into the power grid, new challenges will be introduced into the power system planning and operation. Meanwhile, the V2G power brings more potential benefits to enhance the power quality and system reliability. Using V2G, PEVs can provide many grid services, such as regulation and spinning reserve, load levelling, serving as external storage for renewable sources, generating revenue by buying and selling power at different times according to variable price curves, and providing reactive power support. Battery energy storage and shunt flexible AC transmission system devices such as static VAR compensators and static

compensators (STATCOMs) are capable of very fast and accurate active and reactive power compensation. However, the main drawback of such devices is their high cost and non-mobility. In a SmartPark, a large number of electric vehicles in the parking lot are able to carry out vehicle to grid transactions. The PEVs, while parked in a SmartPark, contains a significant amount of active and reactive power potential and can be utilized for meeting the grid's requirements with little significant infrastructure cost.

With the technological advances in battery technology and the unlimited mobility in contrast to pumped storage, battery banks have been utilized for maintaining the grid's reliability for a few years. The world's largest installed battery bank is the 27 MW 15 minute nickel-cadmium battery bank in Fairbanks, Alaska, switched on in 2003. Earlier this year however, a 36 MW battery storage project was launched in China, using ferrous battery technology from a domestic solar and auto company, BYD.

The battery storage usually suffers from three drawbacks: (1) large upfront and maintenance costs, (2) a limited lifespan, and (3) a small capacity size (especially compared to pumped storage). However, researchers from Stanford University have developed a new electrode that can withstand 40,000 charging/discharging cycles in the laboratory. Even after the test this electrode could still return to more than 80% of its original capacity [5.7]. Fig. 5.2 shows a single container of A123's Smart Grid Stabilization System (SGSS) [5.8].



Fig. 5.2 A single container of A123's Smart Grid Stabilization System (SGSS) [5.8]

The round-trip efficiency (the ratio of the amount of electricity supplied to that consumed) of battery banks can be very high. The current lithium-ion battery bank produced by A123 Systems for grid energy storage claims to be 90% efficient, with a 2 MW output for each container. The table below summarizes the key features about A123’s battery-based energy storage system.

TABLE 5.1 Key Features about a Single Container of A123’s Smart Grid Stabilization System [5.9]

Round-trip efficiency	90%
Cycle life	10,000-multiple 100,000 depending on actual energy throughput
Response time	20 milliseconds
Energy Delivery Duration	15 minutes (at maximum power output)
Power	2 MW
Capacity	500 kWh

Like pumped storage, the operation of battery banks themselves do not generate any emissions. However, electrochemical energy stored in the battery comes from the grid, which in turn comes from a mix of fossil fuels, nuclear and renewables. Besides, improper disposal of batteries can be very harmful to the environment. Appropriate regulation needs be enforced to make sure the battery banks will be properly disposed of when they are retired in the future.

With the development of V2G study, more sophisticated and concrete V2G mathematical model and control strategies have been proposed in the recent studies. Most of the V2G control methods have been verified by the quantitative results collected from simulation or experiment.

Control methods for managing the EV battery energy have been developed depending on the structure of the power network where EVs are connected and the scope of EV interaction with the power grid, electric appliances and other EVs. If the energy management in a single EV is taken into account, the control objectives are chosen to be the minimization of total cost from

the amount of gasoline consumed by combustion engine and the amount of electricity brought from the power grid [5.10]. An emerging concept of vehicle-to-home describes the interaction of a single EV with the other electrical appliances in a single house usually containing small-scale renewable power generation like one wind turbine or several photovoltaic (PV) panels. The other common concepts such as vehicle-to-building (V2B) and vehicle-to-infrastructure (V2I) refers to the power network covering a building or certain region where the power exchange is enabled for EVs, generation resources and electricity consumers [5.11]. Similarly, an optimization scheme is derived for a designated EV charging station composed of a fast charging facility for a number of EVs. These emerging concepts in vehicle-to-grid interaction allow the flexible use of EVs in a particular case and have the merits of simplicity in mathematical model. Due to the limited storage capacity of a single EV, the intelligent control must be able to govern a large number of EVs so that the aggregated V2G power can be sufficient to interact with fluctuating generation as well as regulation signals for system stabilization.

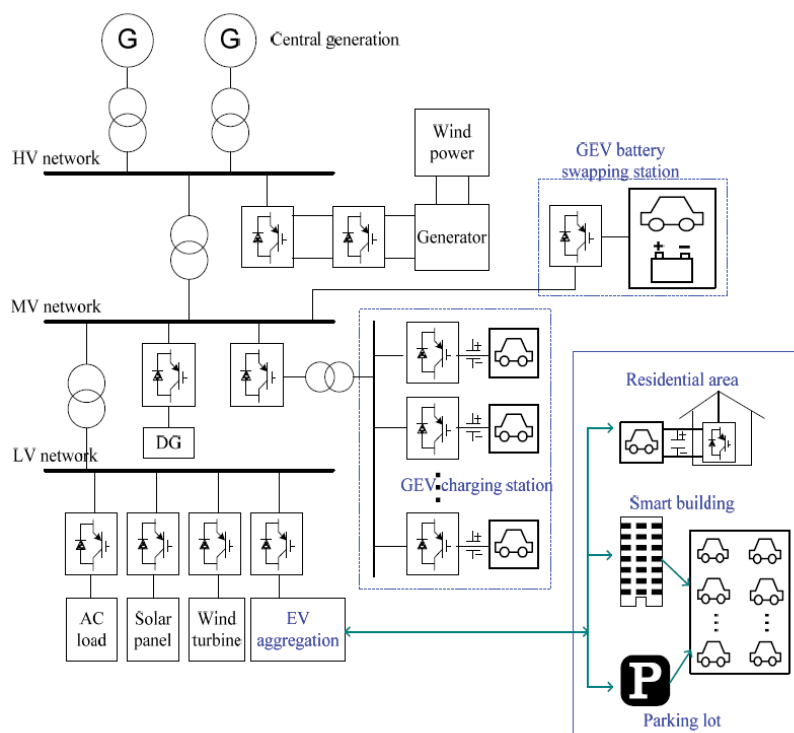


Fig. 5.3 Power electronics-interfaced EV applications in the power grid

Various power electronic converters are employed to implement the optimal control of V2G power, as depicted in Fig. 5.3. For the EVs that are connected to the power grid at the residential buildings, the converter functions to regulate the charging/discharging rate of an individual EV, thus usually being a low-voltage and low-power bi-directional converter [5.12]-[5.13]. EV charging stations are designed to accommodate the simultaneous charging load from a fleet of EVs, resulting in a considerable total charging demand being supplied by the distribution utility. The EV converters can be designed as AC-DC or DC-DC type depending on the structure of the power network normally comprising DC links such as EV charging station, micro-grid and the more complex distribution grid [5.14]-[5.15]. The analysis of the operating characteristics of the EV converters is required to build an accurate mathematical model of V2G system.

5.2 Modelling of Bidirectional Charger Used for V2G Support to Grid

The previous research work lacks a deep technical analysis of power regulation using EVs. To support the grid from EVs when power is needed in grid side, EVs should afford both active power and reactive power to the grid. EVs utilization for grid support through a bidirectional charger is illustrated in this section.

To demonstrate grid support through EVs, the battery is modelled as a source capable of delivering required power during discharging. In case of charging, the battery is modelled as a sink capable of absorbing power from the grid.

Fig. 5.4 shows the schematic diagram of a battery and a bidirectional converter coupled with the distribution node via line reactance X . Power delivered by the battery storage can be written as

$$S_{EV} = VI^* \quad (5.1)$$

where

$$I = \frac{E\angle\delta - V\angle 0}{jX} \quad (5.2)$$

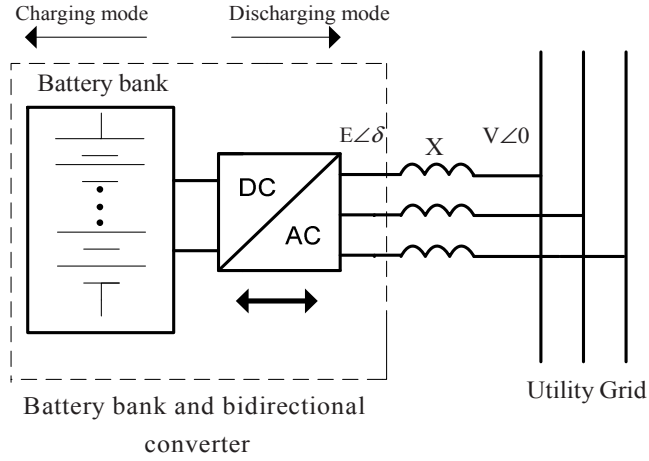


Fig. 5.4 EVs batteries used as a distributed energy source

In (5.1) and (5.2), S_{EV} and I are the power and current supplied by the battery respectively. E and V are the voltages at the sending and receiving ends respectively. δ is the angle between E and V . X is the line reactance between the converter and the utility node. Substituting the value of I , power delivered by the battery system is as follows:

$$S_{EV} = \frac{EV \sin(\delta)}{X} + j \frac{E[E - V \cos(\delta)]}{X} \quad (5.3)$$

From (5.3), active power and reactive power are given below:

$$P_{EV} = \frac{EV \sin(\delta)}{X} \quad (5.4)$$

$$Q_{EV} = \frac{E[E - V \cos(\delta)]}{X} \quad (5.5)$$

Further, considering that phase angle difference δ is typically small, we can assume $\sin(\delta) = \delta$ and $\cos(\delta) = 1$, and consequently,

$$P_{EV} = \frac{EV \delta}{X} \quad (5.6)$$

$$Q_{EV} = \frac{E(E - V)}{X} \quad (5.7)$$

From the Fig. 5.4 and the equations above, with the bidirectional converter, the battery can behave both as a source or a sink, i.e., the vehicles at the charging station can collectively discharge or charge respectively. Hence, EVs with the help of converters can support not only the active power, but also the reactive power. Especially when EVs can afford the reactive power to the grid, the V2G services will attract more and more EV owners willingness to support the grid.

5.3 Aggregator Development of V2G services

The battery storage of an individual EV is too small to impact the grid in any meaningful manner. An effective approach to deal with the negligibly small impact of a single EV is to group together a large number of EVs—from thousands to hundreds of thousands. The aggregation can impact the grid both as a load and a generation/storage device.

The basic idea behind such aggregation is the consolidation of the EVs, so that together they represent a load or a resource of a size appropriate to exploit economic efficiencies in electricity markets. The Aggregator is a new player whose role is to collect the EVs by attracting and retaining them so as to result in a MW capacity that can have a beneficial impact on the grid. The size of the aggregation is indeed the key to ensuring its effective role. In terms of load, an aggregation of EVs represents the total capacity of the batteries, an amount in MWs that constitutes a significant size and allows each EV to benefit from the buying power of a large industrial/commercial customer. There are additional economic benefits that accrue as a result of the economies of scale. The aggregated collection behaves as a single decision maker that can undertake transactions with considerably lower transaction costs than would be incurred by the individual EV owners. As a resource, the aggregated EVs constitute a significant capacity that may beneficially impact the operations of an ISO/RTO. We may view the EV aggregation as a distributed energy resource (DER). The ISO/ RTO deals directly with the Aggregator, who sells the aggregated capacity and energy services that the collection of EVs can provide. The Aggregator's role is to effectively collect the DERs into a single entity that can act either as a

generation/storage device capable of supplying capacity and energy services needed by the grid or as a controllable load to be connected to the energy service provider (ESP) to be charged in a way so as to be the most beneficial to the grid. It is the role of the Aggregator to determine which EVs to select to join the aggregation and to determine the optimal deployment of the aggregation. Fig. 5.5 shows the two main parts of the V2G system. The power grid layer integrates with various renewable energy sources. The power grid is mainly supplied by traditional generators. The gridable vehicle (GV) can draw and store energy from the power grid to support their propulsion systems as well as feeding back power to grid via power converters. GV aggregation layer consists of hundreds or even thousands of GVs which may be plugged in with different power capacity and SOC.

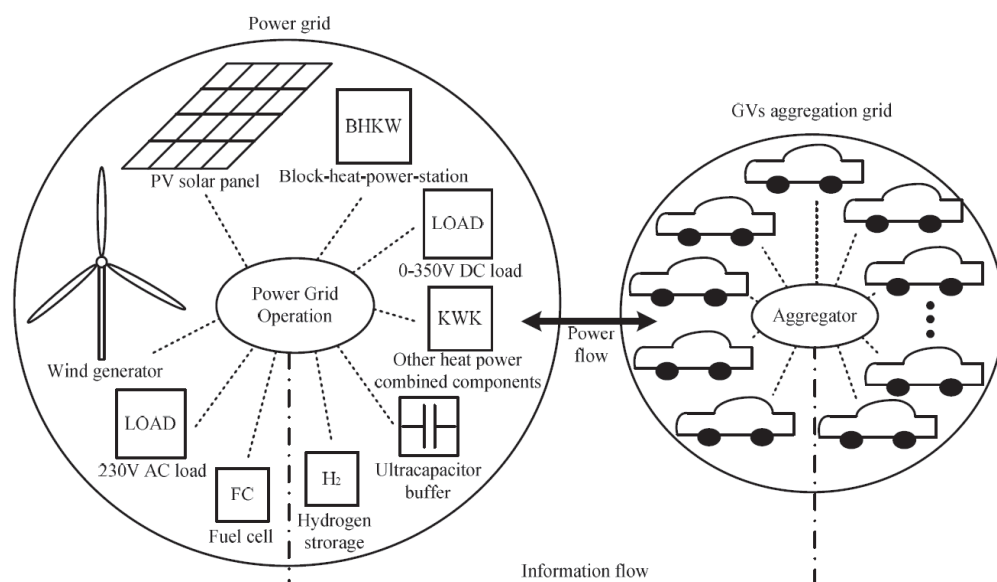


Fig. 5.5 Aggregator in V2G system

An EV aggregation may play a very useful role as a load when the total load created by the aggregation is of sufficient size. As an example, we may consider an aggregation of 12,500 EVs. If we take the average EV battery storage capacity to be 20 kWh and a 5 hour average charging time, the aggregation represents a 50MW load, an amount that has an impact on a system during off-peak conditions. A key objective of deploying the EV aggregation as a load is to levelize the loads during the charging period. The controllability of the load allows the Aggregator to do the

charging of the EV batteries in a way so as to ride out the load fluctuations during the low-load periods. Load levelization requires careful management of the charging periods of the EVs and requires explicit consideration of the SOC of each battery in the aggregation. Without aggregation and without explicit centrally dispatched control to manage the charging periods, the demand by the EVs increases and as a result of lack of levelization so do the requirements for regulation service. Therefore, we conclude that the load levelization control results in reduced energy and reserve requirements compared to the case of no such control.

The EV aggregation can act as a very effective resource by helping the operator to supply both capacity and energy services to the grid. To allow the operator to ensure that the supply–demand equilibrium is maintained around the clock, the EV aggregation may be used for frequency regulation to control frequency fluctuations that are caused by supply–demand imbalances. A battery may provide regulation up or regulation down service as a function of its SOC. Depending on its value for each EV in the aggregation, the collection may be deployed for either regulation up or regulation down at a point in time.

In addition to lowering off-peak regulation needs, the aggregated EVs may be also deployed to provide day-time regulation service to the grid given the fast response capabilities of the EV batteries, of the order of milliseconds. Typically, such service is provided by plants with short response times, of the order of minutes. These plants can be controlled to increase or lower their outputs. The batteries of the EV aggregation can either absorb or discharge energy depending on the SOC of each individual battery, but can do so with a much faster response time than conventional units. The deployment of aggregated EVs for such regulation service may not necessarily involve the supply of energy but simply the use of the capacity they provide. The fast response capabilities of the EV batteries allow the EV aggregation to provide capacity and energy nearly instantaneously. Consequently, they can offer insurance to the system that the load can be met. Aggregated EVs have the potential to play a very important role in improving system operations both on the demand- and the supply-side. However, for the concept to be successful, a careful implementation is required.

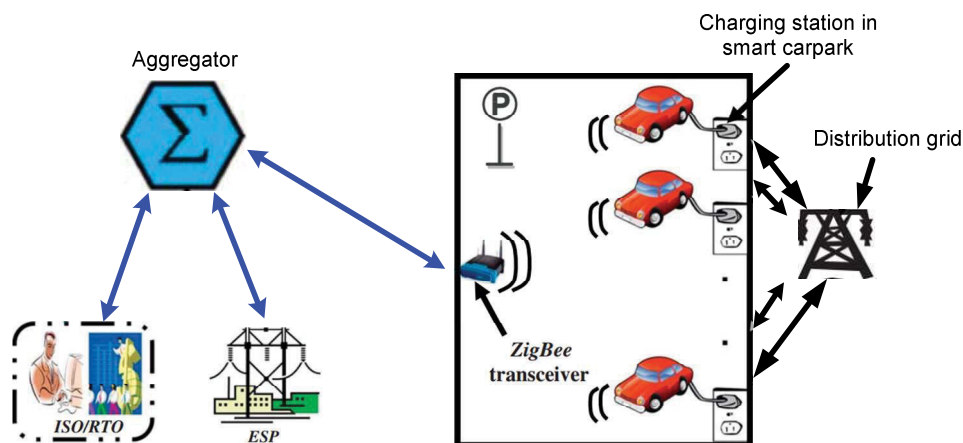


Fig. 5.6 Computer/communication/control network for the framework of V2G system

The implementation of the V2G framework poses a number of challenges. A critically important prerequisite is the construction of the information layer: the establishment of infrastructural computer/communication/control network for the integration of aggregated EVs into the grid. An equally important element whose implementation is essential is a scheme for the aggregator to attract and retain EV owners with the appropriate incentives incorporated.

The computer/communication/control infrastructural network must comprise several subnetworks which need to be seamlessly integrated together to meet the need outlined above. For example, a subnetwork is required at each location where the EVs are plugged into the grid to transmit data over short distances. On the other hand, the transmission of data between the parking lots and the Aggregator involves longer distances. The computer signals sent by the ISO/RTO which need to be broadcasted to each EV in the aggregation have very fast response requirements as do the signals for load levelization control emanating from the ESPs. Given the diversity of applications, the computer/communication/control network must meet some key basic requirements, which include, at a minimum, the following:

- low cost: the additional costs of the installation and maintenance of the communication network for EV integration must be negligibly small compared to the price of the EV;
- fast response: the network must accommodate the speedy delivery of the signals sent to the EVs;

- extensive range: the network must be able to economically integrate each EV in a parking lot;
- flexibility and extend ability: the network must provide the capability to add more EVs willing to participate in the aggregation without incurring major modifications or retrofits;
- high reliability: the reliability of the communication network is critical for the Aggregator to effectively carry out its responsibilities; and,
- security: the cyber security of the communication network must be assured so as to prevent its use in cyber-attacks.

Fig. 5.6 is a schematic which illustrates the interconnection of the components that make up the computer/communication/control network. The elements of the network are the links and the associated subnetworks for communicating with the various players and locations. Specifically, the principal links are the ISO/RTO-Aggregator, the ESP-Aggregator, the Aggregator-parking lot and the Aggregator-residence. In addition, there are the local subnetworks at each location where the EVs can be plugged in at a parking lot or at an EV owner's residence. The bi-directional ISO/RTO-Aggregator link is used for the information transfer to enable the provision of MW and MWh services to the bulk power system. In addition, this pathway serves to transmit the billing data to the ISO/RTO. The fast response times and secure data transmission requirements on this link make computer communications the most appropriate technology to be deployed. Similar requirements and technology solutions hold for the ESP-Aggregator link whose function is to transmit the signals from the ESP to the Aggregator to effectuate the controls to levelize the loads. The Aggregator-parking lot and Aggregator-residence links serve to transfer the signals received by the Aggregator from the ISO/RTO and the ESPs to the various locations where the EVs are plugged into the grid. These pathways also allow the transmission of the EV monitoring data to the Aggregator and the billing information to the EVs. Each local subnetwork in a parking lot or at a residence enables the sending of the command signals from the Aggregator to each individual EV for the charging or the discharging of the EV battery. Each local subnetwork also serves to collect the monitoring data from the aggregated EVs.

We investigated the development of a practical approach for the signal transmission in this subnetwork and assessed and compared different technology alternatives (Other technologies which may be considered include bluetooth and BPL). We selected a wireless network with ZigBee (ZigBee is the name for a combination of high-level communication protocols using small, low-power digital radios based on the IEEE 802.15.4-2006 standard) technology. We picked wireless technology to harness the rapid advances in that technology and to minimize the investments costs. The excellent capabilities of wireless technology can easily meet or exceed the requirements for the whole computer/communication/control network. Indeed, the low cost of a ZigBee transceiver – less than 1% of the costs of a battery – is an attractive feature of this technology. The cost may be further reduced once it is deployed on a large scale. The ZigBee transmission rates of 20–250 kbs are fast enough to transmit the data needed every second as is required for frequency regulation services. The range for the ZigBee technology can easily extend to 400 m and is adequate to reach every EV in a large parking lot with only a small number of transceivers. The use of wireless technology has the flexibility to allow additional devices on a network without modifying its structure. The ZigBee technology offers the ability to connect up to 65,000 devices on a single network. Experience to date indicates that ZigBee is reliable for home appliances and shows remarkable performance [5.16]. The cyber security aspects of ZigBee have been investigated in power systems distribution networks as ZigBee appears to be an important player in demand response applications. The deployment to EVs is rather similar to such networks.

The Aggregators can then pass some or all of the savings to the individual EV owners through the provision of discounts for battery and electricity purchases. In addition, the Aggregators can provide the battery guarantee and maintenance as part of the package deal. The preferential rates for purchasing electricity are very important for individual EV owners in light of the growing concern about the higher energy prices and their marked impacts on a household's monthly expenditures. In addition, because of the provision of battery maintenance and guarantee, EV owners are more inclined to participate and plug in their EVs as they need no longer be concerned about battery degradation due to the operations of the Aggregator. Because EV

owners get preferential rates for acquiring and charging their EV battery, the costs of owning and operating an EV can be reduced for every individual owner from what they would be without the Aggregator.

EV owners also wish to benefit from using “green” transportation. By driving an EV instead of a vehicle with an internal combustion engine, an EV owner may participate actively in decreasing CO₂ emissions. EVs are viewed as more environmentally friendly than conventional internal combustion cars due to no or lower tailpipe emissions. Indeed, studies indicate that EVs are cleaner even if electricity generation uses fossil fuel sources. In addition, the services provided by the EV aggregation allow the delay of the start-up of old power units, thereby consequently decreasing the emissions from older and dirtier plants. The loads due to the charging of EVs during off-peak conditions at night further decrease plant emissions by lowering the need to stop and start-up units for regulation. The inclusion of parking at preferential rates provides incentives for EV owners to plug in so as to be able to actively continue their participation in creating a greener environment.

The Aggregator signs with every individual EV owner a boilerplate contract which specifies what is included in the package deal. The Aggregator can take advantage of the available battery technologies to get a uniform battery technology aggregation which is easier to manage and maintain. Once the Aggregator has signed on a substantial number of EVs, there is an adequately large capacity to be of interest to an ISO/RTO. The services provided by the EVs can be an additional source of income to the Aggregator and some of the revenues may be used to improve the preferential rates to the EV owners. Similarly, because the EVs in the aggregation may be plugged in at locations served by different ESPs, the Aggregator may negotiate with more than one ESP for the purchase of energy at discounted rates. This also allows an EV owner to occasionally plug in the vehicle at a location not served by the ESP providing electricity supply to his residence.

The package deal, thus, provides a way to the aggregator to attract a sufficient number of EV owners to create an aggregation of a sizeable impact. As a result, the EV owner benefits from the preferential rates for the operation and maintenance of the EV.

5.4 V2G Service for Grid Stability from EV Parks

In an electric power system a great variety of different dynamics occur. There are a lot of different dynamical phenomena with different characteristics in a power system. The phenomena could be local, in which case they only involve a minor part of the system or a single component. However they can also involve interactions between different parts of the system that might be geographically far from each other. In many cases these system-wide interactions are initiated by a local disturbance are caused by a local disturbance. In this compendium interactions and phenomena that involve many power system components, e.g. generators and loads, or parts of the system, are dealt with. What these interactions have in common is that they can cause system instabilities that can lead to blackouts in large parts of the system.

Power system stability is the ability of an electric power system, for a given initial operating condition, to regain a state of operating equilibrium after being subjected to a physical disturbance, with most system variables bounded so that practically the entire system remains intact. To achieve a better overview and structure of stability analyses of power systems, it is of great help to classify possible power system stability. The classification to be introduced here is based on the physical mechanism being the main driving force in the development of the associated instability. It could be either the active or the reactive power that is the important quantity.

The classification of power system instabilities is summarised as in Fig. 5.7.

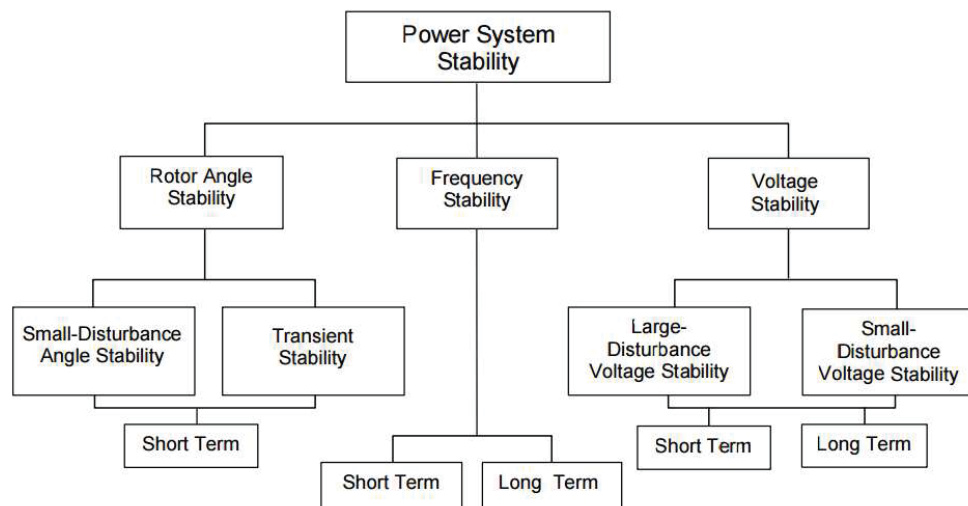


Fig. 5.7 Classification of power system stability

5.4.1 Power system and V2G system modelling in the PSCAD/EMTDC

It is of course almost impossible to develop models that can describe all dynamics in a power system and still being of practical use. Often one has to utilise a model that captures correctly the specific dynamic phenomenon or interaction that is the aim of the particular investigation. Depending on the purpose of the study the appropriate model of a given power system component could vary significantly.

In order to simulate the car park power support to the grid, a power system and V2G model simulation model are constructed using PSCAD/EMTDC software. PSCAD/EMTDC is a simulation language which is very similar to MATLAB but much more used for electrical engineering and it can be used for the transient analysis of an electric power system. PSCAD/EMTDC consists of a set of program which enable the efficient simulation of a wide variety of power system networks. EMTDC (Electromagnetic Transient and DC), although based on the EMTP method, introduced a number of modifications so that switching discontinuities could be accommodated accurately and quickly, the primary motivation being the simulation of a HVDC system. PSCAD (Power System Computer Aided Design) is a graphical Unix-based user interface for the EMTDC program. PSCAD consists of software

enabling the user to enter a circuit graphically, create new custom components, solve transmission line and cable parameters, interact with an EMTDC simulation while in progress and to process the results of a simulation. Its graphical user interface enables all aspects of the simulation to be conducted within a single integrated environment including circuit assembly, run-time control, analysis of results, and reporting. Its comprehensive library of models supports most ac and dc power plant components and controls, in such a way that FACTS, custom power, and HVDC systems can be modelled with speed and precision. It provides a powerful resource for assessing the impact of new power technologies in the power network.

Simplicity of use is one of the outstanding features of PSCAD/EMTDC. It has a great many modelling capabilities and highly complex algorithms and methods are transparent to the users, leaving them free to concentrate their efforts on the analysis of results rather than on mathematical modelling. For the purpose of system assembling, the users can either use the large base of built-in components available in PSCAD/EMTDC or users their own user-defined models.

A. Power system model

A power system model used for the power compensation support from V2G services is a 3-generator-9-bus system. The 3-generator-9-bus system is well-known as the P. M. Anderson 9-bus, which contains 3 generators, 6 lines, 3 loads and 3 two winding power transformers. Fig. 5.8 shows 3 generators and 9 buses power system diagram from western system coordinating council (WSCC).

Fig. 5.9 is the 3 generators and 9 buses power system model. The V2G system is connected at bus 4. The V2G system can support the power grid when there are active power and reactive power needed to keep the stability of the power system. Table 5.2 is the model parameters,

B. V2G system model

In the simulation for the V2G service support to power system, the EVs in a car park can be simulated by the voltage source connected with a bidirectional charger. Through the

bidirectional charger, the voltage source can afford active power and reactive power to the grid according to the grid requirements. EVs in the car park are connected to bus 4.

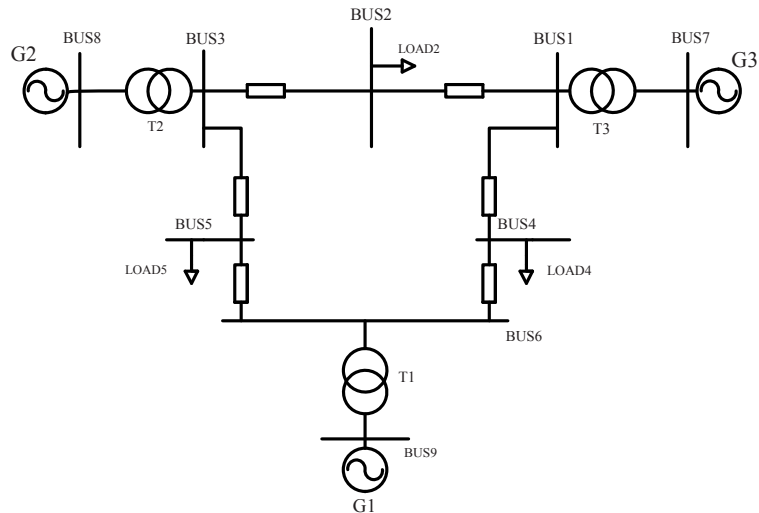


Fig. 5.8 Three generators, 9 buses power system from WSCC

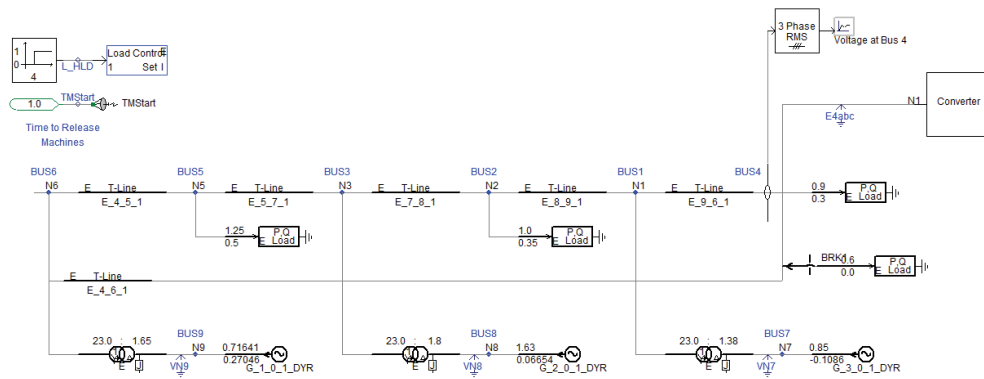


Fig. 5.9 Three generators, 9 buses power system model block diagram in PSCAD/EMTDC

In the PSCAD/EMTDC, the EVs are connected with bidirectional converter and transformer, then connected to the utility node. Fig. 5.10 shows the V2G system model block diagram in PSCAD/EMTDC.

TABLE 5.2 Model Parameters in 3 Generator, 9 Guses Power System Model

System rated frequency	f	50Hz
System rated power	S _B	1MVA
System rated voltage	U _B	23KV
Transformer T1 ratio	K _{T1}	1.65/23
Transformer T2 ratio	K _{T2}	1.8/23
Transformer T3 ratio	K _{T3}	1.38/23
System load 2	Load 2	1+j0.35 MVA
System load 4	Load 4	0.9+j0.3 MVA
System load 5	Load 5	1.25+j0.5 MVA

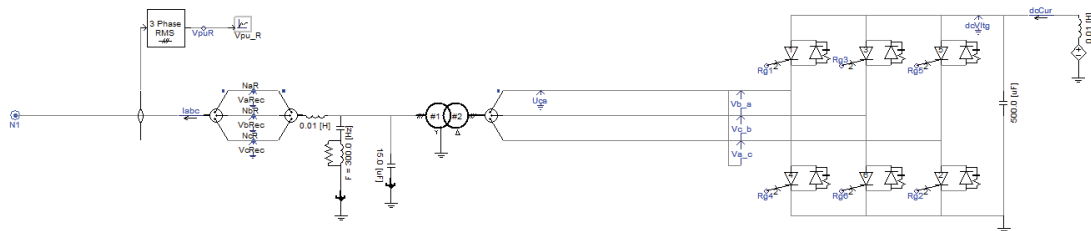


Fig. 5.10 V2G system model block diagram in PSCAD/EMTDC

5.4.2 Power compensation from EVs to the grid

A. Active power compensation

When the imbalance of active power is not local but global, if the total power fed into the system by the prime movers is less than what is consumed by the loads, including losses, this imbalance will influence the frequency of the whole system. The kinetic energy stored in rotating parts of the synchronous machines, and other rotating electrical machines, will compensate for the imbalance resulting in a frequency deviation. If the imbalance is not too

large the generators participating in the frequency control will regulate the active power input from their prime movers, and bring back the frequency deviation to acceptable values. If the imbalance is too large, the frequency deviation will be significant with possible serious consequences. Particularly thermal power plants are sensitive to large frequency drops of long durations, since detrimental oscillations could be excited in the turbines. As a last resort the generators are disconnected, making the situation even more serious. This type of instability is called frequency instability and the time scale could be from a few seconds up to several minutes. Since the involved mechanisms could be quite different, one often distinguishes between short-term and long-term frequency instability.

The primary reason for accurate frequency control is to allow the flow of alternating current power from multiple generators through the network to be controlled. The trend in system frequency is a measure of mismatch between demand and generation, and so is a necessary parameter for load control in interconnected systems. Frequency of the system will vary as load and generation change. Increasing the mechanical input power to a synchronous generator will not greatly affect the system frequency but will produce more electric power from that unit. During a severe overload caused by tripping or failure of generators or transmission lines the power system frequency will decline, due to an imbalance of load versus generation. Loss of an interconnection, while exporting power (relative to system total generation) will cause system frequency to rise. Automatic generation control (AGC) is used to maintain scheduled frequency and interchange power flows. Control systems in power plants detect changes in the network-wide frequency and adjust mechanical power input to generators back to their target frequency. This counteracting usually takes a few tens of seconds due to the large rotating masses involved. Temporary frequency changes are an unavoidable consequence of changing demand. Exceptional or rapidly changing mains frequency is often a sign that an electricity distribution network is operating near its capacity limits, dramatic examples of which can sometimes be observed shortly before major outages. Frequency protective relays on the power system network sense the decline of frequency and automatically initiate load shedding or tripping of interconnection lines, to preserve the operation of at least part of the network. Small

frequency deviations (i.e. -0.5 Hz on a 50 Hz or 60 Hz network) will result in automatic load shedding or other control actions to restore system frequency. Smaller power systems, not extensively interconnected with many generators and loads, will not maintain frequency with the same degree of accuracy. Where system frequency is not tightly regulated during heavy load periods, the system operators may allow system frequency to rise during periods of light load, to maintain a daily average frequency of acceptable accuracy. Portable generators, not connected to a utility system, need not tightly regulate their frequency because typical loads are insensitive to small frequency deviations.

For large grids the presence of many generators and a large distributed load makes frequency management easier because any given load is a much smaller percentage of the combined capacity. For smaller grids, there will be a much larger fluctuation in capacity as delays in matching power supplied are harder to manage when the loads represent a relatively larger percentage of the generated power.

So a battery systems is really designed to keep short-term fluctuations in power requirements from dropping the frequency because of lags in the governors and generators which require a finite time to adjust to the new power requirements. These “frequency regulator” power stations can supply very high power for short bursts to keep the power requirements even so that the other generators do not see too much load faster than they can respond due to mechanical limitations.

When there is frequency fluctuation caused by the change of the active load connected in a power grid, the V2G system can afford the active power to the grid side to stabilize the frequency of the system. In this study, the EVs in V2G system are connected in bus 4 in WSCC 3-generator-9-bus.

The frequency stabilization case is performed to analyse the effect of active power compensation from V2G services using a bidirectional charger to reduce the frequency variation during active load change. In this case study, EVs are connected to bus 4. EVs can compensate

the active power through bidirectional charger to the grid when the active load is changed at bus 4. The simulation analyses are shown as follows,

At 3s, the active power load is increased by 0.8MW at bus 4. To keep the frequency rate at a normal level ($50\pm 0.6\text{Hz}$), the battery bank in EVs is used to make the active power compensation at 3s. Fig. 5.11(a) is the frequency regulation without active power compensation from V2G service; however there is auto frequency correction in Fig. 5.11(a). Fig. 5.11(b) is the frequency regulation with active power compensation from V2G service.

As can be seen in Fig. 5.11, the frequency changes in Fig. 5.11(a) without EVs' active power compensation is more than 0.4Hz which only has the auto frequency correction. On the other hand, the frequency changes in Fig. 5.11(b) with EVs' active power compensation is less than 0.2Hz. From frequency changes comparison it can be concluded V2G service can compensate the active power to the grid with better frequency stabilization than generators with self-auto frequency correction.

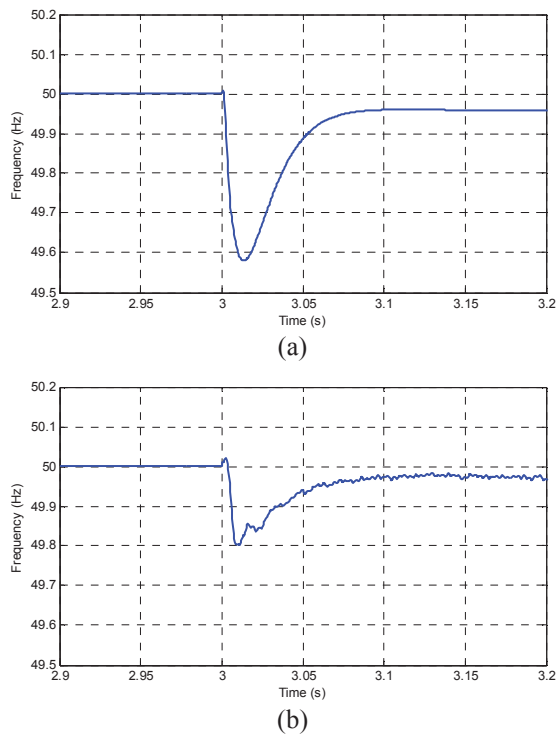


Fig. 5.11 Frequency recovery performance comparison. (a) Without EVs' active power compensation. (b) With EVs' active power compensation.

B. Reactive power compensation

When it comes to reactive power balance the situation is not as clear and simple as concerning active power. There is always a balance between “produced” and “consumed” reactive power in every node of a network. This is in fact a direct consequence of Kirchoff’s first current law. When one talks about imbalance in this context we mean that the injected reactive power is such, normally too small, that the voltage in the node cannot be kept to acceptable values. (At low load the injected reactive power could be high resulting in a too high voltage, possibly higher than the equipment might be designed for. This is of course not desirable but it could usually be controlled in such a way that no instabilities develop) When we talk about imbalance in this case we thus mean that the injected reactive power differs from the desired injected reactive power, needed to keep the desired voltage. If this imbalance gets too high, the voltages exceed the acceptable range.

Reactive power is a more local quantity than active power since it cannot be transported as easily in a power system where normally $X \gg R$. This explains why voltage problems often are local, and often only occur in part of the system. When the imbalances (voltage problems) develop into instabilities these are called voltage instabilities or voltage collapses. In the latter case the instability develops into very low voltages in the system. In principle too high voltages can also occur at a voltage instability. Low voltages arise at high load conditions, while high voltages are associated with low load conditions. Depending on the time scale the voltage instabilities are classified as short-term, a couple of seconds, or long-term, tens of seconds to minutes. The short-term voltage instability involves dynamics of fast acting components such as induction motors, electronically controlled loads, and HVDC converters, while the long-term voltage instability involves slower acting equipment such as tap-changing transformers, thermostatically controlled loads, and generator current limiters. As for rotor angle stability one distinguishes between large-disturbance and small-disturbance voltage stability.

Reactive power compensation not only can help the grid to maintain power quality and reliability [5.17], but also increase the active power transfer limits [5.18]. Currently, in the

United States, as per the NERC Operating Policy-10 [5.19], only the reactive power provided by synchronous generators is considered as an ancillary service to receive financial compensation. However, the reactive power market is foreseen to grow and become more diverse, mainly due to the increase in the number and capacity of PEVs and renewable energy sources connected to the grid [5.20]-[5.22].

Reactive power compensation and voltage regulation have different characteristics compared to demand side management and frequency regulation. In particular, generation of real power requires energy conversion from some other energy resource (such as fossil / nuclear fuel, sunlight, wind power or water flow), whereas reactive power does not. The cost of common reactive power compensators such as shunt capacitors mainly comes from their capital installation (equipment) and operating cost. For the case of PEV-based reactive power compensation, operation can be coordinated by the same charging and discharging scheduling software agents that are foreseen to be used by residential consumers for demand-side management with low additional cost [5.23].

When there is voltage fluctuation caused by the change of the reactive load connected in power grid, the V2G system can afford the reactive power to grid side to stabilize the bus voltage. In this reactive power compensation study, the EVs in V2G system are connected in bus 4 in WSCC 3-generator-9-bus.

The voltage stabilization case is performed to analyse the effect of reactive power compensation from V2G services using a bidirectional charger to reduce the voltage sag during reactive power load changes. In this case study, EVs are connected at bus 4. The EVs can compensate the reactive power through bidirectional charger to the grid when the reactive load changed at bus 4. The simulation analyses are shown as follows,

At 3s, the reactive power load is increased by 0.3MVar at bus 4. Fig. 5.12 is the voltage level variation at bus 4. To keep the voltage at a normal level, the battery bank in EVs is used to compensate reactive power to the grid at 4s. Fig. 5.13 shows the voltage level variation at

different bus nodes when reactive load changed and reactive power compensated at bus 4. From Fig. 5.13, we could observe that the voltage level change in bus 4 is the largest fluctuation since the bus 4 reactive load changed locally at bus 4.

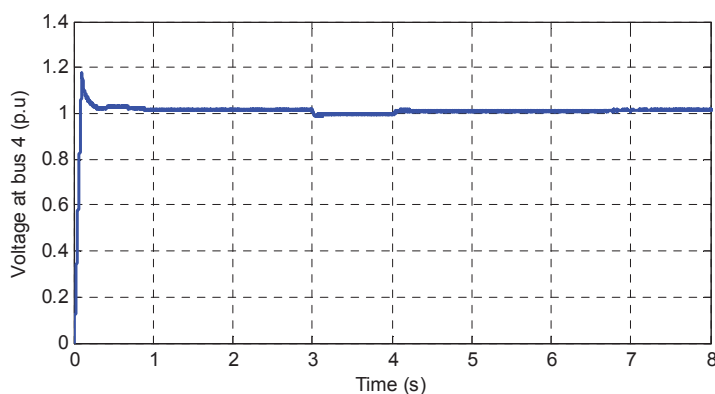


Fig. 5.12 Voltage recovery performance at bus 4 (Increase reactive load at bus 4 and use EVs to compensate the reactive power at 4s)

As can be seen in Fig. 5.12, the voltage drops from 1.01 p.u. to 0.99 p.u. when reactive load increases at 3s. When reactive power is compensated from the battery bank at 4s, the voltage level is back to normal level instantly. From reactive power compensation results, it is concluded that EVs can support the grid locally to level up the voltage with reactive power compensation when the voltage sag occurs caused by the increase of reactive load.

The nine bus nodes voltages are shown in Fig. 5.13. The grid system operates in steady state before 3s, the nine nodes voltages are operating at a normal level. When there is reactive load increase at bus 4, the voltage level variation at different buses are different. As can be seen in Fig. 5.13, when bus 4 is compensated by the reactive power supplied by the EVs, the different nodes have different voltage compensated rates. The voltage compensated rates at different buses depend on the distance between bus 4 and corresponding bus.

Fig. 5.14 shows voltage change comparison results among different bus numbers when there is reactive power load changes and reactive power from EVs compensated at bus 4. As can be seen in Fig. 5.14, the results show that the voltage at bus 4 has been compensated perfectly to the normal level since we compensate the reactive power locally. The voltage level at bus 4 can

be restored to normal level at steady state with almost no difference. On the other hand, the voltages at other buses also have been improved with different rates which can be used for other purposes such as reactive power consumption of equipment connected at other buses. The V2G service can afford reactive power support to the grid when there is voltage sag existing in the grid to improve voltage stability.

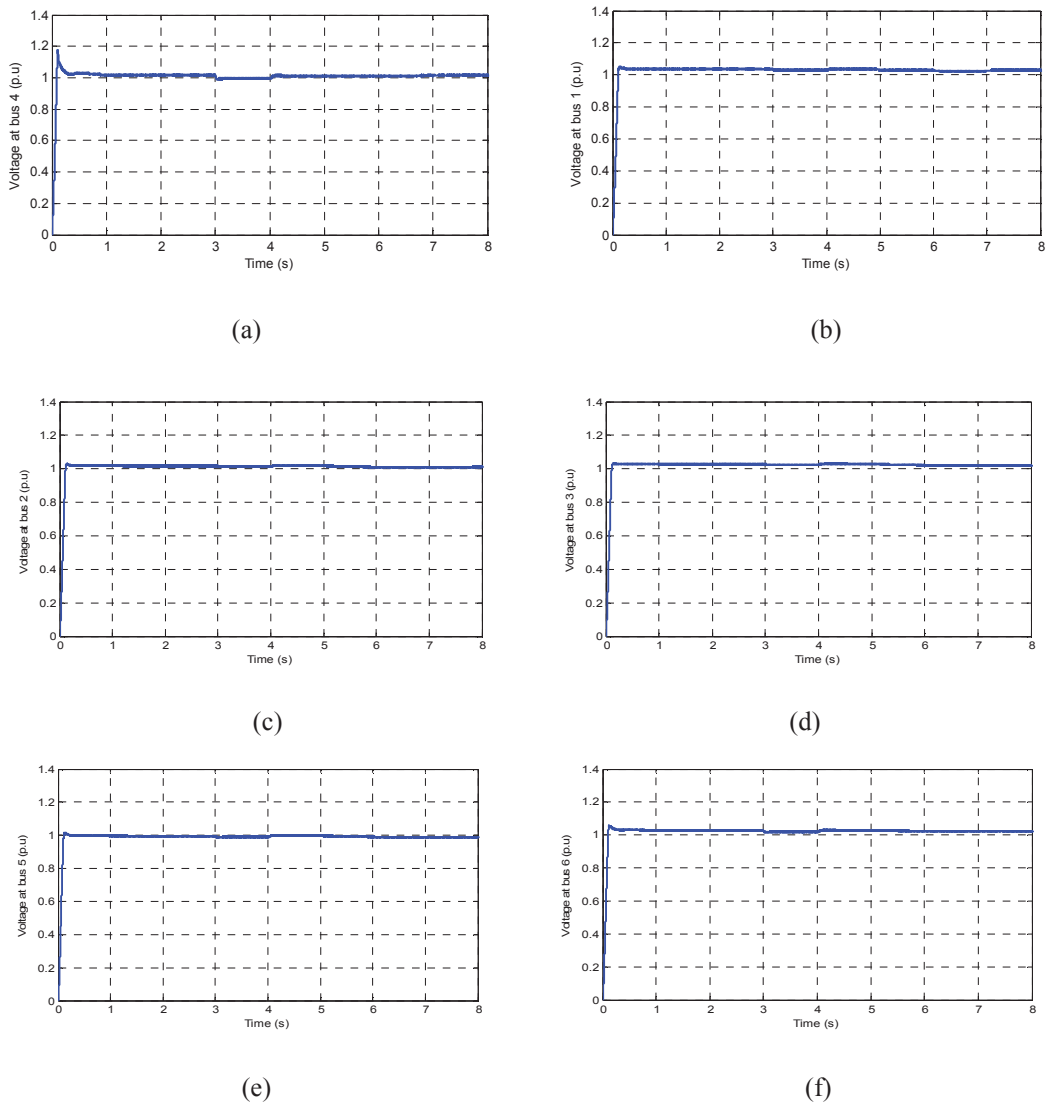


Fig. 5.13 Different buses voltage variation when there is reactive load change at bus 4 and reactive power from EVs compensated at bus 4. (a) Bus 4. (b) Bus 1. (c) Bus 2. (d) Bus 3. (e) Bus 5. (f) Bus 6.

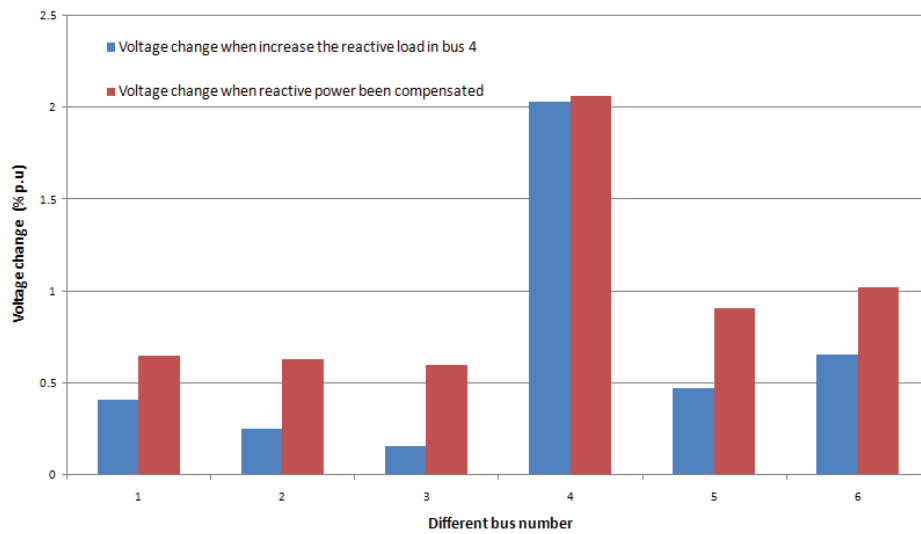


Fig. 5.14 Voltage change comparison results among different bus numbers when there is reactive power load change at bus 4 and reactive power from EVs compensated at bus 4

5.5 Simulation Results and Scaled Down Experimental Test Results for V2G Service

In laboratory, in order to verify the V2G service to support the grid to stabilize the frequency and voltage fluctuation. A scale down experimental test bed has been set up to obtain the results.

Following are the equipment needed for the experimental test.

- 1) Easygen-3000 generator set (2.2 kW) with built-in transmission line model from Woodward company
- 2) Three phase 240 V, 6 A / 120 V, 12 A / 120 V, 12 A transformer
- 3) Three phase resistive load, 110 Ω per phase
- 4) Three phase inductive load, 0.5H per phase
- 5) Three phase capacitive load, 20 μ F per phase

Connect the transformer in Star/Star connection using the winding taps to have 240V/240V as shown in Fig. 5.15.

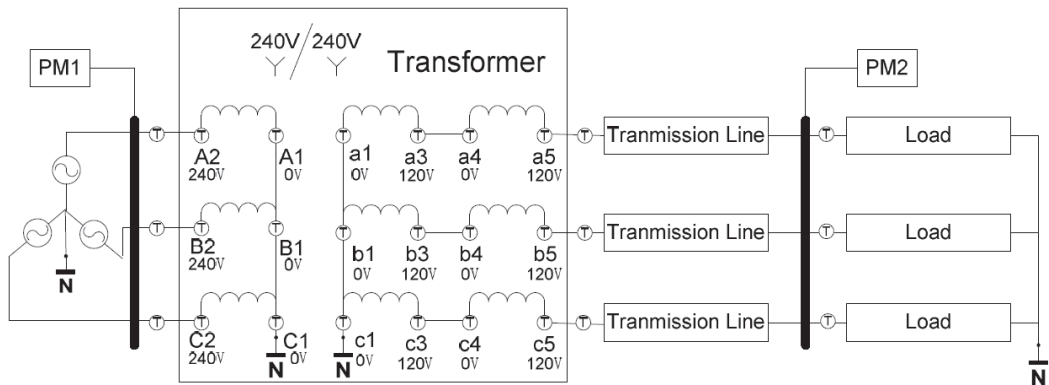


Fig. 5.15 Connection of transformer and load



Fig. 5.16 Display and control panels of Easygen-3000 in the laboratory

Fig. 5.16 is the display and control panels of Easygen-3000. As shown in Fig. 5.16, display and control panel consists of four elements: Power Meter 1 (PM1), Power Meter 2 (PM2), Genset Controller (GENSET) and Programmable Terminal (PT). Fig.5.17 is the PT screen of Easygen-3000. From the PT screen power, voltage and frequency values can be observed during different modes of the experiment.

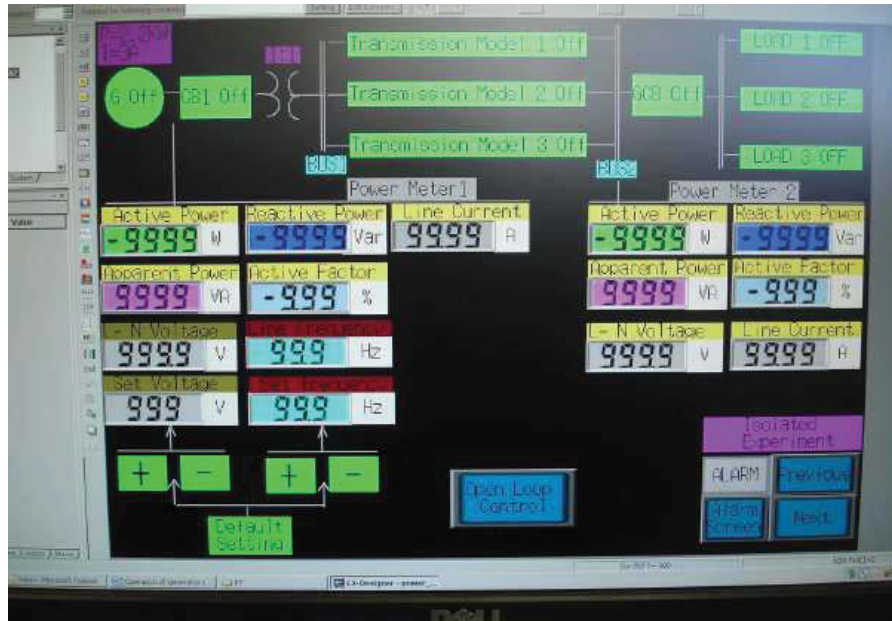


Fig. 5.17 PT screen

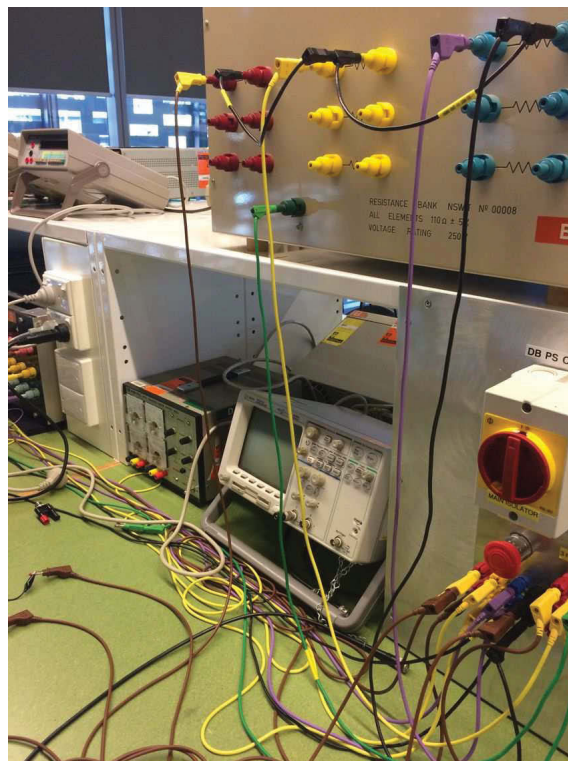


Fig. 5.18 Experimental test bed for the generator when load changes

For the observation of the effect of different loads on the system voltage, the experimental test bed for the generator had been set up in the laboratory. Fig. 5.18 is the experimental test bed for the generator.

5.5.1 Experimental results of the generator performance when load changes

In the different load test experiments, the resistor load was firstly been done to observe output voltage performance of the generator. After the generator starting period, the three phase resistor load was connected to the generator.

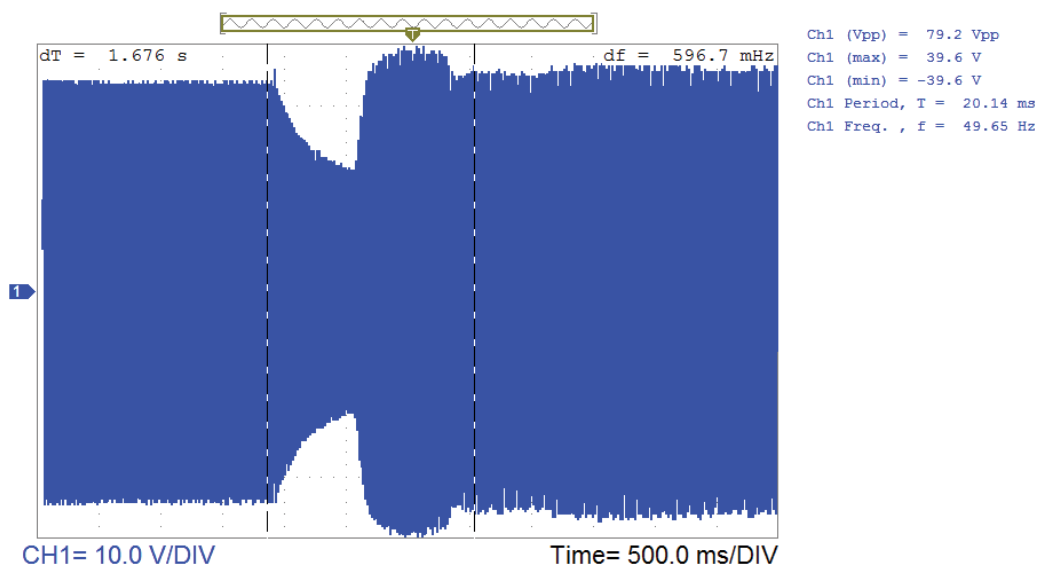


Fig. 5.19 Output voltage waveform of resistor load without V2G support

Fig. 5.19 shows the output voltage waveform of generator when resistor load connected to the generator. From the figure we could observe that the voltage drops and then increases to its normal level since the generator has own ability to adjust the voltage when there is load fluctuation. The adjust period is 1.676s when there is only resistor load connected to the generator.

Fig. 5.20 shows the output voltage waveform of generator when resistor and capacitive load connected to the generator. From the figure we could observe that the voltage performance is

similar with only resistor load connected to the generator. The adjust period is 2.120s which is longer compared with only resistor load connected to the generator.

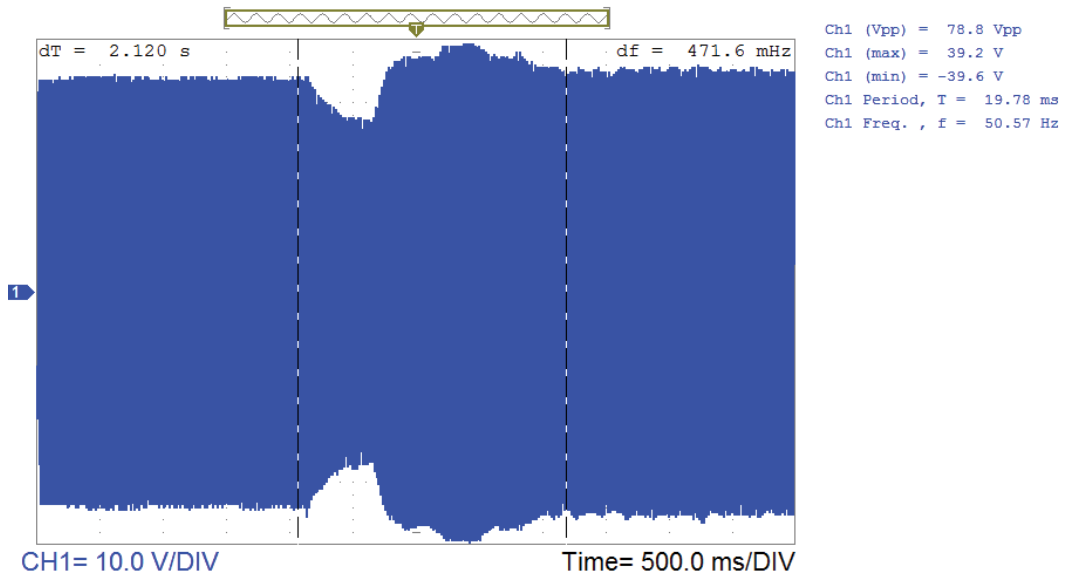


Fig. 5.20 Output voltage waveform of resistor and capacitive load without V2G support

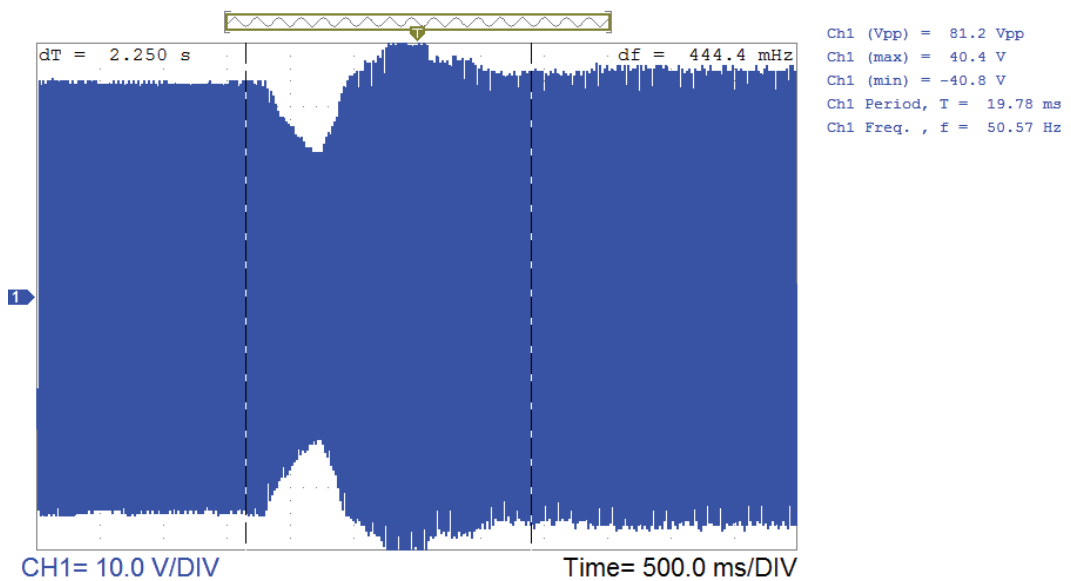


Fig. 5.21 Output voltage waveform of resistor, capacitive and inductive load without V2G support

Fig. 5.21 shows the output voltage waveform of generator when resistor, capacitive and inductive load connected to the generator. From the figure we could observe that the voltage drops and then increases to its normal level since the generator has own ability to adjust the

voltage when there is load fluctuation. The adjust period is 2.250s which is longer compared with the previous two cases.

From the experimental results of load change connected to the generator, we can conclude that the generator has own ability to adjust the voltage. Since there is no V2G support to the generator, the generator voltage adjust period is several seconds. The adjust period is different according different types of load connected.

5.5.2 Simulation results of the V2G support to power system when load changes

In order to verify the result of V2G support to power system, a simulation for the scale down power system corresponding to the Easygen-3000 generator set has been carried out. In the simulation, the V2G service supports the power system to stabilize the voltage when the load changes.

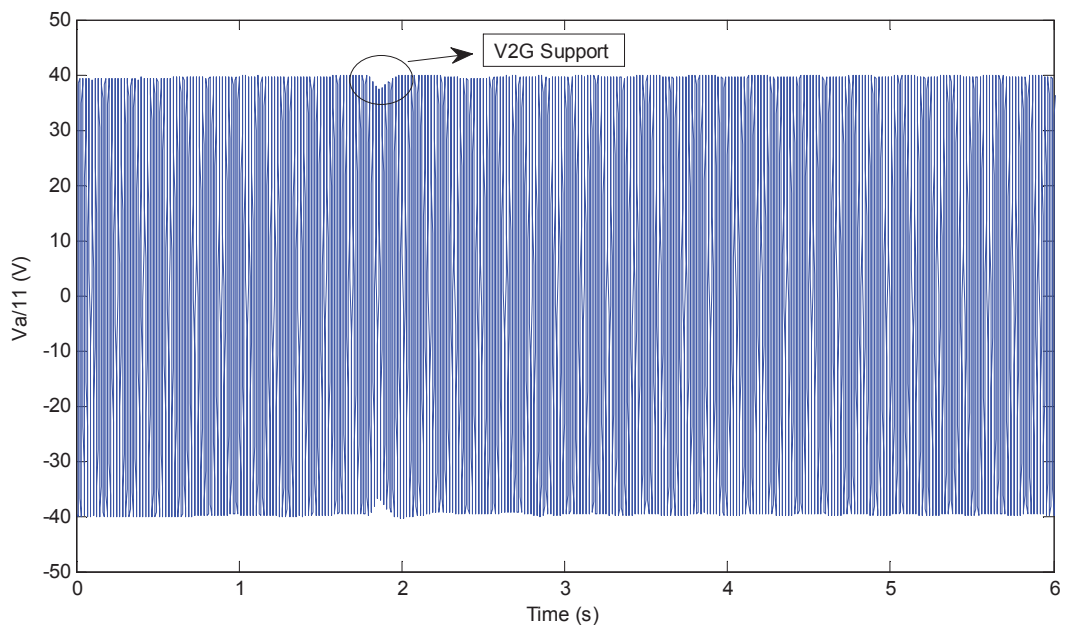


Fig. 5.22 V2G support to power system when load changes

Fig. 5.22 shows the voltage performance of V2G support to the power system when load changes. The load changed at 1.8s, at the same time the V2G service began to support the power system. From Fig. 5.22 it can be observed that the voltage drops slightly and then recovers to

normal level since V2G service support the power system with a fast speed. The adjust speed is less than 0.2s based on the simulation result.

The V2G support to power system has not been carried out yet. From the simulation results it can be concluded that the adjust period of V2G support is very instant. According to the simulation result, the V2G support adjust period is less than 0.2s which is much less than the power system own adjust period obtained from the experimental results. The experimental test of V2G support to the power system is critically desired for the continued work.

5.6 Summary of the Chapter

This chapter introduce the grid support from the EVs in the Smartpark, the aggregator development and the results of active and reactive power support to the grid from EVs. As a main function of Smartpark, the V2G system has control flexibilities to fulfil system reliability and power quality requirements.

Firstly, the modelling of V2G charger is given out. In order to demonstrate grid support from EVs, a battery is modelled as a source capable of delivering required power during discharging. In case of charging, the battery is modelled as a sink capable of absorbing power from the grid. EVs with the help of converters can support not only the active power, but also the reactive power.

However, the battery storage of an individual EV is too small to impact the grid in any meaningful manner. An effective approach to deal with the negligibly small impact of a single EV is to group together a large number of EVs-from thousands to hundreds of thousands. Based on this background, the Aggregator is a new player whose role is to collect the EVs by attracting and retaining them so as to result in a MW capacity that can beneficially impact the grid.

Finally, V2G service for grid stability improvement from EV parks is carried out. In order to stabilize the frequency of system which is a measure of mismatch between demand and

generation, active power can be compensated by the V2G system to grid side to stabilize the frequency of the system. The same principle can be applied for the reactive power compensation to stabilize voltage variation. Energy storage system in EVs makes V2G a strong candidate for supplying grid-balancing power. Put simply, the EVs, while parked in a SmartPark, contains a significant amount of active and reactive power potential which can be utilized for meeting the grid's requirements with little significant infrastructure cost.

References

- [5.1] Car Prototype Generates Electricity, And Cash. 2007 [cited 2012 Jan 20]; Available from: <http://www.sciencedaily.com/releases/2007/12/071203133532.htm>
- [5.2] W. Kempton, J. Tomic, "Vehicle-to-grid power implementation: From stabilizing the grid to supporting large-scale renewable energy," *Journal of Power Sources*, 2005. 144(1): pp. 280- 294.
- [5.3] W. Kempton, J. Tomic, "Vehicle-to-grid Power Fundamentals: Calculating Capacity and Net Revenue," 2005.
- [5.4] W. Kempton, J. Tomic, "Using fleets of electric-drive vehicles for grid support," *Journal of Power Sources*, 2007. 168(2): pp. 459-468.
- [5.5] J. Tomic, W. Kempton, "Vehicle-to-grid power fundamentals: Calculating capacity and net revenue," *Journal of Power Sources*, 2005. 144(1): p. 268-279.
- [5.6] A.N. Brooks, "Vehicle-to-Grid Demonstration Project: Grid Regulation Ancillary Service with a Battery Electric Vehicle," 2002, AC Propulsion, Inc.
- [5.7] "Enabling grid scale battery storage systems," Inside R&D 2011; Available from: http://go.galegroup.com/ps/i.do?id=GALE%7CA275852351&v=2.1&u=duke_perkins&it=r&p=I TOF&sw=w.
- [5.8] <http://www.a123systems.com/products-modules-energy.htm>
- [5.9] "Grid stability battery systems for renewable energy success," Charles Vartanian from A123 system

- [5.10] A. Y. Saber and G. K. Venayagamoorthy, "Resource scheduling under uncertainty in a smart grid with renewables and Plug-in Vehicles," *IEEE Systems Journal*, vol. 6, pp. 103-109, 2012.
- [5.11] Y. Ota, H. Taniguchi, and A. Yokoyama, "Autonomous distributed V2G (Vehicle-to-Grid) satisfying scheduled charging," *IEEE Transactions on Smart Grid*, vol. 3, pp. 559-564, 2012.
- [5.12] O. C. Onar, J. Kobayashi, D. C. Erb, and A. Khaligh, "A bi-directional, high power quality grid interface with a novel bi-directional non-inverted buck-boost converter for PHEVs," *IEEE Transactions on Vehicular Technology*, vol. 61, no. 5, pp. 2018-2031, 2012.
- [5.13] S. Cui, X. Liu, D. Tian, Q. Zhang, and L. Song, "The construction and simulation of V2G system in micro-grid," in *2011 International Conference on Electrical Machines and Systems (ICEMS)*, 2011.
- [5.14] R. Smolenski, M. Jarnut, G. Benysek, and A. A. Kempinski, "AC/DC/DC interfaces for V2G applications - EMC issues," *IEEE Transactions on Industrial Electronics*, vol. 60, pp. 930-935, 2012.
- [5.15] A. K. Verma, B. Singh, and D. T. Shahani, "Grid to vehicle and vehicle to grid energy transfer using single-phase bidirectional AC-DC converter and bidirectional DC-DC converter," in *2011 International Conference on Energy, Automation, and Signal (ICEAS)*, 2011, pp. 1-5.
- [5.16] <http://www.sensorsmag.com/sensors/Wireless+Works/How-ZigBeeCompares/ArticleStandard/Article/detail/393407> (read on April 10, 2009).
- [5.17] B. Kirby and E. Hirst, "Ancillary service details: voltage control," Oak Ridge National Laboratory, Dec 1997.
- [5.18] W. W. Hogan, "Markets in real electric networks require reactive prices," *The Energy Journal*, vol. 14, no. 3, pp. 171-200, 1993.
- [5.19] North American Electric Reliability Council, NERC Operating Policy-10 on Interconnected Operation Services. Draft-3.1, Feb 2000.

- [5.20] N. Ullah, K. Bhattacharya, and T. Thiringer, "Wind farms as reactive power ancillary service providers: Technical and economic issues," *IEEE Transactions on Energy Conversion*, vol. 24, no. 3, pp. 661–672, sept. 2009.
- [5.21] H.-S. Ko, J. Jatskevich, G. Dumont, and G.-G. Yoon, "An advanced lmbased- lqr design for voltage control of grid-connected wind farm," in *Int. J. Electric Power Systems Research*, vol. 78, April 2008, p. 539C546.
- [5.22] H. S. Ko, S. Bruey, G. Dumont, J. Jatskevich, and A. Moshref, "A pi control of dfig-based wind farm for voltage regulation at remote location," in *IEEE Power Engineering Society General Meeting*, June 2007.
- [5.23] M. Kisacikoglu, B. Ozpineci, and L. Tolbert, "Examination of a phev bidirectional charger system for v2g reactive power compensation," in *Applied Power Electronics Conference and Exposition (APEC)*, 25th Annual IEEE, feb. 2010, pp. 458-465.

CHAPTER 6

ECONOMIC ISSUES RELATED TO V2G SERVICES

6.1 Introduction

Today the electricity and transportation systems face a number of challenges related to reliability, security and environmental sustainability. The Electric vehicle is a technology solution with great potential for reducing vehicle emissions and oil dependency. Furthermore, electric vehicles can work as distributed resources and power can be sent back to the utility, which is called “vehicle to grid” (V2G). This function can smooth the load curve, afford backup capacity and improve the reliability of the power system. As a result, V2G offers many advantages to both the electricity and transportation system.

The benefits of vehicle to grid technologies are very clear. It is very efficient in the sense that a sitting car can become a power source for the electrical company. This way, during peak hours of demand, the electrical company can use customer’s cars to help service their electrical grid’s demands, thus creating less demand and stress on other areas of the electrical company’s grid system. The car’s battery ultimately acts as an energy storage system for the electrical company so that they can buy back energy from the electrical vehicle (EV) owner whenever they want to. Ideally, the electric utility company will implement the idea of valley shaving, charging at night when demand is low, and peak shaving, sending power back to the grid when demand is high. Use of V2G capable plug-in electric vehicles (PEVs) can be considered as partial solutions to the global energy crisis at present. A note of importance is that with so many more cars used as generators, the electrical company could build fewer coal and resource depleting power sources as backup power systems. The utility companies can use EVs to stabilize the frequency in the power system [6.1]-[6.2] and improve utility operation. It makes the utility companies more efficient, there is less current flow in feeders, less loss because the energy is generated locally.

Finally, it will help the company use more of renewable energy [6.3]. That helps the environment with less pollution and reduction in global warming.

The economic analysis of V2G technology applied to the current electricity market has been widely studied and reported in open literature. In [6.4] the equations to calculate the capacity for grid power from three types of electric vehicles are proposed to evaluate revenue and costs for these vehicles to supply electricity to electric markets. In [6.5], the strategies and business models are proposed as theoretical support on implementation of V2G to stabilize large-scale wind power production. The cost analysis of electric vehicles to providing peak power in Japan is investigated in [6.6]. In addition, the assessment of V2G technology applied to the UK electricity market is studied in [6.7].

The main attractiveness of V2G is that it can produce income to the vehicle owner, when the car is not needed, maximizing car use, by substituting for the very expensive auxiliary power systems and therefore bringing positive implications for both the system operator and the vehicle owner. This however from the owner point of view has to be done to the extent where the income associated with V2G is higher than its costs. From the system operator point of view there is the advantage of substituting the secondary systems with a cheaper alternative, reducing costs associated with the electrical grid operation, though the system operator needs to guarantee that a minimum number of cars are plugged in at all times in order to assure the stability of the grid.

6.2 V2G System Information Collection for SmartPark

This section presents the various data of V2G system for the development of SmartPark. To carry out the economic analysis of a real-time large scale EVs power flow control, EVs' power requirement model should be provided. The EVs power requirement model contains the number of EVs with different sizes, battery capacity, charging time and energy consumption per mile.

6.2.1 EVs information collection

In the Smartpark there are different EVs types for V2G services. For research purpose, different types of EVs are illustrated here. The specific detail is shown in Table 6.1. Whenever a PEV is connected to the grid, the owner is requested to set the next departure time, and the system will make a record. At the departure time, the state of charge (SOC) of the battery is expected to be above 80%. Therefore, during the following period before the departure time, these PEVs can either be charged or discharged based on the grid's power flow, renewable energy sources output power, and frequency regulation requirement. For a protection reason, during the V2G service, the SOC of the batteries should not go below 20% [6.8].

TABLE 6.1 Parameters for PEVs in Different Sizes

EVs model	Percentage	Battery capacity (kWh)	Energy consumption per mile (kWh/mile)
Compact sedan (Ford Focus)	32.5%	10-20	0.2
Full-size sedan (Toyota Prius)	37.5%	20-30	0.3
Mid-size SUV	20%	30-40	0.45
Full-size SUV	10%	40-50	0.6

In the V2G system, the parking garage is located in some workplace like a company or universities whose office hours are from 9:00am to 18:00 pm. Based on the Central Limit Theorem (the conditions under which the mean of a sufficiently large number of independent random variables, each with finite mean and variance, will be approximately normally distributed [6.9]), the distribution of the EVs arrival and departure time is around 9 am and 6 pm. In this case, the total number of EVs is assumed to be 5,000. The normal distribution of arrival time A is $N\sim(9, 1.2)$, the normal distribution of departure time D is $N\sim(18, 1.2)$. Fig. 6.1 and Fig. 6.2 show the diagram distribution of the two parameters.

With the probability density function of A and D, the joint probability density function of D - A can be founded, which is the daily parking duration time. It is a normally distributed $N \sim (9, 1.2)$. The probability density function of the daily parking duration is shown in Fig. 6.3.

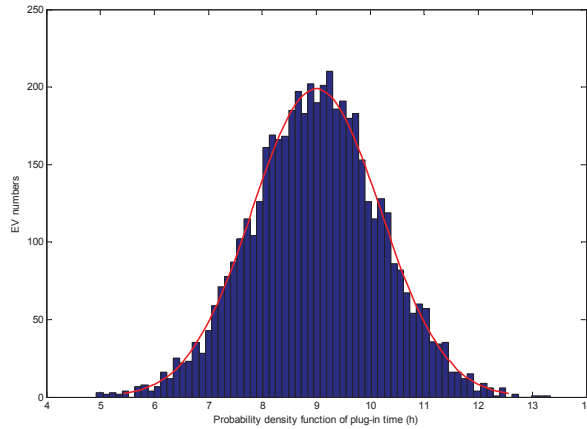


Fig. 6.1 The probability density function of arrival time A

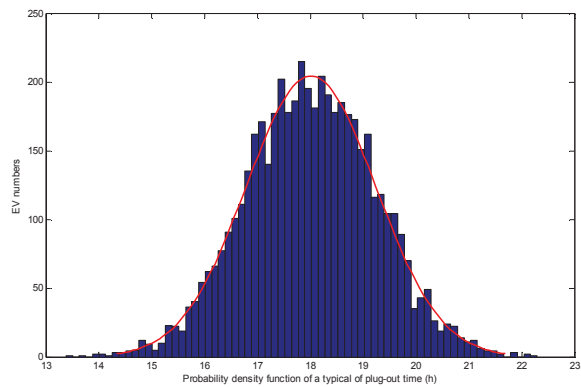


Fig. 6.2 The probability density function of arrival time D

Fig. 6.1 and Fig. 6.2 are the probability density function of arrival time and departure time; they are all normally distributed.

From Fig. 6.1 and Fig. 6.2 we could give out the probability density function of parking duration time as shown in Fig. 6.3. It is also normally distributed, the most numbers of EVs parking duration time is 6 to 12 hours.

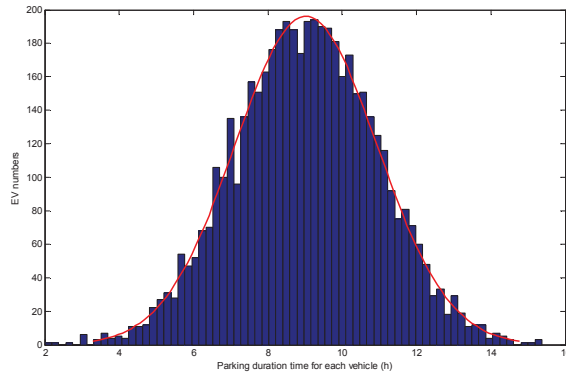


Fig. 6.3 The probability density function of parking time

The estimated power demanded by each individual PEV can be represented by equation,

$$P_{EV} = \frac{M \times E}{D - A} \quad (6.1)$$

M is the estimated number of miles driven daily (in kilometres); E is the energy efficiency for the PEV (in miles/kWh); D is the departure time, A is the arrival time.

$$P_{upco \min g} = \int_t^{t+T} f_A(x, \mu_A, \sigma_A) dt \times N \times P_{EVavg} \quad (6.2)$$

$f_A(x, \mu_A, \sigma_A)$ is the probability density function of grid connecting time A, N is the total number of PEVs in the PEVs network, P_{EVavg} is the average constant power requirement for all PEVs when they are connected to the parking lot. P_{EVavg} can be calculated from the probability density function of PEV.

For the daily travel range M, the following is information collected by the author in 2014,

Fig. 6.4 shows average kilometres travelled, from motor vehicles by state/territory of registration year ended 30 June 2012. From Fig. 6.4, we could calculate the average distance and electricity consumption for a typical plug-in hybrid EV (PHEV) which is shown in Table

6.2. From Table 6.2, we could observe that required electricity per kilometre is 0.25kWh, average running distance per day is 37.8km and average required electricity per day is 9.45kWh.

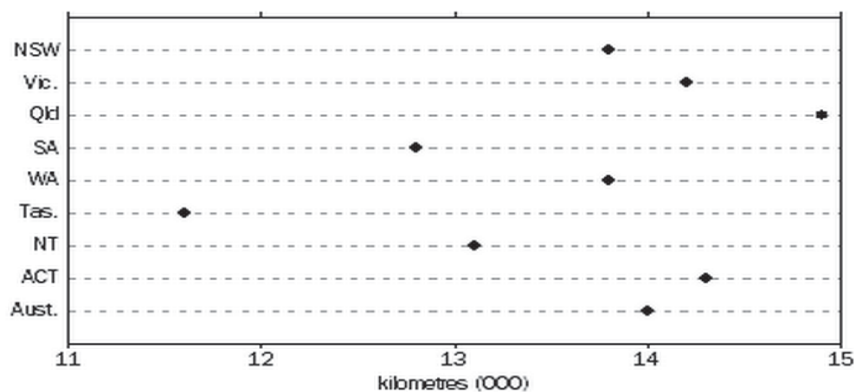


Fig. 6.4 Average kilometres travelled, Motor vehicles by state/territory of registration Year ended 30 June 2012 [6.10]

TABLE 6.2 Average Distance and Electricity Consumption for a Typical PHEV

Required electricity per kilometre (kWh)	Average running distance per day (km)	Average required electricity per day (kWh)
0.25	37.8	9.45

Based on the known driving pattern statistics, the average yearly total miles driven in NSW is 13,800 kilometres with 50% of drivers driving 35 kilometres per day or less, and 80% of drivers driving 40 kilometres or less. So a log normal distribution with $\mu_m = 3.37$, $\sigma_m = 0.5$ is selected to approximate the PDF of M_d , which shows that the total yearly driving distance average is 13,818 kilometres, 48% of the vehicles drive 35 kilometres or less each day, and 83% of the vehicles drive 60 kilometres or less each day, which closely approximates the driving performance results from [1]. The distribution function for M_d is given in (6.3).

$$f_x(x; \mu_m, \sigma_m) = \frac{1}{x\sigma_m\sqrt{2\pi}} \exp\left\{-\frac{(\ln x - \mu_m)^2}{2\sigma_m^2}\right\} \quad (6.3)$$

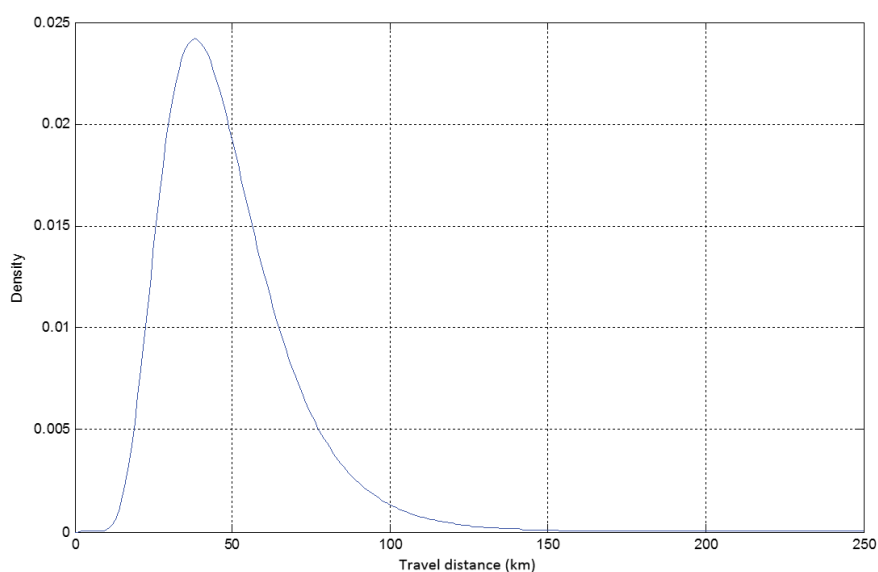


Fig. 6.5 The probability density function of the daily travel distance

To reduce the impact of PEVs charging on the utility AC grid and improve grid stability, during the following period before the departure time, these PEVs can either be charged or discharged based on the grid's power flow. The input data for the objective function include departure time disconnected to the grid, arrival time connected to the grid, estimated miles driven daily, estimated power demanded, electricity price and load power demand.

6.2.2 Grid side information collection

Regulation and load following are the two services required to continuously balance generation and load under normal conditions [6.11]. Fig. 6.6 shows the morning ramp-up decomposed into base energy, load following, and regulation. Starting at a base energy of 3566 MW, the smooth load following ramp is shown rising to 4035 MW. Regulation consists of the rapid fluctuations in load around the underlying trend, shown here on an expanded scale to the right with a ± 55 MW range. Combined, the three elements serve a load that ranges from 3539 to 4079 MW during the three hours depicted.

Load following and regulation ensure that, under normal operating conditions, a control area is able to balance generation and load. Regulation is the use of on-line generation, storage, or load

that is equipped with automatic generation control (AGC) and that can change output quickly (MW/min) to track the moment-to-moment fluctuations in customer loads and to correct for the unintended fluctuations in generation. Regulation helps to maintain interconnection frequency, manage differences between actual and scheduled power flows between control areas, and match generation to load within the control area. Load following is the use of on-line generation, storage, or load equipment to track the intra- and inter-hour changes in customer loads.

Fig. 6.7 is the electricity load demand data in a typical day in NSW (11/3/2015). Based on the electricity load demand data, the load curve and load following line in a typical day in NSW (11/3/2015) are shown in Fig. 6.8.

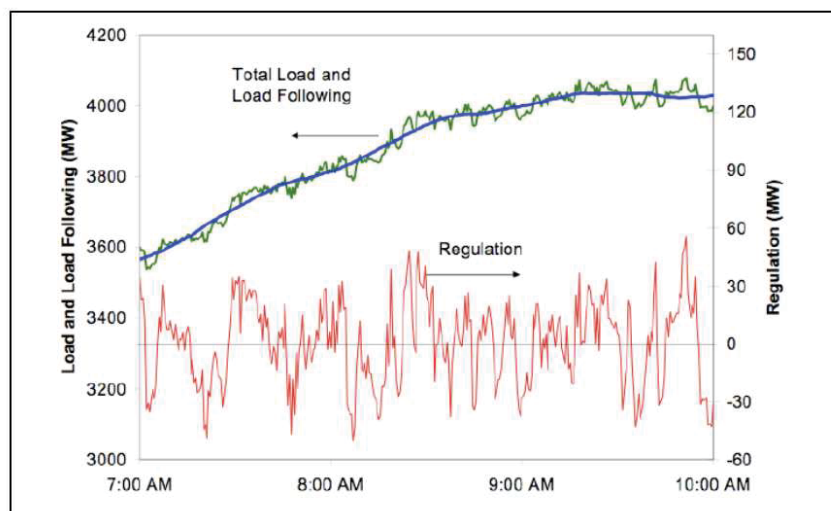


Fig. 6.6 System load following and regulation, where Regulation (red) is the fast fluctuating component of total load (green) while load following (blue) is the slower trend [6.12]

The load following curve is to meet power regulation, the ability to respond to small, random fluctuations around normal load. To smooth the actual load curve is the function of the load following curve.

By using the cftool in MATLAB, the mathematical function of the load following curve is obtained. Then the power needed for regulation is obtained as shown in Fig. 6.9.

	A	B	C	D	P
1	REGION	SETTLEMENTDATE	TOTALDEMAND	RRP	
2	NSW1	2015/3/11 9:10	9190.33	43.5467	
3	NSW1	2015/3/11 9:15	9202.43	42.96832	
4	NSW1	2015/3/11 9:20	9222.47	42.02798	
5	NSW1	2015/3/11 9:25	9226.46	42.21501	
6	NSW1	2015/3/11 9:30	9259.4	42.71748	
7	NSW1	2015/3/11 9:35	9266.26	35.95728	
8	NSW1	2015/3/11 9:40	9238.24	40.43358	
9	NSW1	2015/3/11 9:45	9318.75	41.5782	
10	NSW1	2015/3/11 9:50	9277.38	41.32287	
11	NSW1	2015/3/11 9:55	9294.1	40.57813	
12	NSW1	2015/3/11 10:00	9304.22	36.96964	
13	NSW1	2015/3/11 10:05	9251.41	35.52636	
14	NSW1	2015/3/11 10:10	9313.49	40.35272	
15	NSW1	2015/3/11 10:15	9305.86	38.97488	
16	NSW1	2015/3/11 10:20	9303.38	41.75214	
17	NSW1	2015/3/11 10:25	9290.18	41.56561	
18	NSW1	2015/3/11 10:30	9254.94	41.84315	
19	NSW1	2015/3/11 10:35	9306.24	42.74835	
20	NSW1	2015/3/11 10:40	9254.52	41.52343	
21	NSW1	2015/3/11 10:45	9368.61	42.76036	
22	NSW1	2015/3/11 10:50	9351.74	43.17069	
23	NSW1	2015/3/11 10:55	9336.06	43.27004	
24	NSW1	2015/3/11 11:00	9385	43.06309	
25	NSW1	2015/3/11 11:05	9356	40.83298	
26	NSW1	2015/3/11 11:10	9326.9	37.77853	
27	NSW1	2015/3/11 11:15	9365.28	38.36127	
28	NSW1	2015/3/11 11:20	9389.46	40.87686	
29	NSW1	2015/3/11 11:25	9364.97	40.44057	
30	NSW1	2015/3/11 11:30	9397.74	41.79617	
31	NSW1	2015/3/11 11:35	9375.93	38.058	
32	NSW1	2015/3/11 11:40	9416.41	38.05099	
33	NSW1	2015/3/11 11:45	9441.73	41.67473	
34	NSW1	2015/3/11 11:50	9482.97	38.65193	
35	NSW1	2015/3/11 11:55	9507.66	39.04478	
36	NSW1	2015/3/11 12:00	9478.7	39.1369	
37	NSW1	2015/3/11 12:05	9522.05	39.11411	

Fig. 6.7 Electricity load demand data in a typical day in NSW (11/3/2015)

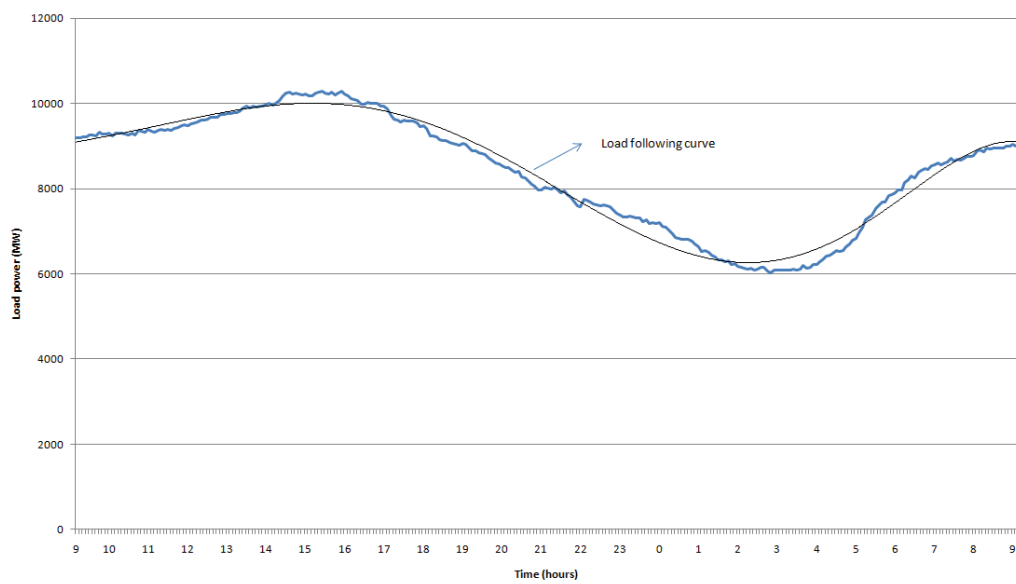


Fig. 6.8 Load curve and load following line in a typical day in NSW (11/3/2015)

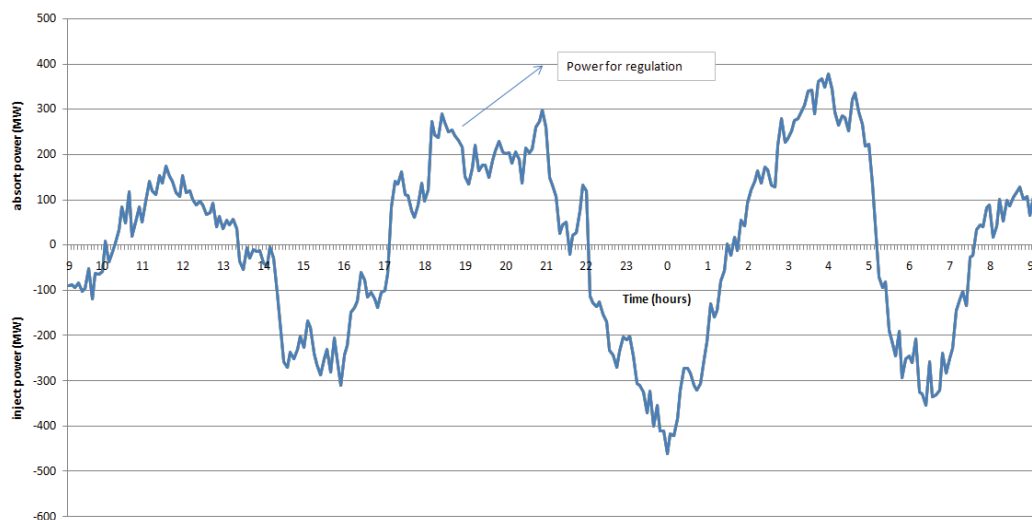


Fig. 6.9 Power regulation pattern in a typical day in NSW (11/3/2015)

Previous figures are about the load data for a day; Fig. 6.10 shows the electricity load demand data in a typical month in NSW (1/12/2014-31/12/2014). It also includes the load demand data in a day for 24 hours.

AE47	T145.25																									
	A	B	C	D	E	F	G	H	I	J	K	L	M	N	O	P	Q	R	S	T	U	V				
1	6524.77	7166.26	7316.73	7119.23	7195.06	6967.96	6484.59	6476.35	6924.05	7004.62	6940.77	6690.64	6747.64	6405.39	6340.31	6847.75	6813.2	6854.5	6979.27	6745.14	6404.21	6531.1				
2	6367.25	6907.86	7066.27	6922.27	6980.66	6679.68	6311.58	6358.52	6703.25	6754.57	6744.08	6449.63	6493.49	6240.32	6236.58	6613.51	6629.76	6618.16	6721.38	6529.23	6224.99	6384.1				
3	6169.01	6603.48	6731.42	6626.84	6647.66	6334.16	6018.76	6145.87	6439.16	6474.28	6430	6165.99	6163.65	5951.33	5969.02	6303.17	6294.65	6348.02	6397.62	6243.95	5976.85	6091.1				
4	6032.11	6430.77	6487.2	6387.34	6404.94	6072.66	5863.2	5988.62	6229.92	6177.62	6181.89	5911.68	5896.16	5751.14	5818.81	6078.55	6038.37	6101.04	6188.26	6004.07	5773.64	5971.1				
5	5948.79	6228.42	6329.66	6265.32	6279.17	5949	5757.77	5888.44	6059.67	6021.23	6060.85	5778.54	5718.3	5670.86	5722.82	5963	5995	5978.09	6064.56	5811.52	5643.35	5811.1				
6	5908.84	6213.17	6288.09	6220.13	6243.29	5881.07	5677.37	5857.95	6001.94	5988.13	6004.03	5677.91	5653.26	5604.63	5669.09	5893.89	5911.13	5890.64	5974.8	5764.98	5580.8	5751.1				
7	5911.02	6204.42	6288.6	6176.13	6231.22	5843.26	5667.78	5890.71	5989.25	6044.2	6011.48	5698.85	5631.14	5558.82	5731.6	5886.12	5913.38	5914.69	5994.8	5719.37	5545.72	5881.1				
8	6002.58	6221.62	6353.98	6227.58	6296.53	5874.61	5685.44	5989.25	6080.13	6142.5	6146	5809.48	5647.68	5560.02	5800.86	5942.98	6026.89	5984.8	6040.16	5713.1	5560.58	5911.1				
9	6284.23	6442.7	6593.09	6474.49	6480.47	6036.94	5746.49	6277.41	6336.34	6367.82	6351.3	6052.18	5750.36	5578.56	6023.65	6138.62	6247.2	6173.37	6254.58	5815.13	5616.21	6104.1				
10	6419.61	6662.88	6782.63	6754.39	6741.48	6037.58	5739.36	6494.59	6541.01	6580.96	6576.54	6246.08	5817.26	5566.64	6207.75	6305.35	6458.48	6403.25	6380.9	5843.05	5587.76	6261.1				
11	6936.71	7179.57	7343.29	7263.5	7253.18	6239.51	5850.22	7079.71	7045.14	7107.76	7035.67	6790.2	6000.59	5659.86	6712.91	6742.93	6918.43	6838.22	6834.66	6014.63	5654.91	6611.1				
12	7547.19	7650.68	7833.93	7756.97	7722.16	6478.84	5982.91	7944.58	7565.29	7570.76	7581.68	7258.51	6152.3	5802.95	7207.47	7173.16	7338.07	7298.4	7221.21	6160.18	5823.47	6981.1				
13	7962.36	8070.46	8304.91	8207.38	8124.55	6766.35	6272.28	8199.32	7987.87	7936.54	7989.87	7575.57	6421.26	5989.41	7461.78	7535.72	7697.05	7603.76	7529.14	6449.58	6010.96	7361.1				
14	8357.45	8397.81	8722.82	8552.9	8483.46	7140.06	6522.39	8439.59	8346.67	8281.23	8356.7	7837.01	6737.39	6295.18	7828.14	7887.67	8014.25	7941.2	7858.21	6743.08	6312.74	7711.1				
15	8540.37	8502.18	8989.15	8749.66	8706.61	7460.2	6820.96	8553.69	8577.11	8519.14	8592.54	7923.21	7038.44	6536.27	8048.36	8118.11	8191.78	8128.73	8079.35	7009.86	6594.64	8022.1				
16	8757.48	8669.89	9144.79	8903.86	8865.15	7673.7	7057.11	8600.13	8700.37	8650.87	8737.5	7956.04	7216.59	6785.82	8126.29	8211.69	8335.55	8294.04	8196.1	7237.82	6867.85	8111.1				
17	8956.96	8882.45	9477.3	9046.88	9004.77	7929.58	7281.22	8816.56	8869.57	8835.9	8877.76	8015.5	7415.9	6915.22	8328.55	8377.92	8453.82	8441.58	8314.6	7390.94	7022.56	8521.1				
18	9051.33	9042.61	9638.89	9114.03	8970.02	7987.53	7391.91	8889.82	8923.38	8906.04	8935.25	8064.47	7403.53	7053.42	8388.53	8441.42	8163.12	8475.94	8379.52	7406.44	7199.04	8601.1				
19	9091.62	9164.32	9840.42	9192.23	9106.77	8055.44	7490.15	9019.66	8949.92	8993.96	8951.63	8103.04	7467.23	7099.61	8507.81	8512.88	8266.22	8536.81	8401.34	7482.7	7287.34	8761.1				
20	9197.23	9308.59	10091.85	9261.99	9279.88	8070.08	7487.93	9113.79	9033.12	9068.23	8946.03	8182.41	7461.09	7089.6	8562.66	8493.19	8459.78	8664.22	8453.17	7404.41	7321.05	8891.1				
21	9234.58	9419.22	10143.02	9238.91	9372.34	8089.27	7620.1	9177.04	9082.55	9056.97	8899.87	8108.15	7386.22	7075.84	8596.79	8446.7	8462.78	8669.4	8370.75	7369.41	7338.3	8951.1				
22	9330.6	9559.46	10322.77	9307.45	9484.5	8089.02	7641.6	9247.18	9144.16	9078.51	8820.92	8055.81	7351.62	7070.04	8655.35	8475.35	8596.23	8675.49	8300.97	7331.06	7374.58	9011.1				
23	9421.4	9632.05	10517.37	9397.07	9573.59	8001.61	7722.5	9352.03	9194.98	9061.64	8733.56	7947.95	7276.85	7033.51	8672.7	8499.5	8546.72	8638.35	8155.08	7264.44	7416.28	9161.1				
24	9500.39	9774.6	10634.93	9509.46	9631.91	8075.93	7828.59	9361.9	9219.6	9111.81	8582.67	7937.99	7153.73	7033.15	8714.92	8515.1	8536.14	8650.67	8091.24	7213.5	7459.45	9301.1				
25	9654.04	9890.58	10842.41	9568.72	9721.83	8085.04	7922.38	9321.28	9198.04	9191.92	8574.72	7885.37	7142.85	7009.62	8776.73	8537.98	8660.51	8664.95	8050.98	7197.14	7505.65	9391.1				
26	9786.17	10137.51	10687.35	9669.08	9820.07	8137.05	7905.37	9187.8	9207.25	9258.03	8536.88	7866.91	7108.09	7025.62	8887.38	8543.46	8609.71	8688.51	8039.36	7206.83	7556.69	9511.1				

Fig. 6.10 Electricity load demand data in a typical month in NSW (1/12/2014-31/12/2014)

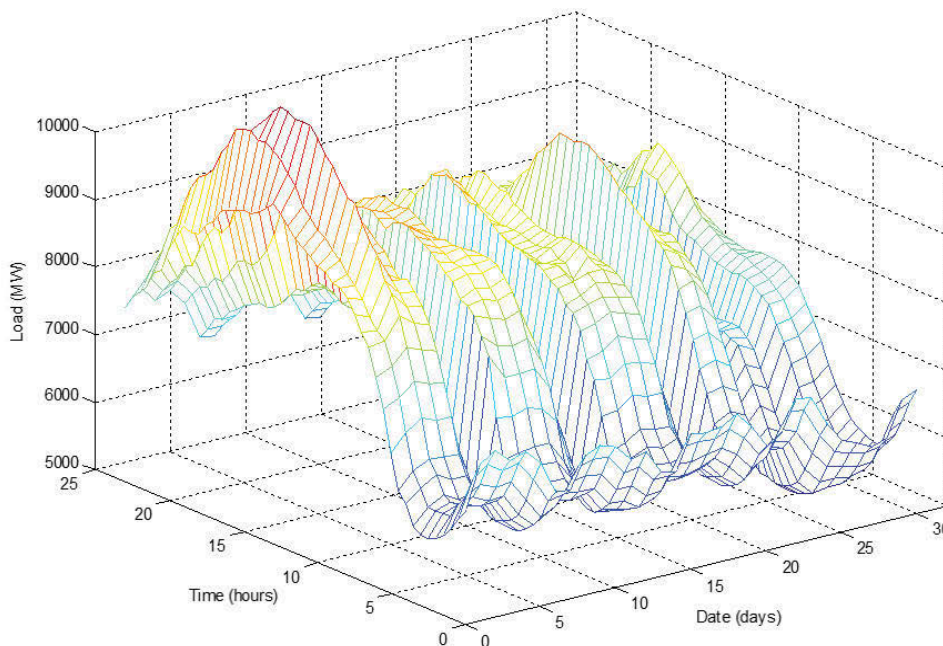


Fig. 6.11 Electricity load demand data in a typical month in NSW 24 hours a day 31 days a month (1/12/2014-31/12/2014)

Fig. 6.11 is the electricity load demand data in a typical month in NSW 24 hours a day 31 days a month (1/12/2014-31/12/2014).

Electricity price variation is essential for V2G economic issues. Fig. 6.12 is the electricity price variation in a typical month in NSW (1/12/2014-31/12/2014), it also includes the price variation for 24 hours a day.

J30		41.63																				
	A	B	C	D	E	F	G	H	I	J	K	L	M	N	O	P	Q	R	S	T	U	V
1	23.43	27.62	27.88	29.76	36.28	27.71	20.19	28.12	29.28	33.32	28.82	23.87	28.05	28.11	25.38	28.78	27.76	31.05	25.5	28.53	20.71	2
2	23.22	24.76	26.43	30.95	32.47	26.66	19.66	27.29	27.6	33.36	28.71	26.14	28.72	27.53	24.7	28.14	27.91	28.81	23.59	27.73	22.93	2
3	21.99	24.04	24.55	28.37	29.93	25.31	18.96	23.97	25.06	30.57	26.77	21.43	24.71	23.51	23.13	28.05	26.34	26.74	24.09	26.05	20.53	2
4	21.39	23.39	24.31	28	27.42	24.35	18.78	23.66	23.68	27.96	24	18.96	23.86	22.14	22.75	25.94	25.81	24.24	24.13	24.46	18.96	2
5	19.46	20.92	24.28	25.85	27.27	24.5	18.3	23.63	23.45	28.14	24.25	18.96	23.66	20.63	21.33	23.59	26.03	24.53	22.09	23.66	18.1	2
6	18.55	20.75	24.17	28.63	25.71	24.36	18.1	23.57	23.61	30.68	22.74	18.89	23.69	18.96	19.56	22.46	26.52	24.01	20.8	23.72	17.58	2
7	18.96	18.96	24.08	26.53	25.29	24.28	18.83	24.16	23.52	34.41	24.07	18.96	23.63	18.96	22.13	23.11	27.7	24.42	24.41	22.06	17.91	2
8	18.56	18.96	24.12	27.68	24.74	24.41	17.77	24.73	24.04	34.51	24.59	18.96	23.64	18.96	23	24.06	28.66	24.66	24.42	18.97	18.47	2
9	22.68	22.7	24.42	28.76	27.81	24.75	18.36	26.15	26.48	39.8	24.99	26.36	24.01	19.67	24.57	26.83	32.46	26.36	26.71	24.28	18.96	2
10	21.22	23.3	24.75	27.83	28.37	19.4	18.29	25.53	24.13	36.3	24.65	24.75	23.67	18.57	24.55	23.16	33.52	24.63	25	18.96	17.8	2
11	21.42	25.08	26.52	31.3	28.13	21.13	18.85	31.1	25.46	40.67	25.72	24.34	23.77	18.96	28.11	26.02	33.77	25.58	24.87	18.96	18.16	2
12	32.49	27.46	29.64	31.51	32.65	24.52	18.96	35.24	29.98	40.91	30	28.37	19.6	18.96	31.19	29.22	34.07	30.13	27.43	18.96	18.73	2
13	32	30.58	32.43	31.86	32.22	24.77	18.96	35.52	33.2	41.81	31.78	29.06	24.48	19.1	30.22	27.77	32.63	32.66	30.51	23.56	18.96	2
14	31.19	31.63	32.73	34.79	33.4	28.46	18.96	35.78	36.36	45.03	36.7	31.76	24.71	20.09	33.11	29.45	33.82	39.14	31.54	28.39	18.96	2
15	31.41	30.58	35.81	34.38	32.28	31.25	22.19	34.84	32.8	44.75	39.97	28.97	24.44	23.97	33.96	28.72	34.01	33.23	31.77	25.31	18.96	2
16	34.11	32	45.56	37.4	32.97	31.43	24.77	42.1	35.78	48.56	40.81	29.08	24.62	26.09	33.38	28.41	35.44	32.08	31.96	27.2	21.17	2
17	37.27	33.03	48.54	41.93	32.82	31.82	25.42	49.61	40.33	48.84	46.37	29.86	25.28	26.92	34.74	29.46	38.29	36.03	31.26	30.71	24.26	2
18	35.57	33.24	47.86	42.06	32.78	31.38	26.6	48.12	40.4	49.58	43.09	31.11	25.41	28.17	36.26	31.18	33.32	35.82	31.27	29.1	25.17	2
19	33.85	32.78	46.97	45.49	32.88	32.37	27.97	49.84	45.85	45.82	49.39	29.33	27.56	28.27	36.84	31.88	37.36	37.38	31.31	28.49	28.17	2
20	34.87	34.73	49.96	48.01	33.22	32.39	28.02	48.75	46.81	43.24	46.16	31.96	28.03	28.25	40.24	31.95	35.98	34.82	31.46	28.16	27.93	2
21	33.89	36.7	49.49	48.91	33.19	32.66	28.29	43.58	46.69	42.93	36.34	32.05	28.12	28.26	40.28	31.73	35.29	39.6	27.93	28.14	28.27	2
22	36.43	35.91	50.5	50.23	34.84	31.7	28.73	45.64	51.01	45.6	45.25	32.33	27.2	28.04	38.72	31.48	42.76	40.55	27.16	28.29	28.91	2
23	37.48	42.84	54.23	49.63	43.42	28.65	28.48	40.86	52	39.74	37.98	30.9	27.67	28.13	36.24	31.58	38.96	40.18	26.85	28.03	30.78	2
24	37.96	45.42	50.68	49.29	46.2	28.03	29.5	39.61	48.59	38.69	35.59	32.25	25.81	26.36	35.5	32.09	35.14	44.67	28.38	28.13	31.81	4
25	43.5	41.55	51.04	48.01	45.87	28.08	29.32	35.97	45.17	38.58	45.46	31.28	27.11	25.42	42.52	32.42	40.9	36.58	28.13	26.6	32.08	4
26	47.66	46.55	50.56	47.75	37.75	28.14	28.03	36.78	45.87	44.32	45.01	28.67	27.92	25.09	43.67	31.83	38.54	35.33	28.63	26.77	32.45	4

Fig. 6.12 Electricity price variation in a typical month in NSW (1/12/2014-31/12/2014)

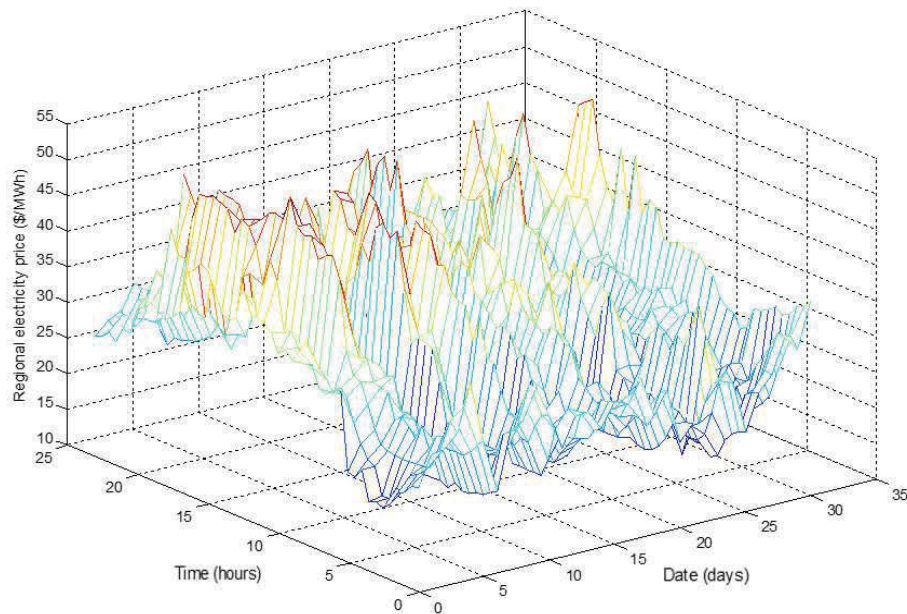


Fig. 6.13 Electricity price variation in a typical month in NSW 24 hours a day 31 days a month (1/12/2014-31/12/2014)

Fig. 6.13 shows the 3D electricity price variation curve in a typical month in NSW 24 hours a day 31 days a month (1/12/2014-31/12/2014).

In the following assumptions, for smart parks it is assumed to have 100 EVs. Three types of EVs are assumed with energy ratings 10 kWh, 16 kWh, and 20 kWh. It is assumed that EVs with different SOC are available at the charging station. Primary job of the EVs are for commuting and hence a minimum SOC value should always be maintained to meet any emergency needs. A minimum state of charge of 50% has been taken here. Two scenarios are developed for calculating the energy available for grid support as well as energy required for charging the EVs. In the first scenario, it is assumed that 390 kWh of energy is available which is shown in Table 6.3. In the second scenario, 192 kWh of energy is available which is given in Table 6.4. These two scenarios together serve as a base case for the study of grid support by EVs.

Similar assumption is made for developing the scenarios for the charging of EVs. SOC level of EVs are assumed to be same as that of discharging. It can be seen from Table 6.5 that charging scenario 1 requires 435 kWh of energy and from Table 6.6, it is clear that charging scenario 2 requires 648 kWh of energy to charge the EVs.

The EVs for grid support should have the minimum SOC value limit, the minimum SOC value should always be maintained to meet any emergency needs. A minimum state of charge of 50% has been assumed here. The total energy available for grid support is shown in Table 6.3 and Table 6.4, the total energy required during charging is shown in Table 6.5 and Table 6.6. For the case of charging from grid to EVs, a maximum state of charge of 100% has been assumed.

These two cases also together serve as a base case for the study of grid support and EV charging case.

Next, the data is obtained for total amount of power regulation, information for EV owners (initial SOC, desired SOC, arrived time, departure time), electricity price, charging facility cost. Objective functions can be carried out for optimal charging.

TABLE 6.3 Total Energy Available For Grid Support

Initial SOC	Energy (kWh)	Number of EVs	SOC required for discharging (%)	Available energy for the grid support (kWh)
30	10	25	-20	-50
60	16	25	10	40
90	20	50	40	400
Total energy for discharging				390

TABLE 6.4 Total Energy Available For Grid Support

Initial SOC	Energy (kWh)	Number of EVs	SOC required for discharging (%)	Available energy for the grid support (kWh)
20	10	20	-30	-60
40	16	30	-10	-48
80	20	50	30	300
Total energy for discharging				192

TABLE 6.5 Total Energy Required During Charging

Initial SOC	Energy (kWh)	Number of EVs	SOC required for discharging (%)	Available energy for the grid support (kWh)
30	10	25	70	175
60	16	25	40	160
90	20	50	10	100
Total energy for discharging				435

TABLE 6.6 Total Energy Required During Charging

Initial SOC	Energy (kWh)	Number of EVs	SOC required for discharging (%)	Available energy for the grid support (kWh)
20	10	20	80	160
40	16	30	60	288
80	20	50	20	200
Total energy for discharging				648

6.3 Optimal Charging Based on Different Objectives

6.3.1 As fast as possible charging (AFAP)

AFAP charging illustrates the situation in which no intelligent device is used to charge the EV. The EV immediately starts charging when connected to the grid and stops charging when either the battery is fully charged or when the EV gets disconnected from the power grid.

The following assumptions are made within our model setting:

- 1) Drivers use their electric vehicles in the same manner as a conventional vehicle.
- 2) The volatile component of end consumer electricity prices change proportionally to wholesale electricity prices.
- 3) Vehicle owners can buy electricity at end consumer prices and sell at wholesale prices. They receive a grid fee reimbursement in the latter case.
- 4) Driving patterns and electricity prices are ex-ante known for the optimization horizon.
- 5) Mobility has to be guaranteed, i.e., the battery is always charged such that the next trips are possible.

- 6) The additional load caused by the small number of charging electric vehicles in our study has no influence on electricity prices. Therefore, electric vehicles are price takers.
- 7) Charging and discharging can only occur when the electric vehicle is parked at home.
- 8) Charging and discharging activity is linear and unrestricted across all possible battery SOC levels.
- 9) The time frame of the analysis is one week with 15 min. time slot resolution ($T=672$).
- 10) The terminal battery level SOC_T must match the initial battery level SOC_0 to ensure a continuous trajectory.
- 11) Battery costs are composed of a linear term ($\psi_e \varphi_t$) reflecting the degradation from energy throughput and a quadratic term ($\psi_p \varphi_t^2$) reflecting power-related degradation.

Table 6.7 provides an overview of the model parameters used in the subsequent analyses.

$$\varphi_t = \begin{cases} \min\{\overline{\varphi}_t, \overline{SOC} - SOC_t\} : \text{if } SOC_t \leq \overline{SOC}, \text{ and } z_t = 1 \\ 0 : \text{if } z_t = 0 \end{cases} \quad (6.4)$$

$$z_t = \begin{cases} 1 : EV \text{ at home during time step } t \\ 0 : \text{otherwise} \end{cases} \quad (6.5)$$

The payment resulting from this strategy is the sum of energy charged in the time slots that are determined by the driving profile and do not incorporate any economic decision-making rationale. The payment is given in (6.6) and consists of energy costs and battery degradation costs:

$$P = \underbrace{\sum_{t=1}^T p_t \cdot \varphi_t}_{\text{Energy costs}} + \underbrace{\varphi_t^2 \cdot \psi_p}_{\text{Power-related battery degradation}} + \underbrace{\varphi_t \cdot \psi_e}_{\text{Energy-related battery degradation}} \quad (6.6)$$

TABLE 6.7 Model Parameters

Storage System and Infrastructure Parameters		
Battery capacity	\overline{SOC}	(kWh)
Charging efficiency	η_c	(%)
Discharging efficiency	η_d	(%)
Energy-related battery degradation cost	ψ_e	(EUR/kWh)
Power-related battery degradation cost	ψ_p	(EUR/kWh ²)
Maximum charging amount per time slot	$\overline{\varphi}$	(kWh)
Initial EV battery SOC	SOC_{init}	(kWh)
Terminal EV battery SOC	SOC_{end}	(kWh)
Infrastructure cost	K_f	(\$/week)
Market and Consumer Parameters		
Price per energy unit at time t	p_t	(\$/kWh)
Energy consumption at time t	d_t	(kWh)
Location of the EV at time t	z_t	
Decision Variables		
Charge parameter for at time t	φ_t	(kWh)
Net charging amount	ϕ	(kWh)
V2G parameter for at time t	λ_t	(kWh)
SOC level for at time t	SOC_t	(kWh)

6.3.2 Maximization of the average SOC for all vehicles at the next time step

The objective function considered in this part is the maximization of the average SOC for all vehicles at the next time step. The energy price, charging time, and current SOC are considered in this model to join the charging system dynamically. In order to make the system more robust, the proposed system will also allow vehicles to leave prior to their expected departure time (i.e., the vehicle is unplugged abruptly). This would result in a serious failure in terms of optimal power allocation, and the PHEV/PEV battery may not be adequately charged (even if it has been plugged-in for a long time) [6.13]. Therefore, the proposed function aims at ensuring some fairness in the SOC-distribution at each time step. This will help ensure that a reasonable level of battery power is attained, even in the event of an early departure.

Maximize the objective function J at any given time k

$$J(k) = \sum_i w_i(k) \cdot SOC_i(k+1) \quad (6.7)$$

$$w_i(k) = f(Cap_{r,i}(k), T_{r,i}(k), D_i(k)) \quad (6.8)$$

$$Cap_{r,i}(k) = (1 - SOC_i(k)) \cdot Cap_i \quad (6.9)$$

where $Cap_{r,i}(k)$ is the remaining battery capacity needed to be filled for the i th vehicle at time step k ; Cap_i is the rated battery capacity (A h) of the i th vehicle. Fig. 6.14 illustrates the relationship between Cap_i and $SOC_i(k)$. $T_{r,i}(k)$ is the remaining time for charging the i th vehicle at time step k ; $D_i(k)$ is the price difference between the real-time energy price and the price that the specific customer at the i th vehicle battery charger is willing to pay at time step k ; $w_i(k)$ is the charge weighting term of the i th vehicle at time step k (this is a function of the energy price, the remaining charging time, and the present SOC); $SOC_i(k+1)$ is the state of charge of the i th vehicle at time step $k+1$.

The weighting term gives a reward proportional to the attributes of a specific vehicle. For example, if a vehicle has a lower initial SOC and less remaining charging time, but the driver is willing to pay a higher price, the controller allocates more power to this vehicle battery charger:

$$w_i(k) \propto [Cap_{r,i}(k) + D_i(k) + 1/T_{r,i}(k)] \quad (6.10)$$

Since the three terms $Cap_{r,i}(k)$, $D_i(k)$, $1/T_{r,i}(k)$ are not on the same scale, all terms need to be normalized in order to assign reasonable importance to each other.

The parking deck operators may also have different interests and assign different importance factors to $c_{r,i}(k)$, $t_i(k)$, and $d_i(k)$ depending on their own preferences, α is this user-defined parameter. Thus,

$$w_i(k) = \alpha_1 c_{r,i}(k) + \alpha_2 t_i(k) + \alpha_3 d_i(k) \quad (6.11)$$

$$\alpha_1 + \alpha_2 + \alpha_3 = 1 \quad (6.12)$$

$$\alpha_1, \alpha_2, \alpha_3 \geq 0 \quad (6.13)$$

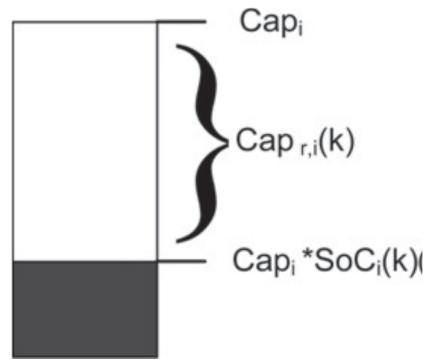


Fig. 6.14 The illustration of the remaining battery capacity

The charging current is also assumed to be constant over Δt .

$$[SOC_i(k+1) - SOC_i(k)] \cdot Cap_i = Q_i = I_i(k) \Delta t \quad (6.14)$$

$$SOC_i(k+1) = SOC_i(k) + I_i(k) \Delta t / Cap_i \quad (6.15)$$

where Δt is the sample time defined by the parking deck operators, and $I_i(k)$ is the charging current over Δt .

The battery model is considered to be a capacitor circuit, where C_i is the battery capacitance (Farad). The model is described as

$$C_i \cdot dV_i/dt = I_i \quad (6.16)$$

Therefore, over a short period of time, one can approximate the voltage change to be linear,

$$C_i \cdot [V_i(k+1) - V_i(k)] / \Delta t = I_i \quad (6.17)$$

$$V_i(k+1) - V_i(k) = I_i \Delta t / C_i \quad (6.18)$$

Since the decision variable is the power allocated to the vehicles, replace $I_i(k)$ with $P_i(k)$

$$I_i(k) = \frac{P_i(k)}{0.5 \times [V_i(k+1) + V_i(k)]} \quad (6.19)$$

Substituting $I_i(k)$ into (6.18) yields

$$V_i(k+1) = \sqrt{2P_i(k)\Delta t / C_i + V_i^2(k)} \quad (6.20)$$

$$SOC_i(k+1) = SOC_i(k) + \frac{2P_i(k)\Delta t}{Cap_i \cdot [V_i(k+1) + V_i(k)]} \quad (6.21)$$

Finally, the objective function becomes

$$J(k) = \sum_i w_i \cdot \left[SOC_i(k) + \frac{2P_i(k)\Delta t}{Cap_i \cdot \left[\sqrt{\frac{2P_i(k)\Delta t}{C_i} + V_i^2(k)} + V_i(k) \right]} \right] \quad (6.22)$$

6.3.3 Maximum revenue static charging scheduling problem (R-SCSP) and minimum cost dynamic charging scheduling problem (C-DCSP)

The electricity market operates on an hourly basis; therefore, we can naturally divide the time domain into timeslots with a duration of 1 h each and consider $T=24$ h as a charging period, starting at 12:00 p.m. (noon). We define a charging schedule for a given charging task i as a vector $\Phi_i = [p_{i,1}, \dots, p_{i,t}, \dots, p_{i,T}]$ in which each entry specifies the charging rate at hour t . the charging schedule is feasible if both customers' demands (specified by charging tasks) and the system loading requirements are satisfied. The charging schedule can be defined for a set of given tasks: $\Phi = \{\Phi_i : i \in \{1, \dots, N\}\}$, where N is the number of charging tasks. We define the static scheduling problems. Given a set of charging tasks $Q = \{(1, s_z, f_1, e_1), \dots, (i, s_i, f_i, e_i), \dots, (N, s_N, f_N, e_N)\}$; base loads $l = [l_1, \dots, l_t, \dots, l_T]$; electricity prices $g = [g_1, \dots, g_t, \dots, g_T]$; regulation prices $a = [a_1, \dots, a_t, \dots, a_T]$; transformer delivery capacity R ; EV battery capacities $C = [C_1, \dots, C_i, \dots, C_N]$; EV battery charging efficiency $E = [E_1, \dots, E_i, \dots, E_N]$, which is the ratio between the effectively stored energy and input energy; and upper and lower charging rate limits $P = [P_1, \dots, P_i, \dots, P_T]$ and $P' = [P'_1, \dots, P'_i, \dots, P'_T]$. The two definition of problems are shown as follows.

Definition 1: The maximum revenue static charging scheduling problem (R-SCSP) seeks a feasible charging schedule Φ for the set of given charging tasks Q such that the corresponding aggregator's revenue $\sum_{t=1}^T \sum_{i=1}^N m_{i,t}$ is maximum among all feasible charging schedules.

Definition 2: The Minimum Cost Static Charging Scheduling Problem (C-SCSP) seeks a feasible charging schedule Φ for the set of given charging tasks Q such that the corresponding total electricity cost $\sum_{t=1}^{t=T} \sum_{i=1}^{i=N} c_{i,t}$ is minimum among all feasible charging schedules.

The dynamic charging scheduling problems are the same as their static counterparts except that the charging task sequence is not assumed to be known in advance. Correspondingly, we call the two problems as the **Maximum Revenue Dynamic Charging Scheduling Problem (R-DCSP)** and the **Minimum Cost Dynamic Charging Scheduling Problem (C-DCSP)**.

For the static problems, they can be formulated as linear programming (LP) problems, which are known to be solvable in polynomial time [6.14]. For the dynamic problems, we present polynomial-time heuristic algorithms.

For easy references, the symbols and major notations are shown in Table 6.8

A. Static charging scheduling

The LP formulation for the R-SCSP, LP-SCSP.

$$\max_{x_{i,t}, p_{i,t}, r_{i,t}} \sum_{t=1}^T a_t \left(\sum_{i=1}^N r_{i,t} \right) + M \sum_{t=1}^T \sum_{i=1}^N p_{i,t} h_{i,t} \quad (6.23)$$

Subject to

$$x_{i,t} = \begin{cases} e_i & \forall i, t = \lfloor s_i \rfloor \\ e'_i & \forall i, t = \lceil f_i \rceil \\ x_{i,t-1} + \frac{E_i h_{i,t-1} p_{i,t-1}}{C_i}, & \text{otherwise} \end{cases} \quad (6.24)$$

$$P'_i \leq p_{i,t} \leq P_i \quad \forall i, t \quad (6.25)$$

$$\sum_{t=1}^T (M + gt) \left(\sum_{i=1}^N p_{i,t} h_{i,t} \right) \leq B \quad (6.26)$$

$$r_{i,t} = u_{i,t} + d_{i,t} \quad \forall i, t \quad (6.27)$$

$$u_{i,t} = \begin{cases} p_{i,t} - P'_i & \forall i, t \text{ s.t. } h_{i,t} = 1 \\ 0, & \text{otherwise} \end{cases} \quad (6.28)$$

$$d_{i,t} = \begin{cases} \min\{\bar{P}_{i,t}, P_i\} - p_{i,t} & \forall i, t \text{ s.t. } h_{i,t} = 1 \\ 0, & \text{otherwise} \end{cases} \quad (6.29)$$

$$\sum_i^N p_{i,t} + l_t + \sum_i^N d_{i,t} \leq R \quad \forall t \quad (6.30)$$

TABLE 6.8 The Symbols and Major Notations

T	The total number of timeslots
N	The number of EVs
M	The mark-up price (\$/kWh)
g_t	The electricity price at timeslot t (\$/kWh)
a_t	The regulation price at timeslot t (\$/kWh)
l_t	The base load at timeslot t (kW)
P_i	The upper charging rate limit of EV i (kW)
P'_i	The lower charging rate limit of EV i (kW)
C_i	The battery capacity efficiency of EV i
E_i	The battery charging efficiency of EV i
e_i	The initial SOC of EV i
e'_i	The desired SOC of EV i
s_i	The starting time of EV i
f_i	The finishing time of EV i
R	The transformer delivery capacity (kW)
B	The cost upper bound
$h_{i,t}$	The EV connection of EV i during timeslot t (h)
$x_{i,t}$	The SOC of EV i at time t
$p_{i,t}$	The charging rate of EV i at timeslot t (kW)
$\bar{P}_{i,t}$	The maximum charging rate limit of EV i at timeslot t (kW)
$r_{i,t}$	The regulation capacity of EV i at timeslot t (kW)
$u_{i,t}$	The regulation-up capacity of EV i at timeslot t (kW)
$d_{i,t}$	The regulation-down capacity of EV i at timeslot t (kW)
$m_{i,t}$	The aggregator's revenue from EV i at timeslot t (\$)
$c_{i,t}$	The cost of charging EV i at timeslot t (\$)

In this formulation, (6.24) assigns a value for the SOC of each connected EV in each hour properly. This way, each EV is guaranteed to be charged to the desired SOC when it is disconnected from the charging network. Note that in these equations, $h_{i,t}$ gives the actual connection time of each EV during each timeslot. An EV may not always arrive at the beginning of a timeslot and leave at the end of a timeslot. Therefore, in a timeslot, the connection time of an EV may be less than 1 h, and this would affect the calculation of regulation capacities, charging energy, and cost. Note that $h_{i,t}$ is not a decision variable, and its value can be precalculated using the following equation once a charging task is given:

$$h_{i,t} = \begin{cases} 1, & \lfloor s_i \rfloor < t < \lfloor f_i \rfloor \\ 1, & t = \lfloor s_i \rfloor, s_i = \lfloor s_i \rfloor \\ \lceil s_i \rceil - s_i, & t = \lfloor s_i \rfloor, s_i \neq \lfloor s_i \rfloor \\ f_i - \lfloor f_i \rfloor, & t = \lfloor f_i \rfloor, s_i \neq \lfloor f_i \rfloor \\ 0, & \textit{otherwise} \end{cases} \quad (6.31)$$

Constraint (6.25) ensures that in each timeslot, the charging rate of each EV is no smaller than its lower limit but no larger than its upper limit. In addition, the total charging cost of an EV should not exceed cost upper bound B, which is guaranteed by constraint (6.26). B is the maximum total cost that customers are willing to pay for charging their EVs, which is specified by customers based on their needs. We make these constraints general enough such that the cost upper bound can be set to any reasonable value based on various factors such as emergency level, the cost without regulation, the minimum possible total cost. Constraints (6.27)–(6.30) calculate the regulation capacities and make sure that there is no violation on the transformer delivery capacity. Note that since the regulation service is provided on an hourly basis, the regulation capacity should be consistent during the whole timeslot. In the hours when the EV arrives or leaves in the middle, regulation service is not considered to be provided by the aggregator. Hence, (6.28) and (6.29) ensure that the regulation capacity will not be accounted for in those hours. Thus LP-C-SCSP:

$$\min_{x_{i,t}, p_{i,t}, f_{i,t}} \sum_{t=1}^T (M + gt) \left(\sum_{i=1}^N p_{i,t} h_{i,t} \right) \quad (6.32)$$

subject to constraints (6.24)–(6.25) and (6.27)–(6.30).

B. Dynamic charging scheduling

Neither the R-DCSP nor the C-DCSP can be solved by solving a single LP problem because the charging tasks are not known in advance. We propose two schemes to solve the dynamic scheduling problems. In the first scheme, we solve an LP problem to find the charging schedule Φ_i every time charging task i arrives (i.e., an EV is connected to the charging network). Once the charging schedule for an EV is calculated, it will not be changed during the whole charging period. The LP problem is presented in the following, which has a much smaller size (the number of constraints and variables) than that previously presented since it is used for a single EV i . Thus LP-R-DCSP (i)

$$\max_{x_{i,t}, p_{i,t}, r_{i,t}} \sum_{t=1}^T a_t r_{i,t} + M \sum_{i=1}^T p_{i,t} h_{i,t} \quad (6.33)$$

Subject to

$$x_t = \begin{cases} e_i & \forall t = \lfloor s_i \rfloor \\ e'_i & \forall t = \lceil f_i \rceil \\ x_{i,t-1} + \frac{E_i h_{i,t-1} p_{i,t-1}}{C_i}, & otherwise \end{cases} \quad (6.34)$$

$$P'_i \leq p_{i,t} \leq P_i \quad \forall t \quad (6.35)$$

$$\sum_{t=1}^T (M + gt) p_{i,t} h_{i,t} \leq B \quad (6.36)$$

$$r_{i,t} = u_{i,t} + d_{i,t} \quad \forall t \quad (6.37)$$

$$u_{i,t} = \begin{cases} p_{i,t} - P'_i & \forall t \text{ s.t. } h_{i,t} = 1 \\ 0, & otherwise \end{cases} \quad (6.38)$$

$$d_{i,t} = \begin{cases} \min\{\bar{P}_{i,t}, P_i\} - p_t & \forall t \text{ s.t. } h_{i,t} = 1 \\ 0, & \text{otherwise} \end{cases} \quad (6.39)$$

$$\sum_{j=1}^i p_{j,t} + l_t + \sum_{j=1}^i d_{j,t} \leq R \quad \forall t \quad (6.40)$$

In this formulation, the objective function and constraints are similar to those in the R-SCSP. However, we only calculate the charging scheduling for the newly arriving EV i . Note that constraints (6.36) and (6.40) are different from (6.26) and (6.30) because we only consider this new EV i and all those EVs that were connected before EV i . Similarly, for the C-DCSP, we solve the following LP:LP-C-DCSP(i):

$$\min_{x_{i,t}, p_{i,t}, d_{i,t}} \sum_{t=1}^T (M + gt)p_{i,t}h_{i,t} \quad (6.41)$$

subject to constraints (6.34)–(6.40).

Although this approach can find a charging schedule with either the maximum incremental revenue (LP-R-DCSP) or the minimum incremental cost (LP-C-DCSP) every time an EV is connected to the network, it cannot guarantee that the solution is optimal for either the R-DCSP or C-DCSP. To improve its performance further, we come up with another scheme, namely, dynamic charging scheduling with updating, which adjusts the charging schedules for the connected EVs every time k more EVs arrive. This can be done by solving an LP problem that is the same as the LP-R-SCSP or LP-C-SCSP, except that the input only includes EVs that are currently connected to the network (instead of all EVs). The smaller the value of k , usually, the better the performance, but the higher the overhead.

6.4 Summary of the Chapter

In this chapter, we have studied economic issues related to the V2G services by considering aggregator's revenue and customer's demands and cost. Different EVs are assumed to be charged at Smartparks, different EV parameters, electricity price and load demand are collected

to carry out the economic effects of V2G services. Finally, different objective functions are studied and compared to solve the optimal charging and discharging of EVs. Although this chapter is not the main point of this PhD thesis, how large a profit V2G services produce is one of the main attraction to the vehicle owner.

References

- [6.1] W. Kempton, J. Tomic, "Vehicle to Grid Power Fundamentals: Calculating Capacity and Net Revenue," *Journal of Power Sources*, vol 144, issue 1, June 2005, pp. 268-279.
- [6.2] J. Tomic and W. Kempton, "Using Fleet of Electric Vehicle Drive Vehicles for Grid Support," *Journal of Power Sources*, vol.169, issue 2, June 2007, pp. 459-468.
- [6.3] W. Kempton and J. Tomic, "Vehicle to Grid Power Implementations: From Stabilizing the Grid to Supporting Large Scale Renewable Energy," *Journal of Power Sources*, Vol.144, issue 1, June 2005 pp. 280-294.
- [6.4] W. Kempton and J. Tomic, "Vehicle to grid fundamentals: calculating capacity and net revenue," *Journal of Power Sources*, vol. 144, no.1, Jun. 2005, pp.268-279.
- [6.5] W. Kempton and J. Tomic, "Vehicle to grid implementation: from stabilizing the grid to supporting large-scale renewable energy," *Journal of Power Sources*, vol. 144, no.1, Jun. 2005, pp.280-294.
- [6.6] W. Kempton and K. Toru., "Electric-drive vehicles for peak power in Japan," *Energy Policy*, vol.28, no.1, Jan. 2000, pp. 9-18.
- [6.7] X. Zhong, A. Cruden, D. Infield and P. Holik, "Assessment of vehicle to grid power as power system support," *Smart grid & Mobility Europe Conference*, 16-17 Jun., 2009.

- [6.8] H. Rahimi-Eichi, U. Ojha, F. Baronti, and M. Chow, "Battery management system: An overview of its application in the smart grid and electric vehicles," *IEEE Ind. Electron. Mag.*, vol. 7, no. 2, pp. 4, 16, Jun. 2013.
- [6.9] L. Cam, Lucien, "The central limit theorem around 1935," *Statistical Science*, pp. 78-91, 1986.
- [6.10] Australian Bureau of Statistics, survey of motor vehicle use, Australia, 12 months ended 30 June 2012.
- [6.11] B. Kirby, E. Hirst. "Customer-Specific Metrics for the Regulation and Load Following Ancillary Services," ORNL/CON-474, Oak Ridge National Laboratory, Oak Ridge, TN, January, 2000
- [6.12] B. Kirby "Frequency Regulation Basics and Trends," Oak Ridge National Laboratory, December 2004, ORNL/TM 2004/291, 2004
- [6.13] S. Han, K. Sezaki, "Development of an optimal vehicle-to-grid aggregator for frequency regulation," *IEEE Trans Smart Grid* 2010;1(1).
- [6.14] M. S. Bazaraa, J. J. Jarvis, and H. D. Sherali, "Linear Programming and Network Flows," 3rd ed. Hoboken, NJ, USA: Wiley, 2005.

CHAPTER 7

CONCLUSIONS AND FUTURE WORK

7.1 Conclusions

In this thesis, energy storage systems and the V2G system have been studied and developed.

Based on the research work in the thesis, the general conclusions can be summarized as:

1. Review of state of art of different types of energy storage system and power system requirements, comprehensive study of advanced control strategies for the power converter used for the bidirectional charger of V2G services.
2. Development of hybrid energy storage system using batteries and supercapacitors which can supply desired energy to both the vehicle and the grid.
3. Development of novel cell balancer for supercapacitor bank based on an active balancing method, which considered strongly discharging over voltaged cells rather than strongly recharging under voltaged ones.
4. Development of a bidirectional charger used for the V2G services to control the power flow of V2G services, which can support both active and reactive power according to the model predictive control approach.
5. Verification of grid support from V2G services to improve power quality and stability of the power system, with active power compensation to stabilize frequency fluctuation and reactive power compensation to stabilize voltage fluctuation.
6. Collection of different Smartparks V2G services information, development of different optimizing charging/discharging objectives based on the information of vehicles owners and grid demand.

7.2 Future Work

The V2G technology is a promising technology for increasing the number of electric vehicles. The unique aspect of power flow in V2G vehicles is that it is bidirectional, meaning the vehicles should be able to take power and provide power from/to the grid. Based on the research progress obtained in this thesis, the continued future work of the research field can be described as

- 1 Based on the cell balancer developed for supercapacitor bank in Chapter 3, develop a cell balancer for a battery bank which uses the same balancing method.
- 2 Construct a hybrid energy storage system using batteries and supercapacitors in the laboratory, develop a battery/supercapacitor management system to monitor the state of the energy storage bank and control the power flow of energy of the storage bank
- 3 Develop a V2G system testing workstation in component level in the laboratory and carry out experiments to test if the V2G charger can achieve the bidirectional power flow under the model predictive control algorithm.
- 4 Further develop the concepts of different Smartparks in different places to act as distributed sources, including the Smartparks model and power system model, economic profit and different optimization objectives, taking into account the vehicle owner's behaviour, energy storage dynamic and electricity market scheduling.

APPENDIX:

PUBLICATIONS BASED ON THE THESIS WORK

Journal Papers

Y. Qu, J. Zhu, J. Hu, X. Shi, "Power regulation of V2G system for grid power quality improvement," *IEEE Trans. Transportation Electrification*, under review.

Conference Papers

Y. Qu, J. Zhu, B. Holliday, J. Hu, "Overview of supercapacitor cell voltage balancing methods for an electric vehicle," *2013 IEEE ECCE Asia Downunder*, IEEE, Melbourne Australia, pp. 810-814.

J. Hu, J. Zhu, Y. Qu, J. M. Guerrero, "A new virtual-flux-vector based droop control strategy for parallel connected inverters in microgrids," *2013 IEEE ECCE Asia Downunder*, IEEE, Melbourne Australia, pp. 585-590.

X. Shi, J. Zhu, L. Li, Y. Qu, "Model predictive control of PWM AC/DC converters for bi-directional power flow control in microgrids," *Power Engineering Conference (AUPEC) 2015 Australasian Universities*, pp. 1-4.